NATIONAL TECHNICAL UNIVERSITY OF ATHENS
SCHOOL OF CIVIL ENGINEERING

SEISMIC PERFORMANCE ASSESSMENT OF INDUSTRIAL FACILITY ATMOSPHERIC LIQUID STORAGE TANKS

DOCTORAL THESIS OF
KONSTANTINOS BAKALIS

Supervised by
D. VAMVATSIKOS
Assistant Professor NTUA

Athens, February 2018

ΕΘΝΙΚΟ ΜΕΤΣΟΒΙΟ ΠΟΛΥΤΕΧΝΕΙΟ
ΣΧΟΛΗ ΠΟΛΙΤΙΚΩΝ ΜΗΧΑΝΙΚΩΝ

ΑΠΟΤΙΜΗΣΗ ΣΕΙΣΜΙΚΗΣ ΕΠΙΤΕΛΕΣΤΙΚΟΤΗΤΑΣ ΑΤΜΟΣΦΑΙΡΙΚΩΝ ΔΕΞΑΜΕΝΩΝ ΒΙΟΜΗΧΑΝΙΚΩΝ ΕΓΚΑΤΑΣΤΑΣΕΩΝ

ΔΙΔΑΚΤΟΡΙΚΗ ΔΙΑΤΡΙΒΗ
ΚΩΝΣΤΑΝΤΙΝΟΥ ΜΠΑΚΑΛΗ

Επιβλέπων
Δ. ΒΑΜΒΑΤΣΙΚΟΣ
Επίκουρος Καθηγητής ΕΜΠ

Αθήνα, Φεβρουάριος 2018

NATIONAL TECHNICAL UNIVERSITY OF ATHENS
SCHOOL OF CIVIL ENGINEERING

SEISMIC PERFORMANCE ASSESSMENT OF INDUSTRIAL FACILITY ATMOSPHERIC LIQUID STORAGE TANKS

DOCTORAL THESIS OF
KONSTANTINOS BAKALIS
Diploma in Civil Engineering, AUTH (2010)
MSc in Earthquake Engineering with Disaster Management, UCL (2011)

The thesis is submitted to the School of Civil Engineering
of the National Technical University of Athens
in fulfilment of the requirements for the Degree of Doctor of Philosophy

ADVISORY COMMITTEE:
1. D. VAMVATSIKOS, Assistant Professor NTUA (supervisor)
2. M. FRAGIADAKIS, Assistant Professor NTUA
3. I. VAYAS, Professor NTUA

EXAMINATION COMMITTEE:
1. D. VAMVATSIKOS, Assistant Professor NTUA (supervisor)
2. M. FRAGIADAKIS, Assistant Professor NTUA
3. I. VAYAS, Professor NTUA
4. S. A. KARAMANOS, Professor UTh
5. C. J. GANTES, Professor NTUA
6. V. PAPADOPOULOS, Associate Professor NTUA
7. D. G. LIGNOS, Associate Professor EPFL

Athens, February 2018

ΕΘΝΙΚΟ ΜΕΤΣΟΒΙΟ ΠΟΛΥΤΕΧΝΕΙΟ
ΣΧΟΛΗ ΠΟΛΙΤΙΚΩΝ ΜΗΧΑΝΙΚΩΝ

ΑΠΟΤΙΜΗΣΗ ΣΕΙΣΜΙΚΗΣ ΕΠΙΤΕΛΕΣΤΙΚΟΤΗΤΑΣ ΑΤΜΟΣΦΑΙΡΙΚΩΝ ΔΕΞΑΜΕΝΩΝ ΒΙΟΜΗΧΑΝΙΚΩΝ ΕΓΚΑΤΑΣΤΑΣΕΩΝ

ΔΙΔΑΚΤΟΡΙΚΗ ΔΙΑΤΡΙΒΗ

ΚΩΝΣΤΑΝΤΙΝΟΥ ΜΠΑΚΑΛΗ
Δίπλωμα Πολιτικού Μηχανικού ΑΠΘ (2010)
Μεταπτυχιακό Δίπλωμα Ειδίκευσης UCL (2011)
«Αντισεισμική Μηχανική και Διαχείριση Καταστροφών»

Η διατριβή υποβλήθηκε στη Σχολή Πολιτικών Μηχανικών του Εθνικού Μετσόβιου Πολυτεχνείου
προς εκπλήρωση των προϋποθέσεων του τίτλου του Διδάκτορος Μηχανικού

ΤΡΙΜΕΛΗΣ ΣΥΜΒΟΥΛΕΥΤΙΚΗ ΕΠΙΤΡΟΠΗ:

1. Δ. ΒΑΜΒΑΤΣΙΚΟΣ, Επ. Καθηγητής ΕΜΠ (επιβλέπων)
2. Μ. ΦΡΑΓΚΙΑΔΑΚΗΣ, Επ. Καθηγητής ΕΜΠ
3. Ι. ΒΑΓΙΑΣ, Καθηγητής ΕΜΠ

ΕΠΤΑΜΕΛΗΣ ΕΞΕΤΑΣΤΙΚΗ ΕΠΙΤΡΟΠΗ:

1. Δ. ΒΑΜΒΑΤΣΙΚΟΣ, Επ. Καθηγητής ΕΜΠ (επιβλέπων)
2. Μ. ΦΡΑΓΚΙΑΔΑΚΗΣ, Επ. Καθηγητής ΕΜΠ
3. Ι. ΒΑΓΙΑΣ, Καθηγητής ΕΜΠ
4. Σ. Α. ΚΑΡΑΜΑΝΟΣ, Καθηγητής Παν. Θεσσαλίας
5. Χ. Ι. ΓΑΝΤΕΣ, Καθηγητής ΕΜΠ
6. Β. ΠΑΠΑΔΟΠΟΥΛΟΣ, Αν. Καθηγητής ΕΜΠ
7. Δ. Γ. ΛΙΓΝΟΣ, Αν. Καθηγητής EPFL

Αθήνα, Φεβρουάριος 2018

ACKNOWLEDGMENTS

I have been waiting for a long time to write up this section, but I can assure you that it was totally worth it! When I decided to pursue a PhD, I came across lots of people who strongly advised against it. However, after 4.5 years, I have come to realise that it was one of the best decisions I ever made, and in my humble opinion the reason I feel this way is highly connected to the people that I met in the process. Therefore, through this section, I would like to express my gratitude to everyone that has contributed, either directly or indirectly, in making this PhD thesis possible.

To begin with, I would like to thank Prof. Anastasios Sextos who took me through my very first steps in the field of Earthquake Engineering, by supervising my undergraduate diploma thesis in Aristotle University of Thessaloniki, while also encouraging my decision to pursue further studies in the field. I would also like to thank Domenico Pennucci for giving me the opportunity to work on a very exciting project for my MSc thesis in University College London, as well as for the support and advice he provided through it.

Special thanks to Damian Grant not only for co-supervising my UCL thesis, but also for sharing his enthusiasm and knowledge on the field. His support and inspiration throughout the course has been outstanding! Damian is also one of the two reasons that I ended up with Prof. Dimitrios Vamvatsikos (aka *DV* in PBEE terms…) as my PhD advisor, so here is something else to thank him for. The other reason is Prof. Tiziana Rossetto, who was the one to introduce me to Dimitrios, when I appeared awfully late in our meeting to discuss potential PhD funding opportunities. I still blame (?) Victoria line by the way…

I am never going to forget the first meeting I had with Dimitrios at Exarcheia square in Athens, entertaining the idea of starting a PhD under his supervision. During that meeting there were two key-questions, the first one being “Are you familiar with OpenSees?”, and the second “Are you familiar with Matlab?”. My negative reply in both of them forced Dimitrios to ask out loud, “So, what am I supposed to do with you?”. “I ‘ve used Abaqus before”, I replied, only to hear “Good luck with debugging…”. That first meeting, followed by many more, gave me a unique opportunity to dive into Dimitrios’ world and face engineering from a totally different perspective. The most important thing, however, is that I had the chance to work with an extremely humble person that is characterised by an endless passion for science and excellence, while treats and respects others as equals even when they are brave enough to spell out the most hilarious questions on linear regression. Believe me, this an extremely rare combination. For those and many other reasons I am going to be eternally grateful for working with him. Don’t get me wrong; he may seem easy-going, yet he is the most demanding supervisor in the world. It’s just the way that he asks for things to be done that makes him special. Anyway, I really hope this is not making Dimitrios as uncomfortable as Amit Kanvinde’s last slide during his presentation at the 42nd Risk, Hazard & Uncertainty Workshop (future PhD students, go look for it... it’s worth the trouble…).

I would also like to thank professors Michalis Fragiadakis, Ioannis Vayas, Spyros Karamanos, Charis Gantes, Vissarion Papadopoulos and Dimitrios Lignos for taking the time to read the document and comment on it. It was a pleasure having you all as members of the examination committee for my PhD viva.

Special thanks to Prof. Michalis Fragiadakis for the support and guidance he provided all these years, by actively co-supervising my PhD thesis. I will certainly miss our debates on the quality of figures for our papers. I would also like to thank Michalis for convincing me to ask for a desk in NTUA. That decision, not only improved my productivity, but also gave me the chance to meet and work alongside some very nice and intelligent people that made my everyday routine extremely pleasant.

Among them I would like to thank Vasileios Melissianos (aka Dr. Bill), Stelios Vernardos and Ilias Thanassoulas for sharing their valuable experience on ADINA and finite element analysis in general, particularly during our Friday-afternoon coffee sessions that were dominated but not limited to engineering-related topics.

Many thanks to Stella Avgerinou for sharing her experience on Abaqus and OpenSees, while being Daphne's biggest fan from day one.

Many thanks to Maria-Eleni Dasiou for ensuring a smooth transition when I was asked to provide teaching assistance on the Steel Structures modules.

I would also like to thank Andrea Spillatura for the very strange mix of football and seismic fragility discussions we had during his short time in NTUA. I already miss the way he could change the subject from median $AvgS_a$ capacity to Alberto Malesani (by the way, I am coming for the pistachio ice-cream, so hang in there… Daphne says hi!).

Many thanks to Athanasia Kazantzi and Mohsen Kohrangi for the support they provided towards the publication of two journal papers. It was a pleasure working with you guys.

I can barely find the words to thank my parents for their invaluable support. They have been my gold sponsor throughout my studies, ensuring a smooth completion of my PhD thesis, particularly when the NTUA financial services failed to deliver a pay check on time.

Last but not least, I would like to thank from the bottom of my heart my loving wife Katerina for being the biggest fan of my work, even though she knows very little about engineering. Special thanks to her for being patient enough with me all this time, particularly in cases where the fact that model A wasn't matching model B was driving me crazy. Another special thanks to her for bearing through the viva presentation more than once… She did spot in advance the part where most people from the audience nearly fell asleep…

So, here we are… Against all odds I had a wonderful time, so please allow me to thank all of you one more time. It's time for me to officially start looking for a new challenge…

Yours,

Konstantinos Bakalis,

NTUA, February 2018

To my family,
for their unconditional love
and support

Η παρούσα έρευνα έχει συγχρηματοδοτηθεί μερικώς από την Ευρωπαϊκή Ένωση (Ευρωπαϊκό Κοινωνικό Ταμείο - ΕΚΤ) και εθνικούς πόρους μέσω του Επιχειρησιακού Προγράμματος «Εκπαίδευση και Δια Βίου Μάθηση» του Εθνικού Στρατηγικού Πλαισίου Αναφοράς (ΕΣΠΑ)– Ερευνητικό Χρηματοδοτούμενο Έργο: ΘΑΛΗΣ. Επένδυση στην κοινωνία της γνώσης μέσω του Ευρωπαϊκού Κοινωνικού Ταμείου. Ερευνητικό πρόγραμμα RASOR (Risk Assessment for the Seismic protection Of industrial facilities).

Ευρωπαϊκή Ένωση
Ευρωπαϊκό Κοινωνικό Ταμείο

ΕΠΙΧΕΙΡΗΣΙΑΚΟ ΠΡΟΓΡΑΜΜΑ
ΕΚΠΑΙΔΕΥΣΗ ΚΑΙ ΔΙΑ ΒΙΟΥ ΜΑΘΗΣΗ
επένδυση στην κοινωνία της γνώσης
ΥΠΟΥΡΓΕΙΟ ΠΑΙΔΕΙΑΣ ΚΑΙ ΘΡΗΣΚΕΥΜΑΤΩΝ
ΕΙΔΙΚΗ ΥΠΗΡΕΣΙΑ ΔΙΑΧΕΙΡΙΣΗΣ

ΕΣΠΑ
2007-2013
πρόγραμμα για την ανάπτυξη
ΕΥΡΩΠΑΪΚΟ ΚΟΙΝΩΝΙΚΟ ΤΑΜΕΙΟ

Με τη συγχρηματοδότηση της Ελλάδας και της Ευρωπαϊκής Ένωσης

This research has been co-financed by the European Union (European Social Fund - ESF) and Greek national funds through the Operational Program "Education and Lifelong Learning" of the National Strategic Reference Framework (NSRF) – Research Funding Program: THALES. Investing in knowledge society through the European Social Fund. Research project RASOR (Risk Assessment for the Seismic protection Of industrial facilities).

European Union
European Social Fund

OPERATIONAL PROGRAMME
EDUCATION AND LIFELONG LEARNING
investing in knowledge society
MINISTRY OF EDUCATION & RELIGIOUS AFFAIRS
MANAGING AUTHORITY

NSRF
2007-2013
programme for development
EUROPEAN SOCIAL FUND

Co-financed by Greece and the European Union

ABSTRACT

Large-capacity atmospheric tanks are widely used to store a variety of liquid-form materials that are deemed necessary for the functionality of any modern community. The devastating consequences of earthquake damage on liquid storage tanks (e.g. Kocaeli 1999, Tohoku 2011) have revealed the vulnerability of such structural systems against strong ground motions, while at the same time have highlighted the need for innovative engineering concepts in order to mitigate the associated socioeconomic losses. Along these lines, the seismic performance of industrial-facility atmospheric liquid storage tanks is examined, in view of providing an easy-to-implement assessment tool that offers reliable results within a reasonable timeframe with respect to structural analysis and the associated post-processing.

Following the concepts of performance-based earthquake engineering, a three-dimensional reduced-order (i.e. surrogate) model is formed to obtain the distribution of the various engineering demand parameters of interest under earthquake loading. Liberated from the need for structure-specific calibration using detailed finite element models, the proposed model is able to represent both anchored and unanchored liquid storage tanks, using ground motion components at multiple principal loading directions simultaneously. Exploiting the virtues of the model in our disposal allows to summarise a considerable volume of analysis results in the form of the fragility curves and perform the subsequent integration with the site hazard of interest to derive the associated mean annual frequency of exceeding certain failure mode thresholds.

In view of a comprehensive seismic risk assessment estimation, both component and system-level damage states are employed. Commonly observed modes of failure such as base plate plastic rotation, elephant's foot buckling, sloshing-wave-induced damage and anchorage failure, are used to form the component-level damage classification. Special attention is paid to the elephant's foot buckling failure mode, as the underlying criterion to signal failure is time and seismic intensity dependent. The aforementioned failure modes are appropriately combined to form the system-level damage classification and thus obtain information for a group of tanks rather than a structural system alone. Several scalar and vector seismic intensity measures are also examined in order to come up with a solution that on one hand minimises the required number of records to achieve numerical fidelity, and on the other renders structural response independent of ground motion characteristics. The geometric mean of spectral accelerations in the range of 0.1s and 4.5 times the fundamental period of vibration is proposed as a potentially optimal solution to perform the seismic risk assessment estimation. The latter is employed to

perform a seismic vulnerability assessment on an indicative tank farm layout, whereby suitable damage indices are defined to estimate the expected loss of stored material and storage capacity following a strong ground motion.

Overall, this study attempts to fill a gap that has comparatively drawn little attention within the earthquake engineering science. The proposed methodology comprises a unique seismic risk assessment tool for liquid storage tanks, by offering a simplified numerical model that effectively tackles the issue of the time required to compile all necessary structural analysis data. The estimation of both the probability and the mean annual frequency of exceeding certain failure mode capacity thresholds, suggests that liquid storage tanks are extremely vulnerable structural systems (for the considered site hazard), particularly prone to elephant's foot buckling and base plate plastic rotation. The assessment procedure may further be refined by adopting state-of-the-art seismic intensity measures, bearing in mind that the concepts outlined for a single structural system may be extended to a tank-farm or even a refinery, where various tank geometries are combined to offer increased storage capacity.

Περιληψη

Οι ατμοσφαιρικές δεξαμενές μεγάλης χωρητικότητας χρησιμοποιούνται ευρέως με σκοπό την αποθήκευση των διαφόρων υγρής μορφής υλικών που είναι απαραίτητα για την εύρυθμη λειτουργία κάθε σύγχρονης κοινωνίας. Οι καταστροφικές επιπτώσεις των σεισμικών βλαβών στις δεξαμενές στο παρελθόν (π.χ. Kocaeli 1999, Tohoku 2011) έχουν καταστήσει σαφή την τρωτότητα των εν λόγω δομικών συστημάτων, τονίζοντας παράλληλα την ανάγκη για καινοτόμες ιδέες στον τομέα της μηχανικής με σκοπό την ελαχιστοποίηση των κοινωνικών και οικονομικών απωλειών. Αντικείμενο της παρούσας διατριβής είναι ο προσδιορισμός της σεισμικής επιτελεστικότητας βιομηχανικών ατμοσφαιρικών δεξαμενών, στοχεύοντας στη δημιουργία ενός εύχρηστου εργαλείου αποτίμησης που προσφέρει αξιόπιστα αποτελέσματα σε ένα εύλογο χρονικό διάστημα, απαραίτητο για τη δομική ανάλυση και τη επακόλουθη επεξεργασία των αποτελεσμάτων.

Ακολουθώντας τις ιδέες που έχουν διατυπωθεί στο πλαίσιο της αντισεισμικής μηχανικής με βάση την επιτελεστικότητα, μορφώνεται ένα απλοποιημένο τρισδιάστατο αριθμητικό προσομοίωμα προκειμένου να καθοριστεί η κατανομή των διαφόρων μέτρων απόκρισης υπό σεισμική φόρτιση. Το προτεινόμενο μοντέλο δύναται να προσομοιώσει τόσο αγκυρωμένες όσο και ελεύθερα εδραζόμενες δεξαμενές, χρησιμοποιώντας χρονοϊστορίες σεισμού σε μια ή περισσότερες από τις κύριες διευθύνσεις φόρτισης ταυτόχρονα, χωρίς να απαιτείται διακρίβωση με λεπτομερή μοντέλα πεπερασμένων στοιχείων. Αξιοποιώντας τα πλεονεκτήματα που παρέχει η εν λόγω αριθμητική προσομοίωση, δίνεται η δυνατότητα για τη δημιουργία ενός σημαντικού όγκου δεδομένων ανάλυσης, τα οποία με τη σειρά τους μπορούν μέσω στατιστικής επεξεργασίας να συνοψιστούν στις καμπύλες τρωτότητας, ή ακόμη να αξιοποιηθούν συνδυαστικά με την καμπύλη σεισμικής επικινδυνότητας προκειμένου να υπολογιστεί η μέση ετήσια συχνότητα υπέρβασης της οριακής κατάστασης μιας οποιασδήποτε αστοχίας.

Για την πληρέστερη αποτίμηση της σεισμικής διακινδύνευσης των ατμοσφαιρικών δεξαμενών, χρησιμοποιούνται κατηγορίες σταθμών βλάβης που αναφέρονται τόσο σε αστοχίες που ενδέχεται να συμβούν τοπικά στην κατασκευή, όσο και σε αυτές που αναφέρονται στο επίπεδο ολόκληρου του συστήματος. Η κατηγοριοποίηση με βάση τις τοπικές βλάβες περιλαμβάνει τις συνήθεις αστοχίες που παρατηρούνται στις δεξαμενές σε περίπτωση σεισμού, όπως η πλαστική στροφή της βάσης της δεξαμενής, ο λυγισμός μορφής πόδα ελέφαντα στο τοίχωμα, οι βλάβες λόγω κυματισμού της ελεύθερης επιφάνειας του αποθηκευμένου υγρού και η αστοχία των αγκυρίων για τις αγκυρωμένες δεξαμενές. Ειδική μνεία γίνεται στην αστοχία λυγισμού μορφής πόδα ελέφαντα, καθώς το κριτήριο που καθορίζει τη συγκεκριμένη αστοχία

είναι συνάρτηση τόσο του χρόνου όσο και του επιπέδου της σεισμικής έντασης. Οι παραπάνω μορφές αστοχίας συνδυάζονται κατάλληλα ώστε να προκύψει η κατηγοριοποίηση των βλαβών στο επίπεδο του συστήματος της δεξαμενής, η οποία δύναται να αξιοποιηθεί κατά την αξιολόγηση μιας ομάδας δεξαμενών, αντί ενός μεμονωμένου δομικού συστήματος. Επιπρόσθετα, εξετάζεται ένα πλήθος βαθμωτών και διανυσματικών μέτρων σεισμικής έντασης με σκοπό τον προσδιορισμό της βέλτιστης λύσης η οποία αφενός θα ελαχιστοποιεί το πλήθος των απαιτούμενων αναλύσεων και αφετέρου θα καθιστά την απόκρισης της κατασκευής ανεξάρτητη από τα διάφορα σεισμολογικά χαρακτηριστικά. Με βάσει αυτές τις κατευθύνσεις, ο γεωμετρικός μέσος των φασματικών επιταχύνσεων για περιόδους που βρίσκονται στο διάστημα μεταξύ 0.1s και 4.5 φορές τη θεμελιώδη περίοδο της κατασκευής προτείνεται ως ένα πιθανό βέλτιστο μέτρο σεισμικής έντασης. Το εν λόγω μέτρο αξιοποιείται στην αποτίμηση της σεισμικής τρωτότητας μιας ομάδας δεξαμενών, όπου μορφώνονται κατάλληλοι δείκτες βλάβης με σκοπό την εκτίμηση των αναμενόμενων απωλειών σε επίπεδο αποθηκευμένου υλικού και ικανότητας αποθήκευσης με το πέρας ενός ισχυρού σεισμού.

Συνοπτικά, η παρούσα έρευνα αποτελεί μια προσπάθεια να καλυφθεί ένα κενό στην επιστήμη της αντισεισμικής μηχανικής, στο οποίο συγκριτικά έχει δοθεί μικρή προσοχή. Η προτεινόμενη μεθοδολογία αποτελεί ένα μοναδικό εργαλείο αποτίμησης των σεισμικών βλαβών για δεξαμενές αποθήκευσης υγρών, η οποία αξιοποιεί ένα απλοποιημένο αριθμητικό μοντέλο το οποίο αντιμετωπίζει αποτελεσματικά το θέμα του απαιτούμενου υπολογιστικού χρόνου ώστε να συγκεντρωθούν τα απαραίτητα δεδομένα μέσω της δομικής ανάλυσης. Η εκτίμηση τόσο της πιθανότητας όσο και της μέσης ετήσιας συχνότητας υπέρβασης των διαφόρων οριακών καταστάσεων αστοχίας, αποκαλύπτει πως οι ατμοσφαιρικές δεξαμενές κρίνονται ως άκρως τρωτά δομικά συστήματα (για την εν λόγω καμπύλη σεισμικής επικινδυνότητας), αναπτύσσοντας πρωτίστως μορφές αστοχίας όπως ο λυγισμός μορφής πόδα ελέφαντα και η πλαστική στροφή του ελάσματος βάσης. Η εν λόγω διαδικασία αποτίμησης μπορεί να βελτιωθεί περεταίρω, αξιοποιώντας καινοτόμα μέτρα σεισμικής έντασης, έχοντας κατά νου πως οι ιδέες που έχουν διατυπωθεί για μεμονωμένες δεξαμενές δύναται να αξιοποιηθούν και στην περίπτωση μιας φάρμας δεξαμενών, ή ακόμη ενός διυλιστηρίου, όπου δεξαμενές διαφορετικής γεωμετρίας συνδυάζονται κατάλληλα.

CONTENTS

List of Figures

List of Tables

Nomenclature

2D	two-dimensional
2DOF	two-degree-of-freedom
3D	three-dimensional
A	absolute response history acceleration
A_f	acceleration coefficient for sloshing wave height calculation
a_h	hardening ratio
a_k	strip model edge spring stiffness modification factor
AN	anchorage damage
$AvgS_a$	average spectral acceleration
C	capacity
CMS	conditional mean spectrum
CS	conditional spectrum
d	sloshing wave height
D	demand
$d_{API\text{-}650}$	sloshing wave height demand per API-650
d_{EC8}	sloshing wave height demand per Eurocode 8
DFM	dominant failure mode
DI	damage index
DM	damage measures
DS	damage state
DV	decision variable
E	Young's modulus
EDP	engineering demand parameter
$EDP(IM)_{50\%}$	median *EDP* demand conditioned on the *IM*
$EDP_{C,50\%}$	median limit state capacities expressed in *EDP* terms
EFB	elephant's foot buckling
E_w	soil stiffness
FE	finite element
FEM	finite element model
FSI	fluid-structure-interaction
f_y	yield strength
g	gravity acceleration
GMPE	ground motion prediction equation
h_c	convective mass effective height
h_f	fluid height
h_i	impulsive mass effective height
h_t	tank height
IDA	Incremental Dynamic Analysis
IM	intensity measure
$IM_{C,50\%}$	median limit state capacities expressed in *IM* terms
K_b	anchor-bolt stiffness per supporting spring on the "Joystick" model
k_{uu}	strip model edge translational spring
$k_{\theta\theta}$	strip model edge rotational spring
L	separation length
LS	limit state
MAF	mean annual frequency
MAREq	mean annual rate of equalling
m_c	convective mass
m_i	impulsive mass
M_r	strip model edge moment
m_r	roof mass
M_w	moment magnitude
n	"Joystick" model base plate rigid beam-spokes

N	"Joystick" model vertical edge-spring force
NaTech	natural-technological events
N_r	strip model edge axial force
p	maximum interior pressure on the tank wall
PBEE	performance-based earthquake engineering
PEER	Pacific earthquake engineering research centre
PGA	peak ground acceleration
p_h	hydrostatic pressure
p_i	impulsive pressure
PSHA	probabilistic seismic hazard assessment
R^2	coefficient of determination
R_t	tank radius
$r_{\beta expl}$	normalised variance explained
S_a	spectral acceleration
SL	sloshing damage
T_1	fundamental period
t_a	annular ring thickness
t_b	base plate thickness
T_c	convective period
T_i	impulsive period
T_r	return period
t_w	tank wall thickness
V	Poisson's ratio
V	strip model uplift force
V_b	"Joystick" model base shear
VPSHA	vector-valued probabilistic seismic hazard analysis
W	uplift
β	total dispersion
β_{EDP}	*EDP*-basis dispersions
β_{IM}	*IM*-basis dispersion
δ	anchorage elongation
δ_u	anchorage ultimate displacement
δ_y	anchorage yield displacement
ε	epsilon
ζ	non-dimensional vertical tank coordinate
θ	transverse component response acceleration orientation
θ_{pl}	base plate plastic rotation
κ_f	fluid damping
λ	mean annual frequency
ξ	non-dimensional radial tank coordinate
ρ_f	fluid density
σ_{c1}	ideal critical buckling stress for cylinders loaded in axial compression
σ_{EFB}	critical elephant's foot buckling stress
σ_m	meridional stress
φ	non-dimensional angular tank coordinate

1 INTRODUCTION

1.1 PROBLEM STATEMENT

Industrial facilities produce, store and deliver some of the most fundamental goods required for a modern community to function and are thus categorised as high-importance structures. Safeguarding the integrity of those facilities against natural hazards is of paramount importance, as the impact of a failing structure may lead to a chain of events varying from business disruption to uncontrolled leakage and/or fire. Despite the strict criteria enforced during design, construction and operation by the pertinent codes of practice and regulations (American Lifelines Alliance 2001a; b; American Petroleum Institute 2007; Azzuni and Guzey 2015; CEN 2006; Godoy 2016; Jaiswal et al. 2007; Ormeño et al. 2015b; Rondon and Guzey 2016, 2017, Spritzer and Guzey 2017a; b), industrial disasters are still occurring. Particularly for earthquakes, these so-called Natural-Technological (NaTech) events constitute a major threat for every community, as the associated aftermath might be related to fiscal factors such as significant death-toll, direct monetary loss and/or downtime, as well as social ones similar to psychological disorders (Önder et al. 2006; Tural et al. 2004).

(a) (b)

Figure 1-1: NaTech events in refineries following (a) the Izmit, Turkey, 1999 earthquake (British Broadcasting Corporation 1999) and (b) the Tohoku, Japan, 2011 earthquake (European Pressphoto Agency 2011).

Recent earthquakes such as those of Izmit (or Kocaeli, 1999) and Tohoku (2011) have revealed significant damage, that led to leakage of the stored materials, widespread fire, and caused a series of structures to collapse while leaving others significantly damaged [Figure 1-1, (Cruz and Steinberg 2005; Hatayama 2015; Sezen and Whittaker 2006)]. The impact that the

Kocaeli earthquake in specific had throughout the energy sector was heavy, leaving oil and gas production facilities severely damaged, despite the fact that the fiscal cost was held down by insurance coverage of fire damage to major oil refineries (Bibbee et al. 2000). Moderate oil and gas pipeline damage was also sustained to municipal distribution systems, while there were additional clean-up costs due to oil and chemicals discharged into the Marmara Sea.

Similarly, the Tohoku earthquake left several nuclear and thermal power plants heavily damaged (Naito et al. 2013), causing a series of hazardous materials to leak that had as an immediate result thousands of hectares of farmland to be ruined. Many large-scale manufacturers were placed off-production, causing a decline in the associated markets (Norio et al. 2011), while significant fluctuations in the global financial markets were also noticed, not only on the day of the earthquake, but also days after, when the seriousness of the nuclear accident became clear. Some of the world's largest reinsurers were speculated to suffer losses in the order of tens of billion U.S. dollars (USD), even after some of the losses were absorbed by primary insurers and grants from the Japanese government. The estimation of the direct economic losses due to the Tohoku earthquake was in the order of several hundred billion USD, regardless of the significant cost for recovery which could be assumed to add-up approximately a few more.

The examples presented above are only a couple, among many, to highlight the importance of protecting industrial facilities against earthquakes. On a European level, a comparison among an indicative map of the available refineries [Figure 1-2(a)] to the corresponding seismic hazard map [Figure 1-2(b), Giardini et al. (2013)] suggests that the exposure of such facilities on earthquakes cannot be ignored. Even for countries that are not traditionally considered earthquake prone (e.g. United Kingdom, Netherlands), it appears that there are industrial facility locations where the ground is capable of producing notable shaking. That kind of exposure, combined with the vulnerability that typically stems from under or poorly-designed existing structural systems, highlights the need for innovative engineering concepts to mitigate the potential casualties and socioeconomic losses.

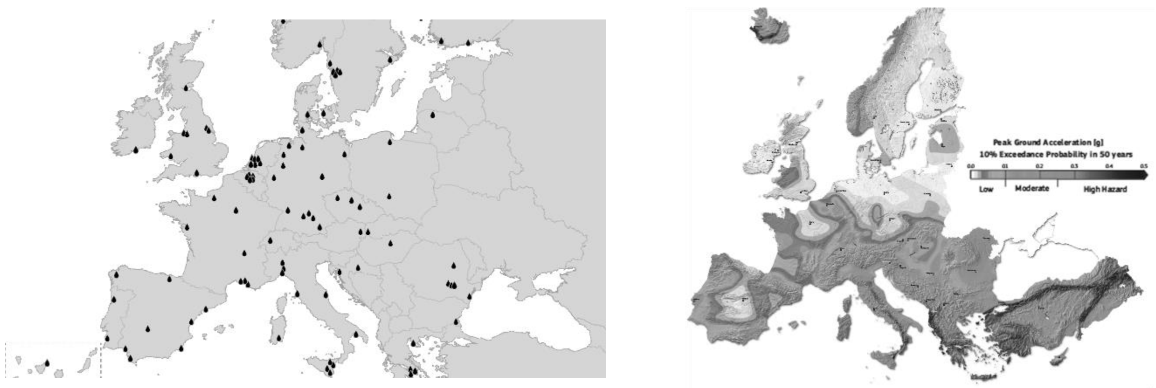

(a) (b)

Figure 1-2: (a) European refineries (Friends of the Earth Europe and Transport & Environment 2017) (b) EU-SHARE seismic hazard map (Giardini et al. 2013).

Undeniably, the production process encountered in industrial facilities is of rather complex nature, as various types of structures are involved to deliver the required goods. Typical kinds of these so-called industrial equipment structures are the process towers [Figure 1-3(a)], the pipe-racks (i.e. steel braced-frames that support the piping, Figure 1-3(b)], the piping itself [Figure 1-3(c)], and the atmospheric liquid storage tanks [e.g., Figure 1-3(d), although other types of tanks may also be encountered within a refinery]. The latter, which are the main subject of this study, serve as the storage space for the final products, or any sort of liquid-form materials that could be exploited during production. Their principal structural element is typically a vertical steel cylinder or shell, which is constructed by welding together a series of rectangular plates, attached on a (usually) flat steel-plated base resting on a prepared foundation.

The industrial facility structures depicted in Figure 1-3 are equally important during the production process, however, from a seismic risk assessment point of view liquid storage tanks comprise probably one of the most vulnerable structural systems within a refinery. The reason why they are considered so important lies on the large quantities of (usually) flammable/pollutive substances that the stored materials contain. As discussed above, an earthquake-triggered leak on a tank could potentially result in drainage of the stored material in the surrounding space, or even in fire that would take days to be controlled. In both these cases, the consequences span from environmental and social, to organisational and monetary, at a magnitude that is always hard to predict.

(a) (b) (c) (d)

Figure 1-3: Typical industrial equipment structures; (a) Process towers (AMACS Process Towers Internals 2016), (b) pipe-rack (Innovative Engicon Solutions PVT 2017), (c) piping (Oil and Gas club 2015) and (d) liquid storage tanks (Trust Subsidiary Production Co 2015).

1.2 PERFORMANCE-BASED EARTHQUAKE ENGINEERING

The procedure that is typically followed for the design of structures by the majority of pertinent codes requires a preliminary member sizing to define the fundamental period (T_1), for which the corresponding design-spectrum spectral acceleration [$S_a(T_1)$] is derived. Strength as well as stiffness checks are then performed using $S_a(T_1)$, in view of verifying the adequacy of the selected member sizes, whereby in the case that the aforementioned conditions are not met, iterations need be performed until the desired structural properties are defined. Similarly, from an assessment point of view, the structural system under investigation is subjected to a series of ground motion records in order to define the distribution of response quantities versus the seismic intensity. The issue with those procedures is that the design $S_a(T_1)$ refers to a fixed value of seismic hazard, typically the 10% in 50 years probability of exceedance, that may significantly differ from the actual site hazard one [Figure 1-4(a)]. On the other hand, both the design and the assessment output rely on that very specific hazard value, thus forming an intensity-based approach that eventually constraints the response distribution (Bradley 2013). This problem stems from a reasonable (in the context of design codes) attempt to oversimplify the rather complex nature of seismic hazard, which according to Figure 1-4(b) forms a surface among the period, the spectral acceleration and the mean annual frequency of exceeding $S_a(T)$ values.

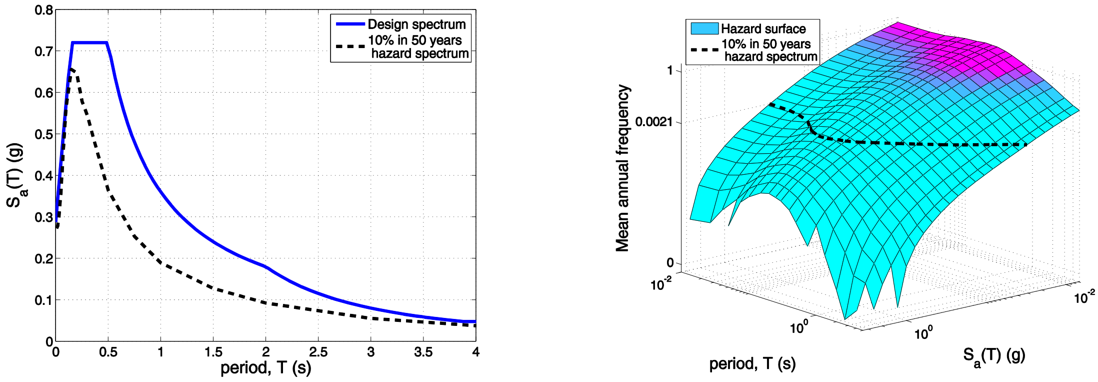

Figure 1-4: (a) Design versus 10% in 50 years hazard spectrum and (b) hazard surface, for the site of Athens.

In that sense, assessing the response capabilities of liquid storage tanks mandates the use of state-of-the-art concepts, such as that of Performance-based Earthquake Engineering (PBEE). The PBEE framework, originally developed by Cornell and Krawinkler (2000) for the Pacific Earthquake Engineering Research (PEER) Centre, serves as an alternative to the well-established Load and Resistance Factor Design, where the former can assess performance based on the mean annual frequency (MAF) of exceeding decision variable (*DV*) thresholds similar to casualties, monetary loss and down time. To perform such an estimation, damage measures (*DM*, e.g. cracking) must be defined based on appropriate engineering demand parameters (*EDPs*, e.g. roof displacement, drift) which are triggered by certain ground motions that correspond to a seismic hazard function $\lambda(IM)$, and can adequately be represented by seismic intensity measures (*IMs*) such as the peak ground acceleration (*PGA*) and the fundamental-period spectral acceleration [$S_a(T_1)$]. The entire PBEE methodology is summarised as

$$\lambda(DV) = \int_{DM}\int_{EDP}\int_{IM} G(DV \mid DM)\left|\mathrm{d}G(DM \mid EDP)\right|\left|\mathrm{d}G(EDP \mid IM)\right|\left|\mathrm{d}\lambda(IM)\right|, \quad (1\text{-}1)$$

where $G(x|\,y)=\mathrm{P}(X>x \mid Y=y)$ is the conditional complementary cumulative distribution function (CCDF) of a random variable X given the value y of another random variable Y.

Figure 1-5 attempts to present the aforementioned equation from a rather simpler perspective. In every PBEE-related application the physical problem (in our case the response of a liquid storage tank under seismic loading) is approximated via a suitable structural model. In the structural analysis context, each dynamic analysis provides a single *EDP-IM* pair, which in view of the uncertainties involved, employs multiple analyses on a considerable number of ground motion records for several levels of seismic intensity. For a given capacity threshold that often refers to a certain failure on the structure, the nonlinear analyses results are statistically processed in order to form the fragility curve. The latter is eventually convoluted with the site hazard curve in order to derive the associated mean annual frequency of exceedance ($\lambda_{failure}$). It should be noted that an additional integration may also be performed, by employing several threshold capacities, in view of obtaining a risk-based representation of response hazard given the desired *EDP* value.

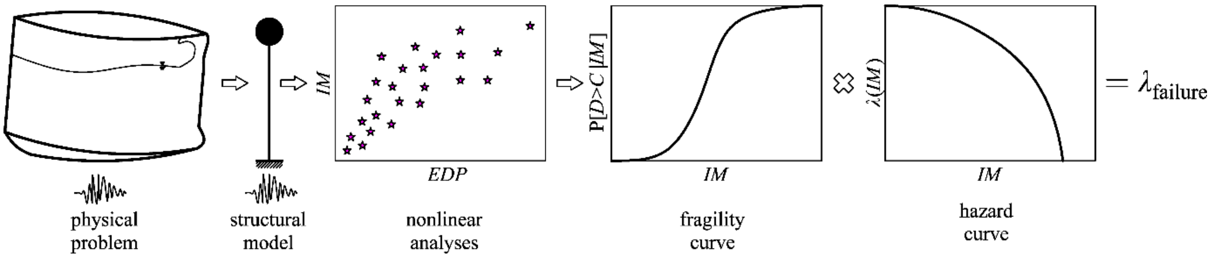

Figure 1-5: PBEE explained; the response of a liquid storage tank under earthquake excitation, approximated using a structural model, to obtain the *EDP-IM* relationship via nonlinear dynamic analysis that is statistically processed to generate the fragility curve, which is convoluted with the site-hazard to derive the mean annual frequency of exceeding a certain failure mode threshold.

1.3 OBJECTIVES AND SCOPE

The goal of this study is to present a comprehensive approach for the enforcement of Performance-based Earthquake Engineering [PBEE, (Cornell and Krawinkler 2000)] concepts on industrial-facility liquid storage tanks. Given that this work primarily aims to offer a methodology that could be applied in a practical way with respect to the estimation of seismic risk (or loss) in the insurance-reinsurance sectors, a simplified model is formed for anchored as well as unanchored liquid storage tanks, capable of performing rapid nonlinear response history analysis. The aforementioned model is exploited to investigate the influence of tank geometry on seismic risk metrics such as fragility curves and mean annual frequency of exceedance, and come up with a suitable seismic intensity measure that satisfies the fundamental criteria of efficiency and sufficiency (Luco and Cornell 2007). Ultimately, the scope is to establish a solid methodology for the seismic risk assessment of a group of tanks (rather than a structural system alone) that are typically encountered in refineries, wineries and tank-farms in general, and thus contribute towards a decision-making process that aims to mitigate the associated losses.

1.4 OUTLINE

Most chapters are designed to be autonomous, each being a self-contained, single paper that has either been published in a scientific journal or is being planned as a future publication.

Chapter 2 aims to get any interested parties acquainted with the fundamentals of liquid storage tanks. It contains information on the typologies that are currently used in the industry, a brief overview of the construction process, and a summary of the actions that liquid storage tanks are typically designed for. It also discusses the response of such structural systems under earthquake loading, by presenting a list of potential modes of failure that have been extensively reported in post-earthquake field investigations.

Chapter 3 discusses the various aspects involved in the modelling of liquid storage tanks, in view of developing a single-mass three-dimensional surrogate physical model. The so-called "Joystick" model consists of beam elements and nonlinear springs, is able to accommodate multiple ground motion components during the analysis, and is thus deemed suitable for rapid seismic performance-based design and assessment of both anchored and unanchored liquid storage tanks. Following the model calibration on the results of shell-dominated finite element models for three different tank aspect ratios, a step-by-step example is presented for a squat liquid storage tank, accompanied by a sensitivity analysis that aims to provide an estimate of the model-parameter uncertainty.

Chapter 4 investigates the seismic risk involved in aboveground cylindrical liquid storage tanks. Using the "Joystick" surrogate model presented in Chapter 3, Incremental Dynamic

Analysis and simplified Cloud are employed to derive the relationships between the various response parameters, that serve in place of the associated failure modes, versus the seismic intensity. Special attention is paid to the so-called ‘elephant’s foot buckling’ formation, whereby its dynamic capacity suggests that failure should be monitored in the time domain. The three tank configurations used in Chapter 3 are also adopted in this instance to perform a set of parametric analyses with respect to appropriately defined component and system-level damage states, by employing metrics such as the median seismic fragility capacity, the associated dispersion, and the mean annual frequency of exceedance.

Chapter 5 refines the methodology presented in Chapter 4, by investigating a series of potentially suitable seismic intensity measures. The selected candidates vary from well-known scalar intensity measures, such as the peak ground acceleration and the first-mode spectral acceleration, to complex combinations of carefully selected spectral ordinates and vector-valued ones. Using state-of-the-art techniques with respect to the ground motion input, selected candidate intensity measures that fully comply with the well-established requirements of efficiency and sufficiency, are promoted as optimal solutions for the seismic risk evaluation of liquid storage tanks.

Chapter 6 extends the concepts presented in all previous chapters for single liquid storage tanks onto a tank-farm level, by considering as a case study an indicative layout of nine tanks with three different geometries. The aim is to offer a decision-making tool with respect to the mitigation of earthquake-related losses, through suitable damage indices that rely on the loss of the stored material as well as the available storage capacity following a strong ground motion.

Chapter 7 summarises the virtues and limitations of the proposed methods, setting directions for future work and improvements. Finally, it provides the overall conclusions and summary of the thesis.

2 LIQUID STORAGE TANKS

2.1 TYPOLOGY

Typology-wise, liquid storage tanks may vary according to the requirements prescribed by the facility owners, and therefore, the choice of the appropriate tank type is often related to the stored material. Thus, they may be categorised as aboveground [Figure 2-1(a)] or belowground [Figure 2-1(b)], depending on whether their construction is performed above or below the ground surface; ground supported [Figure 2-1(a)] or elevated [Figure 2-1(d)], depending on whether the base plate of the tank rests on the ground or a supporting structure; anchored [Figure 2-1(e)] or unanchored [Figure 2-1(f)], depending on the requirement of anchorage at the base; atmospheric or pressurised (low or high pressure), depending on the pressure under which they are designed to operate; flat [Figure 2-1(a)], conical, domed or spheroid bottom, depending on the shape of the base; fixed [Figure 2-1(a)] or floating-roof [Figure 2-1(g, h)], depending on the constraints between the roof and the tank-shell. Note that fixed-roof tanks are further identified by the shape of the roof (i.e. cone, umbrella and dome), while floating-roof tanks may also be categorised as internal (i.e. closed-top) and external (i.e. open-top), based on whether the tank is equipped with a fixed-roof above the floating one [Figure 2-1(g, h)]. In the following, however, only fixed-roof cylindrical steel liquid storage tanks are examined, using both anchored and unanchored support conditions.

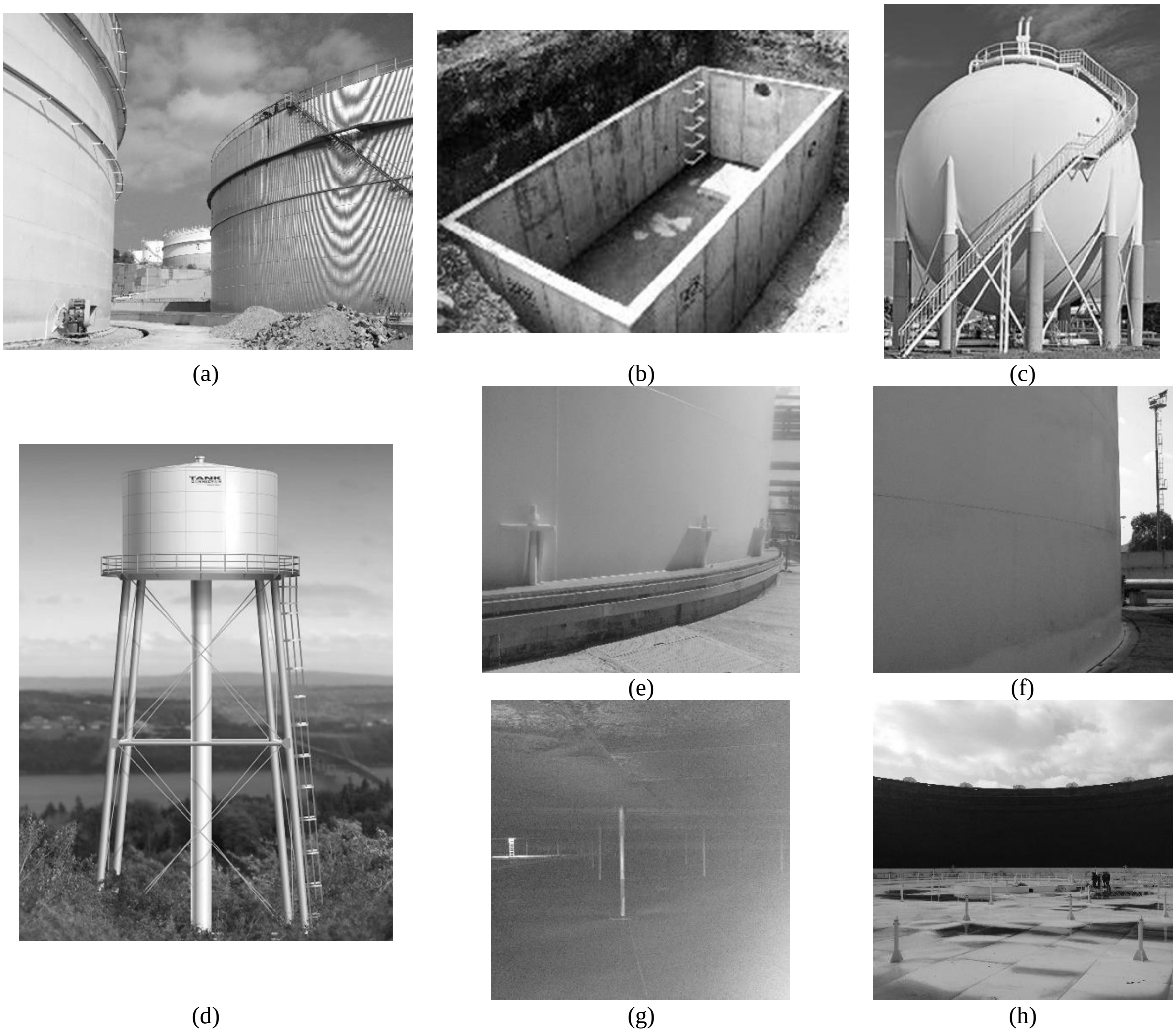

Figure 2-1: Typical liquid storage tank typologies: (a) Cylindrical aboveground fixed-roof, (b) rectangular belowground (MSMAware 2014), (c) spherical (T.F. Warren Group 2016), (d) elevated (Tank Connection 2017), (e) anchored (courtesy of Dr. Vasileios Melissianos), (f) unanchored, (g) floating-roof inner part, (h) floating-roof top.

2.2 CONSTRUCTION

The construction of cylindrical aboveground liquid storage tanks follows a number of stages (Raine 2016). Initially, the tank foundation is constructed using the concrete ring beam/wall approach (although asphalt and sand-pad might also be used instead). The construction of the ring beam follows the principles of reinforced concrete design, by employing longitudinal rebar of appropriate diameter, stirrups for confinement [Figure 2-2(a)], maintaining a uniform thickness throughout the ring [Figure 2-2(b)]. The ring beam is used to perform a variety of functions; however, its most critical aspect is related to whether anchoring (or hold-down) bolts are used to supply the system with additional overturning stability [e.g. against wind or earthquake, Figure 2-1(e)]. In general, the need for anchoring bolts is controlled by the weight of the tank, its aspect ratio (in the sense that a slender tank is going to require a certain amount of anchoring to achieve the same storage capacity compared to a squat one), and more importantly the client specifications. Following the construction of the foundation, the volume defined by the inner surface of the ring wall and the centre of the tank is filled with a suitable material [e.g. soil, gravel, concrete, Figure 2-2(c)] to form a smooth surface [Figure 2-2(d)] where the steel plates that make up the base of the tank [Figure 2-2(e)] are placed for subsequent welding [Figure 2-2(f)].

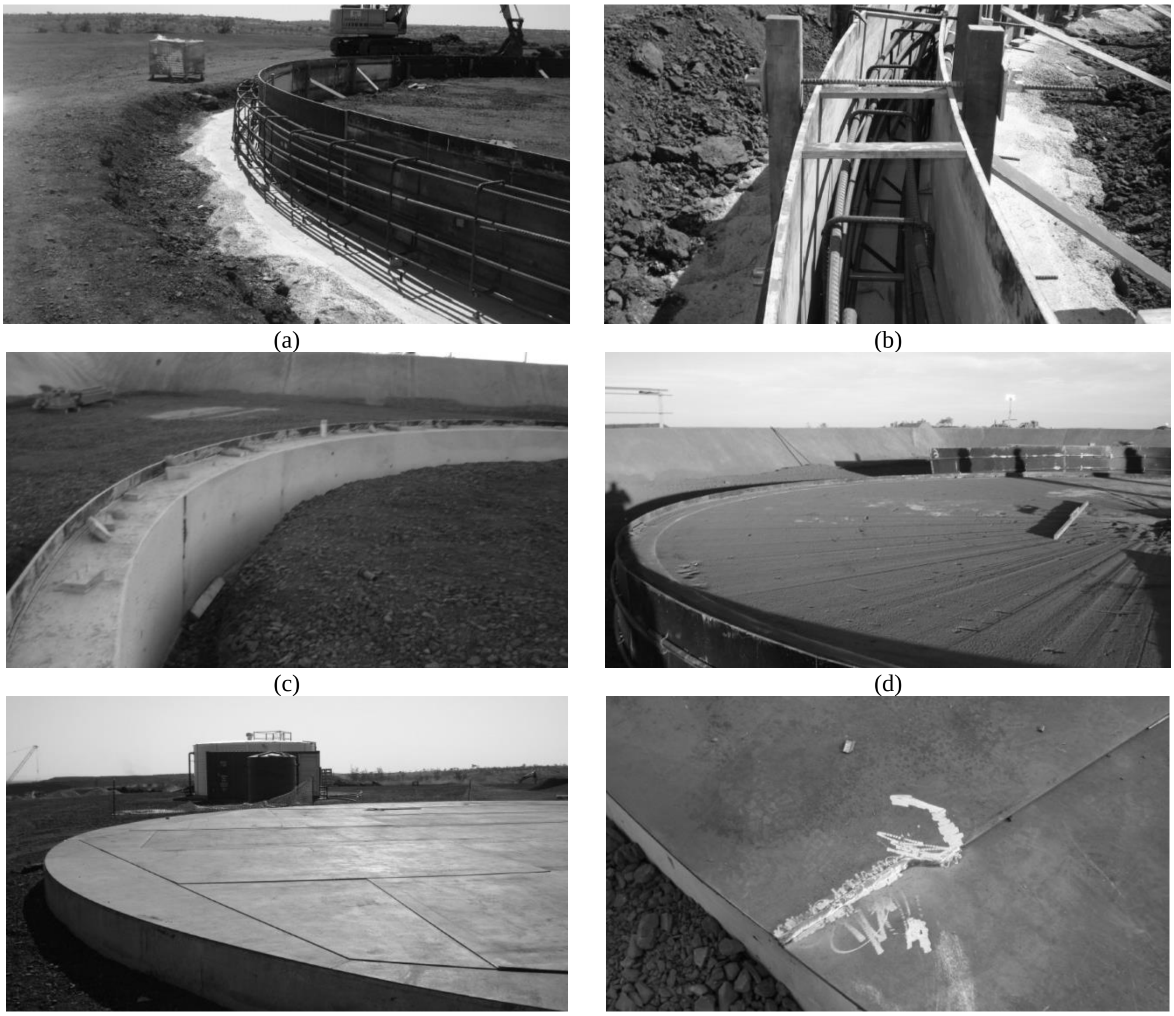

(a) (b)
(c) (d)
(e) (f)

Figure 2-2: Tank foundation construction (Raine 2016); (a, b) ring beam/wall construction, (c) filling the inner part of the ring wall, (d) final stage of the filling process, (e) base plate arrangement on the foundation, and (f) base plate welding.

Once welding of the base plate is complete, the pieces of the tank shell are assembled as shown in Figure 2-3(a). The tank wall is assembled on a sequence of rings rising up from the ground, known as courses. Each course is composed of multiple rectangular plates with appropriate camber to fit the tank wall curvature. Note that the tank wall plates are produced in approximately 3m high plates, which implies that the addition of even a single extra course may significantly modify the (desired) aspect ratio of the tank. As far as the assembly of the roof is concerned, the top course is constructed aside of the rest of the tank shell [Figure 2-3(b)], in view of placing the supporting structure of the roof on it [Figure 2-3(c)]. Then, the roof shell is placed on the supporting structure [Figure 2-3(d)], and the entire block is lifted via a crane [Figure 2-3(e)] to finalise the construction of the liquid storage tank [Figure 2-3(f)].

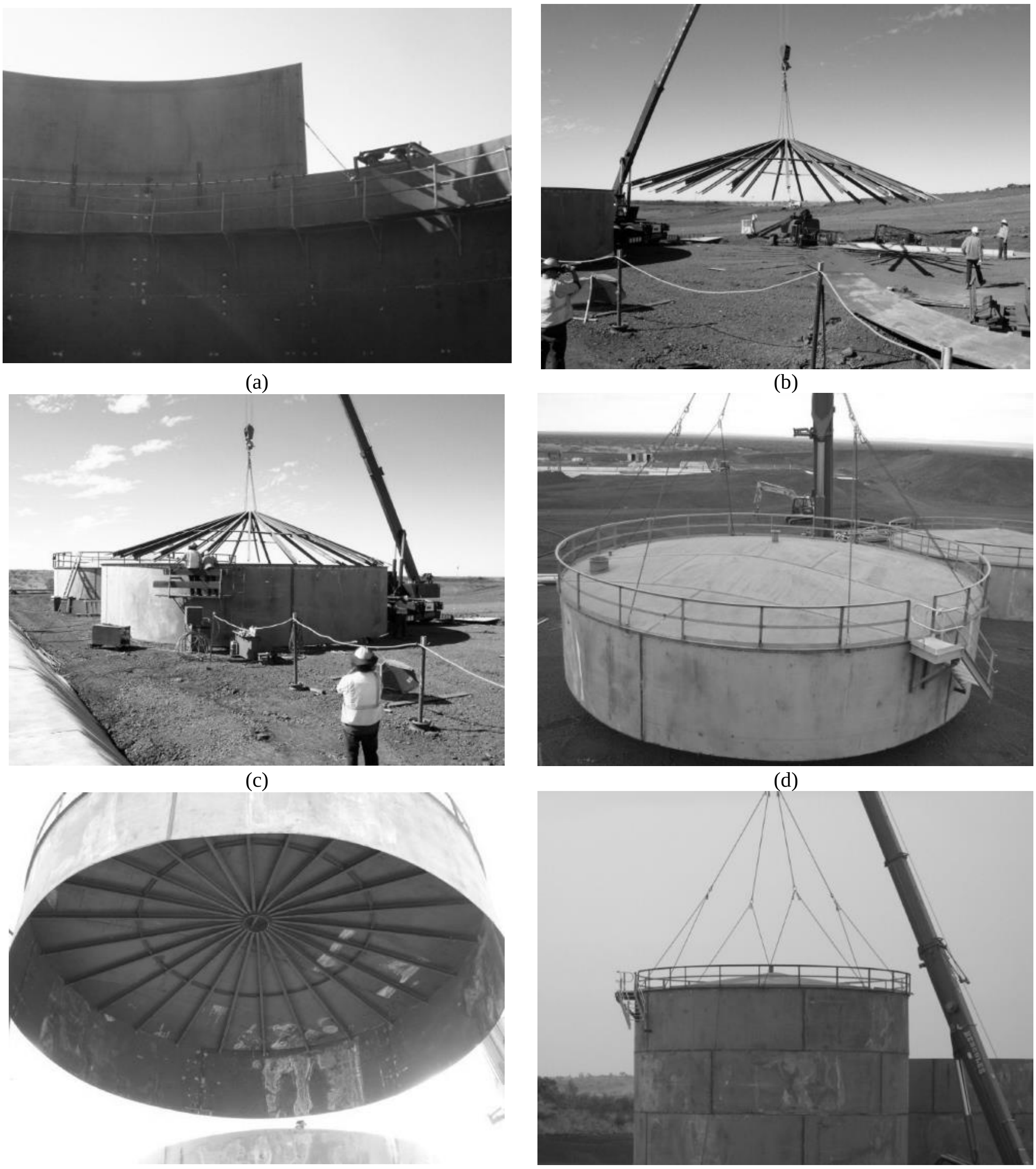

Figure 2-3: (a) Tank wall construction; roof supporting structure (b) lifting and (c) assembly to the top wall-course; roof-wall (d) assembly and (e) lifting; (f) final tank configuration (Raine 2016).

2.3 ACTIONS

Liquid storage tanks are designed using a procedure that combines different engineering disciplines such as hydraulic, mechanical, civil, geotechnical and material (American Petroleum Institute 2007). According to EN1993-4-2 (CEN 2007a), the liquid storage system should be checked for limit states such as global stability and static equilibrium, plastic limit, cyclic plasticity, buckling and fatigue, following the EN1993-1-6 (CEN 2007b) provisions.

In general, the fundamental non-seismic actions that liquid storage tanks are designed against, comprise liquid induced loads; internal pressure loads; thermally induced loads; dead loads resulting from the weight of all component parts of the tank and all components permanently attached to the tank (CEN 2002); insulation loads resulting from the weight of the insulation (CEN 2002); distributed and concentrated live load (CEN 2002); snow (CEN 2003); wind (CEN 2005); suction due to inadequate venting (CEN 2005); loads resulting from connections; loads resulting from pipes, valves and other items connected to the tank; loads resulting from settlement of independent item supports relative to the tank foundation; loads resulting from uneven settlement expected during the lifetime of the tank; emergency loadings from events such as external blast, impact, adjacent external fire, explosion, leakage of inner tank, roll over, overfill of inner tank.

For the design of the base plate in particular, corrosion should be taken into account (Dehghan Manshadi and Maheri 2010), while anchorage should be provided if any of the following conditions can cause the cylindrical shell wall and bottom plate close to it to lift off its foundation: a) uplift of an empty tank due to internal design pressure counteracted by the effective corroded weight of roof, shell and permanent attachments; b) uplift due to internal design pressure in combination with wind loading counteracted by the effective corroded weight of roof, shell and permanent attachments plus the effective weight of the product always present in the tank; c) uplift of an empty tank due to wind loading counteracted by the effective corroded weight of roof, shell and permanent attachments; d) uplift of an empty tank due to external liquid caused by flooding. In such cases it is necessary to consider the effects upon the tank bottom, tank shell etc. as well as the anchorage design; e) uplift of filled tank due to seismic action.

In particular for seismic actions, Eurocode 8 provisions (CEN 2006) rely on two limit states, namely the ‘damage limitation’ and ‘ultimate’ limit state. For the former, there are two additional subdivisions, namely ‘integrity’ and ‘minimum operating level. To satisfy the ‘integrity’ criterion, leak tightness of the system should be verified; adequate freeboard shall be provided to accommodate the maximum vertical displacement of the liquid surface in the tank to prevent damage on the roof due to the pressure of the sloshing liquid or, if the tank has no rigid roof, to prevent undesirable effects of spilling of the liquid; the hydraulic systems which are part of, or connected to the tank, should be verified against stresses and distortions due to relative displacements between tanks or between tanks and soil, without their functions being impaired. For the ‘minimum operating level’ on the other hand, it should be verified that in case of local buckling, collapse is not triggered and damage is reversible.

As far as the ‘ultimate’ limit state is concerned, the overall stability of the tank, which refers to rigid body behaviour and may be impaired by sliding or overturning, should be verified, bearing in mind that a limited amount of sliding may be accepted if the pipe system can tolerate it and the tank is not anchored to the foundation. Inelastic behaviour should be restricted to well-defined parts of the tank. The nature and the extent of buckling phenomena in the shell should be controlled according to the relevant verifications, while the hydraulic systems which are either part of, or connected to the tank should be designed such that they prevent loss of the contents of the tank in the event of failure of any of its components.

2.4 SEISMIC RESPONSE

In the hydrostatic condition cylindrical liquid storage tanks are subjected to axisymmetric pressure caused by the fluid content. To withstand this pressure, hoop tensile forces are developed in the tank wall, thus determining the required wall thickness for the static design. However, in the event of a strong ground motion, the liquid content develops a vibrational motion that interacts with the tank shell. Previous studies have shown that the fluid motion can be divided into several modes of vibration, among which only two are deemed necessary to represent the response of liquid storage tanks under an earthquake excitation (Amiri and Sabbagh-Yazdi 2011, 2012; Haroun 1983; Haroun and Housner 1981; Housner 1957, 1963; Malhotra 2000). The first one, defined as the 'impulsive mode', consists of liquid particles moving in conjunction with the motion of the tank shell. The second one, defined as the 'convective mode', consists of liquid particles near the free surface performing a (mostly) vertical oscillation (Figure 2-4). The inertia effect of the moving liquid particles induces asymmetric hydrodynamic pressure on the tank structure with a magnitude that may reach several times that of the hydrostatic. In response to the hydrodynamic load, axial compressive and tensile stresses as well as additional hoop stress are developed in the tank wall. These stresses are asymmetric, and depending on the seismic intensity may often be greater than the ones developed during the hydrostatic condition. Particularly for unanchored tanks subjected to a sufficiently large resultant overturning moment, a portion of the base plate may be separated from the support foundation, causing the entire system to uplift. Along with the base plate uplift, extensive deformations with significant out-of-round distortion may occur in the tank wall, thus developing a highly nonlinear phenomenon known as 'uplift mechanism'.

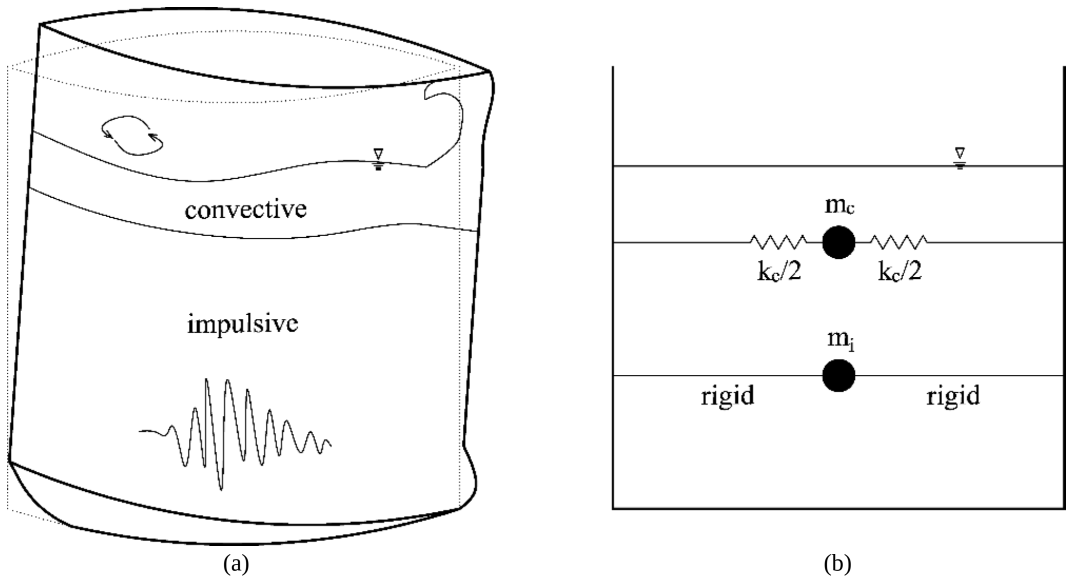

Figure 2-4: (a) Impulsive versus convective component of an unanchored liquid storage tank and (b) spring-mass analogue as developed by Housner (1957, 1963).

2.5 FAILURE MODES

Field investigations after major earthquakes have revealed a variety of failure modes on atmospheric tanks. As seismic waves arrive on site, the impulsive fluid component imposes pressure on the tank wall, causing excessive overturning moments on the system that may in turn lead to sliding and/or uplift of the base plate. The latter results in large-strain deformations on the plate-wall junction that may rupture the base plate, or cause the tank wall to buckle. On the other hand, the convective mode forces the upper part of the contained fluid into a (mostly) vertical displacement that may damage the top parts of the tank, and is known as sloshing. The most common types of failure are shell buckling, plate-wall rupture, sloshing damage to the upper tank shell and roof, anchor-bolt failure (for anchored tanks only) and base sliding. Note that the latter is not necessarily a failure unless it results in pipe rupture, as limited sliding could be beneficial due to the flexibility and damping it provides. These modes of failure derive from the liquid storage system's trend during ground motion shaking to overturning.

2.5.1 Elephant's foot buckling

During an earthquake, the combination of hydrostatic and hydrodynamic effects may lead to high internal pressure on the tank walls. Overturning for those thin-walled shell structures is resisted by axial compressive stresses in the wall. Even though high pressure may increase the capacity against buckling, local yielding may trigger an elastic-plastic buckling failure around the lower course of the tank's perimeter, known as the 'elephant's foot buckling' [EFB, Figure 2-5(a), (Rotter 2006; Vakili and Showkati 2016)]. It should be noted that the very same kind of failure may not be restricted to the lower wall course only, but could also be extended to mid and high courses along the tank elevation, at which case it is refer to as 'elephant's knee buckling' [Figure 2-5(b)].

(a) (b)

Figure 2-5: (a) Elephant's foot buckling developed on the lower wall course; (b) Elephant's knee buckling developed on the mid-high wall course [EFB is also apparent on the lower course of tank wall, (FEMA 2012a)].

2.5.2 Diamond-shaped buckling

Similarly, elastic diamond-shaped buckling may occur along the elevation of the tank wall, as shown in Figure 2-6. This damage pattern, less common than EFB, occurs at small hoop stress levels, and is therefore particularly sensitive to internal pressure and imperfection magnitude. This means that the buckling strength decreases, as the pressure reduces or as the imperfection size increases. Its defining physical characteristic is that there is no protruding outward bulge, but instead a local wrinkling of the tank wall.

(a) (b)

Figure 2-6: Diamond-shaped buckling (Brunesi et al. 2015; Zareian et al. 2012).

2.5.3 Plate-wall junction rapture

When uplift is allowed, either due to absence of anchorage or due to poor detailing of the anchors, the plate-wall junction may exhibit fracture due to the plastic rotation developed at the base of the tank [Figure 2-7, (Cortés et al. 2011; Prinz and Nussbaumer 2012a; Wasicek et al. 2008)].

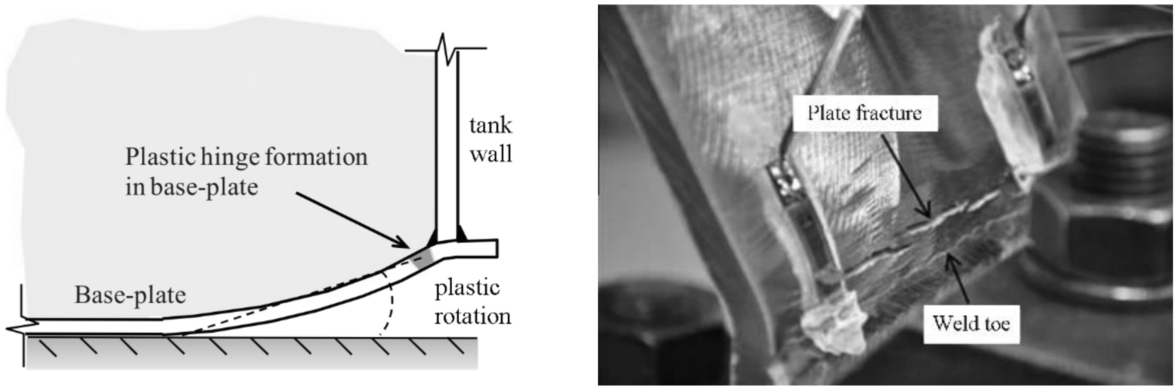

(a) (b)

Figure 2-7: Plate-wall junction fracture (Prinz and Nussbaumer 2012a; b).

2.5.4 Sloshing damage

The excitation of the long period convective mode may cause sloshing of the contained liquid, which may in turn damage the upper parts of the tank (roof, upper course) as shown in Figure 2-8. It is also known to offer additional overturning moments at the base of the system, but its contribution with respect to the impulsive component is marginal for the majority of non-slender tanks, and as a result it is often ignored (Malhotra 2000).

(a) (b)

Figure 2-8: Sloshing damage (Brewer 1992; DuBrowa 2010; FEMA 2012a).

2.5.5 Anchorage failure

For the case of anchored tanks, damage on the anchor bolts constitutes another potential failure mode. Fracturing of the anchors is also affected by the impulsive-component-induced overturning, as the tension developed on the bolts may often exceed their prescribed ultimate strength and ductility. Note that although anchored liquid storage systems are usually considered fully fixed to the ground, their actual performance can incorporate some rocking/uplift, especially when the anchor bolts begin to yield, fracture, or lose their bond with the concrete foundation (Figure 2-9). At this point, part of the base plate is uplifted and the response gradually resembles that of the corresponding unanchored case (Bakalis et al. 2014a, 2017a).

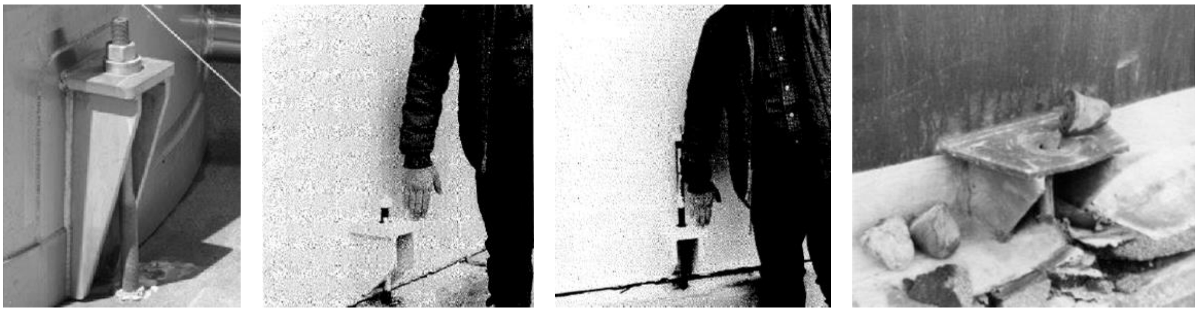

(a) (b) (c) (d)

Figure 2-9: Anchor bolt (a) yielding (Bradley et al. 2017), (b) minor post-yield deformation (Housner et al. 1971), (c) near-fracture post-yield deformation (Housner et al. 1971) and (d) fracture (Vathi 2016).

2.6 EXPERIENCE FROM PAST EARTHQUAKES

Historically, the aforementioned modes of failure have been observed following a series of earthquakes. In particular, during the magnitude ***M*9.2 great Alaska earthquake (1964)**, some oil-storage tanks were bulged outward at the bottom (i.e. EFB), probably by rocking and pounding back and forth due to content sloshing, while the majority located on the dock area were superficially damaged (Thoms et al. 2014). Two steel storage tanks were toppled and destroyed, releasing large quantities of fuel oil (Hansen 1965). Evidence of uplift was reported by Housner et al. (1971) on a wash-water tank after the ***M*6.7 San Fernando earthquake (1971)**, while as Manos and Clough (1985) report, the ***M*6.5 Coalinga earthquake (1983)** caused severe damage on unanchored cylindrical ground supported tanks located at six different sites within the nearby oil production area. Elephant's foot buckling was observed at the base of three moderate-sized tanks, joint rupture and top shell buckling in one large tank, bottom plate rupture of a welded tank and damage to the floating roofs of 11 tanks. In addition, oil was spilled over the top of many floating-roof tanks and secondary damages occurred in pipe connections and ladders.

Similar damage was revealed following the ***M*7.4 San Juan, Argentina (1977)** post-earthquake inventory on anchored wine-tanks (Manos 1991). Mutual observations among the tanks that were examined are the failed anchors and the shell bulging they developed either at the lower shell course or just above the joint between the first and second (from the bottom) courses. Moreover, at locations almost diametrically opposite to bulging (Figure 2-10), there were cases where the weld that joined the bottom shell course with the annular plate ruptured, leading to the sudden release of the contents, which was accompanied by suction and crushing of the upper course of the shell and roof due to absence of a pressure release valve. It should be noted that a pressure release valve became a feature of the wine tank design after this particular earthquake. Other tanks, despite their severely damaged anchors, had no visible signs of shell bulging. Collapsed tanks were also reported following this event, among which liquid was released at a long distance from the bottom part for one of them. The repair effort after the earthquake included in all cases strengthening of the anchoring system, installing stiffeners and thicker plates than the ones used before for the lower courses, and in some cases reducing the maximum allowable fluid level.

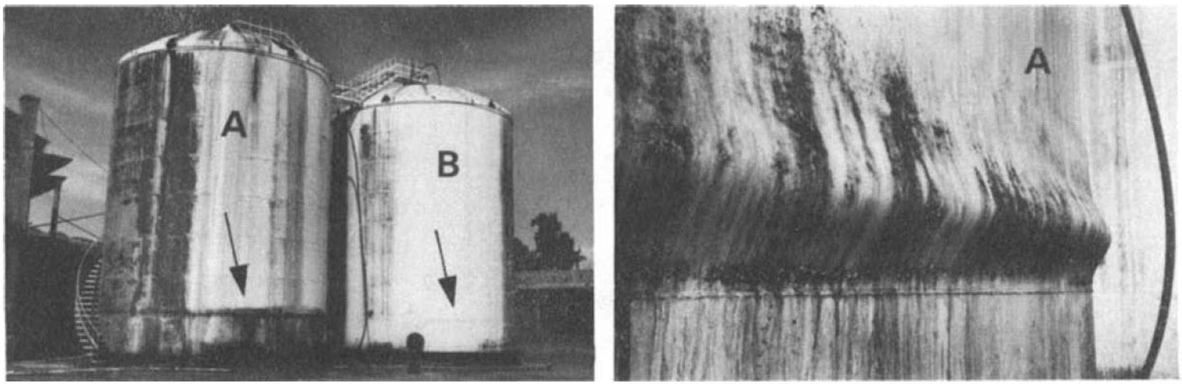

(a) (b)

Figure 2-10: Elephant's foot buckling observed during the M7.4 San Juan, Argentina (1977) earthquake (Manos 1991).

Buckling of approximately 100 wine storage tanks occurred during the ***M*5.5 Greenville-Mt. Diablo (1980) earthquake**, in a winery located approximately 8 miles south-east of the earthquake epicentre (Niwa and Clough 1982). The majority of the tanks that suffered damage were completely full of wine and free to uplift. Elephant's foot buckling was the most common damage in broad tanks (i.e. height-over-radius ratio of about 2). More slender tanks, (i.e. height-over-radius ratio of about 4), suffered diamond-shaped buckling spreading around the circumference. For one particular tank, the elephant-foot buckles were stamped flat during the main shock, leading to leak of the stored material as a result of further damage caused by the subsequent after-shock. In general, even though most of the damaged tanks did not rupture, there was evidence of violent rocking motion of the wine tanks during the earthquake. For instance, big dents at the top of one shell suggested that the tank swayed and collided with adjacent piping systems. Also, a few broken anchor attachments demonstrated the sizeable seismic lateral force that acted on the tanks.

Hazardous material release due to tank failure was apparent during the ***M*7.4 Kocaeli, Turkey (1999)** earthquake. In specific, a number of facilities reported liquid sloshing in storage tanks, indicating that sloshing was the main cause of releases at the plant. Despite the use of containment dikes at almost all the sites, it was apparent that some may not have been of sufficient dimensions to contain the liquid contents in their entirety. In a number of cases, containment walls were not strong enough to withstand the forces generated by the earthquake, and they cracked open. Along with damage to containment dike walls, rupture of pipes and connections resulted in material spills in many instances (Steinberg and Cruz 2004). Some of the more catastrophic examples of hazardous material releases include the intentional air release of 200,000 kg of hazardous anhydrous ammonia, the leakage of 6.5 million kg of toxic acrylonitrile into air, soil, and water from ruptured tanks, the spill of 50,000 kg of diesel fuel into Izmit Bay from a broken fuel-loading arm at a petrochemical storage facility; the release of 1.2 million kg of cryogenic liquid oxygen caused by structural failure of concrete support columns in two oxygen storage tanks at a gas company; the multiple fires in the crude oil unit, naphtha tank farm, and chemical warehouse, the exposure of 350,000 m^3 of naphtha and crude oil directly to the atmosphere; the liquid petroleum gas leakages and oil spills at the port terminal at an oil refinery.

Instability of the tank wall, failure of the anchoring system, failure of welding connection on the plate-wall junction, and failure of connections between piping and tank wall were some of the failures that were observed during the ***M*8.8 Maule (or Bío-Bío), Chile (2010)** earthquake (González et al. 2013; Zareian et al. 2012). For wineries in particular, elephant's foot and diamond-shaped buckling was observed (Figure 2-11). The elephant foot buckling mode took place on squat tanks (e.g. height-over-radius ratio < 2) and was characterized by the appearance of a bulge in the tank shell due to its insufficient thickness. This type of failure was observed just above the tank base and at the point where wall thickness changed from the lower course to the very next. Diamond-shaped buckling was present in slender tanks (e.g. height-over-radius ratio > 2) due to stress concentration in regions where changes of stiffness occurred abruptly, or in other words where large changes in the wall thickness was evident. This mode of failure was also encountered in zones where the tank wall was connected to anchors. In some case, tanks were equipped with anchor bolts to prevent sliding and overturning due to lateral loads. However, inspections revealed that this type of anchorage system failed due to corrosion in anchor bolts, insufficient distance from the connection to the edge of the foundation, and deficient effective embedded bolt length. Some tanks that were not anchored or poorly anchored overturned and slid due to lateral force and impacted other tanks damaging their roofs and walls.

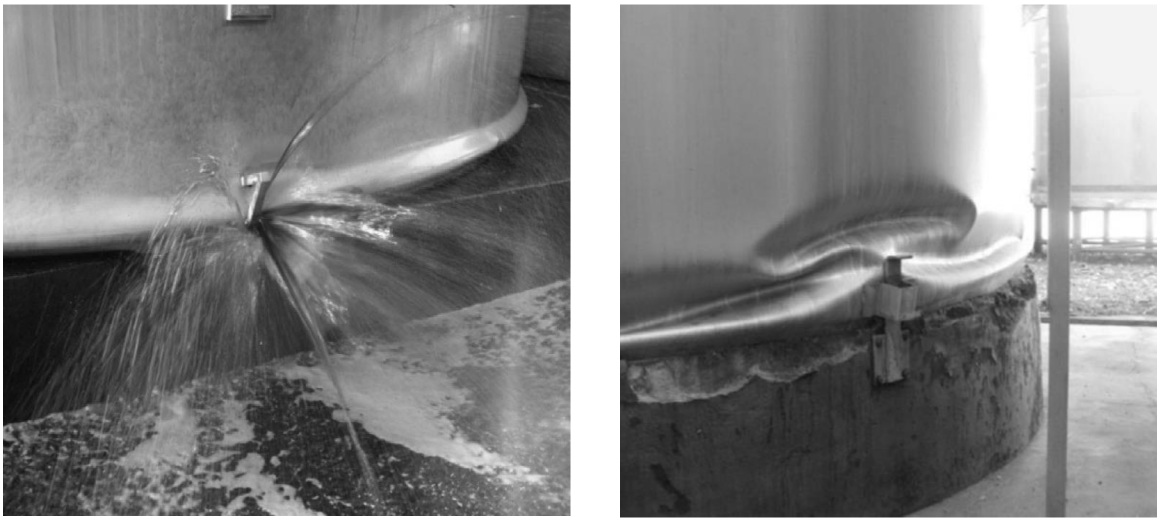

(a) (b)

Figure 2-11: Damage observed during the M8.8 Maule (or Bío-Bío), Chile (2010) earthquake; (a) elephant's foot buckling followed by release of the stored material and (b) diamond-shaped buckling (González et al. 2013).

Of particular interest for this event was the collapse of an unanchored water tank with height-to-radius ratio approximately equal to 1.0, located at the Santiago Airport (Eidinger 2012). The tank was resting on a concrete ring beam, had a series of water pipes attached to its lower course, and was clearly suffering from internal corrosion at the roof level region. On the outside, the tank was properly coated and did not appear to have any significant corrosion. It is believed that at the time of the event the water tank was full. The observed failure modes appeared to be tearing of the bottom course from the steel floor plate, with a nearly uniform tear along one of the vertical welds in the lower courses. This led to collapse of the tank, opening of the tank walls, and coincident buckling and tearing of the steel. This particular case was remarkable for two reasons: a) that kind of performance (i.e. gross collapse) would not be expected for a well-built and well-maintained steel tank, unless the peak ground acceleration (*PGA*) of the ground shaking was in the order of 0.8g or higher; b) there were four adjacent fuel storage tanks that experienced minimal damage, but remained intact overall. It should be noted that these tanks seemed to be designed at the same time as the water tank, using the same coating system and staircase designs. The lack of significant damage suggests that they were possibly no more than 50% full at the time of the earthquake, which is not uncommon in practice.

The most common collapse mechanism encountered during the post-earthquake surveys of the ***M*6.1** and ***M*5.9 Emilia, Italy (2012)** earthquakes, was the classical elephant's foot buckling on flat-base steel tanks (Brunesi et al. 2015). Diamond-shaped buckling, as well as the secondary diamond-shaped buckling of the tank wall were also observed, along with base-anchorage failures. In many cases, excessive inelastic strain demands took place in the anchor bolts, causing their fracture or de-bonding from the concrete pads. Besides the flexural failure occurred in the anchor plates, concrete spalling was also evident, probably induced by insufficient distance between the anchor bolt and the edge of the foundation and low resistance of the concrete. Hence, these systems, poorly anchored and not well-detailed to sustain earthquake-induced demand, collapsed because of lack of proper steel reinforcement around the anchor and inadequate resistance of the foundation concrete.

The ***M*8.3 Tokachi-oki, Japan (2003)** earthquake resulted in the severe damage of seven floating-roof oil storage tanks. Among them, two were damaged by fire; the first suffered the so-called ring fire in which the flame was confined to the rim of the tank roof, while the second suffered sinking of the floating roof resulting in an open-top fire. Another two tanks also suffered sinking of the floating roof, exposing the kerosene to the atmosphere, probably as a result of damage to the roof pontoons due to the large sloshing amplitude (Hatayama 2008). For the devastating ***M*9.0 Tohoku, Japan (2011)** earthquake, although tsunami was the main source of damage, ground shaking led to typical damage of oil storage tanks caused by liquid sloshing (e.g. Niigata and Sakata districts) such as sinking of inner roof, leakage of oil onto deck, deformation of gauge pole, and pontoon fracture. Damage to cylindrical tanks was only limited to the elephant foot bulge of a water tank at Sendai and the extraction of anchor bolts of an oil storage tank at Kashima (Zama et al. 2012).

3 MODELLING OF LIQUID STORAGE TANKS

3.1 ABSTRACT

A three-dimensional surrogate model is presented for the seismic performance assessment of cylindrical atmospheric liquid storage tanks. The proposed model consists of a concentrated fluid mass attached to a single vertical beam-column element that rests on rigid beam-spokes with edge springs. The model is suitable for rapid static and dynamic seismic performance assessment. Contrary to other simplified models for tanks, its properties are determined through a simple structural analysis that can be performed in any nonlinear analysis software, without the need for complex finite-element models. The results compare favourably to those of three-dimensional finite element models on three tanks of varying aspect ratios. A step-by-step example of the modelling procedure is presented for a squat unanchored tank, and a sensitivity analysis is conducted in order to investigate the effect of various modelling parameters on the seismic response of the proposed tank model.

3.2 INTRODUCTION

Large-capacity atmospheric tanks are typical structures of the chemical industry that are widely used to store a variety of liquids, such as oil or liquefied natural gas. The seismic risk of such industrial facilities is considerably higher compared to ordinary structures, since even some minor damage induced by a ground motion may have uncontrollable consequences, not only on the tank but also on the environment. Recent earthquakes have shown that heavy damage on tanks may lead to temporary loss of essential service, usually followed by leakage and/or fire (Girgin 2011; Hatayama 2015). Despite extensive research, earthquakes remain a major threat for the structures both from a social and a financial point of view.

The Performance-Based Earthquake Engineering (PBEE) concept can be employed to better understand and quantify the seismic performance of such critical infrastructure. Appropriate structural models are essential for the successful seismic performance evaluation. Especially for atmospheric liquid storage tanks, detailed finite element models (FEM) require a considerable amount of time even for a single dynamic analysis (Kilic and Ozdemir 2007), while capturing the fluid-structure-interaction (FSI) effect is an onerous task. Although FEM-based procedures may be able to capture complex modes of failure such as buckling (Buratti and Tavano 2014; Kildashti et al. 2018; Virella et al. 2006), their suitability within a probabilistic seismic performance assessment framework may become computationally prohibitive.

Other studies regarding the response of liquid storage tanks have either developed or adopted numerical approximations for the contained liquid (Ahari et al. 2009; Talaslidis et al. 2004; Vathi et al. 2013) in an attempt to minimize the computational time. Simplified modelling techniques that blend efficiency and accuracy are offered by Malhotra and Veletsos (1994a; b; c), who presented a simplified model for the analysis of liquid storage tanks subject to a single component of ground motion [essentially two-dimensional (2D) formulation]. Furthermore, Cortes et al. (2012) also developed a 2D model based on rigid beams and equivalent springs that can be used for rapid response history analysis. The aforementioned approaches cannot be applied with typical commercial structural analysis software. The first approach requires a dedicated analysis algorithm that is not generally available, while the second needs to be calibrated using FEM results.

Building upon the approach of Malhotra and Veletsos, a more sophisticated model that relies on beam-column elements and point springs available in most structural analysis packages, is offered instead. The aim is to develop a three-dimensional (3D) surrogate model that can be subjected to all translational components of ground motion and can be implemented with minimum effort both for anchored and unanchored tanks, using either static or dynamic analysis. The efficiency of the model is assessed with the aid of detailed FE results, while a sensitivity analysis is performed in order to understand the influence of the various properties of the proposed model on its response estimates.

3.3 MODELLING

3.3.1 Background

Modelling of liquid storage tanks is a challenging problem as it requires capturing the dynamic response of the contained fluid and its interaction with the tank walls. During a ground motion the contained fluid of a liquid storage tank interacts with the tank shell in complex nonlinear manner (Veletsos and Tang 1990), which for the purpose of a successful performance evaluation constitutes the structural model adopted a key parameter. There are several approaches to model this severely nonlinear response; for instance, one could adopt a combination of solid and shell elements regarding the fluid and the tank shell, respectively, to obtain a very reliable estimate of the response variables developed throughout the time of the ground motion recording (Ozdemir et al. 2010; Phan et al. 2017b). In view of reducing the computational time required for a single analysis, as well as avoiding convergence issues that are typically encountered in the transient analysis of large-scale finite element problems, the FSI may be taken into account using the added-mass method (Buratti and Tavano 2014; Virella et al. 2006) in place of the solid fluid elements.

The FSI problem may further be approximated by adopting a simplified concept found in codes of practice (American Petroleum Institute 2007; CEN 2006), where the hydrodynamic problem can be summarized in the combination of an impulsive and a convective component (Veletsos and Tang 1990). Part of the contained liquid moves horizontally and follows the movement of the tank walls (impulsive component), while an additional (mostly vertical) component generates the sloshing motion of the free fluid surface (convective component). The period of the impulsive component is typically found in the range of 0.1–0.3 sec, while the convective component is excited at much longer periods that often exceed 5 sec. Although a rigorous eigenvalue analysis may result in several modes of vibration regarding both the impulsive and the convective component, usually the first impulsive and convective modes are more than enough to capture the response. In that sense, liquid storage tanks can be modelled using a two-degree-of-freedom (2DOF) system, where the two masses (impulsive and convective) are considered decoupled (Calvi and Nascimbene 2011; Malhotra et al. 2000; Priestley et al. 1986).

The geometric and modal characteristics of the hydrodynamic problem are determined using equivalent parameters for the impulsive and convective masses. The two components are distinguished with the aid of subscripts "i" and "c", respectively. According to Veletsos and Tang (1990), it is possible to obtain estimates for the natural periods (T_i and T_c), the masses (m_i and m_c) and the effective heights (h_i and h_c) of each component (see also Malhotra and Veletsos 1994c and Eurocode 8-4, CEN 2006). However, other studies (Malhotra 1997; Vathi et al. 2013) have shown that the contribution of the convective mass to the overall response of the structure can be ignored (especially for non-slender tanks with sufficient freeboard), as the impulsive mass is held responsible for the majority of damage that tanks suffer during earthquakes. This concept may result in finite element models that use a loading pattern similar to the one proposed by Veletsos and Tang (1990) for the impulsive and convective pressure components in place of the detailed FSI formulation, on the offset that only nonlinear static analysis can be accommodated. The proposed approach similarly decouples the two components, and considers only the impulsive mass to determine the global response, while the effects of the convective sloshing mode are separately estimated. Note that special care should be exercised for liquid storage systems with insufficient freeboard, as part of the convective mass may become impulsive and the terms m_i and m_c should properly be adjusted (Malhotra 2005).

3.3.2 The proposed "Joystick" model

The proposed "Joystick" model consists of a beam-column element that carries the impulsive mass and is supported by fully rigid beam spokes, which in turn rest on point/edge springs [see Figure 3-1(a), Figure 3-2(a)]. An even number of radially distributed rigid beam-spokes forms the base plate as shown in Figure 3-1(c). The nonlinear behaviour of the system is induced through zero-length edge springs that connect the base plate to the ground. The spring properties refer to a uniform width (b_w) on the base plate

$$b_w = \frac{2\pi R_t}{n}, \tag{3-1}$$

where 'n' is the number of beams used for the modelling of the base plate (preferably $n \geq 8$), and R_t is the tank radius. An elastic nonlinear material is used to idealize the uplift resistance of the edge springs, while the properties of the elastic element that connects the fluid mass to the base are estimated using the equivalent stiffness that corresponds to the fundamental (impulsive) period and mass. Note that the inelastic nonlinear material (with severe pinching hysteresis probably) would be a more realistic model for the edge springs, in particular for systems that rest on flexible foundation, where negative deformations during unloading can be larger than positive. The proposed tank model and its deflected shape are shown in Figure 3-2.

In order to obtain the response of a liquid storage system, a 'pre-analysis' step is necessary to determine the uplift resistance of the supporting edge springs. This step is performed through the analysis of a single base plate strip (Malhotra and Veletsos 1994a), modelled with beam-column elements [Figure 3-1(b)]. Note that although the 'pre-analysis' step may take a few minutes to complete, a single run is only required to calibrate the actual tank model. Once calibrated, the model is capable to perform nonlinear static or dynamic analysis in seconds, without having to repeat the relatively time-consuming 'pre-analysis' step. Another interesting feature of the model is its ability to simulate not only unanchored but also anchored tanks. In the latter case, the equivalent "edge springs" [Figure 3-1(a)] are modified such that their stiffness also takes into account the effect of the bolts that are equally distributed along the perimeter of the base plate (Figure 3-3).

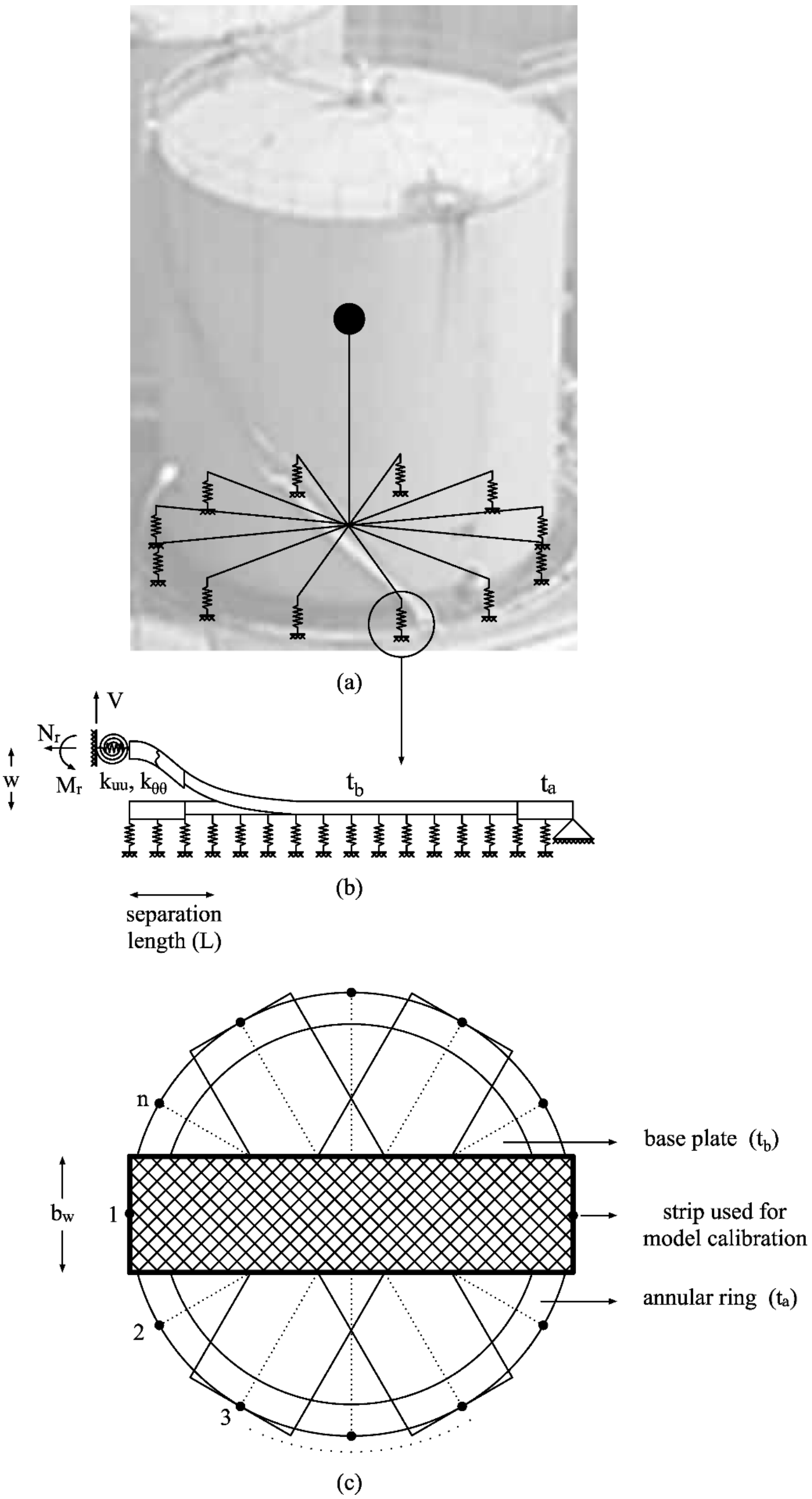

Figure 3-1: (a) Joystick model on an actual liquid storage tank; (b) strip model of the pre-analysis step that provides the response of the springs at the edge of each beam-spoke; (c) base-plate discretisation, shown for the pre-analysis step; a strip is analysed to determine the properties of the spring at the end of each spoke.

3.3.3 Model calibration (pre-analysis)

The *pre-analysis* step requires that the base plate is divided into a number of strips [Figure 3-1(c)]. A single strip is individually examined to determine its uplift resistance and calibrate the model. The resulting strip model shown in Figure 3-1(b) is discretised into a number of force-based fiber beam-column elements, with an approximate element size of $15t_b$, where t_b is the base plate thickness. A uniaxial elastoplastic material is assigned to the fibers, in order to capture the inelastic behaviour of the base plate during uplift. Geometric nonlinearities are also taken into account through the co-rotational formulation. Neglecting large-displacement nonlinearities in the response results in what Malhotra and Veletsos (1994a) call the “bending solution”, which deviates from the true solution as catenary string effects are ignored. This means that in reality as the edge of the tank is uplifted, the base is not only bent but also tensioned.

A series of Winkler springs is used to model the foundation of the strip model [Figure 3-1(b)]. The unanchored liquid storage system is assumed to rest on a uniform soil (or concrete) slab layer, thus implying an analogous base/soil stiffness of modulus E_w (e.g. E_w=1.0 GPa for a practically rigid foundation). The Winkler springs are assigned an elastic-no-tension material, suitable for allowing the tension-free uplift of the base plate. As the tank is uplifted, local buckling tends to develop in the vicinity of the (base) plate-wall joint. In order to capture the (base) plate-wall joint stiffness, edge rotational and axial springs are provided, as shown in Figure 3-1(b). The stiffness of those springs, for a given width of the strip (b_w) and wall thickness (t_w), is determined following the suggestions found in Malhotra and Veletsos (1994a). $k_{\theta\theta}$ is the rotational and k_{uu} the translational (axial) edge stiffness:

$$k_{\theta\theta} = \frac{Eb_w t_w^2 (t_w / R_t)^{1/2}}{2\left[3(1-v^2)\right]^{3/4}} \tag{3-2}$$

$$k_{uu} = \frac{Eb_w (t_w / R_t)^{3/2}}{\left[3(1-v^2)\right]^{1/4}} \tag{3-3}$$

E is the steel Young’s modulus and v the Poisson’s ratio. Malhotra and Veletsos (1994a) also suggested a third term, $k_{\theta u}$, that represents the interaction between rotation and translation. However, this term is neglected, as it cannot be incorporated using uniaxial springs. Sensitivity analyses of $k_{\theta\theta}$ and k_{uu} (presented in a latter section) have indicated that such terms do not have a significant effect anyway. Moreover, a concentrated moment (M_r) and an axial force (N_r) are applied on the plate boundary in order to capture the effect of the hydrostatic pressure (p_h) acting on the tank wall. These actions induce some local uplift on a narrow area close to the base plate-wall joint.

$$M_r = \frac{b_w R t_w p_h}{2\left[3\left(1-v^2\right)\right]^{1/2}} \tag{3-4}$$

$$N_r = \frac{b_w \sqrt{R t_w}\, p_h}{2\left[3\left(1-v^2\right)\right]^{1/4}} \tag{3-5}$$

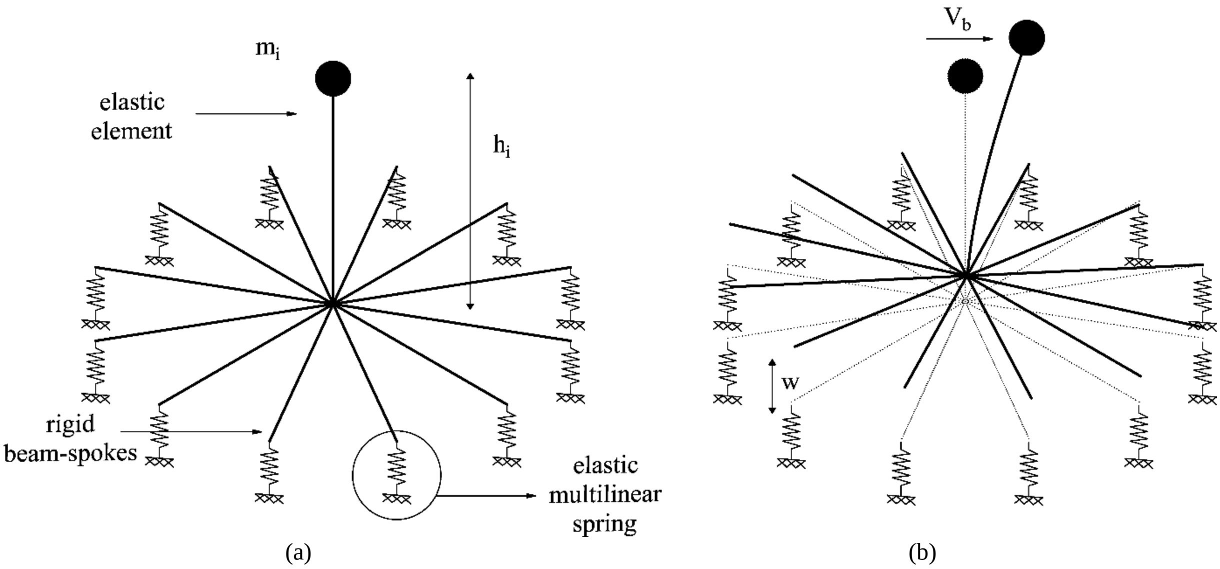

Figure 3-2: (a) Joystick model; (b) its deflected shape.

3.3.4 Anchorage

Appropriate modifications are necessary to model anchored liquid storage tanks. Anchorage is introduced to the "Joystick" model through additional vertically-oriented uniaxial springs, one at the end of each beam-spoke. Each spring is assumed to carry a number of bolts that are equally distributed along the width b_w, as shown in Figure 3-3 [see also Figure 3-1(c), Eq. (3-1)].

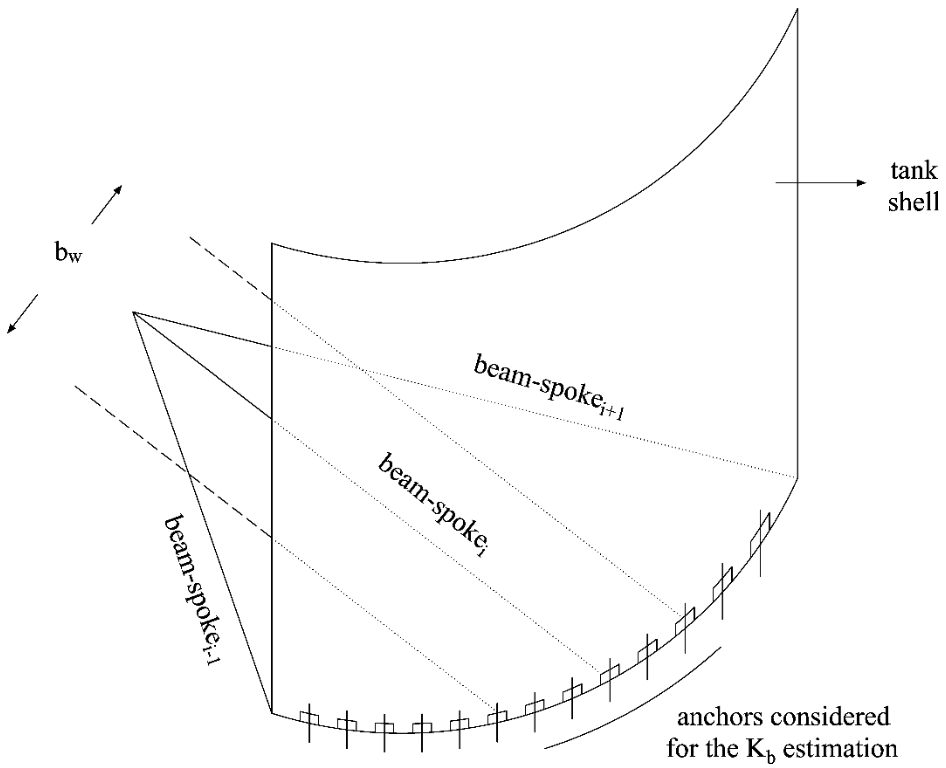

Figure 3-3: Part of an anchored liquid storage tank; the rigid beam-spokes of the proposed model are illustrated, featuring the anchors considered for the stiffness estimation shown in Eq. (3-6).

Assuming that rigid steel flanges connect the anchors to the tank wall, the stiffness may be calculated as

$$K_b = \frac{EA_b}{L_b}, \tag{3-6}$$

where A_b is the total area of the bolts and L_b their respective length. The anchoring springs are thus located on the circumference of the base plate and are introduced to the model through an elastoplastic, no-compression, uniaxial force-displacement relationship. A more faithful representation of the anchors may be achieved: (a) by adding an ultimate displacement δ_u to indicate fracture of the bolted connection and (b) by using a damageable "gap" material for the springs. The latter offers the ability to accumulate damage on the yielding anchors in the form of permanent elongation that causes a characteristic displacement gap before tension is developed in reloading (McKenna and Fenves 2001).

3.4 ENGINEERING DEMAND PARAMETERS

Having such a simple model at our disposal, the failure modes that it is able to capture must be identified. Field investigations after major earthquakes have revealed a variety of failure modes on atmospheric tanks. The most common types of failure are shell buckling, sloshing damage to the upper tank shell and roof, and base sliding. Note that the latter is not necessarily a failure unless it results in pipe rupture, as limited sliding could be beneficial due to the flexibility and damping it provides).

During strong ground motion events, hydrostatic and hydrodynamic effects may lead to high internal pressure on the tank walls. Overturning for those thin-walled shell structures is resisted by axial compressive stresses in the wall. Even though high pressure may increase the capacity against buckling, local yielding may trigger an elastic-plastic buckling failure around the lower course of the tank's perimeter, known as the "Elephant's Foot Buckling" (EFB). When uplift is allowed, either due to absence of anchorage or due to poor detailing of the anchors, the rotation of the plastic hinge in the tank base should not exceed a certain rotational capacity, specified in modern codes (e.g. API-650, American Petroleum Institute 2007 and Eurocode 8-4, CEN 2006). Moreover, the excitation of the long period convective mode may cause sloshing of the contained liquid, which may in turn damage the upper parts of the tank (roof, upper course).

EFB can be captured by comparing the compressive meridional stress against a critical limit such as the formula proposed by Rotter (2006). The EFB stress limit is compared to the corresponding stress estimated through the axial edge spring force recorded during the analysis. The latter implies that the stress estimation is highly connected to the number of edge springs found on the tank circumference. A fine discretisation on the base plate in terms of beam-spokes may allow for a more accurate stress distribution on the edge to be considered. Alternatively, a concentration factor could be applied on a less refined base plate model to take into account the actual stress distribution locally.

As far as plastic rotation is concerned, one may employ direct measurements through the fiber sections adopted for the base plate strips. Alternatively, the direct mapping between uplift (w), separation length (L) and plastic rotation (θ_{pl}) suggested by Eurocode 8-4 (CEN 2006) could be adopted

$$\theta_{pl} = \frac{2w}{L} - \frac{w}{2R_t}, \tag{3-7}$$

which also indicates that the response is closely related to the uplift mechanism of the tank. Viscous damping selected for the model is purely associated with the impulsive mode. Malhotra (1997) suggests different values of impulsive mode damping appropriate for each failure mode, akin to an equivalent approach to account for hysteresis among other issues. Since a single model is only used in our approach to convey all such information at once, a single value of damping [e.g. 2% according to Malhotra (2000) and Eurocode 8-4 (CEN 2006)] is recommended.

The sloshing response may be incorporated by adding the convective mass to the model (similarly to the impulsive component) or alternatively, by ignoring uplift altogether and using the spectral acceleration at the convective mode period only to estimate the wave height according to formulas provided by design codes. For example, $d_{API\text{-}650}$ and d_{EC8} are the maximum sloshing wave height estimates according to API-650 (American Petroleum Institute 2007) and Eurocode 8-4 (CEN 2006) respectively:

$$d_{API-650} = R_t A_f \tag{3-8}$$

$$d_{EC8} = R_t \frac{0.84 S_a(T_{c1}, 0.5\%)}{g} \tag{3-9}$$

A_f is the acceleration coefficient for sloshing wave height calculation and $S_a(T_{c1},0.5\%)$ the elastic response spectral acceleration at the 1st convective mode of the fluid for a damping value equal to 0.5%.

3.5 NUMERICAL EXAMPLE

3.5.1 Detailed finite element model

In order to validate the uplifting mechanism of the proposed model, a comparison is performed against detailed 3D finite element models (Figure 3-4, Figure 3-5, Figure 3-6) for three unanchored tanks of varying geometry and aspect ratio (h_f/R_t). Complex hydrodynamics and fluid-structure-interaction are not tackled. Instead, such effects are taken into account through the Veletsos and Tang (1990) impulsive pressure distribution that is also adopted by Malhotra and Veletsos (1994c) and Eurocode 8-4 (CEN 2006). Bound on this approximation, the performance of the proposed model is assessed versus detailed finite element models with respect to the base plate uplifting mechanism.

The geometric and material characteristics of the tanks are summarized in Table 3-1. The analyses are performed using the general-purpose FE code ABAQUS (2011). Figure 3-4(a), Figure 3-5(a) and Figure 3-6(a) present a typical mesh of the systems considered, where the unanchored tanks rest on a fully rigid surface. For each of those cases, the base plate and the rigid surface form a contact pair that is assigned appropriate interaction properties such that uplift is allowed (Figure 3-7). The rigid surface is modelled using 4-node rigid quadrilateral elements (R3D4), and the tank shell using 4-node reduced integration shell elements (S4R). Special attention is paid to the annular plate as well as to the lower courses of the tank, where modes of failure similar to uplift and EFB are expected to occur. Note that the roof of the tank is not explicitly modelled. Instead, a rigid body constraint is assigned to the upper course top nodes. Although one may argue that the flexibility of the supporting truss of the roof shell could modify the response, this effect can be considered negligible for fixed (non-floating) roof tanks, which is consistent with the assumptions of Malhotra and Veletsos (1994c).

A nonlinear static analysis is conducted in three stages. Figure 3-8 and Figure 3-9 illustrate the loading sequence during the analysis. Gravity loads are initially applied to the "empty" (i.e. zero hydrostatic loads) tank such that contact is established with the rigid surface. Once the tank has settled on the ground, hydrostatic loads are applied on the walls and the base plate of the system. The initial conditions imposed by hydrostatic pressure are followed by the hydrodynamic loading, the distribution of which is obtained through the impulsive pressure equation (Veletsos and Tang 1990):

$$p_i(\xi,\zeta,\varphi,t)=C_i(\xi,\zeta)\rho_f h_f \cos\varphi A(t) \tag{3-10}$$

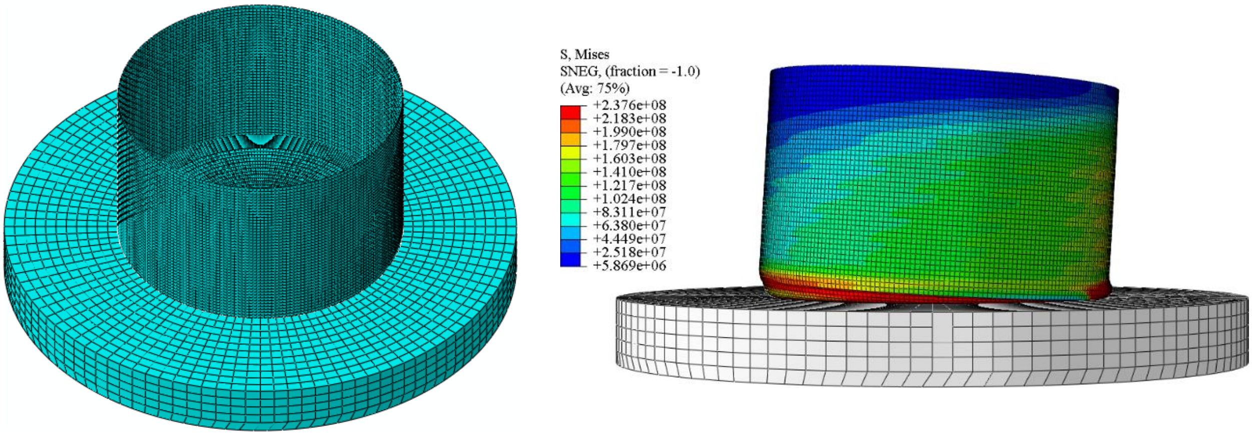

(a) (b)

Figure 3-4: (a) Tank A (h_f/R_t=1.13) detailed 3D finite-element model featuring the contact between the tank and surrounding rigid surface; (b) von Mises stress contour on the deformed shape.

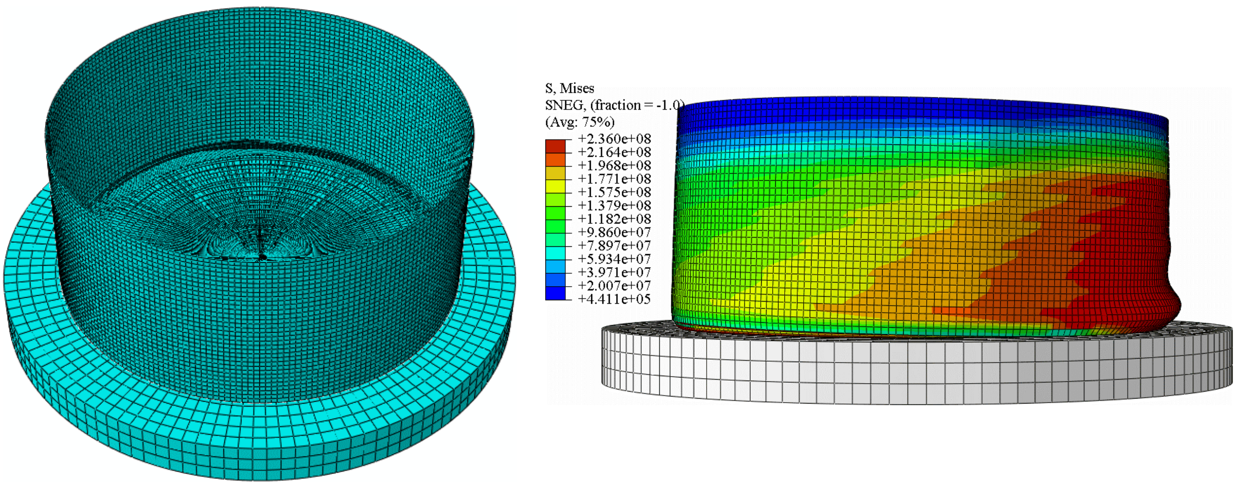

(a) (b)

Figure 3-5: (a) Tank B (h_f/R_t=0.81) detailed 3D finite-element model featuring the contact between the tank and surrounding rigid surface; (b) von Mises stress contour on the deformed shape.

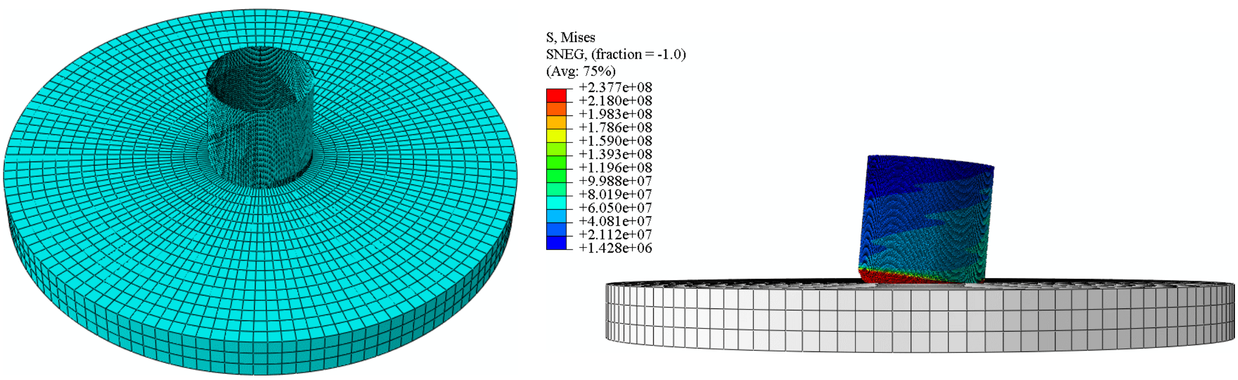

(a) (b)

Figure 3-6: (a) Tank C (h_f/R_t=1.85) detailed 3D finite-element model featuring the contact between the tank and surrounding rigid surface; (b) von Mises stress contour on the deformed shape.

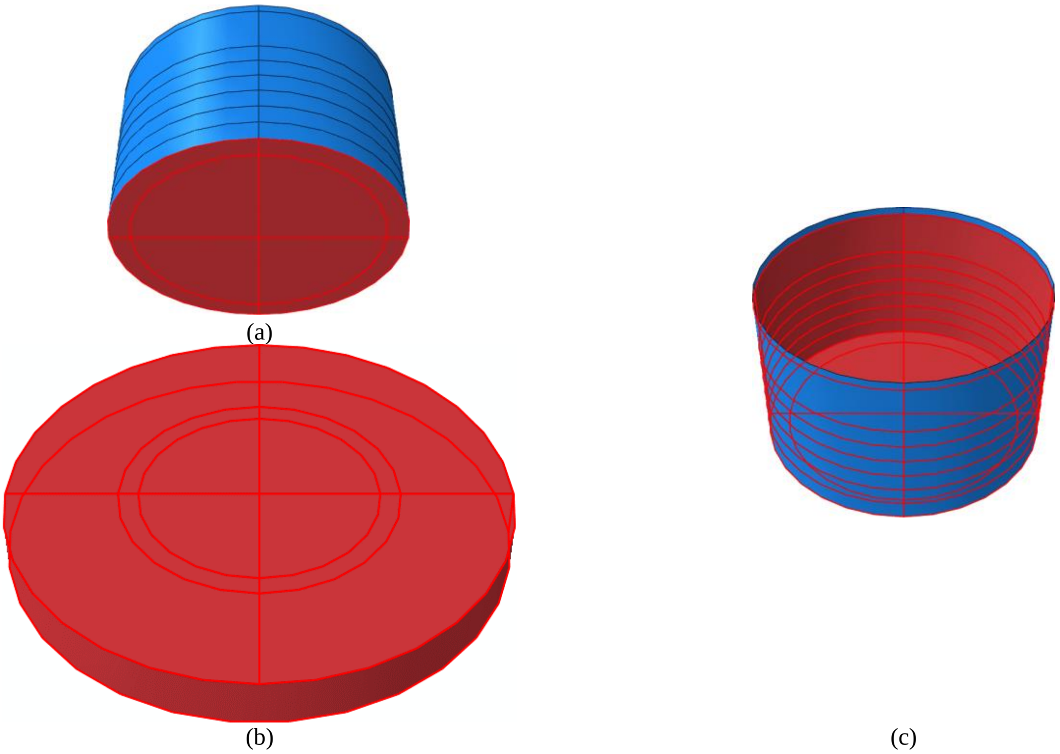

Figure 3-7: Tank A (a) bottom base plate surface, (b) rigid (i.e. ground) surface and (c) inner surface.

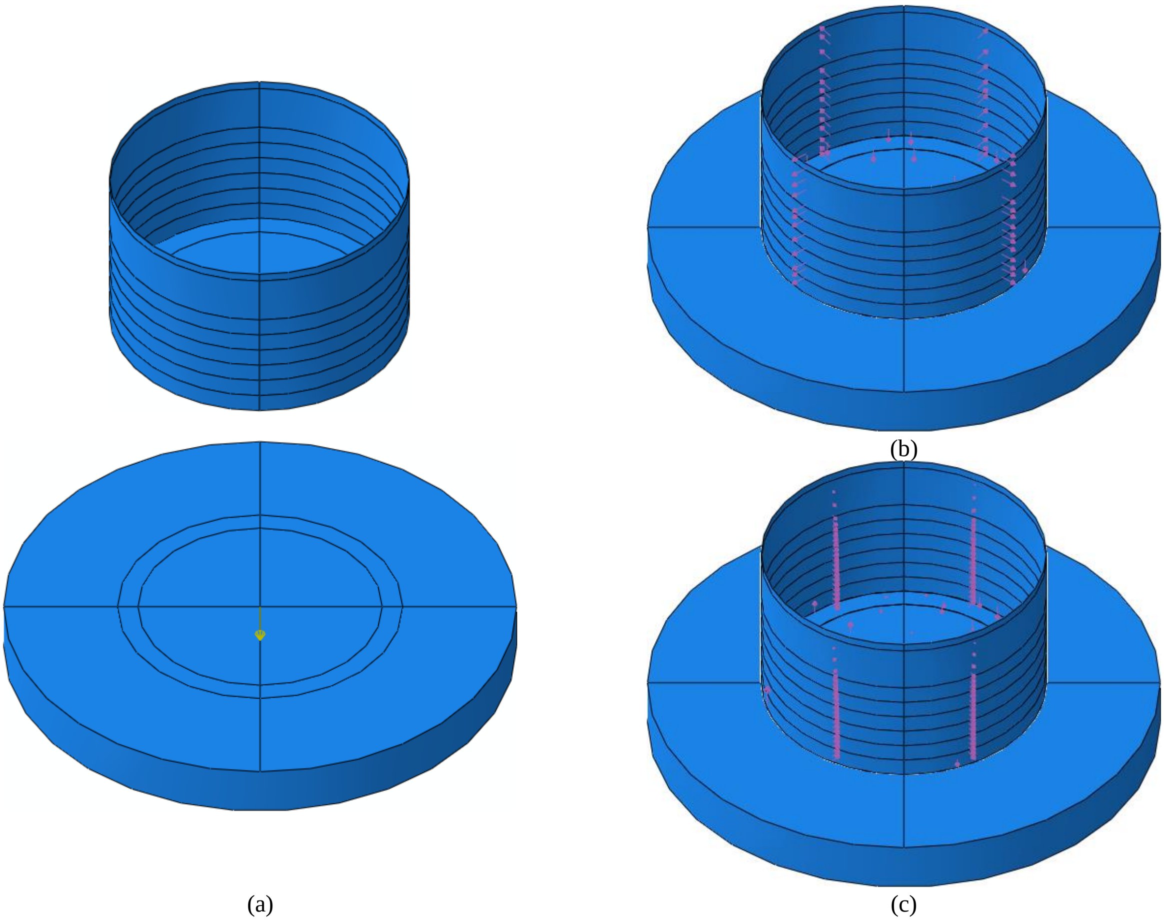

Figure 3-8: Loading steps for Tank A: (a) gravity loads; (b) hydrostatic pressure; (c) hydrodynamic pressure.

C_i is a spatial function for the non-dimensional cylindrical coordinates ξ, ζ, φ (with origin at the centre of the tank bottom and ζ being the vertical axis) and $A(t)$ the earthquake spectral acceleration. Figure 3-10 presents a comparison between the "Joystick" model and the detailed FE model shown in Figure 3-4, for a constant input acceleration of $A(t)$=1.0g and the tank parameters of Table 3-1. The deformability of the model is examined in terms of base uplift (w) versus the separation length (L). A very good agreement is observed for tank A, while small discrepancies are evident for tanks B and C. In particular, for a given uplift of tank B the "Joystick" model underestimates the separation length compared to the FE model, thus implying a slightly stiffer behaviour. In that sense, the response seems to be overestimated for low aspect ratio liquid storage systems similar to tank B by a factor roughly equal to 0.3. Although this kind of difference is borderline acceptable for a simplified model, it occurs following the onset of the Elephant's Foot Buckling where the tank has "failed", and as a result, the edge support conditions on the base are no longer valid. For a slender system such as tank C, the response is clearly underestimated. Initially the factor between the two curves is in the order of 0.15, but as the base uplift approaches the rather large value of 140mm it comes very close to 0.3. Note that the inherent error in the simplifications adopted by Malhotra and Veletsos (1994c) that also appears in the finite element model (e.g. approximate hydrodynamic loading in place of fluid-structure-interaction, Figure 3-8 and Figure 3-9), should also be considered following relevant experimental studies (De Angelis et al. 2009; Ormeño et al. 2015a). In a true performance-based sense, this error (although only roughly estimated) should also be acknowledged in the accuracy of results in terms of model-related uncertainty.

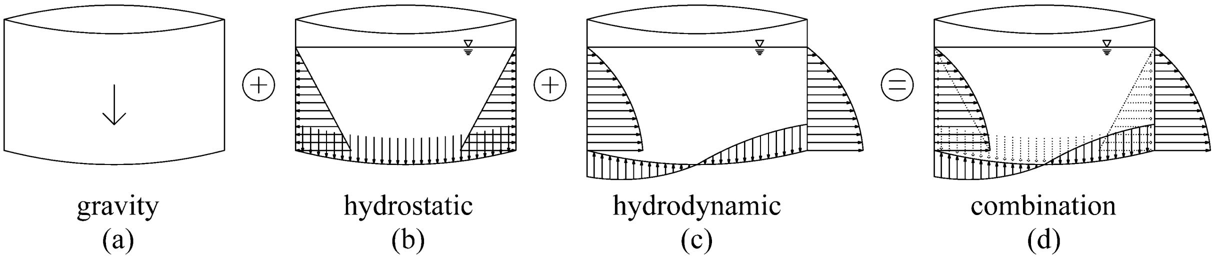

Figure 3-9: Loading steps: (a) gravity loads; (b) hydrostatic pressure; (c) hydrodynamic pressure; (d) combined actions.

Table 3-1: Properties of the Tanks Examined.

Properties	**Variable description**	**Notation (units)**	**Numerical values**		
			Tank A	**Tank B**	**Tank C**
Tank	Radius	R_t (m)	13.9	23.47	6.1
	Height	h_t (m)	16.5	19.95	11.3
	Wall thickness per course	t_w (mm)	17.7;15.7;13.7;11.7;9.7;7.8;6.4;6.4;6.4	22.23;18.93;16.24;13.57;10.9;8.22;8.0;8.0;8.0	9.6;8.0;6.4;4.8
	Base plate thickness	t_b (mm)	6.4	6.4	4.8
	Annular ring thickness	t_a (mm)	8.0	10.0	4.8
	Roof mass	m_r (ton)	35	46	19
Material	Yield strength	f_y (MPa)	235	235	235
	Steel Young's Modulus	E (GPa)	210	210	210
	Hardening ratio	a_h (%)	1	1	1
	Poisson's ratio	v (-)	0.3	0.3	0.3
Fluid	Height	h_f (m)	15.7	18.95	11.3
	Density	ρ_f (kg/m^3)	1000	1000	1000

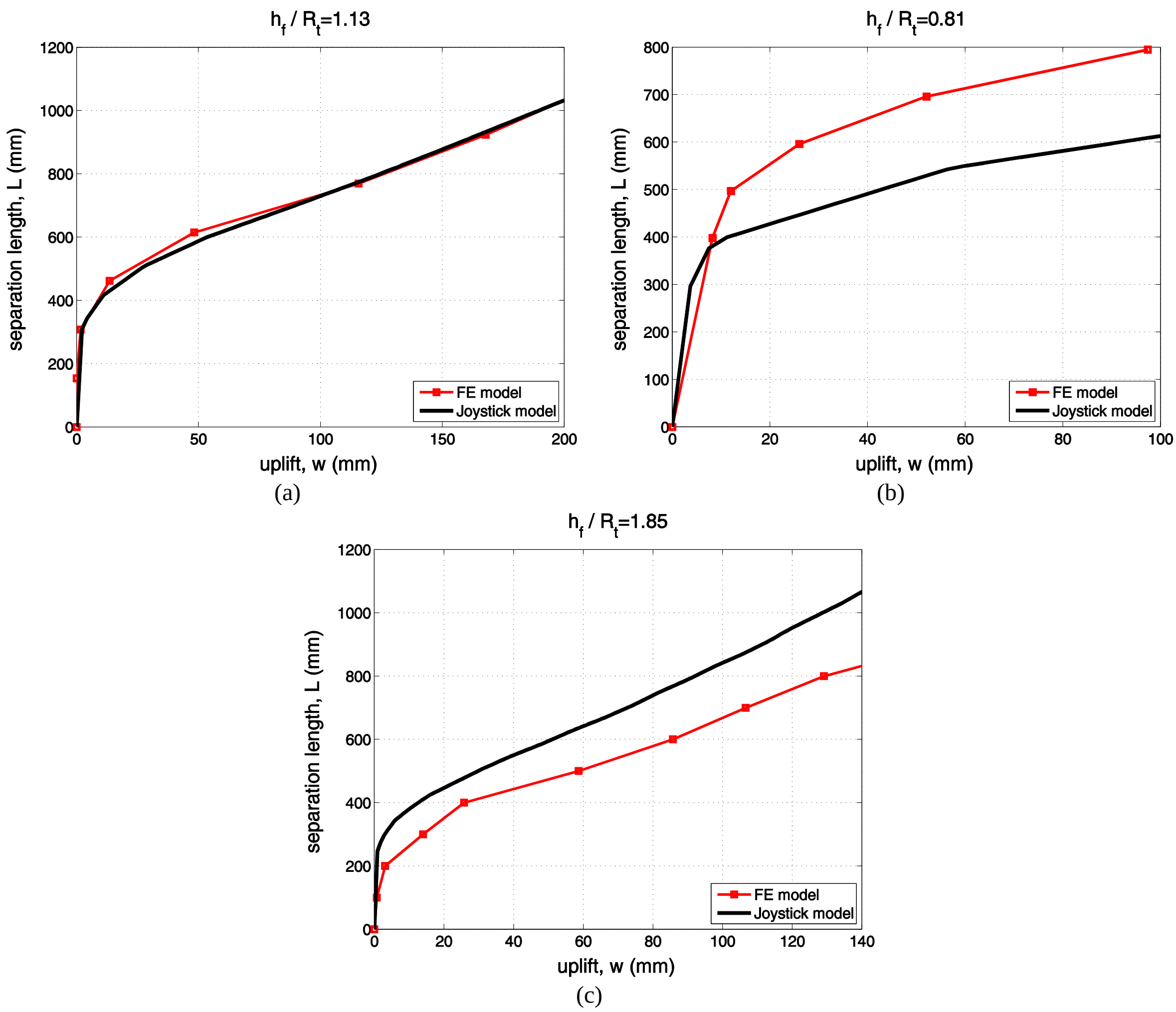

Figure 3-10: Separation length versus uplift for (a) Tank A; (b) Tank B; (c) Tank C.

3.5.2 Performance of the proposed model

The application of the proposed model is presented for the squat tank A that has a radius of R_t=13.9m and is 95% filled with water (Table 3-1). An overview of the strip model response is initially presented through the uplift resistance and plastic rotation plots shown in Figure 3-11. According to Figure 3-11(a), the strip model yields by the time some minor uplift is induced. As the model is further uplifted, stiffness degradation takes place and the response becomes essentially elastoplastic with constant hardening. Figure 3-11(b) compares the recorded model plastic rotation and the corresponding estimate of Eq.(3-7). Apparently, the Eurocode 8-4 (CEN 2006) approximation of the plastic rotation seems to saturate for uplift values greater than 5cm. Thankfully, it presents a conservative approximation compared to the estimates of the proposed model, where the maximum difference between the two curves is in the order of 15%.

The base plate rotational response is shown in Figure 3-12(b). Again, the response is dominated by a very stiff elastic branch that yields when uplift takes place and is then followed by a hardening behaviour, similar to the one observed on the strip model analysis results. The response pattern does not change for the full tank model either, where results are provided both for anchored and unanchored support conditions. Although it is customary to assume fixed boundary conditions for the modelling of anchored tanks, the "Joystick" model provides a more elaborate solution by taking into account the anchorage effect, which according to post-earthquake observations by no means implies zero uplift.

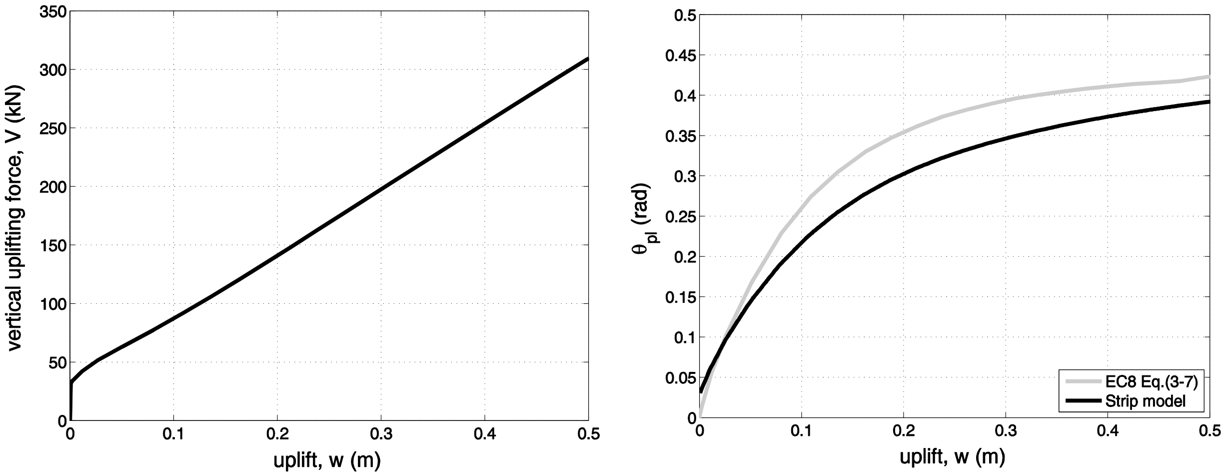

(a) (b)

Figure 3-11: Strip-model (a) uplift resistance; (b) edge uplift versus plastic rotation.

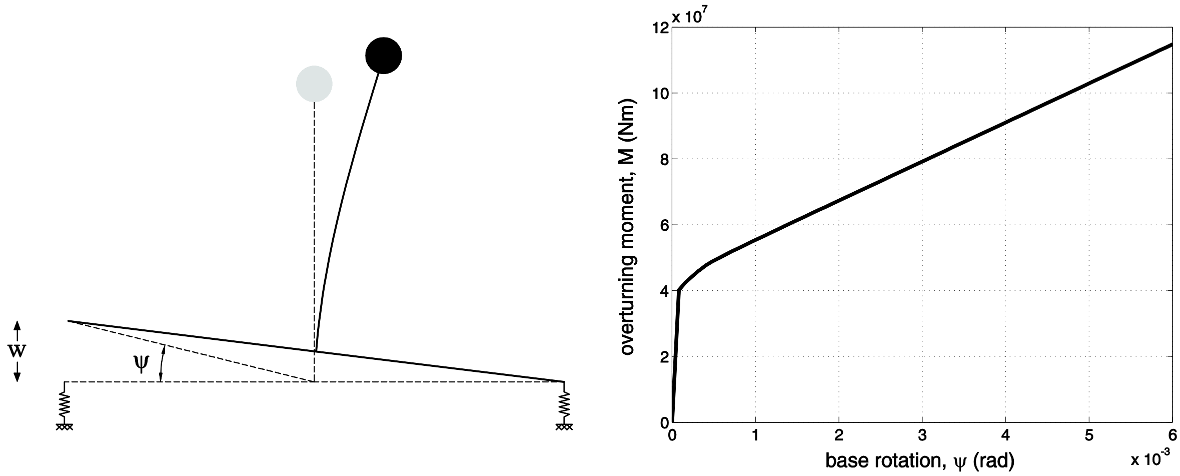

(a) (b)

Figure 3-12: (a) Recorded base rotation ψ; (b) base-plate rotational resistance.

A parametric study is conducted using a range of ultimate displacements for the anchored connections, in order to obtain a deeper understanding on the response of anchored systems. The nonlinear static as well as the time history analysis are employed for ultimate displacement values ranging from δ_u =1cm to δ_u =20cm. This range for δ_u is meant to reflect the potential flexibility of the entire connection, including the bolt and the connecting flange. The results presented in Figure 3-13 show the edge uplift versus the horizontal force that is incrementally applied on the impulsive mass of the tank model. It is evident that the bolts shift the yield point to considerably higher base shear estimates, until the anchors begin to fail and the response of the anchored system changes. A progressive fracture of the connections (followed by a sudden drop of the system's stiffness) takes place, spoke after spoke, until the response becomes similar to that of the unanchored tank. Figure 3-14 and Figure 3-15 present the corresponding time history responses for a scaled version of the El-Centro record. The uplift and rotation histories shown in Figure 3-14 (a, b) and Figure 3-15 (a, b) respectively, fully capture the rocking motion of the tank, while at the same time, the effect of the anchors' ultimate displacement is unveiled during the first 10 seconds of the ground motion. Once again, the bolt connections restrain the system until the progressive failure of the anchors takes place and the response gradually matches that of the unanchored tank.

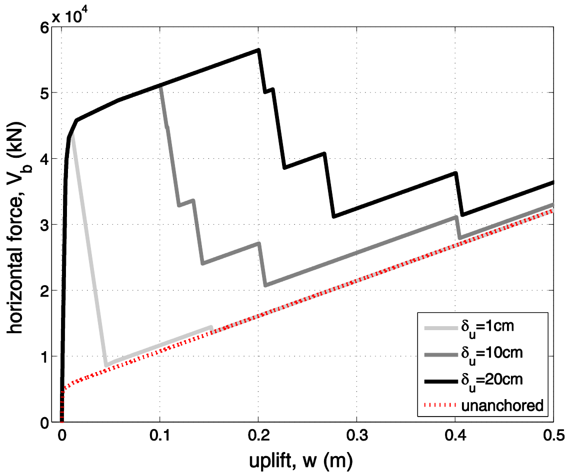

Figure 3-13: Nonlinear static analysis; edge uplift versus horizontal force for a range of ultimate connection displacements (δ_u).

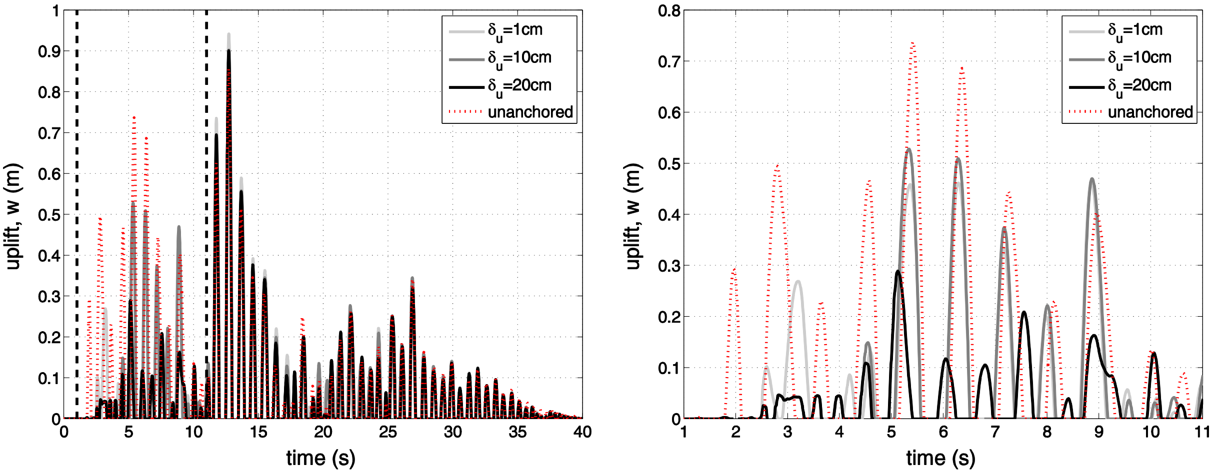

(a) (b)

Figure 3-14: (a) Uplift response history; (b) magnified view at 1 ÷ 11 s featuring the effect of anchors.

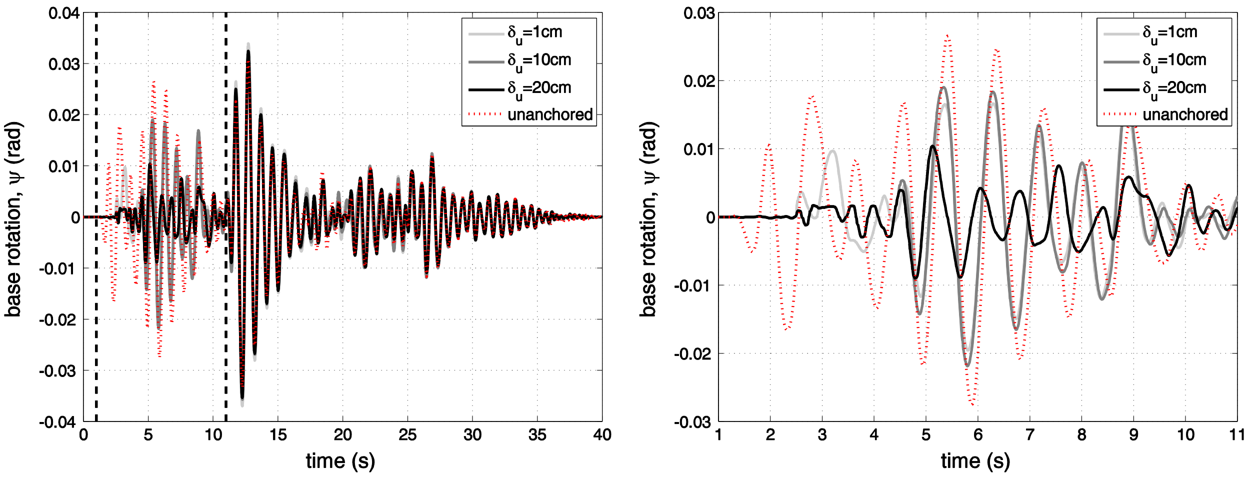

(a) (b)

Figure 3-15: (a) Rotational response history; (b) magnified view at 1 ÷ 11 s featuring the effect of anchors.

3.5.3 Influence of modelling parameters

Figure 3-16 compares various modelling choices in terms of discretisation (mesh) and element type (displacement versus force-based distributed plasticity) used for the strip model 'pre-analysis' step. The displacement-based formulation presents a slightly stiffer response compared to the corresponding force-based solution for an element size not greater than 20t_b. When the discretization is further refined, both formulations exhibit practically identical response. Apparently, at the optimal discretisation level in terms of accuracy (i.e. 15t_b), either can be used bearing in mind that the displacement-based approach is considerably faster. In general, the strip model mesh seems to yield an accurate solution at an element size of approximately 10t_b-15t_b. As an alternative, only the outer quarter of the strip model could be assigned a fine mesh (in the order of 15t_b), in the sense that the plastic hinges are unlikely to form outside this given range. The remaining three quarters may then be modelled using an element size of the order of 45t_b to further improve the computational time.

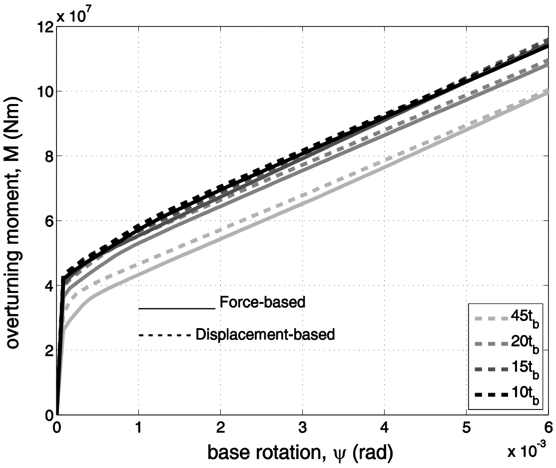

Figure 3-16: Parametric base-plate nonlinear static analysis featuring the element size as well as the displacement versus force-based solutions.

3.6 SENSITIVITY ANALYSIS

Besides the model type uncertainty outlined in the previous sections of this paper, a thorough performance-based approach for practically any earthquake engineering problem should take into account sources of uncertainty such as the model parameter uncertainty, the record-to-record variability and the seismic hazard uncertainty. In this section a sensitivity analysis is conducted in order to determine the effect of different input parameters on the seismic response of the model (i.e model parameter uncertainty). Tank A (Table 3-1) is used as a testbed. Key-parameters such as the steel elastic Young's modulus (E) and the expected yield strength (f_y) are examined. Other geometric parameters examined are: the tank wall thickness (t_w), the annular ring thickness (t_a) and the base plate thickness (t_b) and the contained fluid height (h_f). The edge rotational ($k_{\theta\theta}$) and axial springs (k_{uu}) suggested by Malhotra and Veletsos (1994a) are also considered as potential sources of modelling uncertainty and hence both parameters are included in the sensitivity analysis through a stiffness modification factor (α_k). Finally, the bolts' yield strength (f_b) is included for the case of anchored systems. The aforementioned parameters are summarised in Table 3-2, where the coefficients of variation (CoV) adopted [following either Vrouwenvelder (1997), or engineering judgement] are used to provide upper and lower bound estimates for the majority of variables.

Sensitivity analysis with respect to nonlinear static (Pushover) and dynamic (Incremental Dynamic Analysis, IDA Vamvatsikos and Cornell (2002)] analysis are performed. A set of three nonlinear static analyses is performed for each parameter, corresponding to the response when parameters are assigned their mean, upper and lower bound values. Having eliminated the modelling parameters that the structure has shown small sensitivity to, IDA is performed to provide further insight by taking into account the record-to-record variability. Although it is not presented herein, the effect of the site can be incorporated at a later stage via convolution with the seismic hazard.

Table 3-2: Parameters Considered for the Sensitivity Analysis of the Proposed Model (Bakalis et al. 2014b).

Parameter	Notation (units)	Mean (μ) Expected Values	Values Considered
Young's modulus	E (GPa)	210	216.3;210;203.7
Yield stress	f_y (MPa)	280	299.6;280;260.4
Edge-spring stiffness factor	a_k	1.0	1.3;1.0;0.7
Bolts' strength	f_b (MPa)	900	963;900;837
Equivalent wall thickness	t_w (mm)	13.1	14.41;13.1;11.79
Base plate thickness	t_b (mm)	5.44	6.4;5.44;4.48
Annular ring thickness	t_a (mm)	6.8	8.0;6.8;5.6
Normalized fluid height	h_f /h_t	0.75	0.5;0.6;0.7;0.75;0.8;0.9;0.99

3.6.1 Nonlinear static analysis sensitivity

Figure 3-17 presents the modelling sensitivity in terms of nonlinear static curves for the parameters of Table 3-2. The sensitivity to material uncertainty (E, f_y) is shown in Figure 3-17(a) and (b). It is evident that the material properties are of minor importance as both the upper and the lower bound curves are perfectly aligned to the mean estimates. Other parameters, such as the strip model edge springs, are also strongly related to modelling associated uncertainty. The sensitivity analysis for both rotational and axial edge springs is presented in Figure 3-17(c) and (d) respectively. Although the model is not sensitive to the rotational spring, the axial component affects the response for large uplift deformations (e.g. 0.20m of uplift).

The geometric characteristics comprise another potential source of uncertainty, especially for the case of liquid storage tanks, where loss of material subject to sulphide or seawater corrosion, construction quality and mid-life rehabilitation interventions (typically every 12 years) determine the effective tank wall and base plate thickness. According to Figure 3-17(e), the base plate thickness does not cause any significant change in the response for the given range. The annular ring thickness on the other hand is significant, due to the post-yield response modification shown in Figure 3-17(f). Decreasing t_a reduces the strength of the tank. At the same time, when t_a exceeds its mean value the response becomes stiffer and the plastic hinge formation on the base plate shifts to slightly higher base shear estimates. In general, the base plate thickness modifies the post-yield behaviour of the model for uplift values no greater than 0.25m. One may notice the significance of the annular ring over the base plate thickness, as the former determines response in the critical plastic hinge position. Still, there cannot be a solid prediction regarding the importance of base plate thickness, as the governing parameter is a function of the annular ring (radial) width. For typical design specifications for the annular ring (e.g. American Petroleum Institute 2007), the plastic hinge will form within its width. For the rare case where such specifications are not respected and an insufficiently wide ring is provided, the hinge will form within the base plate and t_b rather than t_a will govern the response. Apart from the base plate properties, the tank wall sensitivity shown in Figure 3-17(g) does not considerably affect the response, except for large uplifts where some minor changes take place on the nonlinear static curves.

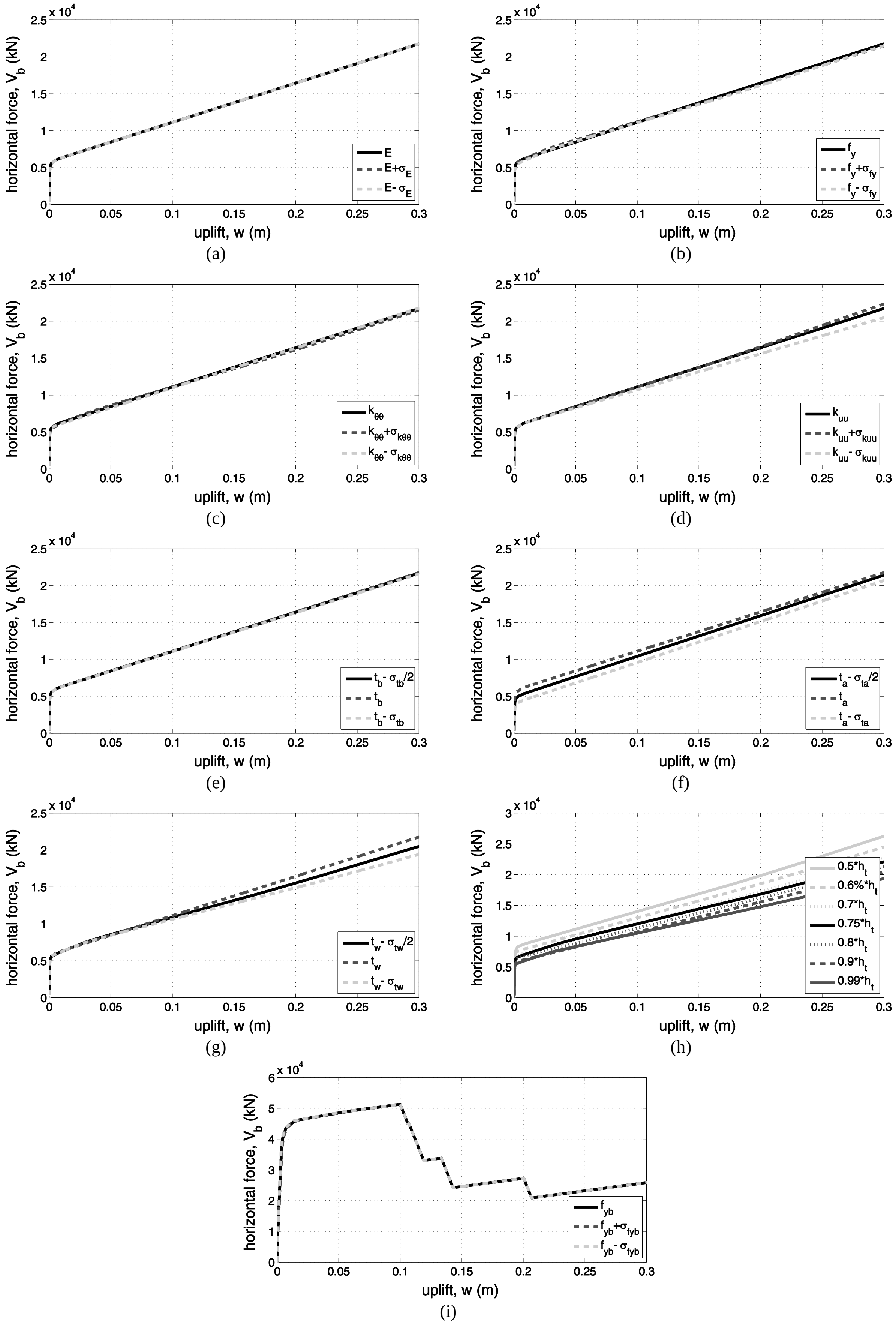

Figure 3-17: Sensitivity analysis using nonlinear static analysis.

The contained liquid height shown in Figure 3-17(h) summarizes the geometric properties evaluation. The fluid height given as a fraction of the total height of the tank, is by far the most influential parameter examined, as the discrepancies found between the $0.50h_t$ and the $0.99h_t$ curves, for a given uplift, are in the order of 35% following the plastic hinge formation. Reducing the fluid stored in the tank results in stiffer models, while as it approaches the maximum storage capacity, the system's strength is significantly reduced, resulting into a more vulnerable structural system. Finally, for the case of anchored tanks, the bolts' yield strength is also examined, where according to Figure 3-17(i) the effect can be considered negligible, in contrast to the significant sensitivity shown for the connection ductility in Figure 3-13.

3.6.2 IDA sensitivity

The nonlinear static analysis results have shown that the most influential parameters are the fluid height, the tank wall thickness, the annular ring thickness and the stiffness of the axial spring. A series of IDAs is performed for these parameters in order to validate the static analysis results. A set of 22 pairs of far-field records (FEMA 2009) is used. The uplift is adopted as the engineering demand parameter (*EDP*) and the peak ground acceleration (*PGA*) as the intensity measure (*IM*). Other *EDPs* are functionally one-to-one related to uplift through the 'pre-analysis' step, hence any conclusions drawn for uplift are also applicable. Regarding the *IM* considered, although *PGA* is expected to inflate the final output of a seismic risk assessment study with additional uncertainty (i.e. it is not the optimal intensity measure), it is intentionally adopted herein in order to make the sensitivity analysis results easier to digest even for readers that are not familiar with terms such as efficiency and sufficiency (Luco and Cornell 2007). In any case, given that there is no obvious optimal intensity measure for the global response of the tank (as the convective spectral acceleration would be for the sloshing wave height for instance), the effect of the parameters examined is not expected to change significantly using any other intensity measure. Either way, when the period falls within a range of 0.1-0.3sec, such as the case of the tanks examined, *PGA* and the fundamental period spectral acceleration provide very similar results. Undeniably, more *IM* options could be tested in order to find the optimal *IM* (e.g. the spectral acceleration at some elongated period for unanchored tanks). However, this is beyond the scope of this study and is expected to be covered in a future direction of our research.

Figure 3-18 presents the median IDA sensitivities. It is evident that geometric parameters such as the tank wall [Figure 3-18(a)] and the annular ring thickness [Figure 3-18(b)] do not introduce any significant demand uncertainty to our model (although the associated capacity may indeed change), as all curves are almost perfectly aligned to each other. The same observation applies for nearly the entire given uplift range of the axial spring stiffness [Figure 3-18(c)]. One may notice that the lower bound deviates from the mean estimate for uplift values greater than 0.22m, yet the difference may be considered statistically insignificant.

Figure 3-18(d) shows that the fluid height introduces a considerable level of uncertainty to the model. Even though the median IDA curves follow the exact same pattern with the nonlinear static analysis results for a fluid height up to 75% of the tank height, it appears that as the fluid height increases, the response changes considerably. The $0.80h_t$ curve coincides with the $0.75h_t$ curve, while both the $0.90h_t$ and the $0.99h_t$ curves develop a substantially stiffer response for peak ground accelerations that exceed 0.1g. The performance obtained summarizes the fluid height uncertainty involved in liquid storage tanks. The paradox of having a more massive (and hence flexible) system (i.e. $0.99h_t$ curve) oscillating at smaller uplifts for a given *IM* level compared to the $0.75h_t$ case, may be attributed to the period effect shown in the Figure 3-19 median spectrum. It appears that as the liquid stored in the tank increases, the impulsive period elongates. Initially, this brings T_i within the ascending branch of the median spectrum and as a result the impulsive spectral acceleration [$S_a(T_i)$] increases too. After the $0.8h_t$ impulsive period [Figure 3-19(b)], a decrease on the median spectral acceleration (for given *PGA*) is observed instead.

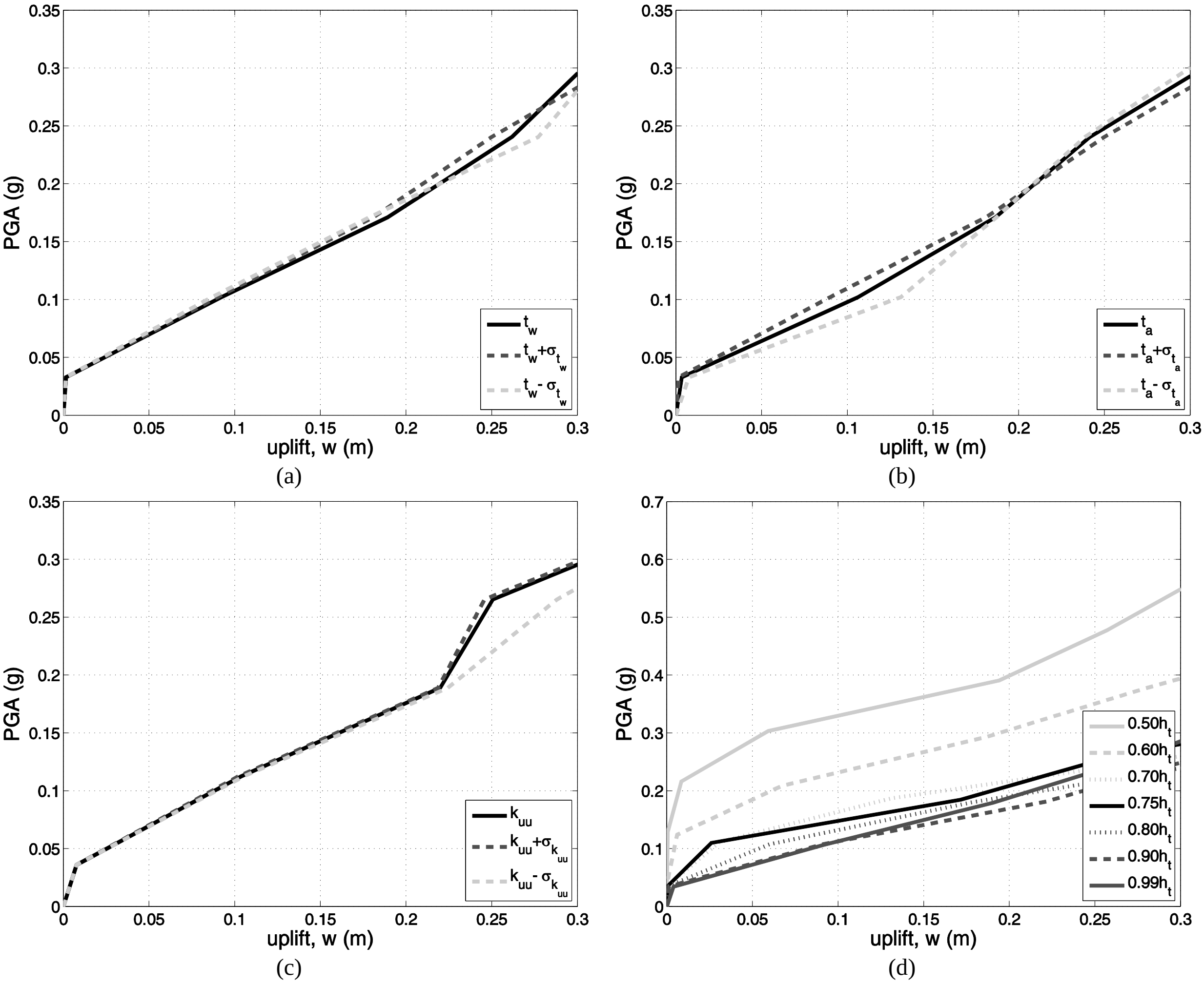

Figure 3-18: Sensitivity analysis using incremental dynamic analysis.

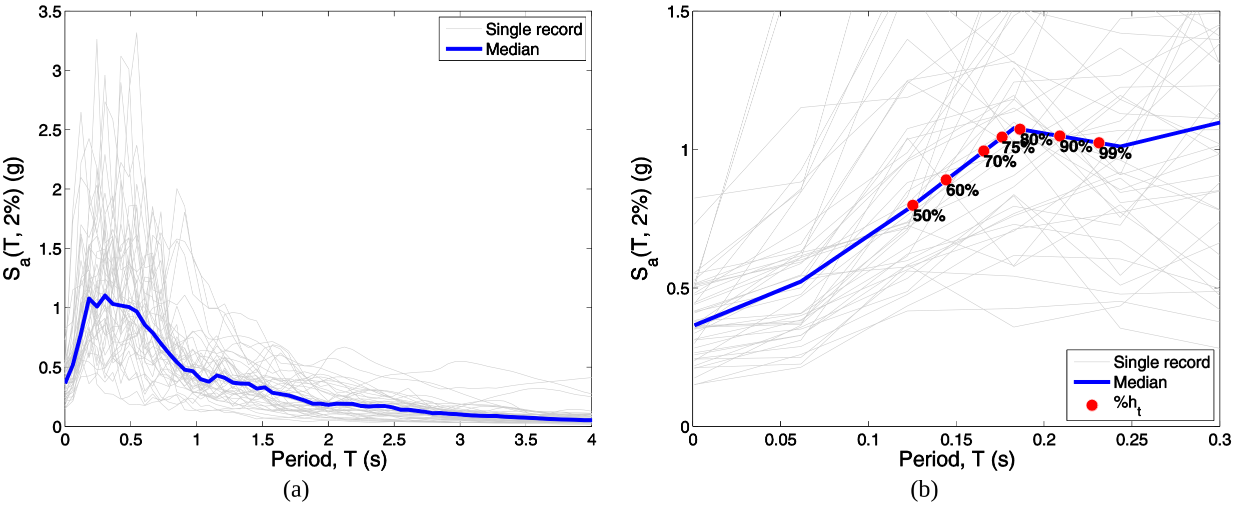

Figure 3-19: (a) Unscaled single record and median spectra (FEMA 2009); (b) magnified view including the 0.5–$0.9h_t$ median $S_a(T_i)$ response.

3.7 CONCLUSIONS

A novel modelling approach has been presented for the rapid analysis of liquid storage tanks. The proposed model offers reasonable accuracy and good computational efficiency compared to detailed FE models. Based on the principles of Malhotra and Veletsos, the proposed model goes one step beyond by providing the ability for three-dimensional analysis of liquid storage systems using multiple ground motion components. It can easily be applied using any general purpose structural analysis software, thus taking advantage of the abilities offered by commercial codes. It is a simplified model suitable for practically any cylindrical fixed-roof liquid storage system, regardless of geometry, material and boundary conditions. The motivation behind this methodology is the need for probabilistic assessment, where numerous scenarios using nonlinear static or dynamic analysis are necessary. All in all, the proposed model forms a concept that employs modern tools for the successful performance-based assessment/design of a single liquid storage system, or maybe even an ensemble of tanks. Part of the work presented in this chapter has been published in the Journal of Structural Engineering (Bakalis et al. 2017a)

4 SEISMIC RISK ASSESSMENT OF LIQUID STORAGE TANKS VIA THE "JOYSTICK" SURROGATE MODEL

4.1 ABSTRACT

A performance-based earthquake engineering approach is developed for the seismic risk assessment of fixed-roof atmospheric steel liquid storage tanks. The proposed method is based on a surrogate single-mass model that consists of elastic beam-column elements and nonlinear springs. Appropriate component and system-level damage states are defined, following the identification of commonly observed modes of failure that may occur during an earthquake. Incremental Dynamic Analysis and simplified Cloud are offered as potential approaches to derive the distribution of response parameters given the seismic intensity. A parametric investigation that engages the aforementioned analysis methods is conducted on three tanks of varying geometry, considering both anchored and unanchored support conditions. Special attention is paid to the elephant's foot buckling formation, by offering extensive information on its capacity and demand representation within the seismic risk assessment process. Seismic fragility curves are initially extracted for the component-level damage states, in order to compare the effect of each analysis approach on the estimated performance. The subsequent generation of system-level fragility curves reveals the issue of non-sequential damage states, whereby significant damage may abruptly appear without precursory lighter damage states.

4.2 INTRODUCTION

Oil and gas products are generally stored in large-capacity atmospheric tanks. Safeguarding the integrity of such industrial facilities against earthquakes is vital not only for maintaining the flow of essential products and energy resources, but also for preventing any associated socioeconomic consequences of a potential disruption (Krausmann and Cruz 2013). Ensuring an "appropriate" level of safety tantamount to the importance of liquid storage tanks, mandates the use of state-of-the-art seismic performance assessment techniques that take into account all possible sources of uncertainty. Nevertheless, the assessment methodology typically undertaken by engineers is based on design code regulations/provisions and can be summarised in a prescriptive approach that may deliver some acceptable (but actually unknown) level of accuracy, by engaging into a deterministic process where blanket safety factors (American Petroleum Institute 2007; CEN 2006) are employed to approximately deliver the required reliability.

In an attempt to rationalise seismic design and assessment procedures, the concept of Performance-based Earthquake Engineering (PBEE) has emerged (Cornell and Krawinkler 2000), thus facilitating a logical decision-making process that relies on the probability of exceeding certain capacity thresholds that even make sense to non-engineers (Yang et al. 2009). Typically, the procedure begins with the *seismic hazard analysis* (Cornell 1968), where ground motion parameters (e.g. peak ground acceleration, *PGA*) known as seismic intensity measures (*IM*) are characterised in terms of mean annual frequency (MAF) by taking into account all potential earthquake scenarios on the site of interest. It may also be used to identify the scenarios that contribute most to the site-hazard and thus select ground motion records suitable for the *structural response analysis.* Of essence in this case is the estimation of the distribution of certain engineering demand parameters (*EDPs*, e.g. stress, strain, displacement) conditioned on the seismic intensity. Different analysis methodologies can be carried out to derive it, and the choice generally relies on a trade-off between accuracy and computational burden. Normally, one can employ Incremental Dynamic Analysis (IDA) (Vamvatsikos and Cornell 2002) for a wide range of ground motion records and seismic intensity levels, to obtain a refined representation of the *EDP-IM* space, bearing in mind that this analysis approach does not allow rigorous record selection to cover up any *IM*-related deficiencies in terms of sufficiency (Luco and Bazzurro 2007). Closely related is the stripe analysis (Jalayer 2003) where different records may be employed at each *IM* level to improve upon an insufficient *IM* (Baker and Cornell 2006a). Cloud analysis may similarly be employed using even unscaled records, but requiring some global or local regression in post-processing, plus perhaps some logistic regression to take care of collapse (i.e. global instability) points where non-convergence appears (Jalayer 2003). The subsequent *damage analysis* conveniently summarises the *EDP* distributions into fragility functions (Bakalis and Vamvatsikos 2018), thus assigning probabilities of exceedance on certain damage state (*DS*) or limit state (*LS*) capacity thresholds. The aforementioned quantities are finally translated into decision variables through the *loss analysis* that relies on cost data for repair, downtime and casualties, with respect to the damage states examined (FEMA 2012b). The final output is normally in the form of the MAF exceeding a (usually monetary) threshold of interest that engages facility owners and stakeholders into comprehensive mitigation actions.

As much as PBEE has reached a mature state for plenty of mainstream civil engineering structures (e.g. buildings, bridges), there are hardly any provisions regarding its application to industrial equipment structures (FEMA 2003). Parameters such as the geometry, the toxicity/flammability of the stored materials, and the intrinsic failure modes, make the problem substantially different from buildings or bridges, as the post-earthquake impact may vary from operational costs, to uncontrollable environmental consequences due to leakage of the stored materials (American Lifelines Alliance 2001a; b; FEMA 2003). The devastating outcome of earthquake events such as Kocaeli (1999) and Tohoku (2011), further enhances the view that comparatively little attention has been paid to liquid storage tanks, even from an academic perspective. Previous research efforts may be summarised to a fragility-based methodology using either costly finite element models (Buratti and Tavano 2014; Talaslidis et al. 2004), or available observational (i.e., historical or empirical) data as shown by O'Rourke and So (2000). Empirical fragility curves are also provided by Salzano et al. (2003) using the probit function to fit the available data, while Berahman and Behnamfar (2007) adopt a Bayesian approach to predict the associated probability of exceedance. Analytical fragility curves for oil storage tanks are available by Iervolino et al. (2004), yet they only cover a single failure mode despite the consideration of various geometric characteristics that affect the dynamic response of the tank.

Other studies (Razzaghi and Eshghi 2015; Salzano et al. 2009) compare large sets of analytical results to observational ones, while there is at least one attempt to extend this train of thought to the entire plant level (Fabbrocino et al. 2005), where fragility curves from various industrial structures (e.g. atmospheric tanks, pressure vessels) should appropriately be combined to estimate the associated risk.

In any case, from a performance-based point of view, there are several pieces in the existing literature (e.g. structural modelling, damage classification, cost assessment) that are either missing or not adequately substantiated to properly translate the analysis output into decision-making variables for liquid storage tanks. Bearing in mind that the individual steps of the PBEE process are all equally important, this work emphasises the structural response and damage (or fragility) analysis that are of particular interest to structural engineers. In specific, it offers an approach that respects proper uncertainty propagation from all pertinent sources and is based on a three-dimensional (3D) surrogate model, appropriate for efficiently running multiple nonlinear response-history analyses, while also allowing to distinguish parts of the tank to offer different levels of damage resolution: Either localised to individual segments and components or generalised to refer to the entire structure, as needed.

4.3 MODELLING OF LIQUID STORAGE TANKS

Adopting the PBEE concept for the case of liquid storage tanks requires a series of tasks to be tackled before the MAF of exceeding a specified *LS* capacity is estimated. Of particular concern is the modelling of such complex structural systems. The fluid-structure-interaction, for instance, imposes several constraints related to the computational effort required, and despite the evolution of computer technology, explicitly modelling the contained fluid and the associated contact properties with the tank shell results in costly finite element models. Given that the number of scenarios considered within a performance-based framework is often significantly larger compared to that of code-based methodologies (e.g. 3 or 7 nonlinear response history analyses according to Eurocode 8 (CEN 2004), vis-à-vis 40-60 analyses for performance assessment (Jalayer 2003; Vamvatsikos and Cornell 2002), simpler surrogate models are required for PBEE applications.

Previous research (Haroun 1983) has shown that earthquake ground motions cause part of the contained fluid to move rigidly with the tank walls (impulsive component), while its remaining portion (convective component) develops a sloshing motion on the free fluid surface [Figure 4-1(a)]. Such observations have led to the development of two-degree-of-freedom (2DOF) approximate models that are suitable for estimating the internal forces and moments, both for anchored and unanchored liquid storage tanks (e.g. Cortes and Prinz 2017; Malhotra 2000). Furthermore, the periods of vibration of the two components (i.e. impulsive and convective) are well-separated for practically any tank, thus allowing the decoupling of their respective responses.

Along these lines, Bakalis et al. (Bakalis et al. 2017a) proposed a 3D single mass surrogate modelling approach for the seismic performance assessment of fixed roof liquid storage tanks. The so-called “Joystick” model is presented in Figure 4-1(b) along with its fundamental modelling details. It consists of a mass (m_i) that represents the impulsive fluid component, attached to an elastic beam-column element, whose properties are estimated such that the fundamental period of the model is fully aligned to the theoretical solution for the impulsive period (Haroun 1983; Malhotra 2000). The elastic element is connected to n rigid beam-spokes that rest on multilinear elastic edge-springs. Those springs are assigned uplift (w) as well as compression resistance properties of a beam (strip) model that extends diametrically on the base plate of the tank, has an effective width b_w=2πR_t/n (where R_t is the tank radius), utilises rotational ($k_{\theta\theta}$) and axial (k_{uu}) springs to model the plate-wall interaction, a concentrated force (N_r) and moment (M_r) to take into account the effect of hydrostatic loads, and is supported by an elastic tensionless Winkler soil/foundation (Bakalis et al. 2017a; Malhotra and Veletsos 1994a) [Figure 4-1(c)]. Essentially, the "Joystick" model is a two-stage model that requires the execution of the base-plate strip model "pre-analysis" step [Figure 4-1(c)] to determine the properties of the "Joystick" model edge-springs (e.g. vertical force (V) versus uplift, separation length (L), etc.). While the "pre-analysis" step requires a few minutes to complete, the "Joystick" model has the ability to perform response history analysis using multiple ground motion components in seconds, without repeating the relatively time-consuming "pre-analysis" step when a different ground motion record or scale factor is adopted. It is also able to take the effect of the anchor bolts into account, simply by modifying the aforementioned edge-springs through a damageable gap-material, the stiffness of which corresponds to the equally-spaced anchor bolts found on the effective width of each beam-spoke (b_w). Similarly, sliding may also be incorporated using suitable friction elements. Overall, the simplified nature of the "Joystick" model offers the ability to model practically any cylindrical liquid storage configuration, regardless of geometry, support conditions and material/fluid properties.

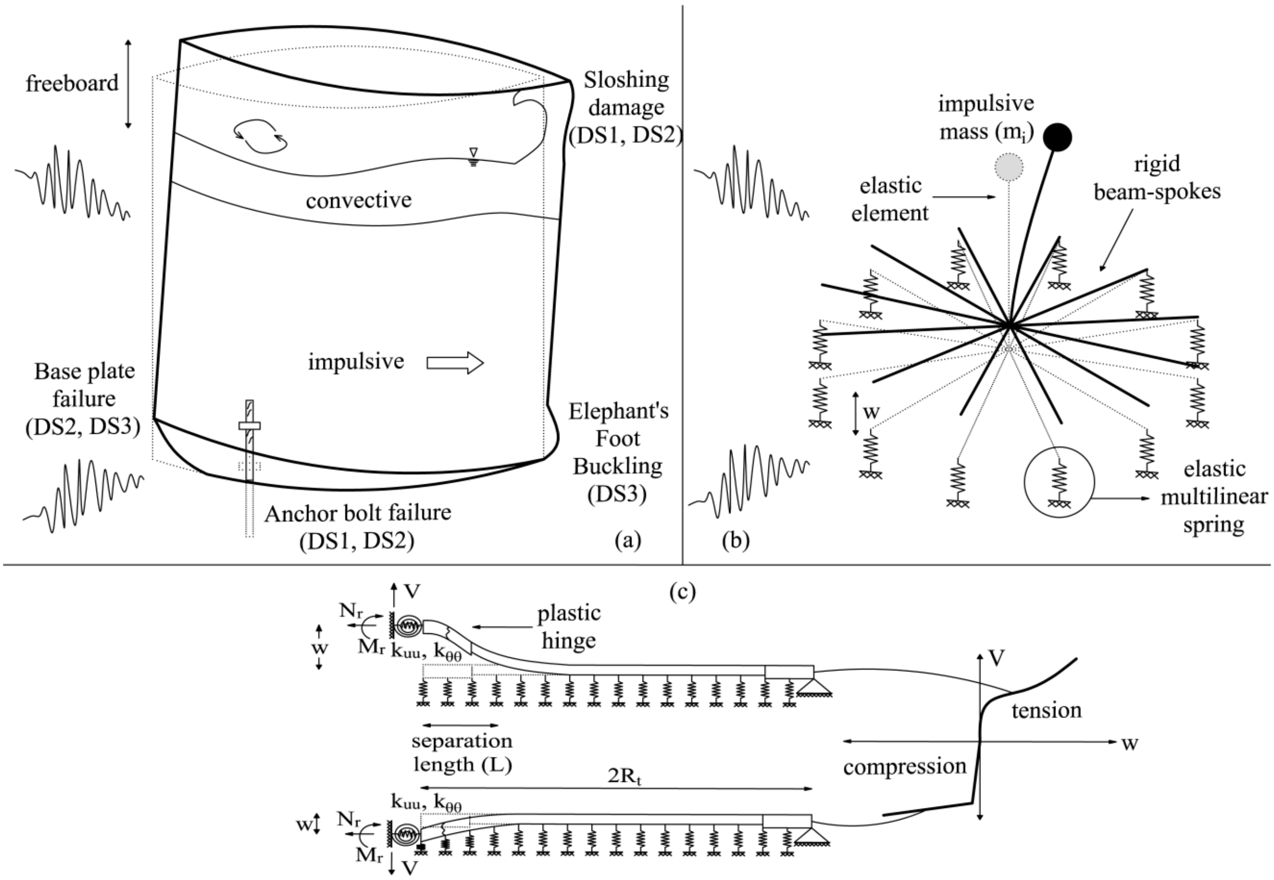

Figure 4-1: (a) Impulsive versus convective fluid component, failure modes and system-level damage state classification on a fixed roof liquid storage tank. Depending on the presence of anchors, the system is either anchored or unanchored. (b) The "Joystick" surrogate model (Bakalis et al. 2017a) and its deflected shape. (c) The strip model under tensile and compressive loading.

4.4 FAILURE MODES

An important consideration for the PBEE application is the ability of simplified models to capture all major modes of failure that may be developed locally on the structural system.

Regardless of support conditions (i.e. anchored or unanchored), commonly observed modes of failure on liquid storage tanks involve fracture of the base plate due to extreme base plate plastic rotations (θ_{pl}), buckling of the tank shell and sliding. These modes of failure derive from the liquid storage system’s trend during ground motion shaking to overturning. As seismic waves arrive on site, the impulsive fluid component imposes pressure on the tank walls, causing excessive overturning moments on the system that may in turn lead to sliding and/or partial uplift of the base plate. The latter results in large-strain deformations on the plate-wall junction that may rupture the base plate. At the same time, the compressive side of the tank suffers from a biaxial stress condition, generated by the compressive meridional and tensile hoop components, which may lead to an elastic-plastic buckling failure. The latter exhibits a characteristic bulge along a considerable part on the tank’s circumference, also known as the Elephant’s Foot Buckling (EFB). For the case of anchored tanks, damage on the anchor bolts constitutes another potential failure mode. Fracturing of the anchors is also affected by the impulsive-component-induced overturning, as the tension developed on the bolts may often exceed their prescribed ultimate strength and ductility. Note that although anchored liquid storage systems are usually considered fully fixed to the ground, their actual performance can incorporate some rocking/uplift, especially when the anchor bolts begin to yield or fracture. At this point, part of the base plate is uplifted and the response gradually resembles that of the corresponding unanchored case (Bakalis et al. 2017a). The convective fluid component on the other hand, determines any kind of damage related to the upper courses of the tank walls and the roof (Kalogerakou et al. 2017). It is also known to offer additional overturning moments at the base of the system, but its contribution with respect to the impulsive component is marginal for the majority of non-slender tanks, and as a result it is often ignored. The failure modes outlined above are depicted in Figure 4-1(a).

4.5 ENGINEERING DEMAND PARAMETERS

Capturing the potential failure modes using surrogate models requires a series of failure criteria to be considered, which are expressed as a function of the engineering demand parameters (*EDPs*) available from the model output. Such criteria are discussed herein for all the aforementioned modes of failure with the exception of sliding, as it requires some elaborate knowledge of the nozzle geometry and mechanical properties. The general view regarding the criteria adopted for the seismic risk assessment of a structure, is that they should remain objective (i.e. neither conservative nor unconservative). In the following, although certain code equations are employed, it should be noted that most of them were presented prior to the development the design codes considered and were not necessarily intended for code-based design. Apparently, the methodology could easily be modified upon the availability of more refined criteria.

4.5.1 Base plate and wall-to-base connection

The deflected shape of the “Joystick” model [Figure 4-1(b)], reveals its ability to simulate the uplift mechanism of liquid storage systems, which provides an indirect mapping to local *EDPs* through the base plate strip model [Figure 4-1(c)]. For instance, the base plate plastic rotation can be estimated using either direct measurements from the simplified uplift response analysis of the base plate strip (Bakalis et al. 2017a; Malhotra and Veletsos 1994a), or with the aid of the Eurocode 8-4 (CEN 2006) equation

$$\theta_{pl} = \frac{2w}{L} - \frac{w}{2R_t}, \tag{4-1}$$

where w is the base uplift and L is the uplifted part of the tank. Note that Eurocode 8-4 provisions suggest a maximum permissible θ_{pl} value of 0.2rad, while experimental studies suggest that this value is overly conservative, proposing a fracture capacity of 0.4rad instead (Cortés et al. 2011). Actually, these values are proposed under the condition that fracture occurs outside the weld that connects the plate to the tank wall; therefore, if a weak weld is suspected to be present, the rotational θ_{pl} capacity may need to be reduced.

4.5.2 Anchorage

Anchorage failure is governed by yielding or fracture of the respective anchor bolts. There are many ways to express this kind of failure (e.g. stress, strain, displacement), and most times the choice of the appropriate *EDP* relies on the structural model that has been chosen to predict the response. When the "Joystick" model (Bakalis et al. 2017a) is adopted, response of the anchor bolts may be estimated through the base uplift that essentially determines their deformation/elongation (δ). Failure may then be captured by assuming that the entire number of anchor bolts corresponding to each spoke (i.e. those along an arc length equal to b_w) are uniformly stressed and respond elastoplastically with a yield-displacement strength (δ_y) and fracture-displacement capacity (δ_u) consistent with the connection ductility.

4.5.3 Sloshing

Sloshing damage is triggered upon the exceedance of the available freeboard d_f, [Figure 4-1(a)], i.e. the available clearance of the free fluid surface (at rest) to the roof. The response is purely dominated by the maximum convective wave height (d) developed during the earthquake. Given the elastic treatment of this problem, Eurocode 8-4 offers the following simplified equation for the sloshing response prediction

$$d = 0.84 R_t S_a(T_c, \kappa_f)/g\,, \tag{4-2}$$

where g is the gravity acceleration and $S_a(T_c, \kappa_f)$ the convective period elastic response spectrum acceleration for an appropriately defined fluid damping [e.g. κ_f=0.5% for water (CEN 2006), bearing in mind that more sophisticated solutions exist (Habenberger 2015)]. API-650 (American Petroleum Institute 2007) also adopts a similar equation using an acceleration coefficient for sloshing wave height calculation in place of the $0.84S_a(T_c,\kappa_f)$ term.

4.5.4 Elephant's foot buckling

Elephant's Foot Buckling depends on the compressive meridional stress demand (σ_m) developed on the tank shell. This mode of failure is slightly more complex to determine, as the edge-spring force (N) recorded from the "Joystick" model must be converted to stress before it is compared to a critical buckling limit (σ_{EFB}). The latter may be estimated, for instance, according to Rotter's (Rotter 2006) formula [also adopted by Eurocode 8-4 (CEN 2006)] as

$$\sigma_{EFB} = \sigma_{c1}\left[1-\left(\frac{pR_t}{t_w f_y}\right)\right]\left(1-\frac{1}{1.12+r^{1.15}}\right)\left[\frac{r+f_y/250}{r+1}\right] \tag{4-3}$$

$$\sigma_{c1} = 0.6E\frac{t_w}{R_t} \tag{4-4}$$

$$r = \frac{R_t/t_w}{400} \tag{4-5}$$

E is the steel elastic Young's modulus, f_y the corresponding yield strength, t_w the wall thickness, σ_{c1} the ideal critical buckling stress for cylinders loaded in axial compression and p the maximum interior pressure acting on the tank wall. The interior pressure is the direct sum of the hydrostatic (p_h) and impulsive component (p_i). The latter may be estimated by adopting a cylindrical coordinate system, using the non-dimensional coordinates ξ (radial), ζ (height), φ (angle), as:

$$p_i(\xi,\zeta,\varphi,t) = C_i(\xi,\zeta)\rho_f h_f \cos\varphi A(t) \tag{4-6}$$

C_i is a function that provides the distribution of p_i along the tank elevation, ρ_f is the fluid density, h_f the contained fluid height and $A(t)$ is the impulsive mass absolute acceleration response history (Malhotra and Veletsos 1994c). As a side note, the EFB check should not be limited to the lower course of the tank shell where the maximum interior pressure occurs, but should rather be extended to the entire tank elevation, especially when the wall thickness is not uniform. Although one could derive a simple relationship for the stress distribution over height, this step may be ignored as in most cases the lowest course is the most critical one.

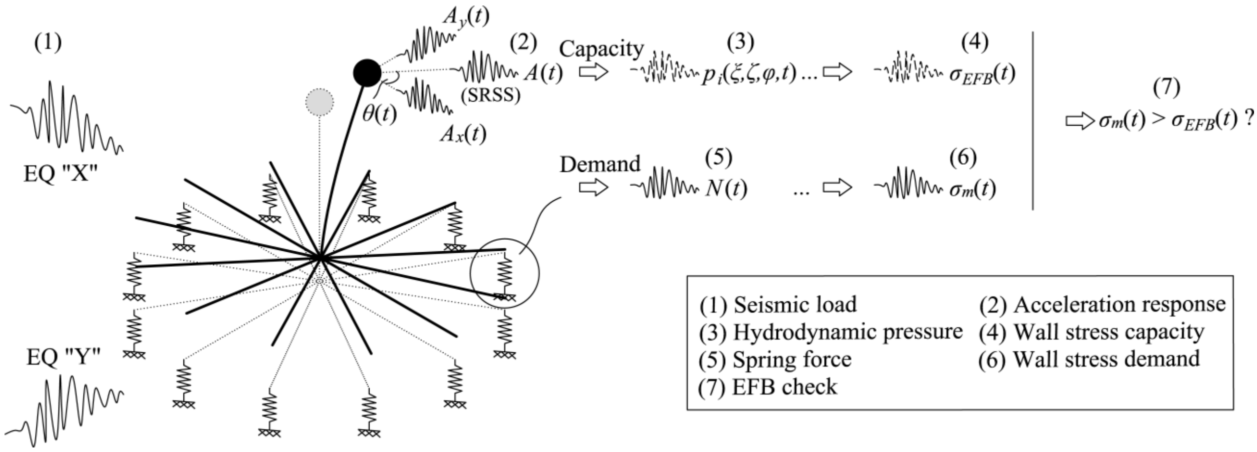

Figure 4-2: EFB violation check using the "Joystick" model instantaneous demand and deterministic capacity estimates.

4.5.5 Special considerations for EFB

4.5.5.1 EFB conditioned on the ground motion record

Eq. (4-3) provides a useful approximation to assess the occurrence of EFB. Still, its accurate application is not as simple since the stress limit (σ_{EFB}) provided is a decreasing function of the impulsive pressure [Eq. (4-6)] at each location (φ), and thus the absolute acceleration demand (and hence the seismic intensity). According to Eq. (4-3)-(4-6), EFB stress capacity is both location and time-dependent, and so is the corresponding stress demand. Thus, at every time step, $\sigma_m(t)$ and $\sigma_{EFB}(t)$ need to be evaluated for each edge-spring on the "Joystick" model, effectively discretising the continuous tank wall (as well as the associated checks) into n positions. It should be noted that the EFB demand appears to be more sensitive to the base plate discretisation, thus requiring 30 to 60 spokes, as opposed to other global response parameters (e.g. uplift) where only 8 spokes are sufficient (Bakalis et al. 2017a; Malhotra and Veletsos 1994b). In general, as the tank radius grows, the number of spokes should be increased to achieve a better discretisation. A good rule-of-thumb would be to target at least an arc length of 2-3m for each spoke.

For a given fraction of time, each evaluation consists of estimating the vector-sum of the longitudinal and transverse component response accelerations [i.e. $A_x(t)$, $A_y(t)$] and its orientation [i.e. $\theta(t)$], vis-à-vis the earthquake (EQ) "X" and "Y" axes (Figure 4-2). Using Eq. (4-6), this results in the instantaneous pressure for each spoke located at an angle φ from the vector of $A(t)$. The sum of p_i and p_h determine the instantaneous $\sigma_{EFB}(t)$ capacity of any single spoke. Conversely, the strip model [Figure 4-1(c)] demand of compressive axial force $N(t)$ at each edge-spring, divided by the corresponding tank wall cross-section, provides the local stress demand $\sigma_m(t)$. Assuming no further uncertainties enter into the estimation of $\sigma_{EFB}(t)$, a straightforward comparison among $\sigma_m(t)$ and $\sigma_{EFB}(t)$ determines violation as shown in Figure 4-3 for the case of a squat tank, the properties of which are summarised in Table 4-1 among other configurations that will later be examined. A preliminary investigation showed that the effect of vertical acceleration was evident on the EFB capacity only (not on any demand), and then for specific tanks and ground motion records. Therefore, the vertical component was not considered in our analyses, although the model adopted can easily accommodate it.

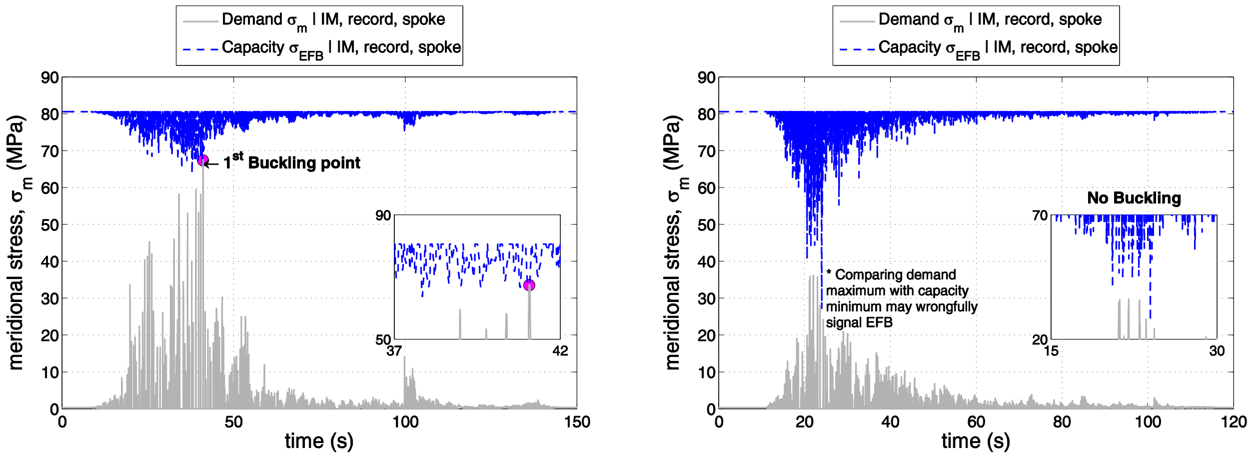

Figure 4-3: IM, record and spoke-specific EFB capacity versus demand response histories for the unanchored tank A (Table 4-1): (a) intersection among time-dependent demand and capacity signals EFB; (b) EFB capacity is not exceeded even though the associated time-independent maximum demand and minimum capacity indicate so.

Capturing EFB becomes more complex when capacity dispersion appears due to uncertainty. Given the time dependence of EFB capacity and demand, the EFB probability of exceedance for a given record, *IM* level and spoke becomes the union of the individual probabilities of EFB occurring at any single moment of time. To avoid a cumbersome bookkeeping and post-processing procedure where entire $\sigma_m(t)$ and $\sigma_{EFB}(t)$ response histories would need to be assessed, the simpler peak "demand-over-capacity" ratio exceeding unity is preferred (Figure 4-3). Evidently, the peak $\sigma_m(t)/\sigma_{EFB}(t)$ ratio provides the demand and capacity values that should be recorded for each spoke during every nonlinear response history analysis.

$$\mathrm{P}[\mathrm{EFB} \mid IM, record, spoke] \cong \mathrm{P}\left[\left(\max_t \frac{\sigma_m(t)}{\sigma_{EFB}(t)}\right) > 1 \mid IM, record, spoke\right] \tag{4-7}$$

4.5.5.2 Extent of damage

Of potential interest is also the extent of EFB damage, as according to studies based on detailed finite element models (e.g. Bakalis et al. 2017; Buratti and Tavano 2014) it is highly unlikely that the examined buckling mode of failure is restrained to small arc lengths covered by a single beam-spoke. Figure 4-4(a), compares the EFB capacity for a given *IM* level and record to the corresponding demand along the circumference of the tank. It seems that although the buckling zone spreads on a significant number of beam spokes, there are several locations where the capacity has not been reached. Lengthwise, buckling spreads on two nearly identical (as well as symmetrical) subzones, a fact that is indicative of the system's tendency (in this case) to rock along a maximum response axis [see also Manos et al. (1989)]. Obviously, these results should be interpreted in tandem with experimental or finite element analysis results, as the weakening of the tank wall, not captured by the “Joystick” model, may indeed promote the spread of buckling beyond our simpler estimates.

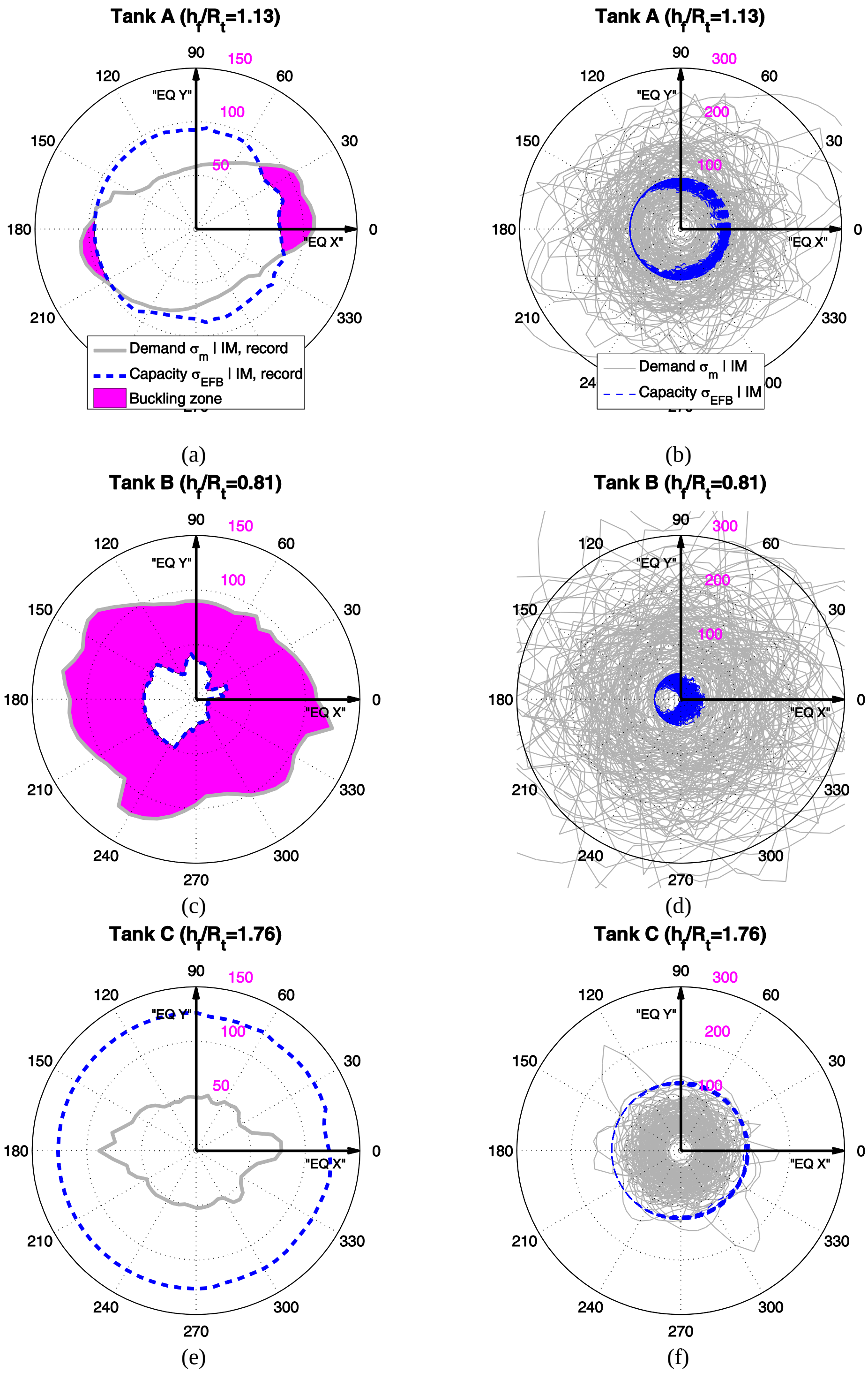

Figure 4-4: EFB capacity versus demand stresses (in MPa) along the circumference of the unanchored tanks presented in Table 4-1, conditioned on PGA= 0.30g: (a) single record pair and (b) 135 record pairs.

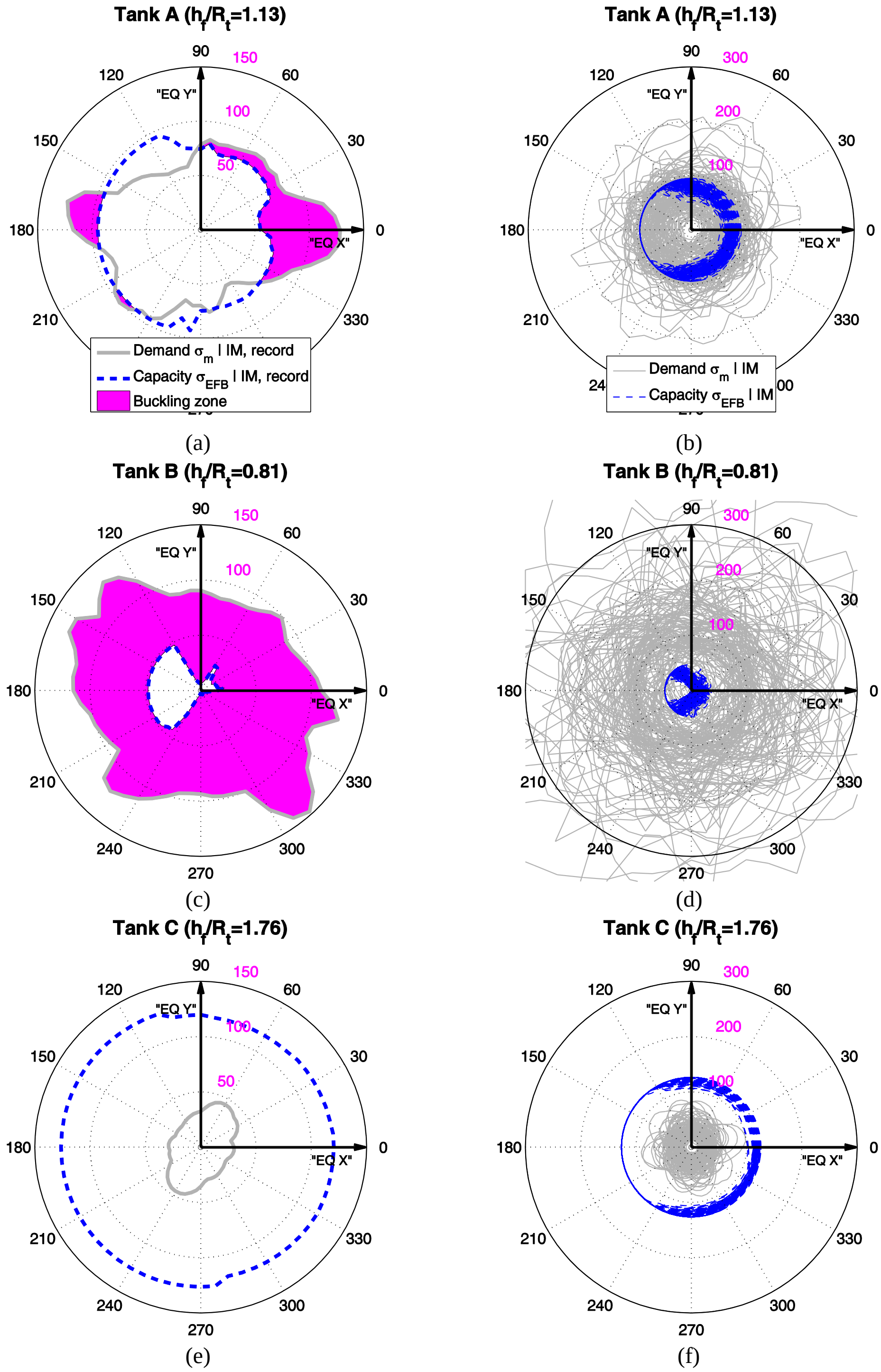

Figure 4-5: EFB capacity versus demand stresses (in MPa) along the circumference of the anchored tanks presented in Table 4-1, conditioned on *PGA*= 0.30g: (a) single record pair and (b) 135 record pairs.

4.5.5.3 EFB conditioned on the *IM* level

Figure 4-4(b) illustrates the EFB capacity and demand along the circumference of the tank, for a given earthquake intensity, using a set of 135 large-magnitude ordinary (i.e. non pulse-like, non long-duration) ground motion pairs obtained from the PEER-NGA database (Ancheta et al. 2013). The considerable variability revealed for the capacity as well as the demand indicates that there are certain records where capacity is not exceeded at any part of the tank, others where it is exceeded everywhere, and some that follow the partial violation pattern shown in Figure

4-4(a). One may also notice the effect of directionality that derives from the combination of longitudinal and transverse earthquake components in time (Figure 4-2), determining a different axis of maximum demand for each ground motion pair.

4.5.5.4 EFB on the IDA plane

A better understanding regarding the detailed representation of EFB may be obtained through IDA (Vamvatsikos and Cornell 2002), for the record suite previously adopted. The results shown in Figure 4-6(a) display the single-record (pair) IDA curves using the meridional stress as an appropriate *EDP* and the peak ground acceleration (*PGA*) as a representative *IM*. It should be noted that the response history analysis is performed using both longitudinal and transverse ground motion accelerograms (Figure 4-2), which implies that a unique scale factor has been applied on both accelerograms for each ground motion pair and that the *PGA* refers to the geometric mean of the two. The light-coloured solid lines form the demand for an arbitrary edge-spring on the “Joystick” model, while the dark dashed ones depict the associated buckling capacity variability for the given range of *IM* levels. The initial buckling capacity at rest (i.e. for a *PGA*=0) refers to the static load case of the liquid storage system, where the maximum internal pressure equals the corresponding hydrostatic. For larger *PGA* estimates, the impulsive pressure adds on to the hydrostatic component on the compressive side of the tank, which results in a significant reduction of the EFB capacity. Intersection among capacity and demand curves for each record provides the individual EFB limit state capacity points.

Figure 4-6(b) shows a more comprehensive representation of EFB. In particular, the entire capacity-demand space is presented through the single-record IDAs for every beam-spoke that forms the base plate of the “Joystick” model. EFB capacity points that represent failure on *any* single spoke (i.e. 1st-spoke failure pattern) are compared to a more extensive state of damage that spreads on 50% of the tank circumference (i.e. multi-spoke failure pattern). The 50% spread of damage is arbitrarily chosen and thus a different value could be used upon the availability of relevant (experimental/structural analysis) data. Comparing the two approaches reveals a clear-yet marginal-shift of the multi-spoke failure to higher *PGA* estimates, which practically triggers the discussion between localised and widely spread buckling.

Traditionally, common approaches for capturing buckling modes conservatively rely on the first point/element on a structure whose demand exceeds the prescribed capacity (e.g. single-spoke failure). Although for the purpose of this study the single-spoke pattern is conservatively adopted to signal EFB, Figure 4-6(b) highlights the abilities of the “Joystick” model to capture limit state capacities that are defined based on the extent of EFB (or any other) mode of failure and could potentially provide a more refined approach in terms of loss. In reality, EFB induces a local instability on the actual tank (not captured by the “Joystick” model) that causes a modification of its properties such that buckling is potentially easier to spread than is shown herein. This is generally tough to quantify, and thus the purpose of this analysis is to indicatively shed some light on the spread of buckling, pending further calibration. The estimate provided remains a useful approximation barring the use of more complex models.

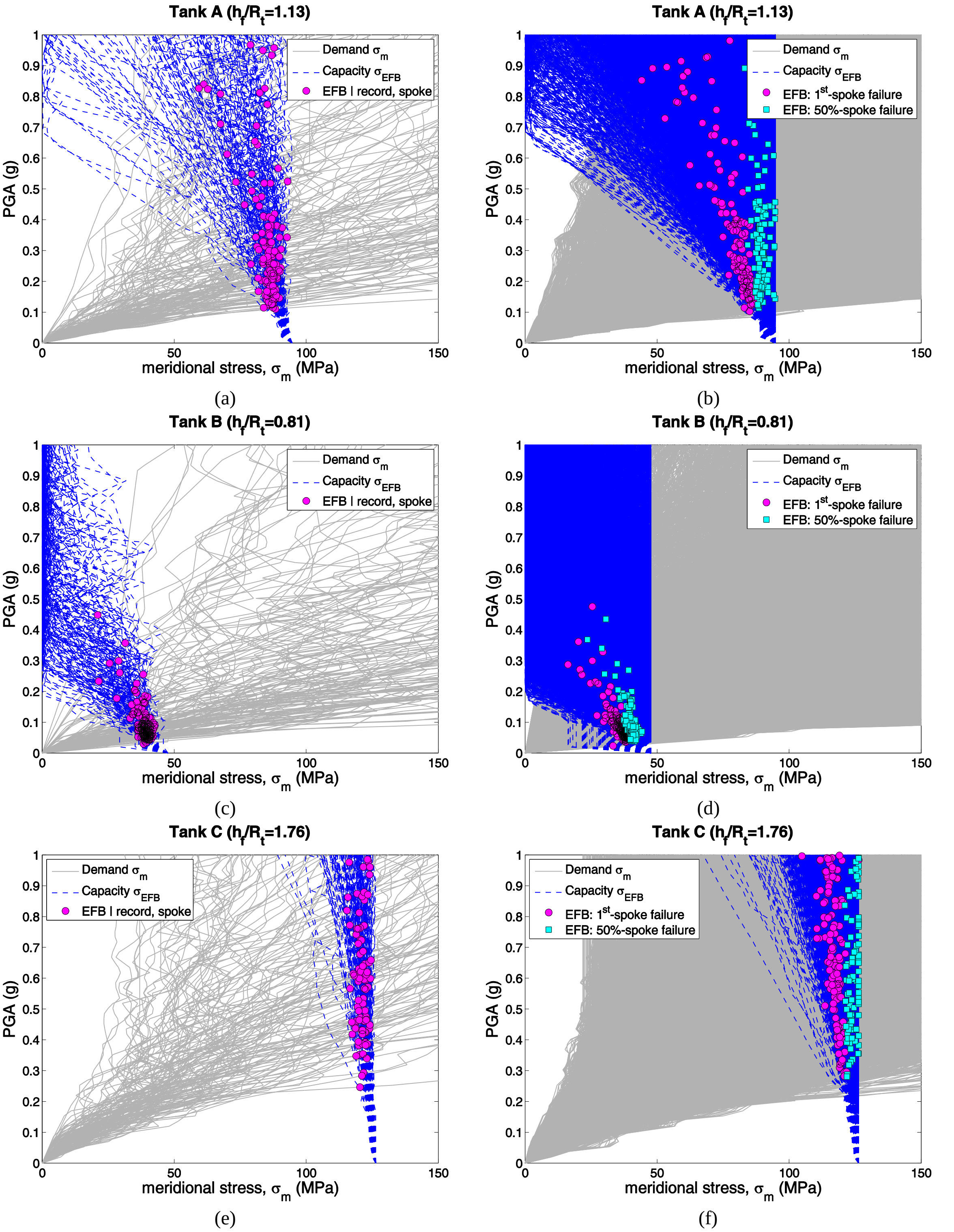

Figure 4-6: (a, c, e) EFB demand versus capacity single-record (pair) IDA curves for an arbitrarily chosen edge-spring on the "Joystick" model. (b, d, f) Single versus multi-spoke EFB failure on the demand-capacity space formed by single-record (pair) IDA curves for the entire set of edge-springs found on the base of the "Joystick" model. The results refer to the unanchored tanks presented in Table 4-1.

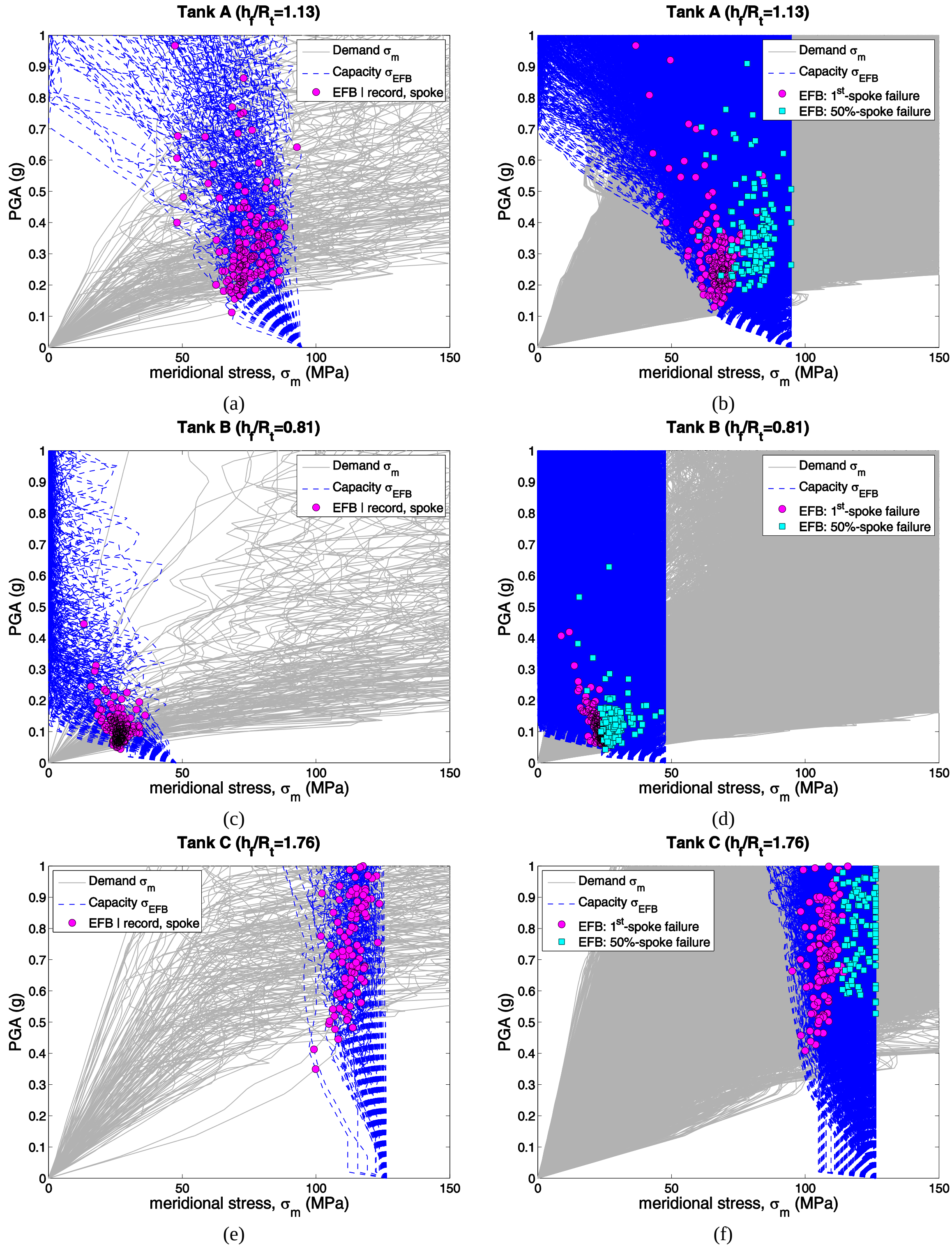

Figure 4-7: (a, c, e) EFB demand versus capacity single-record (pair) IDA curves for an arbitrarily chosen edge-spring on the “Joystick” model. (b, d, f) Single versus multi-spoke EFB failure on the demand-capacity space formed by single-record (pair) IDA curves for the entire set of edge-springs found on the base of the “Joystick” model. The results refer to the anchored tanks presented in Table 4-1.

Table 4-1: Properties of the tanks examined (Bakalis et al. 2017a).

Properties	Variable description	Notation (units)	Numerical values		
			Tank A	Tank B	Tank C
Tank	Radius	R_t (m)	13.9	23.47	6.1
	Height	h_t (m)	16.5	19.95	11.3
	Wall thickness per course	t_w (mm)	17.7;15.7;13.7;11.7; 9.7;7.8;6.4;6.4;6.4	22.23;18.93;16.24;13.57; 10.9;8.22;8.0;8.0;8.0	9.6;8.0;6.4;4.8
	Base plate thickness	t_b (mm)	6.4	6.4	4.8
	Annular ring thickness	t_a (mm)	8.0	10.0	4.8
	Roof mass	m_r (ton)	35	46	19
Material	(expected) Yield strength	f_y (MPa)	280	280	280
	Steel Young's Modulus	E (GPa)	210	210	210
	Hardening ratio	a_h (%)	1	1	1
	Poisson's ratio	v (-)	0.3	0.3	0.3
Fluid	Height	h_f (m)	15.7	18.95	10.74
	Density	ρ_f (kg/m^3)	1000	1000	1000

4.6 DAMAGE STATES

In modern probabilistic seismic assessment framework (Cornell and Krawinkler 2000) damage is discretised into a number of (typically consecutive) damage states that are chosen to represent consequences of increasing severity, based on the failure modes that a structure is prone to exhibit. For instance, design codes for buildings define performance levels similar to "Immediate Occupancy" and "Collapse Prevention". Uncontrollable socioeconomic consequences encountered after past earthquakes (Girgin 2011), however, establish such performance objectives totally unfit for the seismic risk evaluation of industrial facilities. For the case of liquid storage tanks, the most damaging failure modes are the ones that may result in loss of containment, while other modes are mainly confined to structural damage without leakage. Figure 4-8 presents the associated failure modes on the median IDA curve both for an anchored and an unanchored system (Table 4-1). Unlike Figure 4-6 where EFB is examined in detail and hence σ_m is employed as the *EDP*, in this instance the base uplift is shown instead. Although it does not directly relate to the entire set of failure modes outlined in previous sections, the intuition it provides in terms of global (system) deformation is similar to response parameters such as roof displacement and maximum inter-storey drift for buildings, thus allowing for a rough illustration of the damage progression on the tank.

A further classification based on the damage of individual components becomes quite informative, where the upper course of the tank (SL=sloshing), its lower course (EFB), the base plate (θ_{pl}), and the anchors (AN=anchorage failure) are separately examined. Table 4-2 presents the component-level median damage state capacities along with their associated dispersions and engineering demand parameters. In absence of relevant experimental data, the strength-based (for EFB), ductility-based (for θ_{pl}, AN) and displacement-based (for SL) approximations of the FEMA P-58 (FEMA 2012b) guidelines are employed to derive the dispersion around the lognormally distributed capacities of the aforementioned failure modes. Given that the random variables presented in Table 4-2 refer to different parts of the tank, as well as that hardly any relevant data exists, correlation among the capacities of the examined failure modes has been assumed to be zero. Non-zero positive correlation may reasonably be adopted for the capacity of damage states referring to the same component, e.g. θ_{pl} capacity values for consecutive damage states at the same location (i.e. spoke) of a tank. For a more realistic representation, spatial correlation of DS capacity values among different spokes also becomes an issue. Yet, such considerations are beyond the scope of this study as they burden the post-processing considerably.

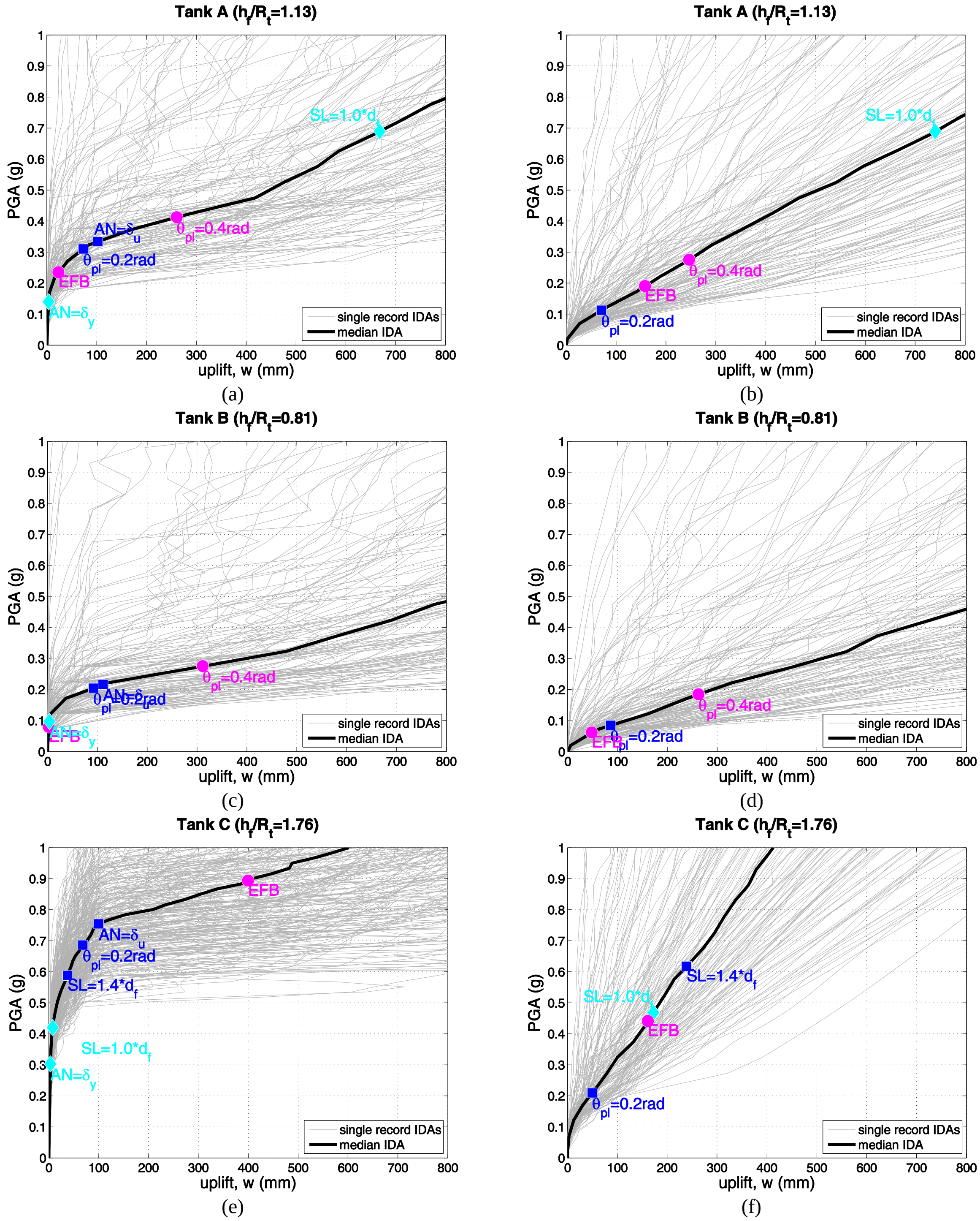

Figure 4-8: Single-record (pair) IDAs along with the associated failure modes on the median IDA curve for liquid storage tank presented in Table 4-1: (a, c, e) anchored and (b, d, f) unanchored support conditions.

In this study, the aforementioned failure modes are appropriately combined to form four damage states of increasing severity, namely no damage (*DS*0), minor (*DS*1), severe without leakage (*DS*2) and loss of containment (*DS*3), as originally proposed in (RASOR 2015; Vathi et al. 2015). It should be noted that the loss of containment is generally the main concern post-earthquake, as it constitutes a paramount source of industrial accidents with severe socioeconomic and environmental consequences (Fabbrocino et al. 2005). Still, structural damage itself (with or without leakage) is also of concern, since its aftermath is not confined to monetary losses only. The reason is that frequent earthquakes of moderate intensity, may trigger a list of actions that include drainage of the tank, repair and refill. This is often inferred as a major disruption of business, the financial impact of which cannot be ignored.

In that sense, for the case of unanchored (or self-anchored) liquid storage tanks, *DS*1 shall represent minor damage induced by a sloshing wave height of the contained fluid equal to the freeboard. *DS*2 shall refer to severe damage at any component of the tank without leakage, where the exceedance of either a sloshing wave height equal to 1.4 times the available freeboard or a plastic rotation of 0.2rad at the base plate shall trigger the damage state violation. *DS*3, finally, shall provide information on the loss of containment through the exceedance of either the EFB capacity (σ_{EFB}) or the base plate plastic rotation of 0.4rad. While some further partitioning of the loss of containment damage states based on the amount of leakage would be desirable, there is little data available to define appropriate *EDP* thresholds. As far as anchored systems are concerned, yielding on the anchors or their connection to the tank may also be considered for *DS*1, while fracture for *DS*2, as shown in Table 4-3. This classification reasonably conveys the extent of system damage, yet one should bear in mind that the different mechanisms involved in a single damage state may be associated with varying degrees of monetary loss or repair actions. For instance, sloshing waves whose amplitude exceeds the available freeboard represent relatively easy-to-repair damage at the top of the tank, compared to the exceedance of a plastic rotation limit at the base, even though both might be categorised as moderate damage. Therefore, it becomes more informative to also classify damage based on the actual component that has failed, as shown in Table 4-2.

Table 4-2: Component-level *DS* classification for anchored and unanchored liquid storage tanks.

Component	**Failure Mode Notation**	**Median EDP Capacity ($EDP_{C,50\%}$)**	**Reference**	**Dispersion*** (FEMA 2012b)
Upper tank course	SL	$1.0\times d_f$ (m)	(American Petroleum Institute 2007)	0.20
		$1.4\times d_f$ (m)	(American Petroleum Institute 2007)	0.20
Lower tank course	EFB	σ_{EFB} (MPa)	(CEN 2006)	0.31
Base plate	θ_{pl}	0.2 (rad)	(CEN 2006)	0.51
		0.4 (rad)	(Cortés et al. 2011)	0.51
Anchors	AN	δ_y (mm)	-	0.51
		δ_u (mm)	-	0.51

*The standard deviation of the log values

Table 4-3: System-level *DS* classification for anchored and unanchored liquid storage tanks.

System Support Conditions	**Damage States**	**Damage State Capacities**
Anchored	*DS*1	$1.0\times d_f$ or δ_y
	*DS*2	$1.4\times d_f$ or θ_{pl}=0.2rad or δ_u
	*DS*3	σ_{EFB} or θ_{pl}=0.4rad
Unanchored	*DS*1	$1.0\times d_f$
	*DS*2	$1.4\times d_f$ or θ_{pl}=0.2rad
	*DS*3	σ_{EFB} or θ_{pl}=0.4rad

4.7 SEISMIC FRAGILITY ASSESSMENT

Under the typical assumption of lognormality for both demand (*D*) and capacity (*C*) (valid for *EDP* demand away from the global instability region only), the probability that the median demand exceeds the associated damage state capacity for a given level of seismic intensity, may be estimated using either of *EDP* or *IM* ordinates (i.e. *EDP*-basis versus *IM*-basis estimation Bakalis and Vamvatsikos 2017; Vamvatsikos and Cornell 2004) through the standard normal cumulative distribution function Φ as:

$$\mathrm{P}\left[D > C \mid IM\right] = \Phi\left(\frac{\ln EDP(IM)_{50\%} - \ln EDP_{C,50\%}}{\beta_{EDP}}\right) = \Phi\left(\frac{\ln IM - \ln IM_{C,50\%}}{\beta_{IM}}\right) \quad (4\text{-}8)$$

$EDP(IM)_{50\%}$ is the median *EDP* demand given the *IM*, $EDP_{C,50\%}$ and $IM_{C,50\%}$ are the median limit state capacities expressed in *EDP* and *IM* terms respectively, while β_{EDP} and β_{IM} the total *EDP* and *IM*-basis dispersions that take into account both aleatory and epistemic sources of uncertainty [see Bakalis and Vamvatsikos (2017) for their explicit definition)].

The parameters found in Eq. (4-8) incorporate the *IM*, and as a result accurately estimating seismic fragility requires an intensity measure that characterises the structural system’s response in an optimal manner. According to Luco and Cornell (Luco and Cornell 2007), the answer to this problem is not distinct, as the well-known criteria of sufficiency, efficiency and practicality must be satisfied. In particular, the optimal *IM* should render the structural response independent of seismological characteristics appearing as variables in the probabilistic seismic hazard assessment (e.g. magnitude, distance, epsilon), it should be able to reduce dispersion in the *EDP*|*IM* (or *IM*|*EDP*) relationship and thus the number of ground motion records required to achieve the same level of accuracy, while at the same time it should be possible to compute the corresponding hazard curve. For the case of liquid storage tanks, either of the *PGA* and the spectral acceleration at the impulsive period [$S_a(T_i)$] is a reasonable choice due to the relatively short impulsive period (T_i); still, the convective response can only be adequately captured through the corresponding convective spectral acceleration that is poorly described by the short T_i. This is an interesting problem that requires delicate handling and is expected to be covered in a future direction of our research.

4.8 PARAMETRIC INVESTIGATION

4.8.1 Component-level evaluation

In order to assess the seismic fragility involved in liquid storage systems, three tanks of varying aspect ratios (h_f/R_t) are considered (Table 4-1), covering a range of broad to slender structural system configurations. The estimation is initially performed on a component-basis (Table 4-2), using the various analysis methodologies discussed above. In this instance, the liquid storage systems are considered unanchored, with the results of this process summarised in Figure 4-10, in terms of median *IM* capacity and the associated dispersion (see also the component fragility curves in Figure 4-12). Offering a detailed view of demand at each *IM* level, IDA is adopted herein as a benchmark solution to discuss the validity and applicability of a simplified (computationally inexpensive) cloud approach that utilises only a single suite of unscaled ground motions and a global power-law fit in the *EDP-IM* space (e.g. Figure 4-9).

Comparing the cloud analysis results to IDA presents a reasonable agreement for certain failure modes. As far as EFB is concerned, a good agreement is observed for all unanchored tanks, despite the slight reduction of the tank B cloud-based dispersion. Regarding θ_{pl} limit states (i.e. 0.2 and 0.4rad), the agreement is very good in terms of median *IM* capacity; however, the dispersions stemming from cloud analysis seem to deviate by scale factors that are in the order of 1.3-2, mostly attributed to the estimation of a single dispersion value by the global fit. Note that the maximum probability of exceedance on the IDA-based fragility output regarding the 0.4rad limit state capacity on tank C, hardly yields 20% (even for large *PGA* estimates), which implies that such a capacity is practically never reached on this particular structural system, and thus the corresponding fragility curve for cloud analysis need not be considered.

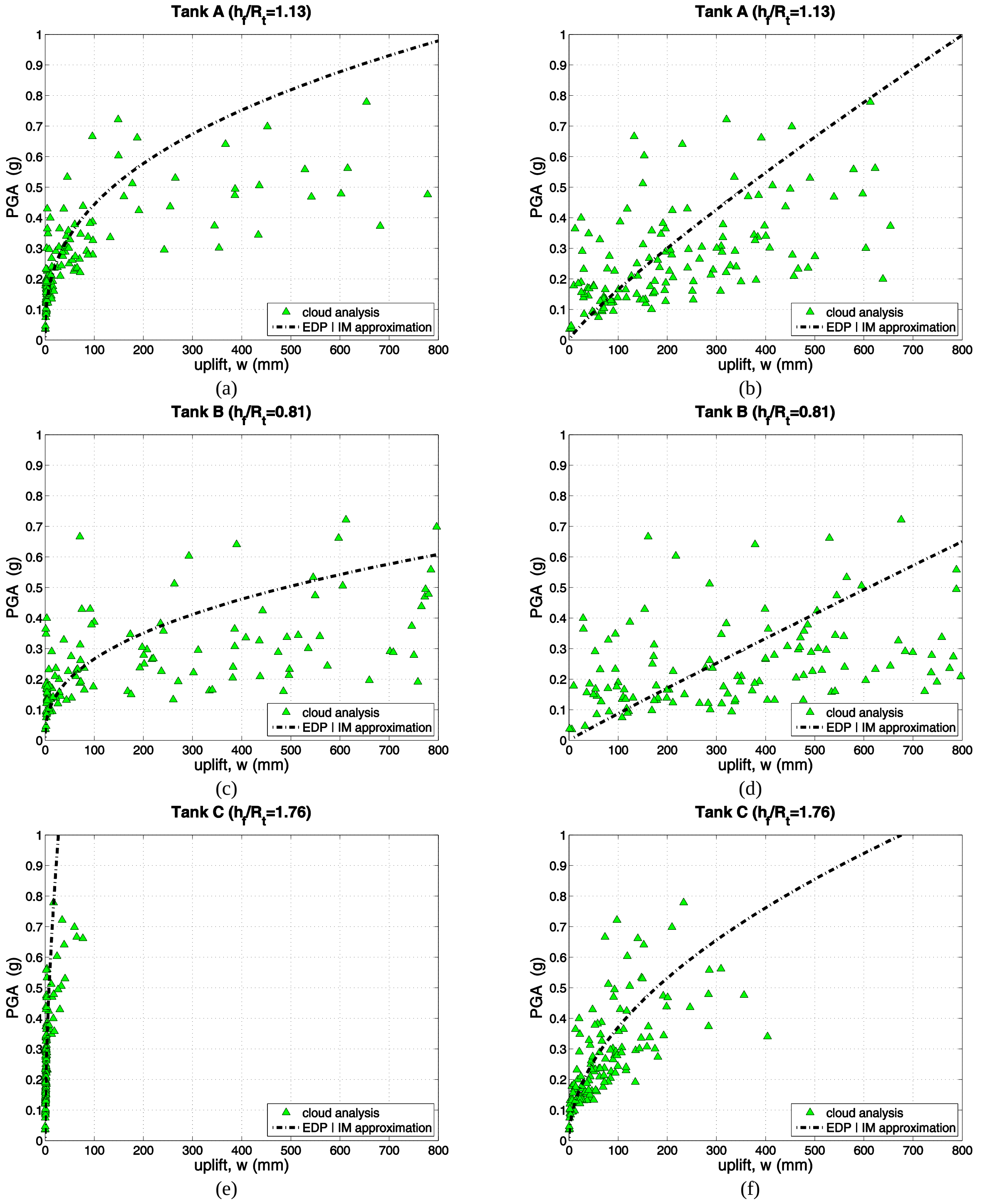

Figure 4-9: Cloud analysis and fitted (global) *EDP-IM* relationship for the liquid storage tanks presented in Table 4-1: (a, c, e) anchored and (b, d, f) unanchored support conditions.

Fragility parameters cannot be estimated for sloshing modes of failure, for all structural systems considered, thus proving the global fit adopted in that instance (combined with the sloshing-insufficient *IM* choice of *PGA*) to be inappropriate.

At this point one may rush into the conclusion that simplified cloud analysis cannot always be trusted within a seismic risk assessment framework, as the assumption that "certain failure modes might not be adequately captured" cannot be overruled. The truth is that some care should be exercised when employing simplified approaches within a PBEE framework. For example, the cloud method adopted is sensitive to pre-processing tasks such as the record selection and the associated scaling. These parameters essentially determine the extent of the *EDP-IM* space, and thus the ability to capture certain damage state capacities that are found in rather large response parameter values. Undeniably, our case study also suffers from such issues, as the (unscaled) record-set that has been used does not provide an adequate number of analysis data points around certain *EDP* capacities of interest, that would otherwise lead to a more accurate regression analysis output. Note that the simplified cloud-based assessment cloud also be refined by adopting a local fit in place of the global one shown in Figure 4-9. Despite the aforementioned problems and their rather complex nature, cloud analysis still remains probably the best alternative to IDA, for cases that the latter is deemed computationally prohibitive.

4.8.2 System-level evaluation

Following the comparison of the various analysis methodologies and their effect on the seismic fragility parameters, the system-level evaluation is performed for the entire set of liquid storage tanks, considering both anchored and unanchored support conditions (Table 4-3). The aim is to assign a single damage state that could be useful in several instances such as regional loss assessment or the assessment of an entire tank-farm, similar to the HAZUS methodology (FEMA 2003). For the sake of brevity, only the IDA-based fragilities for unanchored support conditions are illustrated in Figure 4-12. The entire seismic fragility assessment procedure is summarised in Table 4-4, where parameters such as the median *IM* capacity ($IM_{C,50\%}$) and the associated (total) dispersion (β) are provided for the corresponding fragility curve construction. The dominant failure mode (DFM) as well as the order that each damage state appears during a strong ground motion, are also provided in order to highlight the complexities involved in the assessment of cylindrical liquid storage systems. Special attention is paid to the compound system-level damage states (i.e. damage states that depend on the union of the exceedance of two or more failure mode capacities, e.g. *DS*2 and *DS*3 for unanchored tanks), where a simple Monte Carlo integration is required to estimate the associated probability of exceedance (Bakalis and Vamvatsikos 2018). A good example to appreciate the importance of this procedure can be given through the final fragility product of *DS*2 and *DS*3 for the unanchored tank A [Figure 4-12(b)]. According to Figure 4-12(a), it appears that although the plastic rotation clearly dominates the response of *DS*2, a similar conclusion cannot be drawn for *DS*3 as the plastic rotation appears to influence lower *IM* levels contrary to EFB that is more probable for higher ones.

A closer look on the results of Table 4-4 suggests that even though the sloshing mode governs the response for all unanchored systems with respect to *DS*1, the corresponding response for anchored tanks is dominated by yielding of the anchor bolts, for considerably smaller median PGA estimates. *DS*2 on the other hand, reveals the plastic rotation as the dominant failure mode for every case of unanchored tanks, while for the case of anchored ones the prevalent response cannot be distinguished among the failure modes considered, and therefore it is deemed "inconclusive". In addition, EFB is the mode of failure that controls *DS*3 for all systems examined (both anchored and unanchored). The beneficial effect of the anchors is also highlighted through the seismic fragility estimation of *DS*2 and *DS*3, where each failure mode (unrelated to anchors) is developed for significantly higher intensities, as shown in Table 4-4. Finally, another major conclusion that can be drawn from the assessment procedure, is that the damage states developed do not follow a priori the intuitive order which dictates that increasing intensities result in increasing levels of damage. This issue of non-sequential damage states highlights the fact that certain tanks may progress directly to catastrophic levels of damage without any warning (e.g. progression through lesser damage states).

Table 4-4: System-level seismic fragility assessment of the tanks examined.

Tank	DS1			DS2			DS3			Order of *DSi*
	$IM_{C,50\%}$ (g)	β	DFM*	$IM_{C,50\%}$ (g)	β	DFM*	$IM_{C,50\%}$ (g)	β	DFM*	
Unanchored A	0.689	1.349	SL	0.117	0.758	θ_{pl}	0.168	0.620	EFB	2-3-1
Anchored A	0.130	0.479	AN	0.274	0.383	inconclusive	0.233	0.359	EFB	1-3-2
Unanchored B	1.069	1.382	SL	0.090	0.829	θ_{pl}	0.056	0.767	EFB	3-2-1
Anchored B	0.089	0.480	AN	0.187	0.441	inconclusive	0.076	0.385	EFB	3-1-2
Unanchored C	0.468	1.012	SL	0.201	0.631	θ_{pl}	0.378	0.628	EFB	2-3-1
Anchored C	0.265	0.566	inconclusive	0.512	0.622	inconclusive	0.672	0.344	EFB	1-2-3

*Dominant Failure Mode

4.9 SEISMIC RISK ASSESSMENT

The ultimate goal of seismic assessment lies in the mean annual frequency (λ) estimation for any set of consequences (or decision variables in the terminology of the (Cornell and Krawinkler 2000) PBEE framework). This may be achieved, e.g., for monetary losses either by defining them at the global system-level in a manner similar to HAZUS (FEMA 2003), or by employing the more detailed local component-level *DS* classification and appropriate cost functions, thus adopting a format akin to FEMA P-58 (FEMA 2012b). With such data available, the implementation according to any of the two standards should be straightforward [see also D'Ayala et al. 2015)].

The simpler estimation of the MAF of discrete limit-states is normally performed through an integration on the product of the site-specific hazard function $\lambda(IM)$, typically obtained through probabilistic seismic hazard analysis (PSHA), with any of the aforementioned fragility curves (i.e. P[D>C|IM]) (Vamvatsikos 2013; Vamvatsikos and Cornell 2004):

$$\lambda(DS) = \int_{IM} \mathrm{P}[D > C|IM]\,|\mathrm{d}\lambda(IM)| \qquad (4\text{-}9)$$

For the purposes of this study, the Elefsina, Greece hazard curve is adopted (Giardini et al. 2013), targeting a site of major refineries. The results shown in Figure 4-14 summarise the component as well as system-level seismic risk assessment in terms of mean return period (T_r=1/λ). As expected, from a qualitative perspective, the results are not any different from the ones shown in the seismic fragility section (Figure 4-12). In fact, the discrepancies noticed among the various structural systems and analysis methodologies are nearly identical. However, the view they offer is of a slightly different nature, as they essentially provide an indication of how rare a certain failure mode (or state of damage) is on the site under investigation, or in other words the failure modes that each system is prone to experience during earthquakes consistent with the site. What really matters in this case is the order of magnitude of the various return periods.

For instance, sloshing modes of failure can generally be considered rare events (for the given combination of site and tanks), as the mean return periods they develop are considerably higher compared to plastic rotation and EFB. The well-known return periods that correspond to "10% in 10 years" and "10% in 50 years" probability of exceedance (i.e. 95 and 475 years respectively) are also provided as reference lines, potentially useful as *DS*1 and *DS*2 performance targets respectively. As a general remark, the system-level results closely follow the worst of the relevant component-level ones, unless the dominant failure mode is highly inconclusive. At the same time, the majority of failure modes develop return periods that cannot even capture the indicative "10% in 10 years" objective, which highlights the vulnerability of the structural systems considered against the chosen site hazard. Catastrophic damage (i.e. *DS*2, *DS*3) can be several times more probable than light sloshing damage (i.e. *DS*1 for unanchored tanks), a direct consequence of the long convective period component that is not sufficiently excited by the moderate magnitude events and the rocky profile of the Elefsina site. The aforementioned observation stands regardless of the analysis approach, despite the considerable differences in terms of mean return period.

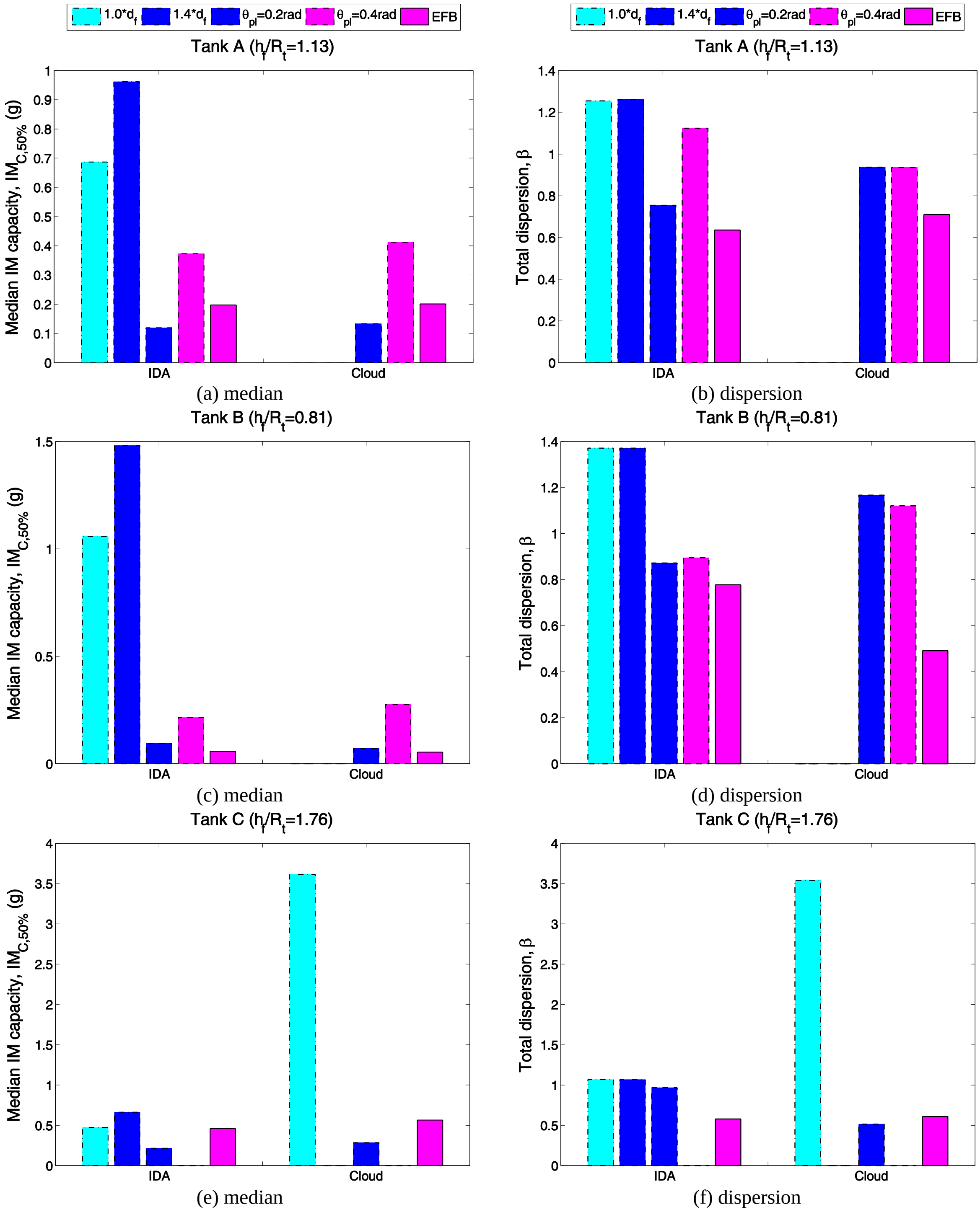

Figure 4-10: IDA versus cloud-based component-level seismic fragility evaluation: [(a), (c), (e)] median *IM* capacity and [(b), (d), (f)] total dispersion. The results refer to the liquid storage tanks of Table 4-1 for unanchored support conditions.

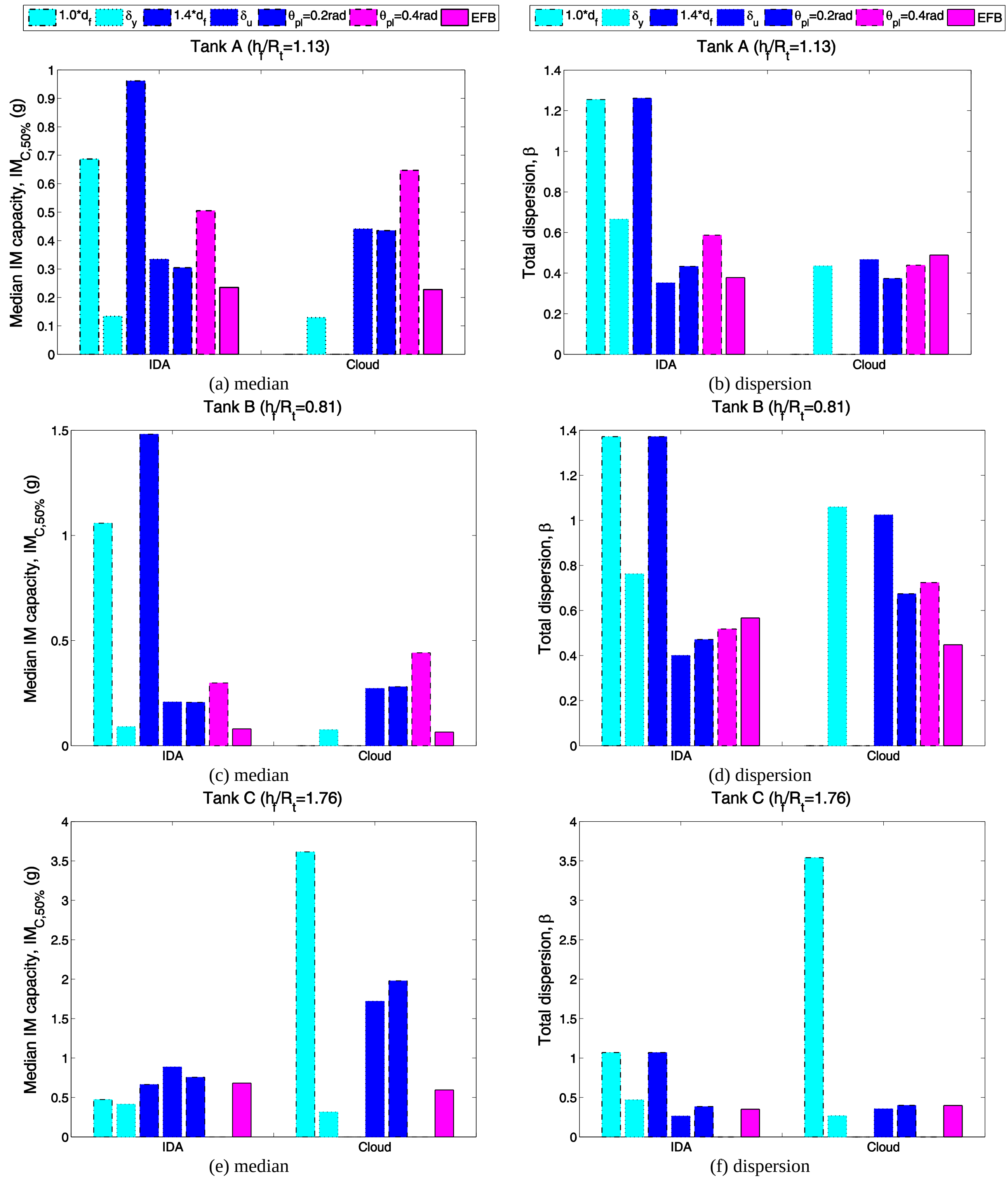

Figure 4-11: IDA versus cloud-based component-level seismic fragility evaluation: [(a), (c), (e)] median *IM* capacity and [(b), (d), (f)] total dispersion. The results refer to the liquid storage tanks of Table 4-1 for anchored support conditions.

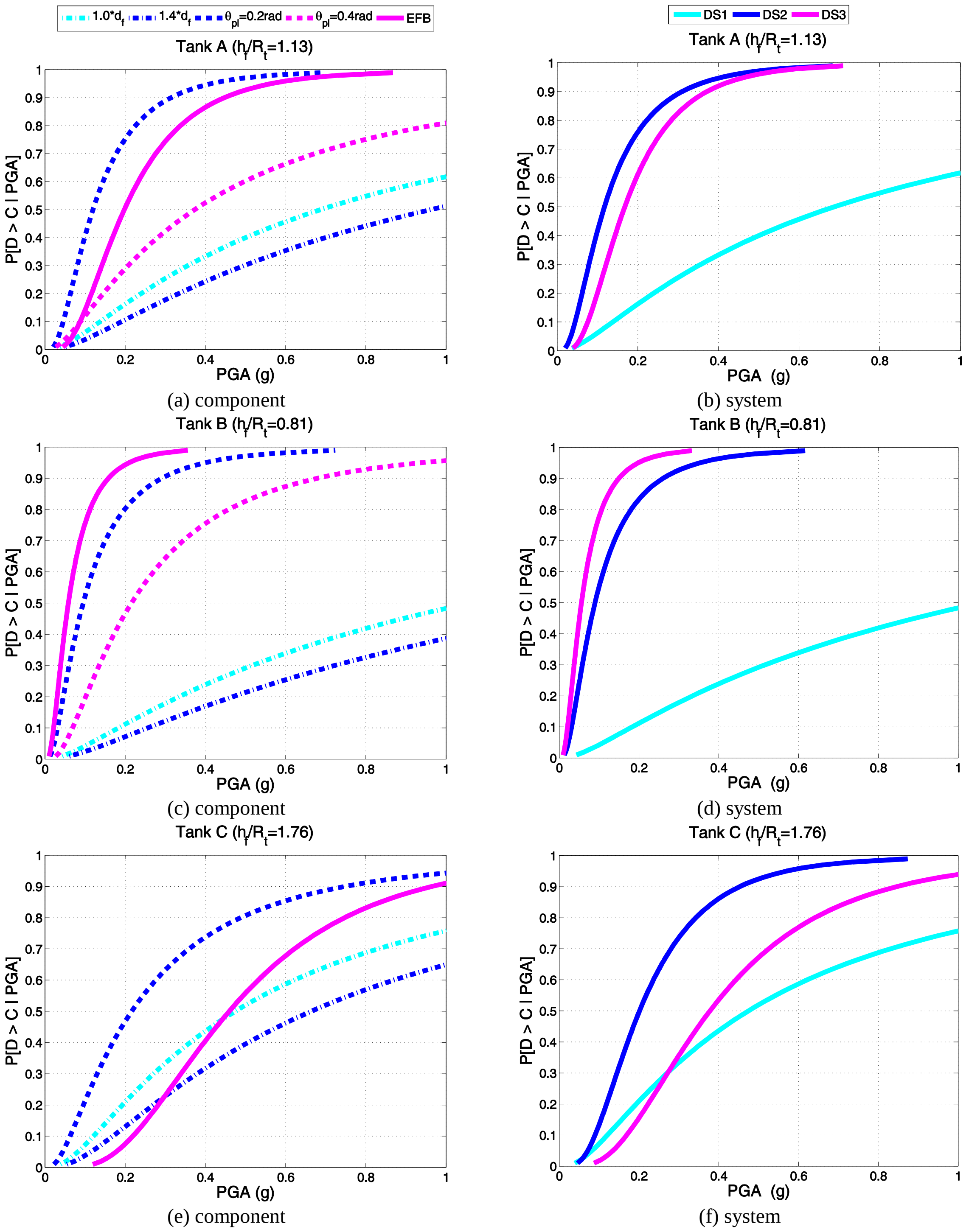

Figure 4-12: IDA-based component [(a), (c), (e)] versus system-level [(b), (d), (f)] seismic fragility evaluation. The results refer to the liquid storage tanks of Table 4-1 for unanchored support conditions.

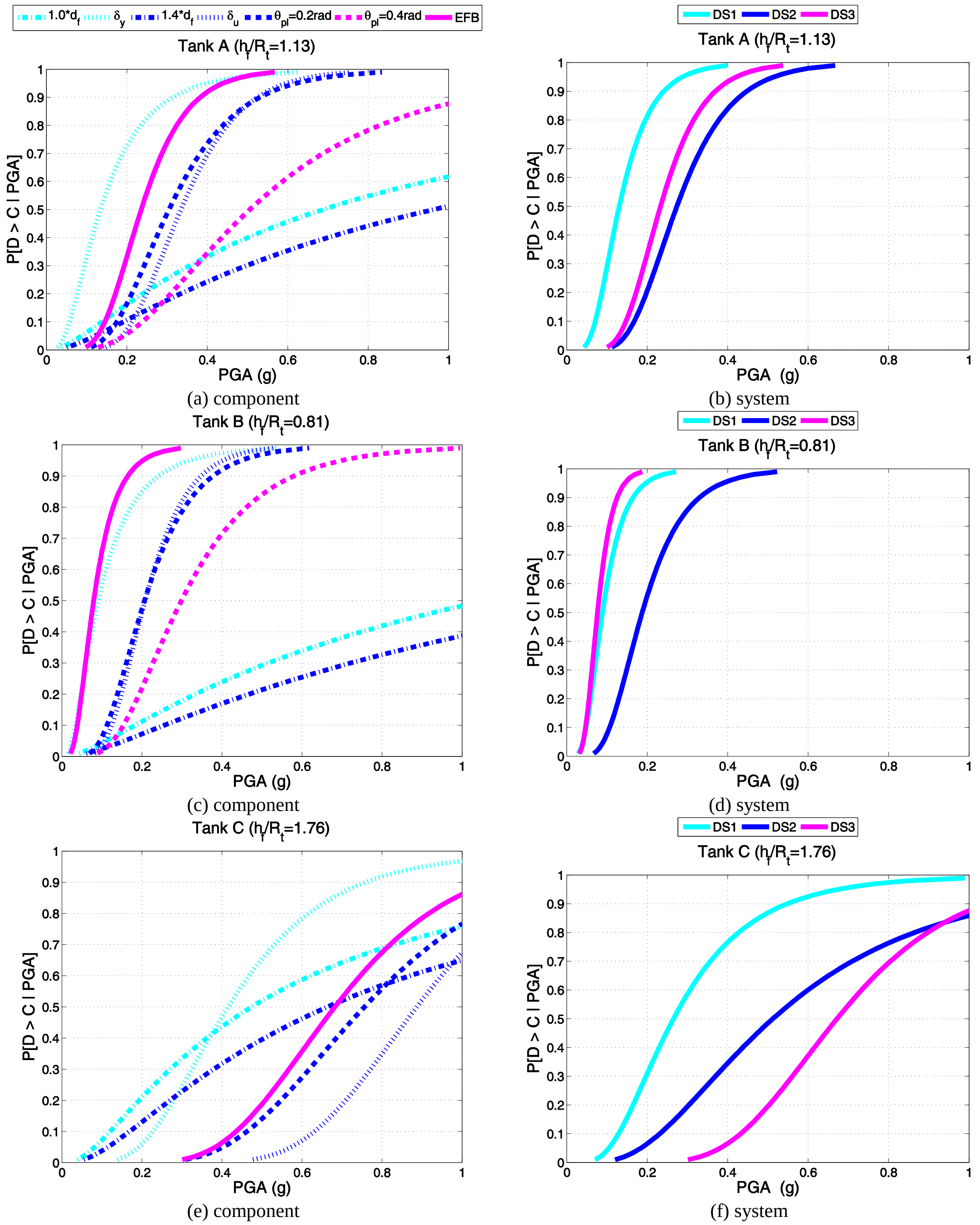

(a) component (b) system
(c) component (d) system
(e) component (f) system

Figure 4-13: IDA-based component [(a), (c), (e)] versus system-level [(b), (d), (f)] seismic fragility evaluation. The results refer to the liquid storage tanks of Table 4-1 for anchored support conditions.

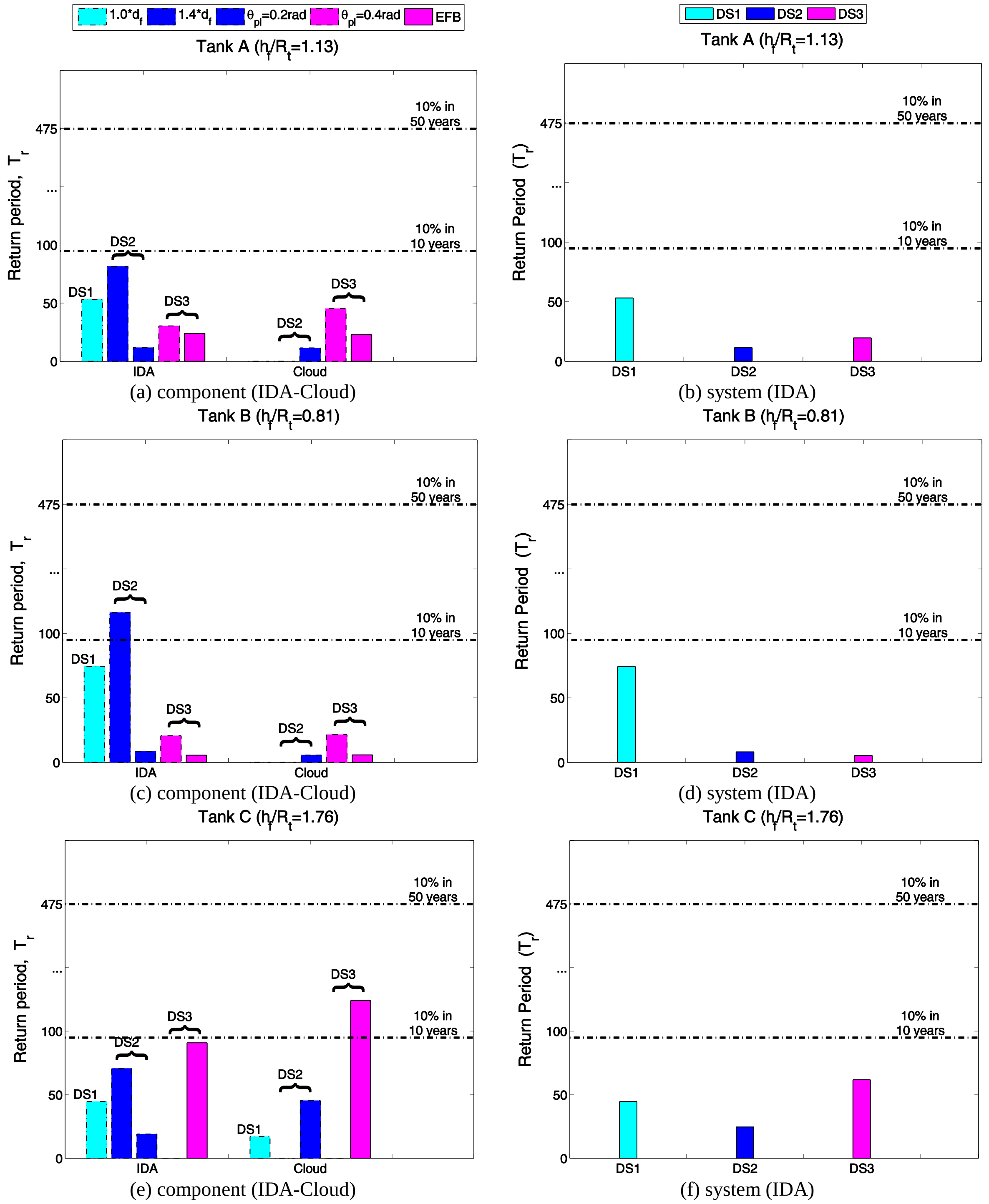

Figure 4-14: [(a), (c), (e)] Component (IDA and cloud) versus [(b)-(d)-(f)] system-level (IDA) mean return period evaluation. The results refer to the liquid storage tanks of Table 4-1 for unanchored support conditions.

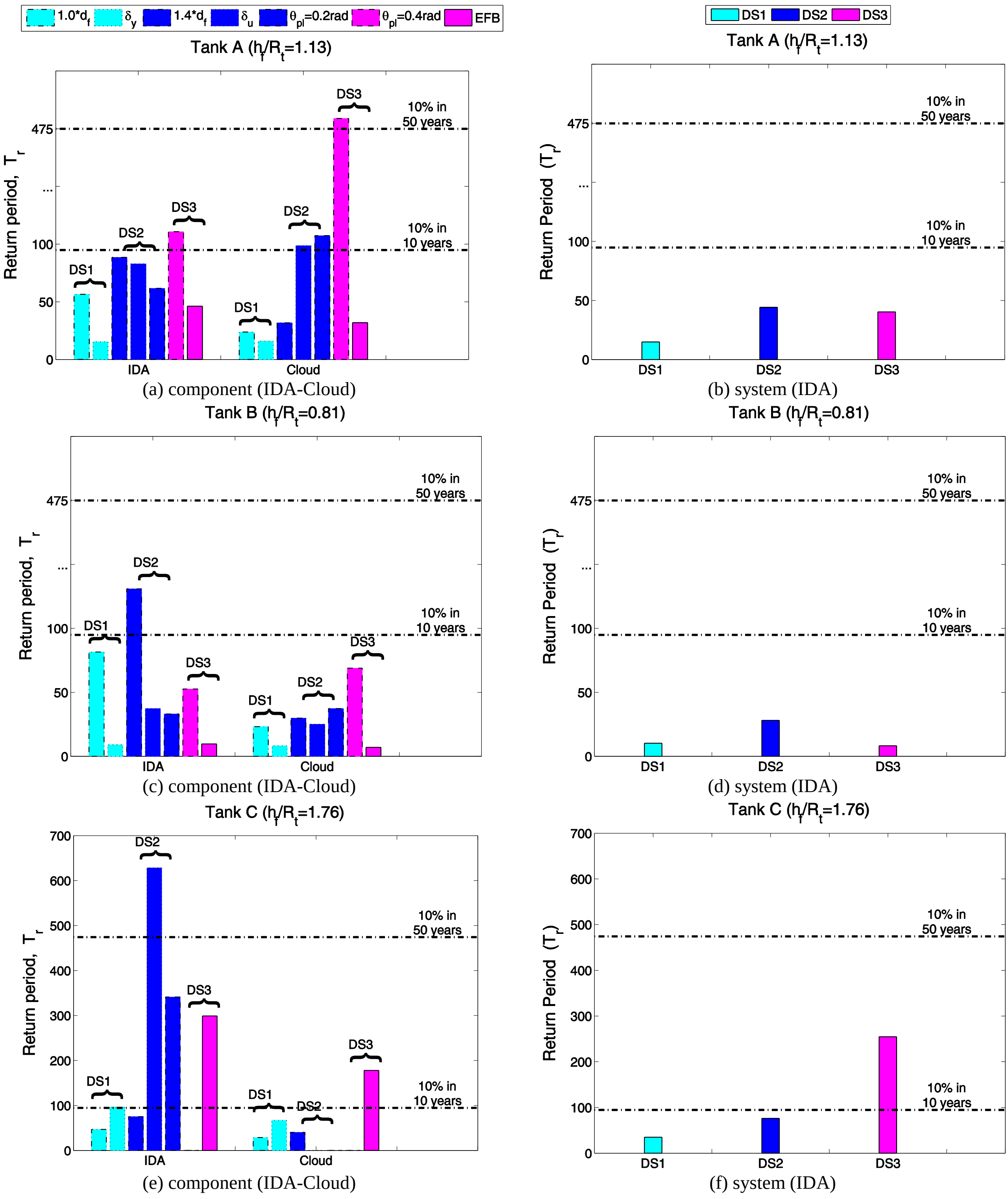

Figure 4-15: [(a), (c), (e)] Component (IDA and cloud) versus [(b)-(d)-(f)] system-level (IDA) mean return period evaluation. The results refer to the liquid storage tanks of Table 4-1 for anchored support conditions.

4.10 CONCLUSIONS

A reliability PBEE assessment methodology has been developed using a simplified surrogate model for liquid storage tanks. Both component and system-level damage states are outlined, favouring the seismic risk assessment of a single liquid storage unit or an entire group of tanks, respectively. Using the simplified cloud analysis to determine the *EDP-IM* relationship, and thus the corresponding fragility curves and mean return period, presents a fairly straightforward and rapid assessment approach, on the onset that some margin of error cannot be avoided compared to more refined dynamic analysis methods such as IDA. In most cases, the margin of error can further be improved by considering a larger number of records or even through rigorous post-processing techniques (e.g. a more refined local fit). The benchmark solution adopted herein through IDA provides a detailed representation of the *EDP-IM* space, although it is slightly more expensive from a computational point of view (under the condition that a surrogate model is available). On the downside, post-processing the IDA output is considerably more demanding, especially if *IM* stipes are not available (Vamvatsikos and Cornell 2002). Regardless of the analysis approach, EFB requires special attention, not only regarding the demand but also the capacity representation. Their underlying (negative) correlation makes the buckling capacity point substantially more difficult to determine, while at the same time suggests that this problem can probably be effectively tackled using a 3D surrogate model. Finally, unlike well-studied structural systems (e.g. moment resisting frames) where increasing seismic intensity triggers higher states of damage, the progression of failure on liquid storage tanks is non-sequential (using the limit state capacities considered), as quite often a higher damage state appears first, hinting at the onset of severe damage with little or no warning. Part of the work presented in this chapter has been published in the Journal of Earthquake Engineering and Structural Dynamics (Bakalis et al. 2017b).

5 SEISMIC INTENSITY MEASURES FOR LIQUID STORAGE TANKS

5.1 ABSTRACT

A series of scalar and vector intensity measures is examined to determine their suitability within the seismic risk assessment of liquid storage tanks. Using a surrogate modelling approach on a squat tank that is examined both under anchored and unanchored support conditions, incremental dynamic analysis is adopted to generate the distributions of response parameters conditioned on each of the candidate intensity measures. Efficiency and sufficiency metrics are employed in order to perform the intensity measure evaluation for individual failure modes, while a comparison in terms of mean annual frequency of exceedance is carried out with respect to a damage state that is mutually governed by the impulsive and convective modes of the tank. The results reveal combinations of spectral acceleration ordinates as adequate predictors, among which the average spectral acceleration is singled out as the optimal solution. The sole exception is found for the sloshing-controlled modes of failure, where mainly the convective-period spectral acceleration is deemed adequate to represent the associated response due to their underlying linear relationship. A computationally efficient method in terms of site hazard analysis is finally proposed to serve in place of the vector-valued intensity measures, providing a good match for the unanchored tank considered and a more conservative one for the corresponding anchored system.

5.2 INTRODUCTION

Liquid storage tanks comprise a vital link between the exploration/exploitation of petrochemical energy resources and the distribution of their products to the public. To ensure the structural integrity of such important structures against the (potentially) devastating socioeconomic impact of a major earthquake, state-of-the-art techniques should be employed (Cornell and Krawinkler 2000). Previous earthquake events [e.g. Alaska 1964 (Thoms et al. 2014), Izmit 1999 (Girgin 2011), Tohoku 2011 (Hatayama 2015)] have revealed several levels of damage on tanks, spanning from easy-to-repair structural damage to complete loss of the stored material, often associated with one or more modes of failure. Although they might relate to varying degrees of repair actions, these failure modes form a union of events that govern the violation of a specific system (global) damage state (*DS*) (Bakalis et al. 2017b; RASOR 2015). In the course of seismic performance assessment, capturing the aforementioned failure modes requires employing appropriate engineering demand parameters [*EDPs*, e.g. stress, strain, (Vathi et al. 2017)], the pertinent thresholds (Vathi et al. 2017), a suitable structural model (Bakalis et al. 2017a) and multiple ground motion records, characterised by pertinent intensity measures (*IMs*) such as the peak ground acceleration (*PGA*) and the first-mode spectral acceleration $S_a(T_1)$ (Jalayer 2003; Vamvatsikos and Cornell 2002).

The information provided above may be efficiently blended into the Performance-Based Earthquake Engineering (PBEE) concept, originally developed by Cornell and Krawinkler (2000) for the Pacific Earthquake Engineering Research (PEER) Centre, whereby the end-product is typically given in terms of the mean annual frequency (MAF) 'λ' of exceeding e.g. monetary loss or downtime thresholds. Nevertheless, the seismic assessment is often conveniently performed using the intermediate product of MAF of exceeding *DS* thresholds (Eads et al. 2013; Jalayer 2003), by integrating the associated *IM*-conditional probability that demand (*D*) exceeds capacity (*C*) with the annual rate of exceeding *IM* values as:

$$\lambda(DS) = \int_{IM} \mathrm{P}(D > C \mid IM)\ |\mathrm{d}\lambda(IM)| \tag{5-1}$$

In Equation (5-1), P($D>C|IM$) is referred to as the 'fragility function', while d$\lambda(IM)$ is the differential of the seismic hazard curve for the *IM* of interest, which is commonly obtained using a probabilistic seismic hazard analysis [PSHA, Cornell (1968)]. Regardless of whether one seeks the MAF of a *DS* or level of loss, the sole parameter that always remains present is the hazard curve, which provides information on the rates of exceeding certain levels of seismic intensity in terms of MAF. Evidently, the *IM* becomes a key element for every assessment-related study, serving as an interface variable among the various parameters that affect 'λ'.

Adopting an *IM* to perform the seismic risk evaluation on a liquid storage tank is not straightforward and the reason mainly lies in the complex response that these structural systems tend to develop during earthquakes. Under ground motion excitation, the contained fluid is essentially divided into two modal masses that are typically considered decoupled [Bakalis et al. (2017a); Malhotra (2000), Figure 5-1(a)]. The translational response is then dominated by a short-period (e.g. T_i=0.1-0.3s) mode of vibration, also known as the (rigid-) impulsive component, and is highly associated with modes of failure such as buckling, plastic rotation and anchor-bolt failure. On the other hand, the remaining portion of the contained fluid is excited at (ultra) long-period modes of vibration (e.g. T_c=4.0-7.0s), refers to the sloshing of the free fluid-surface, and is tied to roof and upper-course damage on the tank. This so-called convective component seldom contributes noteworthy overturning actions on the tank and thus the decoupling among impulsive and convective may reasonably be taken for granted especially for squat tanks (Ozdemir et al. 2012; Spritzer and Guzey 2017a). Evidently, from an assessment point of view, it appears that one is left with a single system influenced by two (largely uncorrelated) spectral acceleration ordinates [e.g. $S_a(T_i)$ and $S_a(T_c)$], and little information available on the existing literature regarding the *IM* that better suits this particular case (Phan et al. 2017a; Phan and Paolacci 2016). The aim of this study is to explore the choice of the *IM* for liquid storage tanks based on quantitative metrics, and come up with the 'optimal' solution from a pool of candidate *IMs*, ranging from simple to complicated ones.

5.3 SCALAR OR VECTOR?

A suitable *IM* should not only serve as an index of the ground shaking severity, but also as a good predictor of the *EDPs* of interest in the structure. In general, the choice of the intensity measure is important and the first reason comes down to a single parameter, i.e. variability. Reducing variability implies that a smaller number of records is required to achieve the same level of confidence on the numerical output (Vamvatsikos and Cornell 2005a). Such an effect can easily be realised by performing a comparison between *PGA* and $S_a(T_1)$ for the case of a mid- to high-rise building, whereby the *EDP-IM* relationship expressed through Incremental Dynamic Analysis [IDA, Vamvatsikos and Cornell (2002)] would provide a much wider range of *IM* values (given the *EDP*) for *PGA* than it would for $S_a(T_1)$. This comes as no surprise, since the fundamental period of a multi-story building falls far away from the range of short periods that the *PGA* might be able to capture, thus inflating the response with additional uncertainty. This is the well-known requirement of *efficiency* according to Luco and Cornell (2007). The second reason is *sufficiency*, which states that the *IM* should render the structural response independent of other seismological or ground motion characteristics [e.g. magnitude (M_w), distance, pulse duration, epsilon (ε)], thus removing the bias introduced when this dependence is ignored in Equation (5-1). Obviously, any sort of discussion around efficiency, sufficiency and bias makes sense so long as the hazard curves of the intensity measure under investigation can actually be computed (Giovenale et al. 2004; Padgett et al. 2008). Further desirable properties have been proposed for *IMs* (Padgett et al. 2008), but in the opinion of the authors they can be folded back to the above two fundamental ones without loss of generality.

5.3.1 Scalar intensity measures

Traditionally, the intensity measure is a scalar variable represented by well-known spectral quantities, such as *PGA* and $S_a(T_1)$. As much as the aforementioned *IMs* may seem useful for the assessment of certain structural systems (e.g. low and/or mid-rise frame-structures respectively), their suitability cannot be taken for granted for the entire range of civil engineering structures. The reason is that individual spectra carry too much variability that cannot always be captured by $S_a(T_1)$ or *PGA* alone; in fact, there are several cases in recent literature where alternative scalar *IMs* or even complex combinations of them are adopted to adequately represent the seismic input on a given structural system (Kohrangi et al. 2016b; Vamvatsikos and Cornell 2005a). For instance, the first-mode inelastic spectral displacement and its combination with higher mode spectral ordinates have been proposed for pulse-like and non-pulse-like ground motions (Tothong and Cornell 2008; Tothong and Luco 2007), while the geometric mean of the $S_a(T_1)$ values along the longitudinal and transverse directions of a three-dimensional (3D) moment resisting frame is considered (Baker and Cornell 2006b) in place of the arbitrary $S_a(T_1)$ ground motion component, especially for cases that the fundamental period of the structure does not predominately favour either of the building axes.

Along these lines, research efforts have resulted in the generation of seismic intensity measures that often consider the product of multiple spectral acceleration ordinates. Such *IMs* normally involve $S_a(T_1)$ along with a modification factor that accounts for spectral shape. This was initially proposed by Cordova et al. (2001) incorporating the geometric mean of $S_a(T_1)$ and $S_a(2T_1)$, attempting to capture the apparent ‘elongation’ of the fundamental period due to structural damage, and was further studied by Vamvatsikos and Cornell (2005) who added higher mode periods. This idea has evolved into the average spectral acceleration ($AvgS_a$) whereby one employs *m* spectral ordinates at equally-spaced multiple periods T_{Rj} within a range $[T_L, T_H]$ that includes T_1 and is defined by a lower (T_L) and higher (T_H) bound:

$$AvgS_a = \left[\prod_{j=1}^{m} S_a\left(T_{Rj}\right)\right]^{1/m} \tag{5-2}$$

Studies by many researchers have shown that a wide variety of *IMs* defined according to the general frame of Equation (5-2) can offer substantial efficiency and sufficiency for building structures (Bojórquez and Iervolino 2011; Eads et al. 2015; Kazantzi and Vamvatsikos 2015; Kohrangi et al. 2016b, 2017b; Mehanny 2009; Tsantaki et al. 2017).

5.3.2 Vector-valued intensity measures

Despite the amount of work performed to date, it seems that most scalar *IMs* are always going to suffer from some level of insufficiency, particularly when the *EDP|IM* relationship strongly depends on certain ground motion parameters. In view of further improving the accuracy with respect to the MAF estimation, the concept of vector-valued intensity measures has emerged, thus offering the ability to effectively tackle both sufficiency and efficiency, on the offset that the vector-valued probabilistic seismic hazard analysis (VPSHA) input is required (Bazzurro and Cornell 2002). Their applicability does not meet any particular constraints, other than the ability to compute the required VPSHA (which by no means should be taken for granted) and perform the corresponding integrations.

There are several examples to highlight the importance of vector-valued IMs, such as the case of tall or irregular buildings, where the second or even higher modes of vibration are expected to be significant. Therein, a vector of $S_a(T_1)$ with the ratio of spectral acceleration at an elongated period [e.g., $S_a(1.5T_1)$] over $S_a(T_1)$ (Bazzurro and Cornell 2002; Kohrangi et al. 2016b; Vamvatsikos and Cornell 2005a), or with the well-known seismological parameter of epsilon (Baker and Cornell 2005), has proved to be more effective than other simple scalar *IMs*. An out-of-the-ordinary example is the case of buried pipelines under fault crossings, whereby the fault displacement is inevitably adopted as a representative *IM*, and its 3D motion during an earthquake suggests that the vector of the associated fault displacement components should be used as shown by Melissianos et al. (2016).

In spite of the accuracy offered, the use of vector-valued *IMs* increases the complexity of application, requiring a multi-dimensional fragility and VPSHA results. Another issue is the analysis methodology that is carried out to determine the *EDP|IM* relationship (Baker 2007) and thus the fragility surface (Gehl et al. 2013). This is the well-known 'curse of dimensionality' whereby increasing the dimensions of the *IM* the fragility function necessitates even more samples for reliable estimation, further complicating the analysis. For practical purposes, these complexities have naturally decelerated the use of vector-valued *IMs*, which are currently confined within the academic environment, mainly aiming towards the validation and quantification of the accuracy of scalar ones.

5.4 MODELLING, DAMAGE STATES AND EDPS

The surrogate modelling approach proposed by Bakalis et al. (2017a) [Figure 5-1(b)], is adopted to carry out the nonlinear dynamic analyses required for this study. The so-called "Joystick" model consists of radially spaced rigid beams, that essentially form the base plate of the tank, and are supported by vertically-oriented elastic multilinear springs. The tensile and compressive properties of those edge-springs are assigned the uplift resistance of a $2R_t$ long (where R_t is the radius of tank), uniformly loaded (due to hydrostatic loading) beam (strip) model, as explicitly shown in Bakalis et al. (2017a; b). The base plate is connected to an elastic element that carries the impulsive mass of the tank, and is assigned properties such that the fundamental period of the entire system equals the prediction offered by Malhotra (CEN 2006; Malhotra 2000). This model is able to simulate (either directly or indirectly) commonly observed modes of failure such as shell buckling, base plate plastic rotation, uplift and anchor bolt deformation [where anchorage is necessary to supply the system with additional stability on top of self-weight anchoring, American Petroleum Institute (2007)]. Sloshing response is not explicitly modelled; instead, it is taken into account through the Eurocode 8 (CEN 2006; Malhotra 2000) equation (A.15) that presents a linear relationship between the sloshing wave height and the elastic convective period spectral acceleration for an appropriately defined fluid damping.

To facilitate the application of the PBEE concept, the aforementioned failure modes are combined to form system damage states of increasing severity for both anchored and unanchored liquid storage tanks (Bakalis et al. 2017b; RASOR 2015). For instance, minor damage on the roof and/or upper course of the tank due to sloshing of the contained fluid, as well as yielding of the foundation anchor bolts, may be characterised as slight structural damage (i.e. *DS*1). Moderate plastic rotations (i.e. order of 0.2rad) on the base-plate, significant roof damage, and fracture of the foundation anchor bolts may be deemed as severe structural damage without leakage of the stored material (i.e. *DS*2). Similarly, the leakage potential (i.e. *DS*3) may be triggered either due to an elastic-plastic buckling failure known as the elephant's foot buckling (EFB), or extreme base-plate plastic rotations (i.e. order of 0.4rad). Table 5-1 summarises the *DS* classification for liquid storage tanks, with respect to the system support conditions (i.e. anchored versus unanchored). As discussed above, the violation of each *DS* is triggered when an *EDP* value (i.e. d for sloshing wave height, δ for anchor bolt deformation, θ_{pl} for base plate plastic rotation, and σ_m for tank wall meridional stress) exceeds the prescribed *EDP* capacity: the available freeboard d_f for sloshing, the anchor bolt yield δ_y and fracture δ_u deformation (e.g. δ_u=100mm), the 0.2rad and 0.4rad limits for base plate plastic rotation, and the σ_{EFB} limit for EFB (Bakalis et al. 2017b; CEN 2006). The simultaneous effect of both impulsive and convective-controlled *EDPs* on certain damage states (e.g. *DS*1 for anchored tanks only and *DS*2 for both anchored and unanchored) constitutes the applicability of conventional *IMs* (e.g. *PGA*) questionable for the seismic risk assessment of liquid storage tanks, as extensively discussed in the following.

Table 5-1: Damage state classification for anchored and unanchored liquid storage tanks.

System Support Conditions	Damage States	Damage State Violation
	*DS*1	$d>1.0\times d_f$ or $\delta>\delta_y$
Anchored	*DS*2	$d>1.4\times d_f$ or $\theta_{pl}>0.2$rad or $\delta>\delta_u$
	*DS*3	$\sigma_m>\sigma_{EFB}$ or $\theta_{pl}>0.4$rad
	*DS*1	$d>1.0\times d_f$
Unanchored	*DS*2	$d>1.4\times d_f$ or $\theta_{pl}>0.2$rad
	*DS*3	$\sigma_m>\sigma_{EFB}$ or $\theta_{pl}>0.4$rad

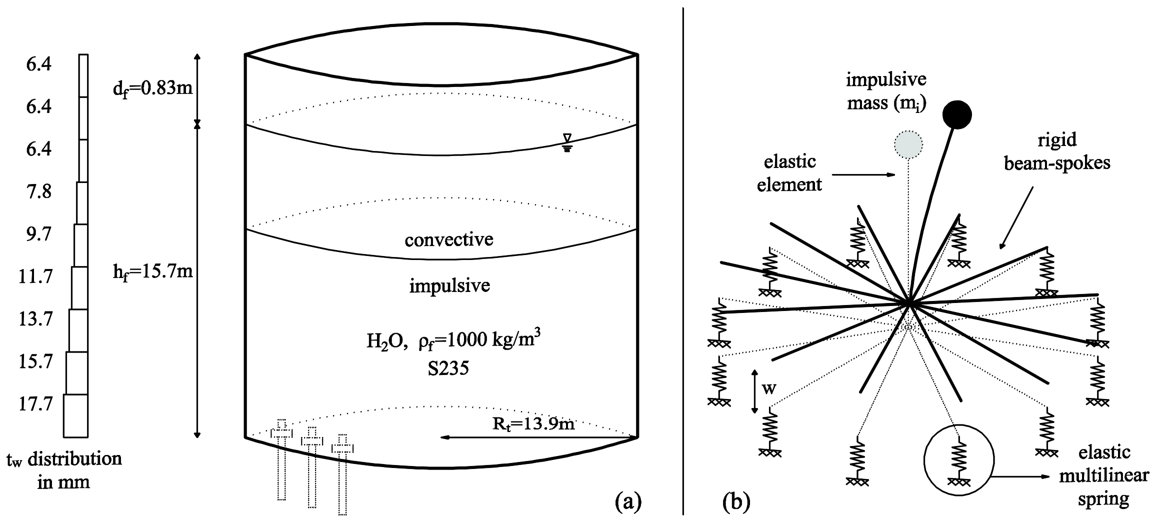

Figure 5-1: (a) Impulsive versus convective fluid component, and properties of the case study liquid storage tank; depending on the presence of anchors, the system is either anchored or unanchored; (b) the "Joystick" surrogate model (Bakalis et al. 2017a) and its deflected shape.

5.5 IM SELECTION

Several candidate *IMs* (Table 5-2) are selected to investigate their suitability within the seismic risk assessment of liquid storage tanks. Besides the obvious choice of $S_a(T_i)$, the relatively short fundamental period of tanks (i.e. T_i=0.1-0.3s) allows also considering *PGA*. Another obvious choice is that of $S_a(T_c)$, which by default is going to be the perfect predictor for the sloshing-related modes of failure [due to their inherently linear relationship assumed for the 'Joystick' model (CEN 2006; Malhotra 2000)], and a rather poor one for the rest of *EDPs* and failure modes. Attempting to bridge the wide gap between the impulsive and convective periods, the geometric mean of various spectral quantities is considered. Combinations of $S_a(T_i)$ with $S_a(T_c)$, $S_a(T_i)$ with spectral accelerations at elongated impulsive periods of vibration (i.e. $1.5T_i$), *PGA* with $S_a(T_c)$, as well as the (scalar) state-of-the-art $AvgS_a$ for various ranges of period (i.e. 0.1s-0.6s, 0.1s-1.0s and 0.1s-1.5s) are taken into account. It should be noted that behind the choice of such high period upper bounds for the $AvgS_a$, lies in the nonlinear-elastic nature of the "Joystick" model, which forces the system to remain on the low-stiffness hardening branch during loading/unloading and reloading, in contrast to the elastic segments of unloading/reloading of an elastic-hardening system. In general, the concept of combined S_a values may also be deemed a strong candidate *IM* for the seismic risk evaluation of a group of tanks with varying geometry (and thus T_i and T_c) (Kazantzi and Vamvatsikos 2015; Kohrangi et al. 2016b, 2017b). This is an interesting problem that requires thorough investigation and is expected to be covered in a future direction of our research. Finally, the vectors of $\{PGA, S_a(T_c)\}$ and $\{S_a(T_i), S_a(T_c)\}$ are considered as a potentially more accurate way of incorporating the effect of T_c without compromising that of T_i as done in a scalar combination. Note that, without loss of generality, the second element of the above vectors may be replaced by its ratio over the first, as indicated in Table 5-2; this transformation will be used to better distinguish the effect of each vector component having the first element being scalable and the second constant for any given record (Vamvatsikos and Cornell 2005a).

Table 5-2: Candidate *IMs* for the seismic risk assessment of a liquid storage tank with T_i=0.22s and T_c=5.6s.

Intensity Measures*		Abbreviation
Scalar		
PGA		IM_{s1}
$S_a(T_i)$		IM_{s2}
$S_a(T_c)$		IM_{s3}
$\sqrt{S_a(T_i)\cdot S_a(T_c)}$		IM_{s4}
$\sqrt{S_a(T_i)\cdot S_a(1.5T_i)}$		IM_{s5}
$\sqrt{PGA\cdot S_a(T_c)}$		IM_{s6}
$AvgS_a=\left[\prod_{j=1}^{m} S_a(T_{Rj})\right]^{1/m}$	$0.1\text{s} \le T_{Rj} \le 0.6\text{s}$ $(\approx 2.7T_i)$	$IM_{s7\text{-}1}$
	$0.1\text{s} \le T_{Rj} \le 1.0\text{s}$ $(\approx 4.5T_i)$	$IM_{s7\text{-}2}$
	$0.1\text{s} \le T_{Rj} \le 1.5\text{s}$ $(\approx 6.8T_i)$	$IM_{s7\text{-}3}$
Vector		
$\{PGA, S_a(T_c)\}$, or equivalently $\{PGA, S_a(T_c)/PGA\}$		IM_{v1}
$\{S_a(T_i), S_a(T_c)\}$, or equivalently $\{S_a(T_i), S_a(T_c)/S_a(T_i)\}$		IM_{v2}

*All spectral ordinates refer to the geometric mean of the longitudinal and transverse earthquake recordings

5.6 SEISMIC HAZARD AND RECORD SELECTION

A site of major oil refineries in Elefsina, Greece with coordinates of (23.507°N, 38.04°E) is adopted to perform all PSHA and VPSHA-related computations, the results of which are summarised in Figure 5-2 for both the scalar and vector *IMs* examined. OpenQuake (Pagani et al. 2014), open-source software for seismic hazard and risk assessment developed by the Global Earthquake Model Foundation is used to perform the seismic hazard and disaggregation computations of this study. PSHA and VPSHA are based on the SHARE Project (Giardini et al. 2013) area source model and the ground motion prediction equation (GMPE) proposed by Boore and Atkinson (2008) is used for all purposes of this study. It should be noted that VPSHA computations are based on the *indirect* approach (Kohrangi et al. 2016a).

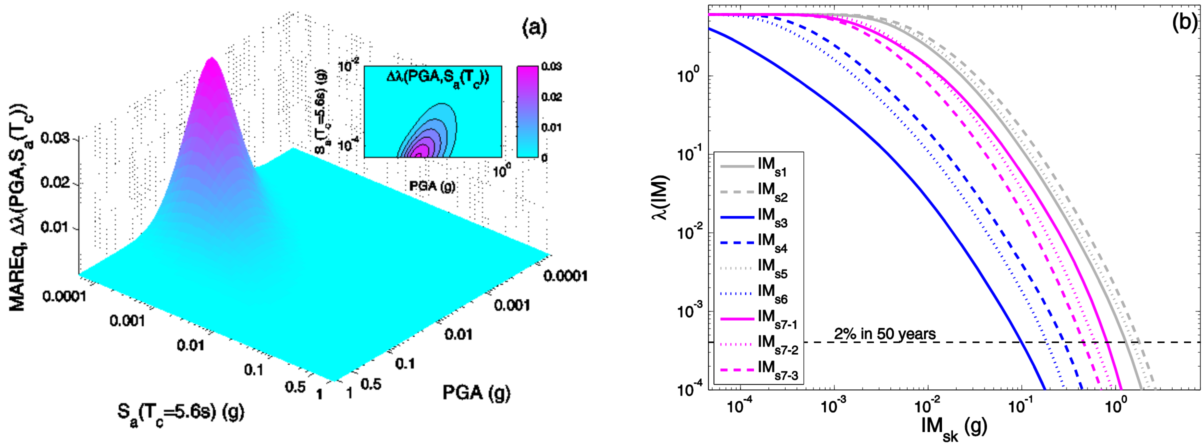

Figure 5-2: Probabilistic seismic hazard analysis; (a) mean annual rate of equalling (MAREq) joint values of $\{PGA, S_a(T_c{=}5.6\text{ s})\}$, i.e. IM_{v1}; hazard surface and contour; (b) mean annual frequency of exceeding IM_{sk} values, where $k \in \{1, 2, 3, 4, 5, 6, 7\text{-}1, 7\text{-}2, 7\text{-}3\}$.

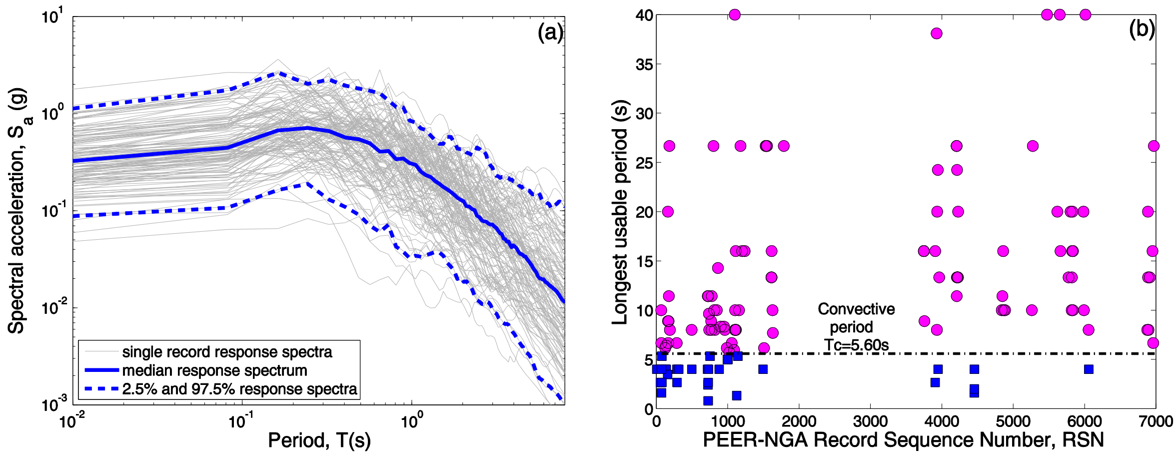

Figure 5-3: GMset-plain; (a) spectra and (b) longest usable periods versus the PEER-NGA record sequence numbers. Squares and circles indicate records with longest usable period less and greater than T_c=5.6s.

The structural response is significantly dependent on the seismicity of the site where the structure is located. Record selection provides the link between the site hazard and the structural response, therefore, it is important for the ground motion set used for response history analysis to be compatible with the seismicity at the site. Herein, two approaches are employed for selection of the records to use in response history analysis. Initially, a set of 135 ordinary ground motion record pairs (i.e. non-pulse-like, non-long-duration) obtained from the PEER-NGA database (Ancheta et al. 2013) is adopted, hereafter referred to as GMset-plain. Note that this record set is ‘not’ used for risk assessment herein; it is only employed to evaluate efficiency

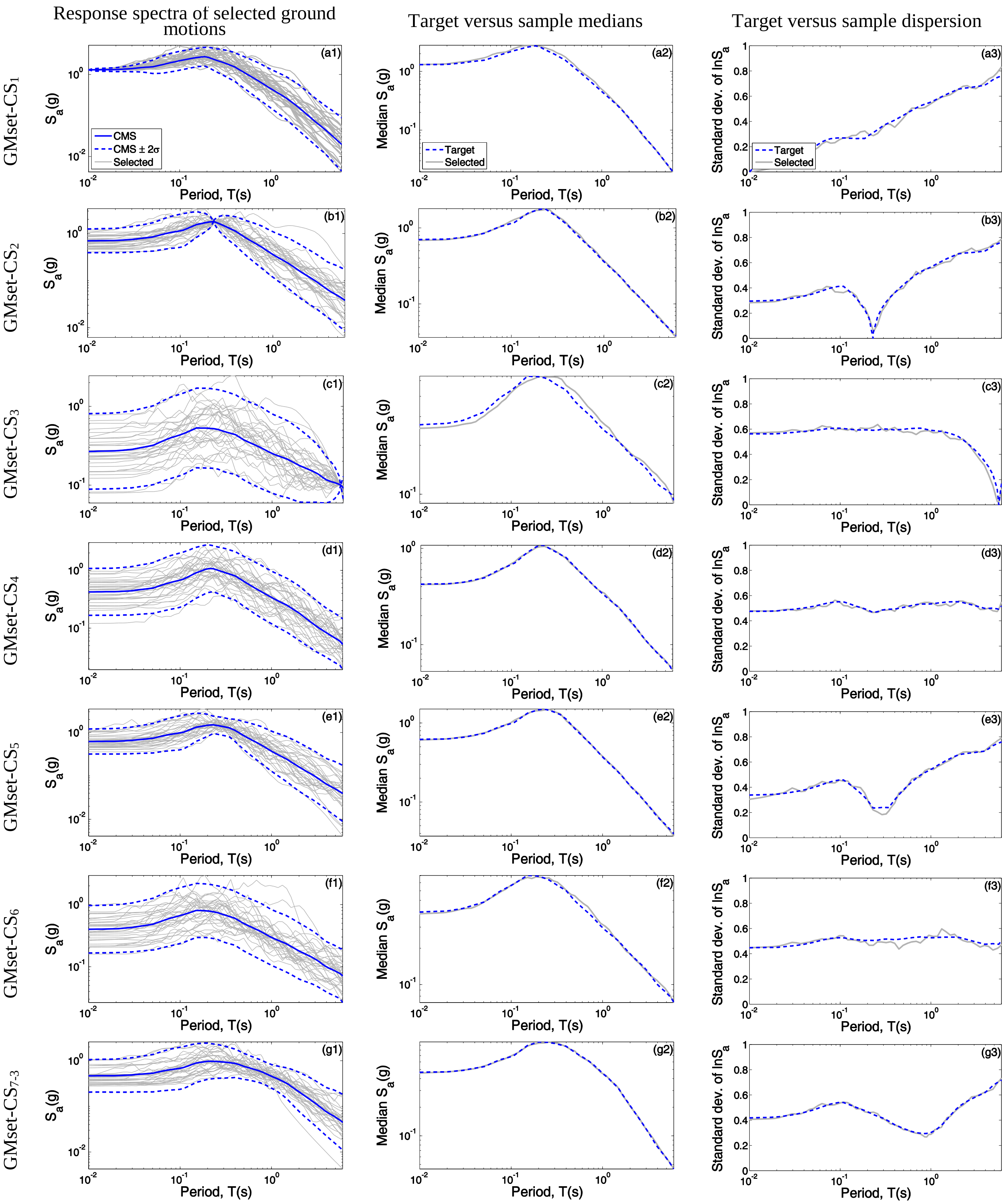

Figure 5-4: CS record selection for scalar *IMs* of Table 5-2. The left column shows the selected ground motion spectra along with the associated median (or conditional mean spectrum, CMS), 2.5th and 97.5th percentiles (CMS ± 2σ); middle and right columns show the comparison of target versus sample median and standard deviation, respectively. For brevity, only $IM_{s7\text{-}3}$ is presented from the $AvgS_a$ candidates.

and sufficiency of the tested *IMs* and thus acquire an early grasp on the performance of each of the candidate *IMs*. Figure 5-3 presents the response spectra of the GMset-plain as well as their longest usable periods. Records with longest usable period lower than T_c are excluded from GMset-plain to avoid biasing the ratio of spectral values in T_i versus T_c due to record processing. In addition to this record set and to maintain the hazard consistency in evaluation of the seismic risk of the case study liquid storage tanks for scalar *IMs*, Conditional Spectrum [CS, Kohrangi et al. (2017a); Lin et al. (2013)] based record selection is adopted. For each of the candidate scalar *IMs*, a set of 30 records corresponding with its 2% in 50 years return period that best match with the CS target are selected using the algorithm of Jayaram et al. (2011). These sets are referred to as GMset-CS$_k$, where $k \in \{1, 2, 3, 4, 5, 6, 7\text{-}1, 7\text{-}2, 7\text{-}3\}$ corresponds to the indices of scalar *IMs* in Table 2. These record sets serve as the state-of-the-art input for IDA and thus the risk-based evaluation of both the individual failure modes and the (global) system-level damage states. Note that, in contrast to GMset-plain, CS selected sets were not screened for appropriate longest usable periods. The reason is that the 'Joystick' model does not include actual periods higher than T_i; T_c is only applied through post-processing and the CS selection approach guarantees that the appropriate distribution of spectral ratio between T_i and T_c is maintained.

Figure 5-4 summarises the CS record selection results for the majority of the considered scalar *IMs*. For each candidate *IM*, the single record spectra are presented on the first column of the panels that compose Figure 5-4, along with the median, 2.5th and 97.5th percentiles. The second and third columns depict the comparison between the target and sample median as well as standard deviation, respectively. Note that, to further simplify the problem, we used a single set of records for all *IM* levels to perform IDA instead of selecting multiple sets for multiple *IM* levels (Jalayer 2003). This may slightly bias the results presented herein because the spectral shape changes by the intensity level, nevertheless, this bias is expected to be insignificant (Kohrangi et al. n.d.). Vector *IMs* have not received a similar comprehensive treatment of CS selection as the relevant methods are only now appearing in the literature (Kishida 2017; Kohrangi et al. n.d.). Still, by nature, vector *IMs* are considered to offer higher sufficiency thus the corresponding GMset-CS records of the primary element [i.e. *PGA* and $S_a(T_i)$] of IM_{v1} and IM_{v2}, respectively, are employed.

5.7 INCREMENTAL DYNAMIC ANALYSIS

A squat liquid storage tank that has a radius R_t=13.9m, height h_t=16.5m and is 95% filled with water (i.e. fluid density ρ_f=1000kg/m^3), is used to showcase the effectiveness of the *IMs* presented above. The thickness of the base plate is t_b=6.4mm, while that of the annular plate is t_a=8mm. A total of 9 wall courses with varying thickness is provided to form the tank shell. In particular, the thickness distribution (in mm) from the lower to the upper course of the tank is 17.7, 15.7, 13.7, 11.7, 9.7, 7.8, 6.4, 6.4 and 6.4 respectively, as shown in Figure 5-1(a). The roof mass is m_r=35t and the material that has been used is steel S235 with a post-yield hardening ratio equal to 1%.

IDA is employed to derive the distribution of the various *EDPs* given the seismic intensity, using the GMset-plain shown in Figure 5-3. Each 3D analysis is conducted using both longitudinal and transverse recordings as an input. The process of capturing any of the aforementioned modes of failure on the "Joystick" model is presented in detail by in Bakalis et al. (2017b). Figure 5-5 illustrates the single-record IDA curves for each failure mode (and thus *EDP*) of interest, along with various (potential) *EDP* capacities and the associated *IM* values that will further be exploited during the efficiency-sufficiency testing. Besides component-level *EDPs* such as plastic rotation, sloshing wave height and meridional stress, uplift is also examined for the unanchored tank in view of obtaining a wider understanding through a global response parameter. Given the dependence of the majority of failure modes on the impulsive component of the tank, the IDAs shown in the columns 1, 2 and 5 of Figure 5-5 indicatively adopt *PGA* as the *IM*. The sloshing wave response of Figure 5-5(a3, b3) also adopt *PGA* in order to display its inappropriateness (at least) in terms of efficiency, compared to $S_a(T_c)$ that is going to be a perfect predictor according to the definition of the sloshing wave height, *d* (CEN 2006), as shown in Figure 5-5(a4, b4). It should be noted that the nonlinear-elastic nature of the "Joystick" model does not allow the development of the characteristic IDA flatlines (Vamvatsikos and Cornell 2002) that signal collapse of the structure, which is consistent with damage observed in the past, where collapse was mainly triggered due to the cascading/secondary effects of the earthquake (e.g. fire, tsunami) rather than the earthquake itself (Girgin 2011; Hatayama 2015).

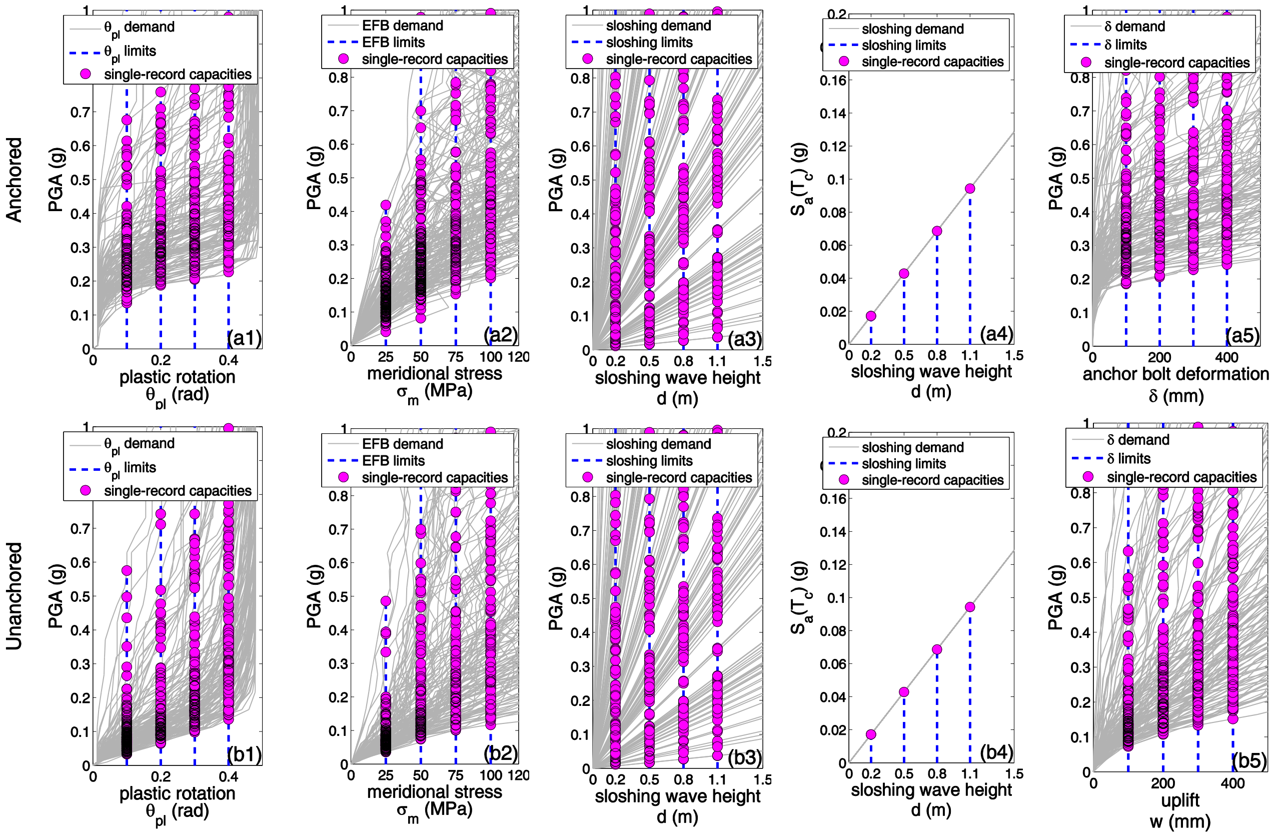

Figure 5-5: GMset-plain single-record IDAs and four indicative *EDP* capacities for each failure mode: (a1) and (b1) base plate plastic rotation, (a2) and (b2) meridional stress, (a3), (a4), (b3) and (b4) sloshing wave height, (a5) anchor bolt deformation, (b5) uplift. The results presented in row (a) refer to the anchored tank shown in Figure 5-1(a), while the ones in row (b) to the corresponding unanchored system.

5.8 IM TESTING

The *IM* evaluation is performed by employing metrics of efficiency and sufficiency. In contrast to the original work of Luco and Cornell (2007), whereby efficiency and sufficiency were tested singularly for the entire range of *EDP* response, the approach of Kazantzi and Vamvatsikos (2015) is employed. In particular, 100 equally spaced *EDP* values are employed to determine corresponding *IM*|*EDP* capacities, termed IM_C values. These offer a high-resolution test for efficiency and sufficiency of each *EDP* and level of response. For scalar *IMs*, each set of IM_C values (i.e. for a single *EDP* threshold) appears as a vertical stripe in the typical 2D representation of IDA curves (e.g. as shown in Figure 5-5). For vector *IMs* of two elements, a 3D visualisation of IDA is adopted (Vamvatsikos and Cornell 2005a), whereby the first vector element [i.e. *PGA* or $S_a(T_i)$] is used to forecast the level of intensity, while the second element [i.e. $S_a(T_c)$] is normalised by the first to become a constant [Figure 5-6(a)]. Then, IM_C values appear on a horizontal plane slice through the 3D IDA curves, as shown in Figure 5-6(a, b). Therein, the additional resolution offered by a vector becomes apparent, as higher values of the *IM* ratio always indicate a more aggressive record, whereby spectral ordinates tend to increase with period. On the other hand, low values of the *IM* ratio provide little information about periods lower than T_c, where it is unknown whether they are high or low, vis-à-vis *PGA* or $S_a(T_c)$. According to the top left part of Figure 5-6(b), extreme *IM* ratio values do indicate low IM_C capacities, and their variability is near perfectly captured [Figure 5-6(C)]. Therefore, vector *IM* sufficiency and efficiency testing shall only focus on the murkier area of $S_a(T_c)/PGA<0.5$ [or $S_a(T_c)/ S_a(T_i)<0.2$] [bottom part of Figure 5-6(b)] where large variability (larger than a cut-off value of approximately 0.20) is still apparent and unexplained by any of the two vectors (IM_{v1} and IM_{v2}) employed. It should be noted that the sample of 135 IDAs provided in Figure 5-5 is narrowed down to 103 to comply with the aforementioned limitation in the longest usable period [Figure 5-3(b)]. Furthermore, the *EDP*-response hazard curves are extracted to provide an additional source of information regarding the applicability of the candidate *IMs*, while the MAF of the compound *DS* involving both impulsive and convective-governed modes of failure are ultimately estimated in view of determining a single predictor for the risk-based evaluation of liquid storage tanks.

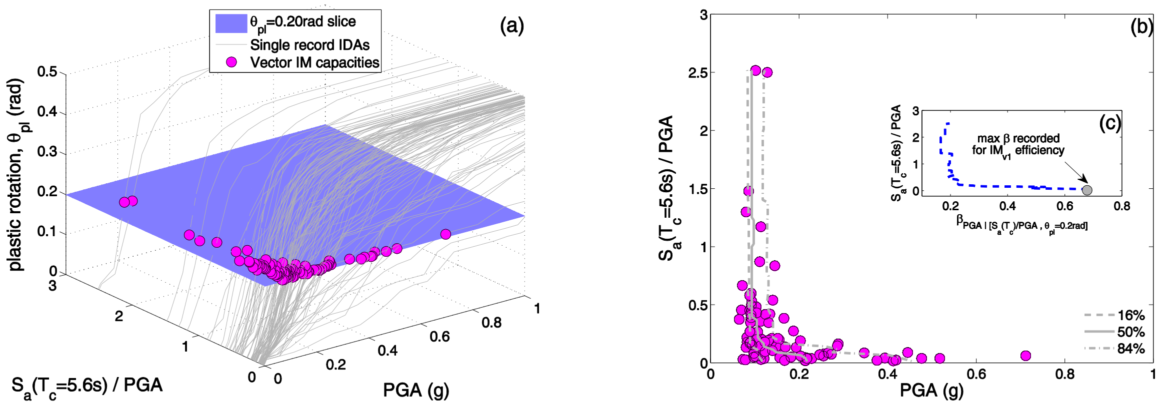

Figure 5-6: (a) Single-record IDAs based on the GMset-plain set of records for the unanchored tank of Figure 5-1(a); plastic rotation versus the vector of {PGA, $S_a(T_c)/PGA$} showing the characteristic saturation of θ_{pl} at high levels of intensity (Bakalis et al. 2017a), featuring the 0.2rad *EDP* slice; (b) joint values of *PGA* and $S_a(T_c)/PGA$; (c) recorded dispersion for the vector *IM* efficiency testing.

5.8.1 Efficiency

The efficiency testing for scalar *IMs* is performed by estimating the standard deviation of the 103 IM_C natural logarithm values ($\beta_{IM|EDP}$) estimated at each *EDP* level. For vector *IMs* this dispersion needs to be further conditioned on the value of $S_a(T_c)/PGA$ [or $S_a(T_c)/ S_a(T_i)$]. Due to lack of data at every value of the vector *IM* element ratio, this conditional dispersion is evaluated by assuming lognormality and employing the 16%/50%/84% running quantiles of *PGA* [or $S_a(T_i)$] versus the corresponding ratio $S_a(T_c)/PGA$ [or $S_a(T_c)/ S_a(T_i)$]. Then, $\beta_{IM\,|[S_a(T_c)/IM,EDP]} = 0.5\left[\ln IM^{84\%}_{S_a(T_c)/IM,EDP} - \ln IM^{16\%}_{S_a(T_c)/IM,EDP}\right]$, as indicatively shown in Figure 5-6(b) and C for θ_{pl}=0.2rad and *IM*=*PGA*. As discussed earlier, only the higher values of $\beta_{IM\,|[S_a(T_c)/IM,EDP]}$ appearing in the lower part of Figure 5-6(c) are of interest.

The results presented in Figure 5-7 refer to the geometry of the tank shown in Figure 5-1(a) using both anchored and unanchored support conditions. A general conclusion that can be drawn regarding the failure modes that are predominantly governed from the impulsive component of the tank (i.e. plastic rotation, EFB, uplift and anchor bolt failure), is that their capacities are less dispersed when the geometric mean of multiple spectral ordinates close to T_i is adopted as in IM_{s5} and IM_{s7} [Figure 5-7(a1), (b1), (a2), (b2), (a4), (b4)]. For the unanchored tank, $IM_{s7\text{-}2}$ and $IM_{s7\text{-}3}$ appear to be two potentially optimal intensity measures as they develop the smallest dispersion estimates throughout the *EDP* range considered, the former performing better for low/moderate values and the latter elsewhere. $IM_{s7\text{-}1}$ is another decent alternative, while the geometric mean of $S_a(T_i)$ and $S_a(1.5T_i)$ (=IM_{s5}) appears to be a reasonable option too, as the pertinent dispersion estimates do not fall far away from those of $IM_{s7\text{-}1}$, at least for moderate *EDP* values. Similarly, combinations of $S_a(T_i)$ and *PGA* with $S_a(T_c)$ (=IM_{s4} and IM_{s6}) may also be deemed applicable for a certain range of *EDP* values regarding plastic rotation and meridional stress [Figure 5-7(b1, b2)]. On the contrary, *PGA* and $S_a(T_i)$ alone (=IM_{s1} and IM_{s2}) cannot be considered acceptable predictors for the aforementioned *EDPs*, as they develop considerably larger dispersions compared to the rest of candidate *IMs*.

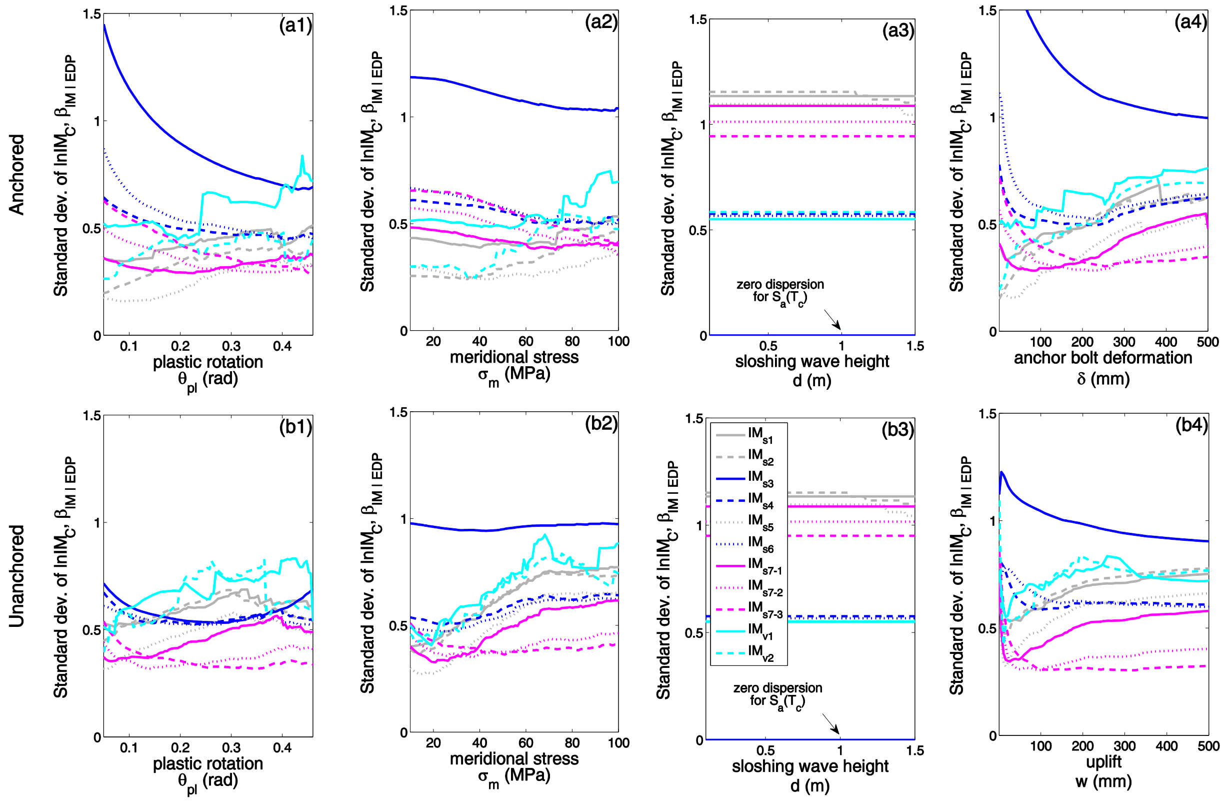

Figure 5-7: *IM* efficiency testing; (a1) and (b1) base plate plastic rotation, (a2) and (b2) meridional stress, (a3), (a4), (b3) and (b4) sloshing wave height, (a5) anchor bolt deformation, (b5) uplift; the results presented in row (a) refer to the anchored tank shown in Figure 5-1(a), while the ones in row (b) to the corresponding unanchored system. IDA results using GMset-plain.

As far as the anchored tank is concerned, the response of impulsive controlled *EDPs* is slightly different from that of the unanchored tank. In particular, IM_{s5} stands out as a potentially optimal solution, while $S_a(T_i)$ (=IM_{s2}) appears as an acceptable alternative for certain *EDPs* [e.g. Figure 5-7(a2) and Figure 5-7(a1) for low θ_{pl} capacities]. Regarding $AvgS_a$ candidates, $IM_{s7\text{-}1}$ appears to be superior compared to $IM_{s7\text{-}2}$ and $IM_{s7\text{-}3}$, for certain ranges of the *EDP* capacities considered. Once again there is no singularly optimal *IM* at all *EDP* ranges of interest. This effect is mainly evident for plastic rotation capacities that exceed 0.3rad [Figure 5-7(a1)] and anchor bolt deformations larger than the prescribed fracture capacity of 100mm [Figure 5-7(a4)], although Figure 5-7(a2) implies that a similar effect would be observed for EFB should σ_m capacities over 100MPa were examined. Such an effect suggests that failure of anchors on a single spoke of the 'Joystick' model changes the response considerably, where the system begins to exhibit partial rocking (Bakalis et al. 2017a), an effect that is difficult to capture using a single *IM* throughout the response range.

Regardless of anchorage conditions, vector *IMs* appear to be following the trend of their respective primary element [i.e. *PGA* or $S_a(T_i)$] for impulsive-controlled modes of failure, occasionally providing larger dispersion estimates due to the conservative criterion presented in Figure 5-6(c). On the other hand, $S_a(T_c)$ (=IM_{s3}) appears to be the only *IM* that can efficiently predict the response related to the convective component of the tank [Figure 5-7(a3), (b3)], thus confirming the initial speculations outlined in the *IM* selection section. It is also evident that nearly all other candidate *IMs* develop considerably larger dispersion estimates of sloshing, an issue which is partially solved when certain spectral ordinates are combined with $S_a(T_c)$ (e.g. IM_{s4}, IM_{s6}, $IM_{s7\text{-}3}$, IM_{v1} and IM_{v2}), but still clearly deviates from the optimal solution of $S_a(T_c)$.

5.8.2 Sufficiency

Sufficiency aims to ensure that an *IM* is independent of seismological parameters such as epsilon and moment magnitude. Quantifying sufficiency is often performed via a linear regression of lnIM_C values against the aforementioned seismological characteristics as

$$\ln IM_C = a_M + b_M M_w + e_M \tag{5-3}$$

$$\ln IM_C = a_\varepsilon + b_\varepsilon \varepsilon + e_\varepsilon \tag{5-4}$$

where b_ε, b_M are the slopes, a_ε, a_M the intercepts and e_ε, e_M the normally distributed errors of these two straight lines in log space. Sufficiency essentially determines the statistical significance of each *IM* and is quantified by extracting there levant p-value from the regression output. Based on an earlier discussion for vector *IMs*, only IM_C values below the cut-off value of $S_a(T_c)/PGA$=0.5 or $S_a(T_c)/\ S_a(T_i)$=0.2 are employed in Equations (5-3) and (5-4).As an example, Figure 5-8 presents the linear regression of *PGA* values conditioned on the θ_{pl} capacity of 0.2rad versus ε and M_w, which constitutes the backbone of the process (Luco and Cornell 2007) that is used to generate the results that are further presented in Figures 5-9 and 5-10. It should be noted that p-values higher than 0.05 are generally acceptable indicators of low statistical significance and thus high *IM* sufficiency (Luco and Cornell 2007).

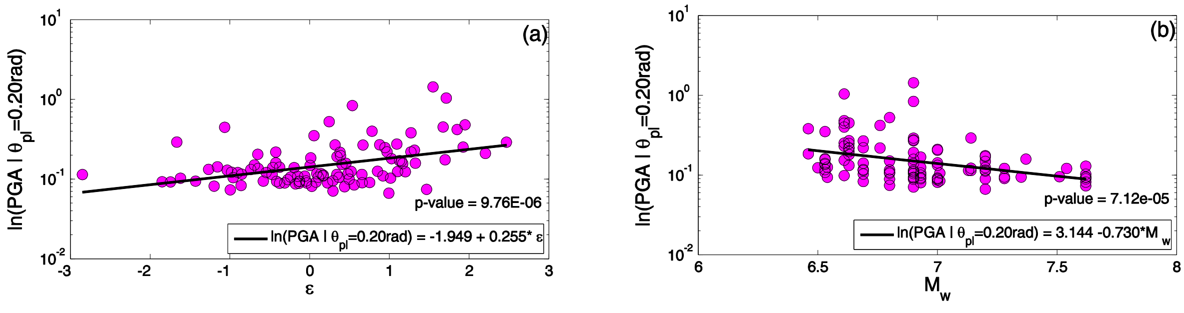

Figure 5-8: Linear regression of ln($PGA|\theta_{pl}$=0.20rad) values versus (a), ε and (b), M_w for the unanchored tank of Figure 5-1(a).

According to Figures 5-9 and 5-10, all *EDPs* besides sloshing wave height seem to be suffering from low p-values, when either of the *PGA* (=IM_{s1}), $S_a(T_i)$ (=IM_{s2}), $S_a(T_c)$ (=IM_{s3}), the geometric mean of $S_a(T_i)$ with $S_a(T_c)$ (=IM_{s4}), and that of $S_a(T_i)$ with $S_a(1.5T_i)$ (=IM_{s5}) is adopted as the *IM*, even though the latter presents acceptable p-values for the anchored tank prior to the fracture of the respective anchors, an effect that is also obvious for the $AvgS_a$ candidates $IM_{s7\text{-}2}$ and $IM_{s7\text{-}3}$. In general, $IM_{s7\text{-}1}$ appears as the most sufficient solution for the anchored system, bearing in mind that its sufficiency with respect to M_w is ensured only up to the point where anchors fracture. For the unanchored system on the other hand, $AvgS_a$ (=IM_{s7}), S_a combinations containing $S_a(T_c)$ (=IM_{s4} or IM_{s6}) and the vector *IMs* provide acceptable p-values for certain

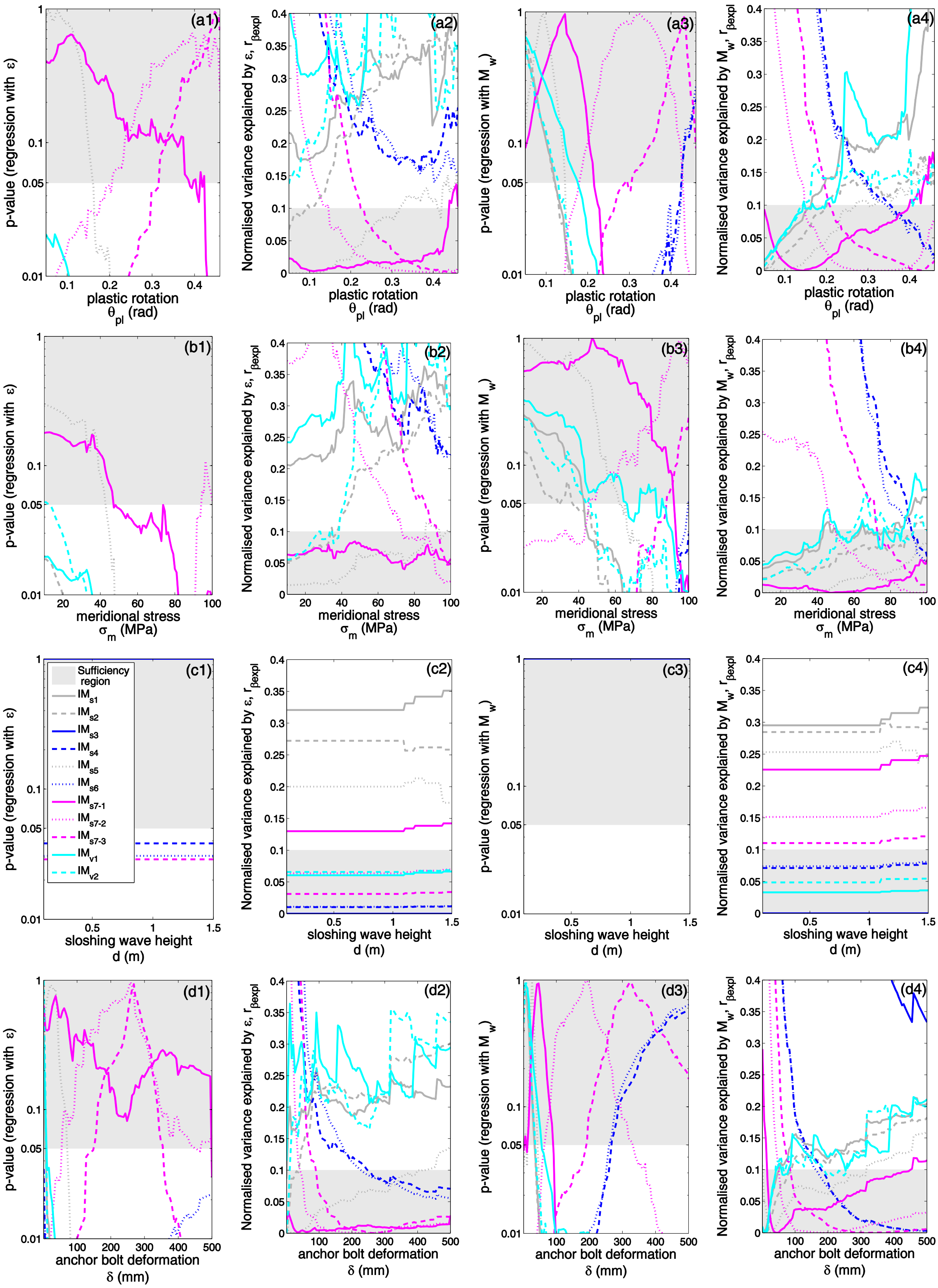

Figure 5-9: *IM* sufficiency for the *EDPs* of the anchored tank of Figure 5-1(a) using the GMset-plain; the columns from left to right present the p-values when the regression is performed against ε, the variance explained by ε normalised to the total $S_a(T_i)$ variance, the p-values when the regression is performed against M_w and the variance explained by M_w normalised to the total $S_a(T_i)$ variance, respectively.

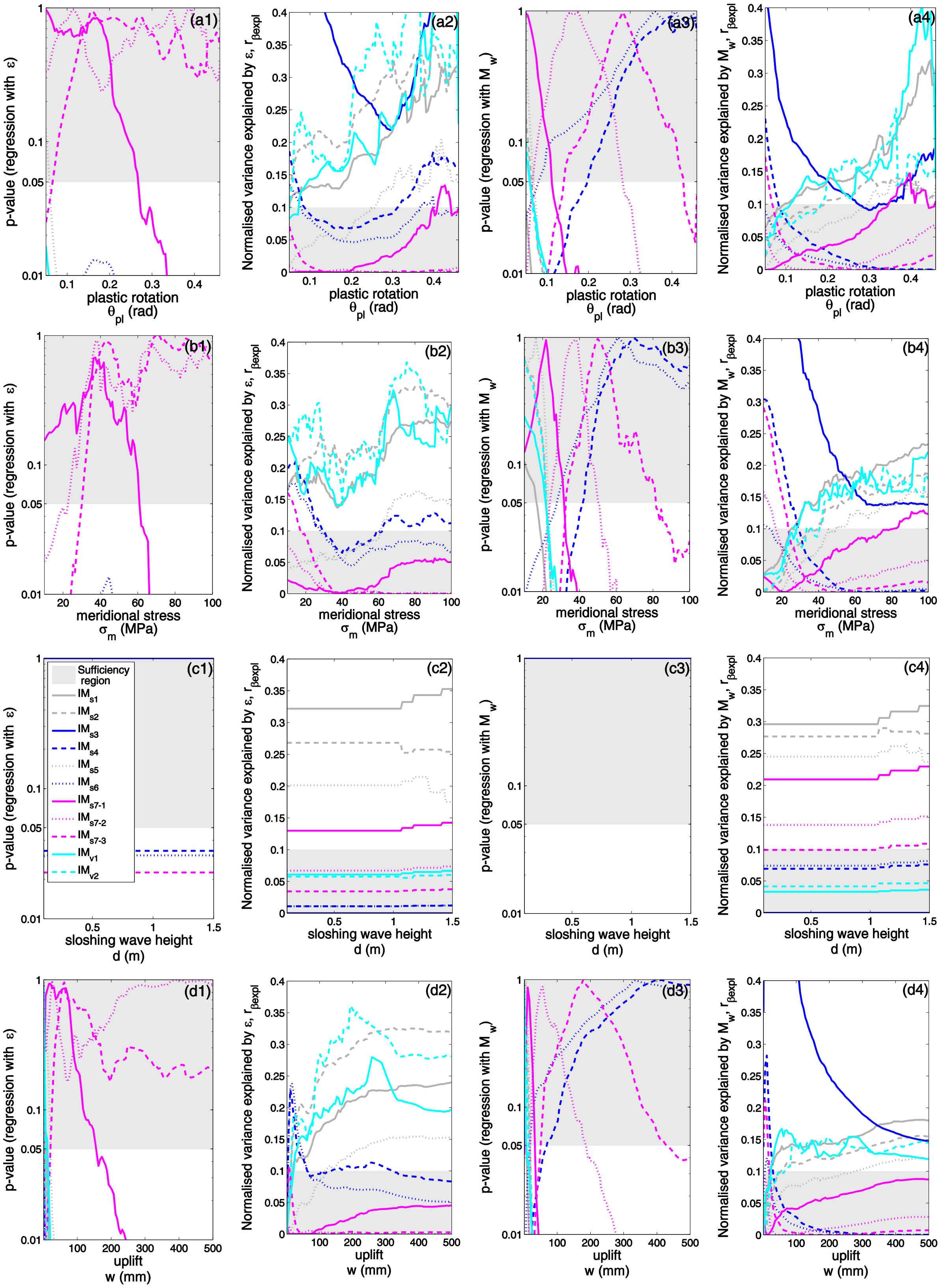

Figure 5-10: *IM* sufficiency for the *EDPs* of the unanchored tank of Figure 5-1(a) using the GMset-plain; the columns from left to right present the p-values when the regression is performed against ε, the variance explained by ε normalised to the total $S_a(T_i)$ variance, the p-values when the regression is performed against M_w and the variance explained by M_w normalised to the total $S_a(T_i)$ variance, respectively.

ranges of *EDP* capacities only, even though the former appears to be highly dependent on the range of periods considered for each $AvgS_a$, particularly when testing for M_w.

In any case, the p-values of Figures 5-9 and 5-10 do not point towards a single *IM* that is sufficient for the entire range of the response. At the same time, one should also bear in mind the several instances found in the literature where the use/interpretation of p-values is strongly criticised [e.g. Kazantzi and Vamvatsikos (2015); Nuzzo (2014)]. This is a common issue within the scientific community, which is often attributed to the confusion of two completely different terms such as *significance* and *relevance*. Undeniably, a small p-value might be an indicator of *IM* dependence (in our case) with M_w or ε, yet the extent of this effect remains unknown. Therefore, the question one should be asking ought to be in the context of magnitude of the effect rather than the effect itself. For example, one could easily improve all p-values by using a smaller set of records, thus removing statistical significance via inadequate sampling rather than an improved *IM*. Along these lines, the authors decided to provide an alternative metric of *IM* sufficiency, i.e. the variance explained by ε (or M_w) normalised to the total variance of $S_a(T_i)$, $r_{\beta expl}$, or normalised variance explained by ε (or M_w) in short:

$$r_{\beta expl} = \frac{R^2 \beta^2_{IM|EDP}}{\beta^2_{S_a(T_i)|EDP}} \tag{5-5}$$

$r_{\beta expl}$ describes the proportion by which the variance of the prediction errors shrinks, and is estimated herein using the product of the coefficient of determination (R^2) and the total IM_C variance, over the total variance of $S_a(T_i)$ capacities. In essence, low variance-explained values (e.g. < 0.10) imply *IM* sufficiency, meaning that M_w or ε do not offer any appreciable change to the determination of IM_C, thus their omission does not bias the relevant fragility (i.e. cumulative distribution function of IM_C). Therefore, according to Figures 5-9 and 5-10, the $AvgS_a$ $IM_{s7\text{-}1}$ is clearly promoted as the best option available for impulsive-driven modes of failure of anchored tanks, while all $AvgS_a$ are viable candidates for unanchored tanks. It should be noted that the aforementioned *IMs* as well as the vectors considered seem to be working for sloshing wave height too, only in absence of $S_a(T_c)$ (=IM_{s3}), though, which is by default the optimal solution in this particular case.

5.8.3 EDP-hazard

A further comparison among the candidate *IMs* is performed by extracting the response hazard curves for the *EDPs* of interest through Equation (5-1). The results presented in Figure 5-11 refer to the tank shown in Figure 5-1(a), using both anchored and unanchored support conditions, for each of the *IMs* outlined in Table 5-2. Discrepancies among the various response hazard curves by the *IM*, an argument that obviously needs a considerable amount of data to be supported for tank configurations other than the one examined herein (e.g. non-squat). Shape-wise, for anchored support conditions, the plastic rotation hazards [Figure 5-11(a1)] seem to display characteristic changes in steepness in the range of 0.02-0.05rad, which can be attributed to the sudden increase in dispersion, stemming from the uplift that the system begins to exhibit.

Overall, comparing the *EDP*-hazards for various candidate intensity measures cannot offer any significant insight on its own, as it essentially lacks a baseline solution, which means that any scatter observed among them may only be attributed to epistemic uncertainty inherent in the state-of-the-art approach of employing CS selection to remove any *IM* insufficiency. *EDP*-hazard curves are certainly useful to distinguish the outliers among the candidate *IMs*, combined to other relevant information such as efficiency and sufficiency (Figures 5-7, 5-9 and 5-10). Along these lines, *PGA* (=IM_{s1}) and $S_a(T_c)$ (=IM_{s3}) may be deemed unfit predictors for the evaluation of impulsive-controlled modes of failure, while at the same time it should be noted that the $AvgS_a$ candidates ($=IM_{s7}$) appear to serve as the central value among the rest of candidate *IMs*, regardless of the *EDP*.

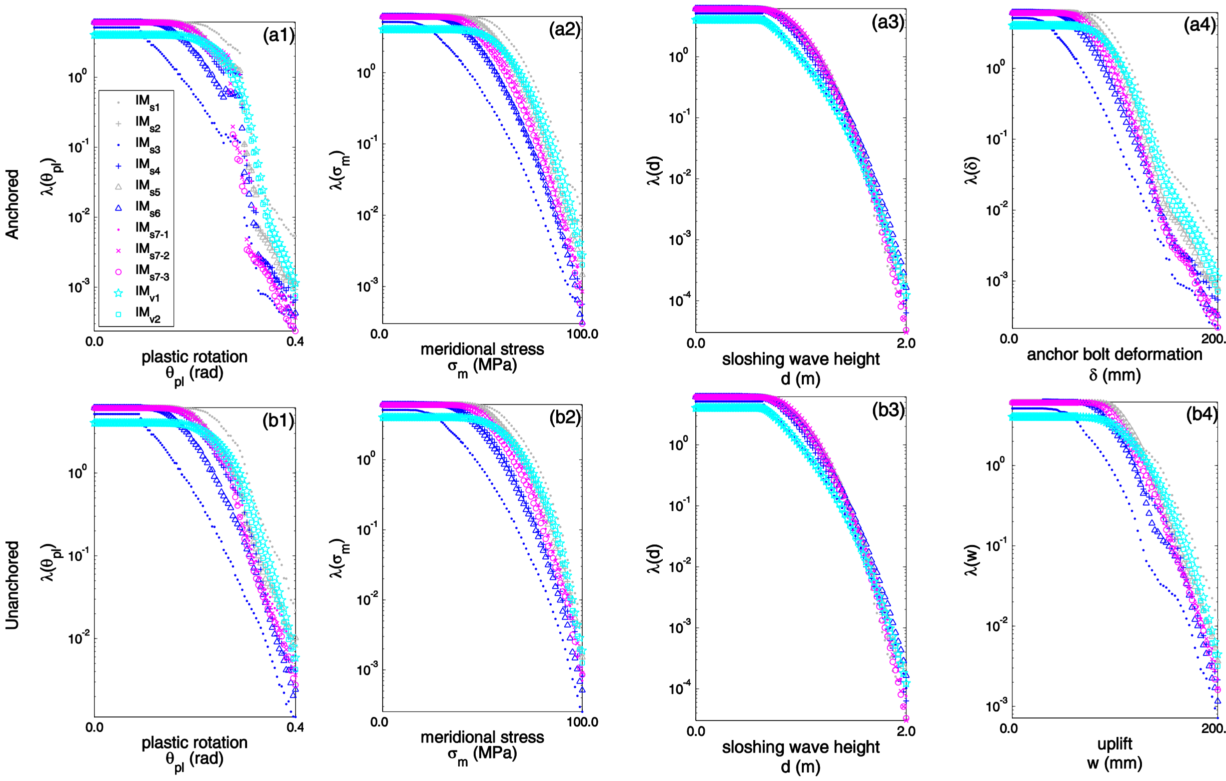

Figure 5-11: *EDP* hazard curves featuring the *IMs* of Table 5-2; (a1) and (b1) base plate plastic rotation, (a2) and (b2) meridional stress, (a3) and (b3) sloshing wave height, (a4) anchor bolt deformation, (b4) uplift. The results presented in row (a) refer to the anchored tank of Figure 5-1(a), while the ones in row (b) to the corresponding unanchored system. IDA results for GMset-CS.

5.8.4 Compound damage states

The information outlined so far is useful for the assessment of modes of failure determined by a single *EDP*. Still, it provides little insight on the issue of compound system-level damage states, controlled by two or more *EDPs*, as for example *DS*2. The latter is defined as the union of two and three events for unanchored and anchored tanks, respectively, involving both impulsive and convective modes of failure (Table 5-1). The latter, for the case of vector *IM* candidates, implies the necessity to generate the fragility surfaces appearing in Figure 5-12 for anchored and unanchored tanks, estimated by adopting a lognormal assumption in conjunction with the running quantiles of Figure 5-6(b) at each *EDP* level.

Due to specific definition of *DS*2 and the near-zero correlation among spectral ordinates at the widely spaced periods of T_i and T_c (Baker and Cornell 2006c; Inoue 1990), one may achieve a decomposition of the fragility and the MAF estimate for a 2-component vector $IM_v=\{IM_A, IM_B\}$, thus proposing a computationally cheap in terms of site hazard analysis alternative. For a union of two events *A*, *B*, each depending solely on IM_A, IM_B, respectively, this becomes

$$\begin{aligned}\lambda_{DS,IM_v} &= \iint \mathrm{P}\left(DS \mid IM_A, IM_B\right) \mathrm{d}\lambda\left(IM_A, IM_B\right) \\ &= \sum_p \sum_q \mathrm{P}\left(DS \mid IM_A^p, IM_B^q\right) \Delta\lambda\left(IM_A^p, IM_B^q\right) \\ &\approx \sum_p \sum_q \begin{bmatrix} \mathrm{P}\left(A \mid IM_A^p, IM_B^q\right) + \mathrm{P}\left(B \mid IM_A^p, IM_B^q\right) \\ - \mathrm{P}\left(A \mid IM_A^p, IM_B^q\right)\mathrm{P}\left(B \mid IM_A^p, IM_B^q\right)\end{bmatrix} \Delta\lambda\left(PGA_p, S_a(T_c)_q\right)\end{aligned}$$

where P[$DS|IM_A$, IM_B] is the corresponding fragility surface. Due to failure modes A, B being dependent only on a single IM, the double sum (or integral) involving a second irrelevant quantity simplifies to the classic scalar IM sum (or integral) of Equation (5-1). Thus:

$$\lambda_{DS,IM_v} \approx \lambda_{A,IM_A} + \lambda_{B,IM_B} - \lambda_{A,IM_A}\lambda_{B,IM_B} \tag{5-6}$$

Similarly, for a DS being a 3-event union of A, B, C, dependent on IM_A, IM_B, IM_A, respectively:

$$\begin{aligned}\lambda_{DS,IM_v} \approx\ & \lambda_{A,IM_A} + \lambda_{B,IM_B} + \lambda_{C,IM_A} - \lambda_{A,IM_A}\lambda_{B,IM_B} \\ & - \lambda_{A,IM_A}\lambda_{C,IM_A} - \lambda_{B,IM_B}\lambda_{C,IM_A} + \lambda_{A,IM_A}\lambda_{B,IM_B}\lambda_{C,IM_A}\end{aligned} \tag{5-7}$$

Equations (5-6) and (5-7) are essentially the intersection probability of two and three events in MAF space, respectively.

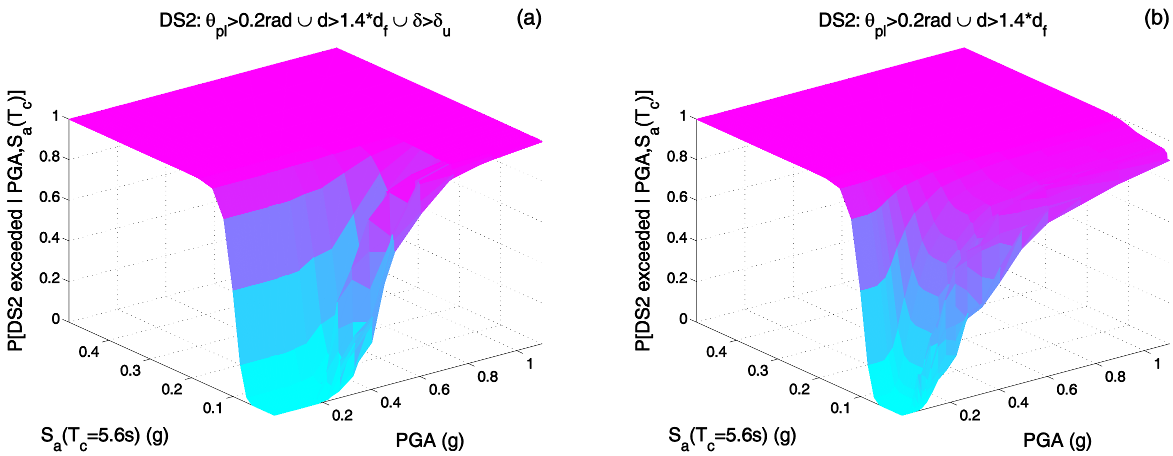

Figure 5-12: Probability of exceeding $DS2$ versus IM_{v1}; (a) anchored and (b) unanchored support conditions.

A comparison among the $DS2$ MAFs ($\lambda_{DS2,IM}$) is presented in Figure 5-13 with respect to the candidate IMs examined so far. Given that $DS2$ consists of a union of events that involve both impulsive and convective-controlled modes of failure (Table 5-1), the vector-valued IM_{v2} is indicatively adopted as a baseline solution thanks to its (slightly) better performance over IM_{v1}. Thus, the $DS2$ MAFs are normalised with respect to the corresponding MAF value $\lambda_{DS2,IMv2}$. As expected (Figures 5-7 and 5-11), Figure 5-13 reveals poor behaviour of the PGA (=IM_{s1}) for both anchored and unanchored support conditions, with respect to IM_{v2}. For the unanchored system, IM_{v1} and $IM_{v1,\mathrm{Eq(5\text{-}6)}}$ reveal a response similar to the PGA (=IM_{s1}), thus highlighting its dominant effect on the vector-valued IM. On the other hand, $S_a(T_i)$ (=IM_{s2}), IM_{s5}, the $AvgS_a$ candidates (=IM_{s7}) and the solution proposed through Equation (5-7) appear to be very close to the baseline solution of IM_{v2}. For the anchored system, however, there is no obvious candidate to be named as optimal. Actually, due to the change in system behaviour introduced by fracturing anchors, one cannot claim that IM_{v2}, which is neither efficient (Figure 5-7) nor sufficient (Figure 5-9), is an optimal choice. It is still employed as a baseline solution in this case to preserve consistency in the comparison of the pertinent IMs and structural systems (i.e.

anchored versus unanchored), bearing in mind that a vector of $AvgS_a$ and $S_a(T_c)$ might be a good way to get relatively efficient and sufficient results, at least if combined with a simple approximation that eliminates the need for a fragility surface and VPSHA. Considering those limitations, the sole outcome that can be drawn from Figure 5-13(a) is that the $AvgS_a$ candidates (=IM_{s7}) provide similar MAF estimates for $DS2$, and may thus be deemed appropriate. Also, the simplified estimate of Equations (5-6) and (5-7) is matching the results at least for IM_{v2}, offering a simpler way of employing vector IMs for tank assessment.

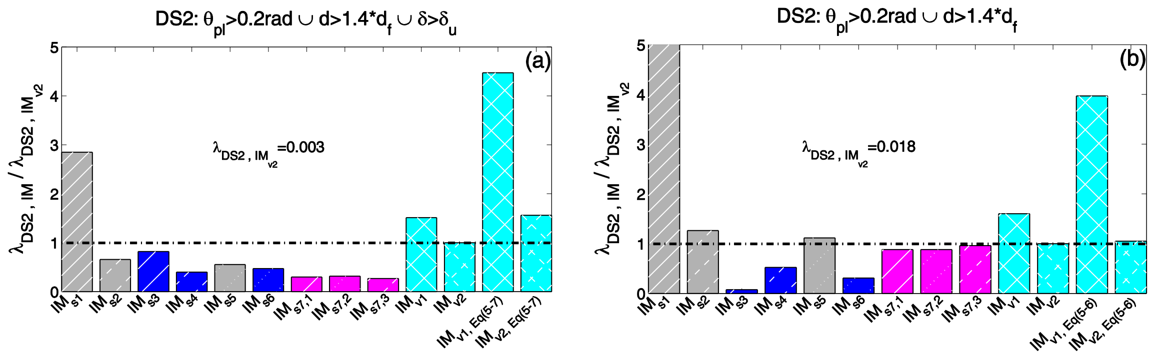

Figure 5-13: $DS2$ mean annual frequencies normalised to that of IM_{v2} for all candidate IMs; (a) anchored and (b) unanchored support conditions.

5.9 CONCLUSIONS

The applicability of several seismic intensity measures has been demonstrated for the seismic risk assessment of a squat liquid storage tank that is examined both under anchored and unanchored support conditions. Given that the motivation of this study is to propose an IM that is predominately able to reliably estimate the seismic risk for damage that is mutually controlled by the impulsive and convective fluid components of the tank, a dilemma/challenge arises regarding the nature of the IM that should eventually be nominated. On one hand, it is fairly obvious that the aforementioned problem can be adequately described using a vector of IMs, which admittedly is not very handy within the context of loss estimation due to the VPSHA and the fragility surface it demands; on the other hand, scalar IMs may need to be overly complex to achieve an acceptable solution for such diverse structural response, thus requiring a 'trial and error' process similar to the quest for suitable predictors in regression.

Altogether, the substantial difference in response for tanks with anchored and unanchored support conditions does not encourage the nomination of a single IM for their simultaneous seismic risk assessment, e.g. in a tank farm. For unanchored tanks, a potentially optimal solution is the average spectral acceleration $AvgS_a$ for a period range of [0.1s, 4.5T_i], while other similar period ranges or geometric mean combinations of T_i and 'elongated' T_i ordinates also perform reliably. For anchored tanks, the fracture of anchors clearly separates the response into two different regions, whereby pre-fracture assessment is better performed with the geometric mean of $S_a(T_i)$ and $S_a(1.5T_i)$ (an elastoplastic system), while post-fracture, one of the $AvgS_a$ candidates works well (a nonlinear elastic system). In addition, vector IMs can be employed with ease without vector PSHA and surface fragility burdens, by adopting a simple approximation for potentially superior efficiency and sufficiency.

Besides the outcome of this study itself, it is worth discussing the procedure that has been followed in order to reach the aforementioned conclusion. Each of the metrics that have been adopted for the IM evaluation provides useful information. For instance, dispersion in response offers an indication of IM efficiency, p-values are traditionally used to test sufficiency, while variance explained appears as a more reliable test for the latter, as it is not adversely influenced by the number of data points or the efficiency of the *IM*. The problem is that none of these metrics can stand on its own, which is quite intriguing, as individual parameters such as efficiency may fulfil the requirements to let a candidate *IM* be promoted as a potentially optimal solution, yet the cross examination with sufficiency for instance may indicate otherwise (although this is known to be a very rare scenario). Still, even in the case where all these properties are well within the allowable limits, the lack of a crystal-clear baseline solution may create additional obstacles in determining the optimal solution, as for instance in the case of *DS*2 for the anchored tank examined herein. In any case, the procedure that has been presented is straightforward, and the results could further be refined upon the availability of more reliable (or better studied) fracture capacities of the anchors. Part of the work presented in this chapter has been submitted for publication in the Journal of Earthquake Engineering and Structural Dynamics (Bakalis et al. 2018b).

6 SEISMIC VULNERABILITY ASSESSMENT OF LIQUID STORAGE TANK FARMS

6.1 ABSTRACT

A seismic vulnerability estimation procedure is developed for liquid storage tank-farms, specifically ensembles of atmospheric tanks that are interconnected to provide enhanced storage capacity for a given liquid product. All pertinent sources of uncertainty are considered together with associated intra- and inter-structure correlations, while particular attention is paid to the effect of uncertainty on damage state threshold values. Appropriate decision variables are defined in view of enabling decision-making for the mitigation of seismic losses at the level of the system, rather than the individual structure, focusing on (a) the leakage of stored product and (b) the loss of storage capacity. A case study of nine tanks, evenly split in three types, is undertaken. Whenever uncertain damage state thresholds are considered, Monte-Carlo simulations reveal a significant potential for loss of containment for average spectral accelerations ($AvgS_a$) of 0.30g. While storage capacity is proportionately impacted, a remarkable 30% of the total farm storage volume can survive an $AvgS_a$ of 0.5g, thus leaving considerable room for the drainage and repair of damaged tanks in typical operation scenarios.

6.2 INTRODUCTION

Oil & Gas industry products are normally stored in large-capacity atmospheric tanks. Safeguarding the integrity of such industrial facilities against earthquakes is vital not only for maintaining the flow of essential products and energy resources, but also for preventing any associated socioeconomic consequences. Ensuring an "appropriate" level of safety tantamount to the importance of liquid storage tanks, mandates the use of state-of-the-art techniques that take into account all possible sources of uncertainty, in the form of Performance-Based Earthquake Engineering [PBEE, Cornell and Krawinkler (2000)].

The assessment methodology typically undertaken by engineers is based on the design code and can be summarised in a prescriptive approach that may only deliver some acceptable (but actually unknown) level of accuracy by engaging in a deterministic process, where the associated dispersion is either inadequately defined or completely missing. It appears that current design codes and guidelines have not fully adopted the PBEE concept, while its application to industrial facilities is very limited and usually dependent on the respective client.

Despite the devastating outcome of recent earthquake events such as Kocaeli (1999) and Tohoku (2011), little attention has been paid to industrial facilities even from an academic point of view. Previous research efforts may be summarised to a fragility-based methodology using either computer-intensive finite element models (Buratti and Tavano, 2014; Talaslidis et al., 2004), or available empirical data as shown by O'Rourke and So (2000). Along these lines, a systematic PBEE methodology based on a surrogate (i.e., reduced-order) modelling approach was recently developed by Bakalis et al. (2015b, 2017a; c), thus offering an alternative to the existing procedures. Still, this only concerns a single tank rather than an ensemble.

Modern refineries accommodate a variety of industrial components that blend harmoniously to deliver high quality oil and gas products. The component topology is normally very strict and follows certain design criteria to meet health and safety measures. Large-capacity atmospheric tanks are normally constructed according to specific requirements to suit the volume produced and the physical characteristics of each liquid product in the refinery. Each design is typically constructed in multiples to avoid design and procurement iterations. Still, even for the same product, one may find adjacent liquid storage tanks that do not share similar geometric characteristics, either due to different year of construction, or due to the varying demand in fluid capacity prescribed by the client. Such a topology is presented in Figure 6-1 where the difference between the group on the left (indicated by yellow arrows) and the group on the right (indicated by red arrows) is evident.

This study aims to extend the existing framework by evaluating the seismic vulnerability of a set of liquid storage tanks. A typical tank-farm within a modern refinery is examined in view of defining the correlation of damage between adjacent structural systems with varying geometric characteristics, subject to the same ground excitation. Several scenarios are considered, taking into account the intra- and inter-structure correlations that befit a system of closely-spaced and constructionally related tanks.

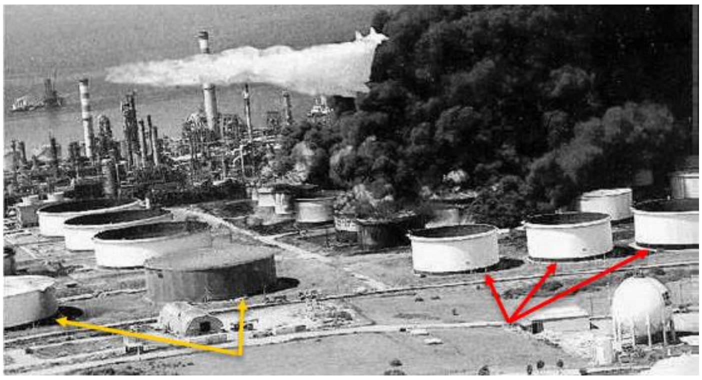

Figure 6-1: Damage on the Izmit refinery during the Kocaeli (1999) earthquake.

6.3 CASE STUDY DESCRIPTION

In an attempt to capture the seismic vulnerability involved in a modern industrial complex, a simple 3x3 layout is adopted, as shown in Figure 6-2. Three different structural systems are considered: Tanks A have a radius (R_{tA}) equal to 13.9m and a total height (h_{tA}) of 16.5m. The bottom course wall (t_{wA}) is 17.7mm thick, while the corresponding base plate (t_{bA}) and annular ring (t_{aA}) thickness are 6.4mm and 8.0mm respectively. In the same sense the geometric characteristics for Tanks B may be summarised as R_{tB}=23.47m, h_{tB}=19.95m, t_{wB}=22.23mm, t_{bB}=6.4mm and t_{aB}=10.0mm, while for Tank C as R_{tC}=6.1m, h_{tC}=11.3m, t_{wC}=9.6mm, t_{bC}=4.8mm and t_{aC}=4.8mm.

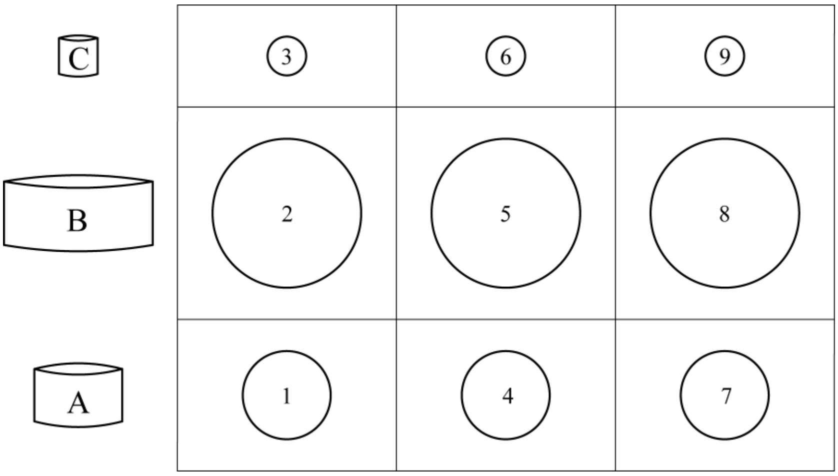

Figure 6-2: Case study layout of liquid storage tanks.

6.4 STRUCTURAL ANALYSIS

The surrogate modelling approach developed by Bakalis et al. (2017a) is adopted in view of offering a balanced "computational efficiency versus accuracy" compromise for nonlinear time-history analysis (Figure 6-3). The modelling approach is based on the work of Malhotra and Veletsos (1994) for liquid storage systems, where the uplift mechanism of unanchored tanks is modelled in detail. The response is defined using two decoupled masses that represent the rigid-impulsive motion of the tank on one hand and the sloshing of the fluid (convective mass) on the other. The latter is considered to offer very little in terms of overturning action on the tank (at least of the dimensions that are of interest herein), which means that it may be neglected during the modelling process, and that sloshing response may individually be obtained through a simple response spectrum analysis (CEN 2006; Malhotra 2000; Vathi and Karamanos 2017). Figure 6-4(a) presents the associated response for unanchored tanks A, B and C at their maximum fill level, under varying levels of earthquake loading. Single-record and median Incremental Dynamic Analysis (IDA) curves (Vamvatsikos and Cornell 2002) are plotted for a set of 30 pairs of records that have been selected using the conditional spectrum approach (Kohrangi et al. 2017a; Lin et al. 2013b). The base uplift is adopted as the engineering demand parameter (*EDP*), while the geometric mean of spectral accelerations [i.e. the so-called average spectral acceleration, $AvgS_a$, (Cordova et al. 2001; Eads et al. 2015; Kazantzi and Vamvatsikos 2015; Kohrangi et al. 2016b; Vamvatsikos and Cornell 2005a)] is employed as a suitable intensity measure (*IM*). Relevant research conducted by the authors (Bakalis et al. 2018b) has revealed the superiority of $AvgS_a$ over traditional (scalar) intensity measures such as the peak ground acceleration (*PGA*), while it has also shown that the range of low and high periods [T_L, T_H] that should be considered for it is [0.1s, 4.5T_i], where T_i is the impulsive mass vibration period of the liquid storage tank.

The most common failure modes are depicted on the median IDA curves (solid lines) in Figure 6-4, where θ_{pl} corresponds to the plastic rotation that may be developed on a tank's base plate when uplift is allowed, and EFB stands for the well-studied elastic-plastic buckling failure, known as the elephant's foot buckling. A third mode of failure, related to convective mode sloshing damage (SL) to the top of the tank wall is also considered. Still, as shown in Figure 6-4(b), this may occasionally appear at excessive $AvgS_a$ values due to the ultra-long convective period (T_c). Similarly, excessive plastic rotation at the base (i.e. order of 0.4rad), may also be difficult to reach for slender tanks such as Tank C. For the purpose of the vulnerability estimation presented below, a system-level damage state (*DS*) classification is adopted, similar to the one proposed by Vathi et al. (2017). The definition follows an increasing severity pattern,

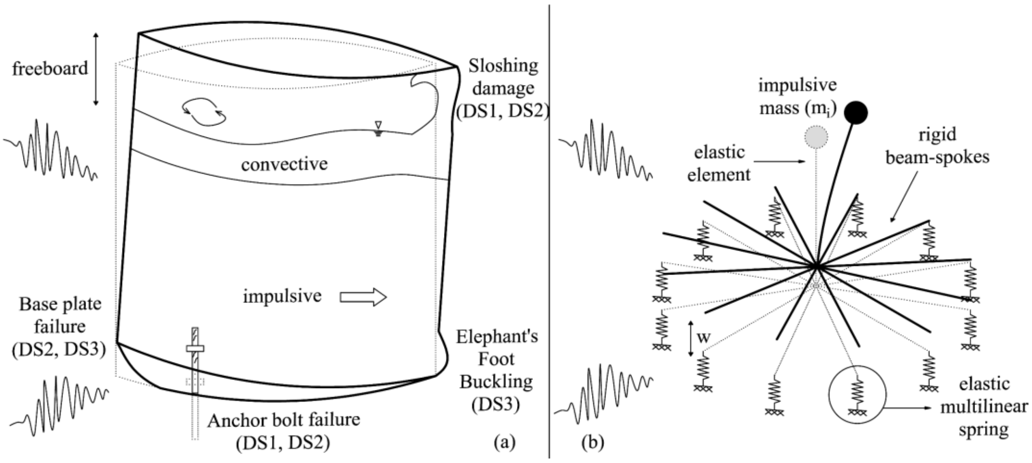

Figure 6-3: (a) Impulsive versus convective fluid component, failure modes, and system-level damage state classification on a fixed roof liquid storage tank. Depending on the presence of anchors, the system is either anchored or unanchored. (b) The "Joystick" surrogate model and its deflected shape (Bakalis et al. 2017b).

where *DS*0 represents no damage, *DS*1 slight damage, *DS*2 severe damage without leakage and *DS*3 loss of containment. For the case of unanchored systems, *DS*1 may be controlled by the sloshing response of the contained liquid only, *DS*2 though, is governed by the exceedance of either a sloshing wave height capacity equal to 1.4 times the available freeboard or a plastic rotation of 0.2rad at the base plate. *DS*3, finally, provides information on the loss of containment either through the EFB formation, or the exceedance of a base plate plastic rotation capacity equal to 0.4rad [Figure 6-3(a)].

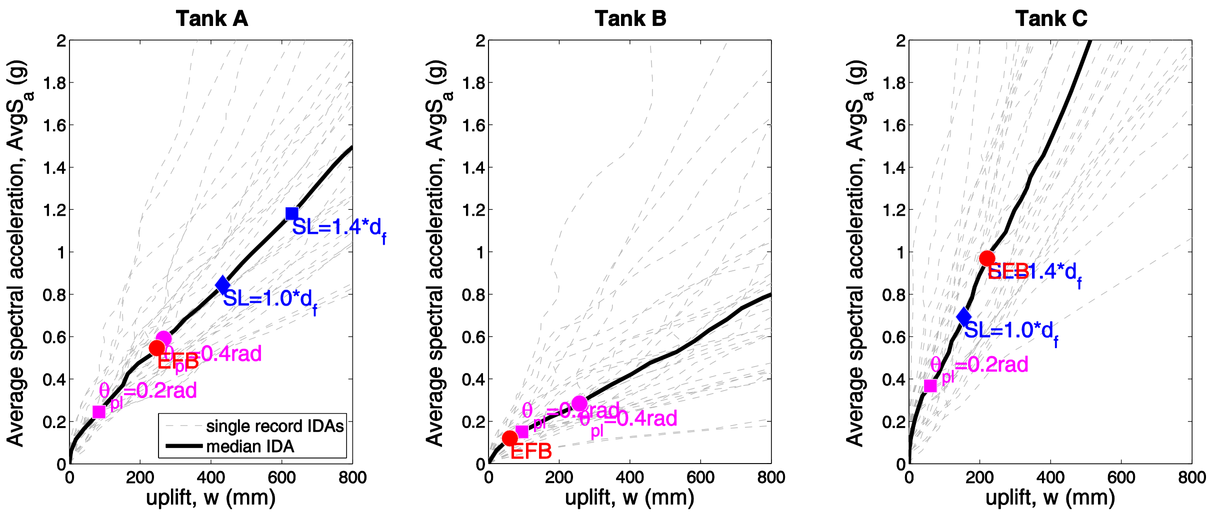

(a) (b) (c)

Figure 6-4: Single-record and failure mode capacities on the median IDA curves for Tanks (a) A, (b) B and (c) C at their maximum filling level.

6.5 VULNERABILITY FRAMEWORK

Predicting the seismic loss has been a major challenge for the earthquake engineering community. Complex structural systems may cause additional difficulties due to the increased level of uncertainty that requires even more runs to determine median and dispersion response estimates (Fabbrocino et al. 2005; Salzano et al. 2003). Fragiadakis and Vamvatsikos (2010) have extensively discussed the issues associated with uncertainty estimation not only through

Static Pushover procedures, but also using Incremental Dynamic Analysis (Vamvatsikos and Fragiadakis 2010), where the computational time is significantly increased. Recently, Bakalis et al. (2017a) investigated the potential sources of uncertainty for the surrogate model used herein. Parameters such as the ground motion uncertainty, the tank wall (t_w), the base plate (t_b) and annular ring (t_a) thickness were found to be of some importance, yet, the fluid height (h_f) serves as the one parameter that could critically modify the response of the system.

The sources of uncertainty associated with the case study considered may be summarised into the seismic load (i.e. the ground motion record to occur), and the structural properties (i.e. plate/shell thickness, fluid height). Structural elements may suffer a significant loss of thickness, mostly due to the chemical composition of liquids stored in a tank. Oil products typically contain sulphides or other substances (e.g. seawater in crude oil) that can severely corrode steel plating, having a significant impact on the structural capacity both locally and globally. Fluid height on the other hand is highly depended on the operation of the storage facility (e.g. within a refinery). Thus, it is evident that significant uncertainty will be present in any tank assessment.

Having established a performance-based framework where the structural variability is well defined, one may argue that the vulnerability estimation is only a few calculations away. That may be true for the case of a single liquid storage unit, but the application of the procedure on a tank-farm becomes more complex, as correlations regarding uncertainty both in the structure considered (intra-structure) and the farm (inter-structure) need to be considered. Bradley and Lee (2010) have already highlighted the component correlation significance by offering a structure-specific seismic loss procedure, where different correlation assumptions can significantly affect the results for certain cases. It appears that correlation has drawn a lot of attention since, as research efforts such as Kazantzi et al. (2014) and Vamvatsikos (2014) also take it into account in view of an accurate seismic performance estimation. Furthermore, interconnectivity of infrastructure is a topic of considerable importance that has grown considerably in the literature (e.g., Pitilakis et al. 2014). The fire hazard due to leakage ignition is a significant issue (Alessandri et al. 2017b; a; Fabbrocino et al. 2005), which however, is not tackled herein.

Regarding the different variables within a tank (i.e. intra-structure), zero intra-structure correlation is assumed. Plate/shell thicknesses may serve as the primary source of uncertainty, due to the effect they may have on the predefined failure mode capacities such as EFB and θ_{pl}. Following the sensitivity analysis results found in Bakalis et al. (2017a), it is reasonable to assume that the demand is not affected. The steel plates are already extremely thin compared to tank dimensions, and as a result, a reduction of thickness at the order of 30% is not expected to significantly modify either the local or the global demand for the tank. This observation reduces the computational load by far, as the model cases that must be considered correspond to tanks with varying fluid height only. Even damage state capacities that could be construed to be correlated due to similar corrosion damage, e.g. tank wall buckling resistance and base plate plastic rotation, are actually modelled uncorrelated as design codes stipulate a thickness-independent limiting value for θ_{pl}. Similarly, sloshing damage is only a function of the available freeboard (CEN 2006; Malhotra 2000).

For the case where two adjacent tanks are examined (i.e. inter-structure), the correlation may be deemed perfect across all tanks (types A, B and C) under the assumption that they are used to store the same product and filled/drained uniformly. Apparently, this is highly depended on the operating procedures within the refinery, thus implying strong correlation for sloshing damage states as they are a function of the available freeboard and hence the fluid height. Zero correlation may be assumed for the damage state capacities of different tanks, bearing in mind that parameters such as the year of construction and the inspection/repair schedule will reduce any dependence: To avoid a significant reduction in storage capacity of the tank-farm, repairs are performed serially rather than in parallel, resulting in tanks with different corroded states at the time of the earthquake. However, for a very large storage facility that could afford to inspect and repair tanks in parallel, strong correlation may be a better option. As far as ground motion records are concerned, they may be applied uniformly on the entire tank-farm, given the same site conditions and the relatively small distance between them, thus implying full correlation. To be more precise, perfect correlation can only be achieved among structural systems that share the same dynamic properties, i.e. the impulsive (T_i) and convective (T_c) periods of vibration. Even for the same type of tanks, the aforementioned variables are strongly tied to the fluid height ratio (i.e. a certain percentage of the maximum allowable fluid height prescribed for a liquid storage system), leading to a strong but not necessarily perfect correlation.

6.5.1 Monte Carlo sampling

With the basis of the vulnerability framework adequately defined, the sample matrix may be formed in a few steps. A series of assumptions that define both intra and inter-structure correlation is more than necessary at this point in order to come up with realistic scenarios at the minimum computational cost. Fluid height levels of interest are defined to describe common

Table 6-1: Sample matrix without *DS* threshold uncertainty. All possible combinations of 5 fluid heights times 30 record pairs are considered for each tank.

#	Tank 1	Tank 2	...	Tank 9
30 records * h_{f1}	$0.55h_{fA,max}$ record 1	$0.55h_{fB,max}$ record 1	...	$0.55h_{fC,max}$ record 1
	$0.55h_{fA,max}$ record 2	$0.55h_{fB,max}$ record 2	...	$0.55h_{fC,max}$ record 2
	…	…	...	…
	$0.55h_{fA,max}$ record 30	$0.55h_{fB,max}$ record 30	...	$0.55h_{fC,max}$ record 30
30 records * h_{f2}	$0.65h_{fA,max}$ record 1	$0.65h_{fB,max}$ record 1	...	$0.65h_{fC,max}$ record 1
	$0.65h_{fA,max}$ record 2	$0.65h_{fB,max}$ record 2	...	$0.65h_{fC,max}$ record 2
	…	…	...	…
	$0.65h_{fA,max}$ record 30	$0.65h_{fB,max}$ record 30	...	$0.65h_{fC,max}$ record 30
… …	… …	… …	… …	… …
30 records * h_{f5}	$0.95h_{fA,max}$ record 1	$0.95h_{fB,max}$ record 1	...	$0.95h_{fC,max}$ record 1
	$0.95h_{fA,max}$ record 2	$0.95h_{fB,max}$ record 2	...	$0.95h_{fC,max}$ record 2
	…	…	...	…
	$0.95h_{fA,max}$ record 30	$0.95h_{fB,max}$ record 30	...	$0.95h_{fC,max}$ record 30

Table 6-2: Sample matrix with *DS* threshold uncertainty. For each tank, all possible combinations of 5 fluid heights times 30 record pairs, times *Np*=8 damage state capacities are considered.

#	Tank 1	...	Tank 9	...	Tank 9
30 records * h_{f1}*$EDP_{C,j,Np}$	$0.55h_{fA,max}$ record 1 $EDP_{C,1,1}$	...	$0.55h_{fC,max}$ record 1 $EDP_{C,9,1}$	...	$0.55h_{fC,max}$ record 1 $EDP_{C,9,Np}$
	$0.55h_{fA,max}$ record 2 $EDP_{C,1,1}$	...	$0.55h_{fC,max}$ record 2 $EDP_{C,9,1}$	...	$0.55h_{fC,max}$ record 2 $EDP_{C,9,Np}$
	…	...	…	...	…
	$0.55h_{fA,max}$ record 30 $EDP_{C,1,1}$	...	$0.55h_{fC,max}$ record 30 $EDP_{C,9,1}$	...	$0.55h_{fC,max}$ record 30 $EDP_{C,9,Np}$
30 records * h_{f2}*$EDP_{C,j,Np}$	$0.65h_{fA,max}$ record 1 $EDP_{C,1,1}$	...	$0.65h_{fC,max}$ record 1 $EDP_{C,9,1}$	...	$0.65h_{fC,max}$ record 1 $EDP_{C,9,Np}$
	$0.65h_{fA,max}$ record 2 $EDP_{C,1,1}$	...	$0.65h_{fC,max}$ record 2 $EDP_{C,9,1}$	...	$0.65h_{fC,max}$ record 2 $EDP_{C,9,Np}$
	…	...	…	...	…
	$0.65h_{fA,max}$ record 30 $EDP_{C,1,1}$	...	$0.65h_{fC,max}$ record 30 $EDP_{C,9,1}$	...	$0.65h_{fC,max}$ record 30 $EDP_{C,9,Np}$
… …	… …	… …	… …	… …	… …
30 records * h_{f5}*$EDP_{C,j,Np}$	$0.95h_{fA,max}$ record 1 $EDP_{C,1,1}$	...	$0.95h_{fC,max}$ record 1 $EDP_{C,9,1}$	...	$0.95h_{fC,max}$ record 1 $EDP_{C,9,Np}$
	$0.95h_{fA,max}$ record 2 $EDP_{C,1,1}$	...	$0.95h_{fC,max}$ record 2 $EDP_{C,9,1}$	...	$0.95h_{fC,max}$ record 2 $EDP_{C,9,Np}$
	….	...	….	...	….
	$0.95h_{fA,max}$ record 30 $EDP_{C,1,1}$	...	$0.95h_{fC,max}$ record 30 $EDP_{C,9,1}$	...	$0.95h_{fC,max}$ record 30 $EDP_{C,9,Np}$

practice scenarios. h_f is assumed to be uniformly distributed in [$0.5h_{f,max}$, $1.0h_{f,max}$], where $h_{f,max}$ is the maximum allowable fluid height for each tank type. Stratified sampling is performed on the aforementioned fluid heights of interest, resulting in five different structural systems for each tank that need to be subjected to Incremental Dynamic Analysis, based on the associated j^{th} sample of fluid height ($h_{f,j}$). For the case study examined, it is assumed that all nine tanks are uniformly filled to same fluid height ratio at any given time. Obviously, the amount of the liquid in a tank is affected by the operations performed within a refinery, yet some uniformity of the filling height is a plausible assumption, given that the same product is assumed to be stored in all tanks. Table 6-1 shows the sample matrix with all the available scenarios considered when no damage state uncertainty is employed. Therefore, only scenarios associated with fluid height and ground motion uncertainties are presented.

A more realistic representation is possible if the damage states are examined from a probabilistic point of view, where their capacities are considered lognormally distributed around their median estimates (EDP_c). Bearing in mind the zero correlation already assumed, Table 6-1 may be augmented following a random permutation pattern (due to zero inter-structure correlation) of the uncertain capacities for each tank. A reasonable sample size (i.e. N_p=8) is considered for the Monte Carlo simulation and stratified sampling is performed in order to define equiprobable damage state capacities, as shown in Table 6-2.

6.5.2 Damage index

Seismic vulnerability is typically illustrated using appropriate decision variables. They may be used to quantify seismic loss in terms of cost or damage, depending on the application. For the case of liquid storage tanks two damage indices (*DI*) are defined.

*DI*1 shall represent the loss of containment ratio,

$$DI1 = \frac{\text{Volume loss post event}}{\text{Volume contained pre event}} \tag{6-1}$$

under the assumption that the exceedance of the *DS*3 capacity triggers a complete loss of the stored product within the tank. *DI*2 on the other hand shall provide information on the available volume capacity through the following equation:

$$DI2 = \frac{\text{Volume capacity loss post event}}{\text{Volume capacity pre event}} \tag{6-2}$$

The concept behind the aforementioned damage indices is to enable a decision-making process using parameters that make sense even to non-engineers. They provide information both on the loss of the stored material and on the capacity of the facility following an earthquake event. Both indices are obviously controlled through *DS*3, while *DI*2 is affected by *DS*2 too, in view of the significant damage that may render the tank unusable. *DS*1 is not considered in this calculation, as it represents relatively easy-to-repair damage on the upper course of the tank whose repair may require draining the tank but can be scheduled with relative ease.

Figure 6-5(a) presents the 16%, 50% and 84% fractiles for *DI*1, without considering *DS* threshold capacity uncertainty. It is evident that the tank farm examined suffers an immediate loss of containment, at the order of 35%, which may be attributed to the exceedance of the θ_{pl}=0.4rad capacity as well as the EFB allowable stress for type ‘B’ tanks (i.e. 2-5-8 in Figure 6-2). According to Figure 6-4, the aforementioned capacities are developed for relatively moderate $AvgS_a$ estimates (order of 0.15-0.30g), when the contained liquid reaches the maximum allowable height, thus verifying the results observed in the first ascending branches of Figure 6-5(a) fractiles. Moreover, both EFB and θ_{pl}=0.4rad capacities of type 'A' tanks are slightly higher (order of 0.55-0.60g) compared to the corresponding type 'B' values, fully justifying the loss of another 30% of the total volume stored in the facility. Evidently, type 'C' tanks are held responsible for the loss of the remaining volume, as the loss of containment damage state capacities are developed for significantly larger seismic intensities. It should be noted that the response of the type 'C' tanks never reaches the θ_{pl}=0.4rad limit, and as a result *DI*1 is solely controlled by EFB for that particular case.

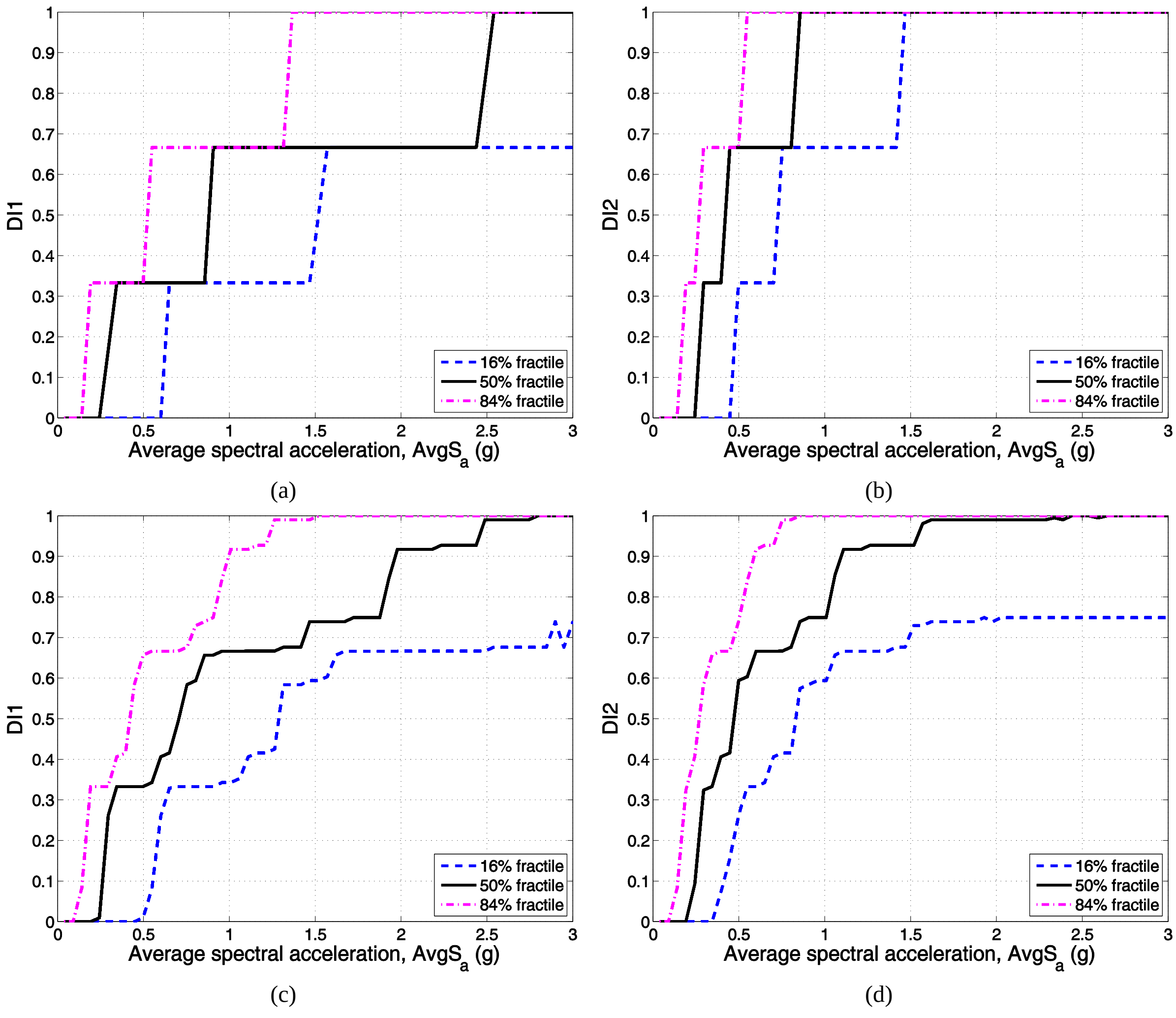

Figure 6-5: (a) *DI*1 without *DS* threshold uncertainty, representing the system loss of containment, (b) *DI*2 without *DS* threshold uncertainty, featuring the system loss of capacity, (c) *DI*1 with *DS* threshold uncertainty and (d) *DI*2 with *DS* threshold uncertainty.

The results discussed above are presented from a system capacity point of view in Figure 6-5(b). 16%, 50% and 84% fractiles are illustrated for *DI*2, thus providing an alternative representation of the system response, where the available capacity suddenly drops (on average) down to (approximately) 30%, once an $AvgS_a$ at the order of 0.30g is reached. The two graphs provide similar, yet not identical information. For instance, one may notice the considerably larger variation among the fractiles in Figure 6-5(a), which cannot be attributed to the record-to-record variability. In fact, *DI*1 is strongly tied to the fluid height ratio compared to *DI*2 that is only affected by the actual height of the tank. Hence, this extra source of uncertainty appears in the representation of the results.

Damage indices 1 and 2 are reproduced taking the *DS* threshold uncertainties into account. It appears that uncertainty significantly removes the abrupt nature of the previous results for *DI*1 and *DI*2. Comparing the median vulnerability curves of Figure 6-5(c) and Figure 6-5(d) for any given *IM* level, reveals that *DS* uncertainty forces the onset of minor loss to appear at lower $AvgS_a$ values, yet significant losses are delayed until much higher intensity levels, at least for *DI*2. Regarding *DI*1, an $AvgS_a$ equal to 0.60g results in a median loss of containment slightly over 40% when the *DS* uncertainties are taken into account, while a 35% loss is estimated for the case that the aforementioned uncertainties are ignored. Similar conclusions are drawn for *DI*2, as according to Figure 6-5(b) and Figure 6-5(d), for an $AvgS_a$ level equal to 0.60g, both median system capacities suffer a 65% loss, respectively.

The differences observed among the two different assumptions are significant. There is no question that properly accounting for *DS* uncertainty is important, but at the same time it comes at an additional computational cost. Ignoring this important source of variability may simplify the analysis, yet at the same time it introduces an unknown error that may or may not be conservative, thus degrading the fidelity of one’s conclusions.

6.6 CONCLUSIONS

A seismic vulnerability assessment methodology has been developed for the mitigation of seismic losses within a typical tank-farm. The damage indices developed aim to enable a rapid decision-making process through the estimation both of the loss of containment and the available capacity, following a strong ground motion event. Potential assumptions are discussed in view of defining intra and inter-structure correlation, of the effect of considering or neglecting damage state capacity uncertainty is examined. Although the majority of assumptions are reasonably defined, further modifications to the existing framework could extend the accuracy as well as the applicability of the methodology. Employing a leakage ratio for *DI*1, instead of the assumption that a full loss of containment takes place upon the *DS*3 capacity exceedance, would be a good example to illustrate this. The latter may enhance the quality of the methodology outlined, and it is expected to be covered in a future direction of our research. Part of the work presented in this chapter has been submitted for publication in the 16th European Conference on Earthquake Engineering.

7 CONCLUSIONS

7.1 SUMMARY

In the preceding chapters a PBEE driven methodology has been presented with respect to the seismic performance assessment of liquid storage tanks.

Following a brief introduction (**Chapter 2**) that summarises the design and construction practice as well as the seismic response of liquid storage tanks, **Chapter 3** presents a reduced order model that aims to capture commonly observed modes of failure under earthquake loading. The aim of this modelling approach is to eliminate the need for detailed finite element models that are traditionally used to calibrate simpler ones that are able to provide a certain volume of analysis results within a reasonable timeframe. Therefore, the response of the so-called "Joystick" model is compared to shell-element-based finite element models under static pushover loading patterned after the impulsive mode, revealing an acceptable match for each of the case studies considered. Despite the (minor) differences observed among the two modelling approaches, what really matters in this instance is the establishment of low bias for the "Joystick" model and the quantification of the so-called model-type uncertainty, which could easily be incorporated in the PBEE assessment process, bearing in mind that both may further be refined using more elaborate finite element models. Besides the ability to accommodate simultaneous ground motion recordings in all principal loading directions (i.e. horizontal, transverse and vertical) during the analysis, one of the key features of the "Joystick" model is an option that enables the modelling of both self-supported (i.e. unanchored) and anchor-bolt-supported (i.e. anchored) liquid storage tanks. It should be noted that the response of the "Joystick" model was found to be sensitive to modelling parameters such as the fluid height (predominantly) and the wall thickness. Similarly, the estimation of the buckling stress demand was found to be sensitive to the base plate discretisation, requiring a number of approximately $2.5R_t$ spokes (R_t in meters), while global response parameters such as uplift would only require $0.35R_t$ spokes for the response to be unaffected.

A more elaborate representation of earthquake damage on liquid storage tanks is presented in **Chapter 4**, using representative component and system-level PBEE framework products such as fragility curves and mean annual frequencies of exceedance. Considering the assumptions performed in the course of this study, a general remark that can be drawn regarding liquid storage tanks, is that they comprise extremely vulnerable structural systems that should be adequately safeguarded against earthquakes. This is not only highlighted by the onset of damage in relatively low seismic intensities, but also from the fact that the progression of damage does not follow the well-known pattern where slight damage precedes moderate and severe. Thereby, severe structural damage may abruptly appear with little or zero warning.

In the process of extracting the probability of exceeding response parameter thresholds for the associated modes of failure, various challenges are encountered with respect to elephant's foot buckling, mostly stemming from the fact that its capacity is dependent on the time step as well as the seismic intensity of the ground motion. Such observation leads to the conclusion that (according to the proposed framework) EFB should be monitored in the time domain, where only the intersection of the demand and capacity response histories may signal failure. This is very crucial, as there are cases where demand response history maxima exceed the associated capacity minima, but still occur on a different time steps. Another significant contribution regarding EFB, is the ability to capture the extend of its damage along the circumference of the tank. At a first glance, this may seem rather unnecessary, as an engineer would typically be interested in whether the EFB capacity is exceeded anywhere on the structure; however, considering the piping that is often attached on industrial facility liquid storage tanks, establishes the extent of EFB damage a critical parameter with respect to the loss of containment damage state, as the EFB-imposed displacement on the pipes may lead to rupture and immediate release of content.

The PBEE framework extensively discussed in Chapter 4, is further refined by investigating a series of seismic intensity measures in terms of efficiency, sufficiency and *EDP*-hazard curves in **Chapter 5**. Besides ordinary scalar *IMs* such as *PGA* and $S_a(T_1)$, several combinations of spectral acceleration ordinates are examined in view of coming up with a solution that renders structural response independent of seismological characteristics, while at the same time minimises the number of ground motion records required to achieve the same numerical output. Vector-valued *IMs* are also examined, in order to serve as baseline solutions for the applicability of the aforementioned scalar ones with respect to the assessment of damage states that are mutually controlled by both impulsive and convective modes of failure. Among the selected candidates, the geometric mean of spectral accelerations in a range of [0.1s, $4.5T_i$] stands out as a potentially optimal solution. This is a very promising finding with respect to the assessment of a group/class of tanks that are often encountered in industrial facility complexes, as it enables the use of a state-of-the-art *IM* that is able to represent the spectral shape information in a more sophisticated manner compared to the widely used *PGA* and $S_a(T_1)$.

The aforementioned *IM* is adopted for the seismic vulnerability assessment of a case-study tank-farm layout in **Chapter 6**. The layout under investigation is used to discuss potential decision-making approaches in view of minimising the expected earthquake-induced losses. In that instance, two damage indices are proposed with respect to the post-earthquake capacity of the facility and the corresponding loss of content. The vulnerability of liquid storage tanks that has already appeared in previous chapters of this study is also highlighted on a tank-farm level. Still, the most important aspect of this chapter is the consideration or not of the uncertainty of the *EDP* capacities. Ignoring uncertainty allows for an easier-to-apply damage index estimation which is counterbalanced by the accuracy offered. Taking uncertainties into account increases the post-processing workload, yet it provides a more realistic view of the expected seismic losses within the tank farm.

7.2 LIMITATIONS AND FUTURE WORK

The work presented in this study is bound to the "Joystick" modelling approach and thus its own limitations. Therefore, a more refined calibration of the "Joystick" may improve upon the robustness of the results provided. This could be achieved by simply considering more case study tanks, by using finite element models that explicitly take into account the fluid-structure-interaction, or by modifying the hydrodynamic pressure distributions found in the literature (Housner 1957, 1963; Malhotra 2000; Malhotra and Veletsos 1994c; Veletsos and Tang 1990) via experimental tests. The aforementioned approaches may slightly modify the response and/or the model-parameter uncertainty; still, the procedure outlined regarding the modelling as well as the seismic risk assessment of liquid storage tanks is expected to be unaffected.

Seismic risk assessment alone, is clearly tied to the proposed damage state classification. Adopting different response parameter thresholds to signal failure on a component-level approach, or even different failure mode combinations to control system-level damage, is expected to modify the fragility curves as well as the mean annual frequencies (or return periods) of exceedance. For the latter, it should be noted that performing the seismic risk assessment on a different site would certainly provide different MAF estimates; still, fragility curves should remain unchanged when an efficient/sufficient *IM* is employed (Kohrangi et al. 2017b; Luco and Cornell 2007). In addition, the case studies considered for anchored tanks herein consist of unanchored tank designs that are indicatively equipped with anchor-bolt properties to provide intuitive results for anchored tanks too. Thus, realistic designs of anchored liquid storage tanks should be examined in order to enhance the validity of the results, particularly for the optimal *IM* proposed in Chapter 5. In a similar manner, the tank farm vulnerability framework presented in Chapter 6 is limited by the chosen case study farm.

Future work on liquid storage tanks may include the application of the methodology on an actual tank farm or refinery, by explicitly taking into account the correlation of *EDP* capacities as well as the interconnectivity of liquid storage tanks with other industrial equipment structures such as piping and pipe-racks. It would also be interesting to generate a code-compatible assessment approach which could be achieved via a static pushover approach for liquid storage tanks (Bakalis et al. 2015a, 2018a, Vamvatsikos and Cornell 2005b, 2006). The latter could be beneficial to the earthquake engineering community not only regarding liquid storage tanks, but also nonlinear-elastic systems in general, as current literature is in lack of suitable 'strength ratio-ductility-period' relationships to derive the associated structural demand using a simple static pushover analysis. Finally, as PBEE concepts evolve in time, it would be an opportunity to exploit the "Joystick" model capabilities and investigate potential performance-based design approaches such as the "Yield Frequency Spectra" proposed by Vamvatsikos and Aschheim (2016) [see also Bakalis and Vamvatsikos (2015); Katsanos and Vamvatsikos (2017)].

7.3 OVERALL CONCLUSIONS

The application of the PBEE framework for liquid storage tanks has extensively been discussed. Bearing in mind the fundamentals provided by Cornell and Krawinkler (2000), the "Joystick" surrogate model is formed in order to obtain the distribution of certain response parameters of interest versus the seismic intensity. Using appropriate component and system-level damage state classifications for individual tanks, as well as suitable damage indices for tank farms, the vulnerability of liquid storage tanks against earthquakes is revealed, as even moderate-intensity ground motions may result in significant damage. Adopting state-of-the-art intensity measures does not alter the aforementioned conclusions; yet it provides a more robust tool to assess seismic performance. The latter finds great application for the assessment of groups of tanks, whereby structural systems of various geometric properties are encountered, thus providing a promising package for the estimation of seismic losses in industrial-facility complexes.

8 REFERENCES

ABAQUS Documentation (6.11). (2011). Dassault Systèmes, Providence, RI, USA.

Ahari, M. N., Eshghi, S., and Ashtiany, M. G. (2009). “The tapered beam model for bottom plate uplift analysis of unanchored cylindrical steel storage tanks.” *Engineering Structures*, Elsevier Ltd, 31(3), 623–632.

Alessandri, S., Caputo, A. C., Corritore, D., Giannini, R., Paolacci, F., and Phan, H. N. (2017a). “Probabilistic risk analysis of process plants under seismic loading based on Monte Carlo simulations.” *Journal of Loss Prevention in the Process Industries*, Elsevier Ltd, (Article in press).

Alessandri, S., Caputo, A. C., Corritore, D., Renato, G., Paolacci, F., and Phan, H. N. (2017b). “On The Use of Proper Fragility Models for Quantitative Seismic Risk Assessment of Process Plants in Seismic Prone Areas.” *Proceedings of the ASME 2017 Pressure Vessels & Piping Division Conference*, Waikoloa, Hawaii, United States.

AMACS Process Towers Internals. (2016). “Oil Refinery Towers and Petrochemical in Sarjeant.” <https://www.amacs.com/winning-plant-turnarounds-come-standard/oil-refinery-towers-and-petrochemical-iain-sarjeant/> (Nov. 14, 2017).

American Lifelines Alliance. (2001a). *Seismic fragility formulation for water systems: Part 1-Guideline*. ASCE.

American Lifelines Alliance. (2001b). *Seismic Fragility Formulation for Water Systems Part 2-Appendices*. ASCE.

American Petroleum Institute. (2007). *Seismic Design of Storage Tanks - Appendix E, Welded Steel Tanks for Oil Storage*. API 650, 11th Edition, Washington, D.C.

Amiri, M., and Sabbagh-Yazdi, S. R. (2011). “Ambient vibration test and finite element modeling of tall liquid storage tanks.” *Thin-Walled Structures*, 49(8), 974–983.

Amiri, M., and Sabbagh-Yazdi, S. R. (2012). “Influence of roof on dynamic characteristics of dome roof tanks partially filled with liquid.” *Thin-Walled Structures*, 50(1), 56–67.

Ancheta, T., Darragh, R., Stewart, J., Seyhan, E., Silva, W., Chiou, B., Wooddell, K., Graves, R., Kottke, A., Boore, D., Kishida, T., and Donahue, J. (2013). *PEER NGA-West2 Database, Technical Report PEER 2013/03*. Pacific Earthquake Engineering Research Center, Berkeley, CA.

De Angelis, M., Giannini, R., and Paolacci, F. (2009). “Experimental investigation on the seismic response of a steel liquid storage tank equipped with floating roof by shaking table tests.” *Earthquake Engineering & Structural Dynamics*, 39(4), 377–396.

Azzuni, E., and Guzey, S. (2015). “Comparison of the shell design methods for cylindrical liquid storage tanks.” *Engineering Structures*, Elsevier Ltd, 101, 621–630.

Bakalis, K., Fragiadakis, M., and Vamvatsikos, D. (2015a). “Surrogate Modelling of Liquid Storage Tanks for Seismic Performace Design And Assessment.” *5th ECCOMAS Thematic Conference on Computational Methods in Structural Dynamics and Earthquake Engineering, COMPDYN 2015*, Crete Island, Greece.

Bakalis, K., Fragiadakis, M., and Vamvatsikos, D. (2017a). "Surrogate Modeling for the Seismic Performance Assessment of Liquid Storage Tanks." *Journal of Structural Engineering*, 143(4), 4016199.

Bakalis, K., Kazantzi, A. K., Vamvatsikos, D., and Fragiadakis, M. (2018a). "Seismic performance evaluation of liquid storage tanks using nonlinear static procedures." *Journal of Pressure Vessel Technology*, (Under revision).

Bakalis, K., Kohrangi, M., and Vamvatsikos, D. (2018b). "Seismic Intensity Measures for Liquid Storage Tanks." *Earthquake Engineering & Structural Dynamics*, (Accepted).

Bakalis, K., and Vamvatsikos, D. (2015). "Direct Performance-Based Seismic Design for Liquid Storage Tanks." *SECED 2015 Conference: Earthquake Risk and Engineering towards a Resilient World*, Cambridge, UK.

Bakalis, K., and Vamvatsikos, D. (2018). "Seismic Fragility Functions via Nonlinear Response History Analysis." *Journal of Structural Engineering, ASCE*, (Accepted).

Bakalis, K., Vamvatsikos, D., and Fragiadakis, M. (2014a). "Seismic Reliability Assessment of Liquid Storage Tanks." *Proceedings of the 2nd European Conference on Earthquake Engineering and Seismology*, Istanbul, Turkey.

Bakalis, K., Vamvatsikos, D., and Fragiadakis, M. (2014b). "Surrogate Modelling and Sensitivity Analysis of Steel Liquid Storage Tanks." *8th Hellenic National Conference of Steel Structures*, Tripoli, Greece, 2-4 October 2014.

Bakalis, K., Vamvatsikos, D., and Fragiadakis, M. (2015b). "Seismic Fragility Assessment of Steel Liquid Storage Tanks." *Volume 8: Seismic Engineering*, ASME, Pressure Vessels and Piping Conference, Boston, Massachusetts, USA, V008T08A023.

Bakalis, K., Vamvatsikos, D., and Fragiadakis, M. (2017b). "Seismic risk assessment of liquid storage tanks via a nonlinear surrogate model." *Earthquake Engineering & Structural Dynamics*, 46(15), 2851–2868.

Baker, J. W. (2007). "Probabilistic structural response assessment using vector-valued intensity measures." *Earthquake Engineering & Structural Dynamics*, 36(13), 1861–1883.

Baker, J. W., and Cornell, C. A. (2005). "A vector-valued ground motion intensity measure consisting of spectral acceleration and epsilon." *Earthquake Engineering and Structural Dynamics*, 34(10), 1193–1217.

Baker, J. W., and Cornell, C. A. (2006a). "Spectral shape, epsilon and record selection." *Earthquake Engineering and Structural Dynamics*, 35(9), 1077–1095.

Baker, J. W., and Cornell, C. A. (2006b). "Which spectral acceleration are you using?" *Earthquake Spectra*, 22(2), 293–312.

Baker, J. W., and Cornell, C. A. (2006c). "Correlation of response spectral values for multicomponent ground motions." *Bulletin of the Seismological Society of America*, 96(1), 215–227.

Bazzurro, P., and Cornell, C. A. (2002). "Vector-Valued Probabilistic Seismic Hazard Analysis (VPSHA)." *Proceedings of the 7th U.S. National Conference on Earthquake Engineering*, Boston, Massachusetts, USA.

Berahman, F., and Behnamfar, F. (2007). "Seismic Fragility Curves for Un-Anchored On-Grade Steel Storage Tanks: Bayesian Approach." *Journal of Earthquake Engineering*, 11(2), 166–192.

Bibbee, A., Gonenc, R., Jacobs, S., Konvitz, J., and Price, R. (2000). *Economic Effects of the 1999 Turkish Earthquakes: An Interim Report*. *OECD Economics Department Working Papers, No.247*.

Bojórquez, E., and Iervolino, I. (2011). "Spectral shape proxies and nonlinear structural response." *Soil Dynamics and Earthquake Engineering*, 31(7), 996–1008.

Boore, D. M., and Atkinson, G. M. (2008). "Ground-Motion Prediction Equations for the Average Horizontal Component of PGA, PGV, and 5%-Damped PSA at Spectral Periods between 0.01 s and 10.0 s." *Earthquake Spectra*, 24(1), 99–138.

Bradley, B. A. (2013). "A comparison of intensity-based demand distributions and the seismic demand hazard for seismic performance assessment." *Earthquake Engineering & Structural Dynamics*, 42(15), 2235–2253.

Bradley, B. A., and Lee, D. S. (2009). "Component correlations in structure-specific seismic loss estimation." *Earthquake Engineering & Structural Dynamics*, 39(3), 237–258.

Bradley, B., Comerio, M., Cubrinovski, M., Dellow, S., Dizhur, D., Elwood, K., Giaretton, M., Green, R., Horspool, N., Hughes, M., Ingham, J., Johnson, L., Massey, C., Seville, E., Simkin, G., Stevenson, J., Wilson, R., and Wotherspoon, L. (2017). *QuakeCoRE, GEER, and EERI Earthquake Reconnaissance Report: M7.8 Kaikoura, New Zealand Earthquake on November 14, 2016*.

Brewer, L. (1992). "Buckled water tank lifted off base by Landers earthquake." *National Oceanic and Atmospheric Administration, US Department of Commerce*, <https://www.ngdc.noaa.gov/hazardimages/picture/show/344>.

British Broadcasting Corporation. (1999). "In pictures: The search for survivors." <http://news.bbc.co.uk/2/hi/europe/423588.stm> (Nov. 14, 2017).

Brunesi, E., Nascimbene, R., Pagani, M., and Beilic, D. (2015). "Seismic Performance of Storage Steel Tanks during the May 2012 Emilia, Italy, Earthquakes." *Journal of Performance of Constructed Facilities*, 29(5), 4014137.

Buratti, N., and Tavano, M. (2014). "Dynamic buckling and seismic fragility of anchored steel tanks by the added mass method." *Earthquake Engineering & Structural Dynamics*, 43(1), 1–21.

Calvi, G. M., and Nascimbene, R. (2011). "Progettazione sismica dei serbatoi." *Progettare i gusci*, IUSS Press, Pavia, Italy, 537–672.

CEN. (2002). *Eurocode 1: Actions on structures —Part 1-1: General actions - Densities, self-weight, imposed loads for buildings*. *European Committee for Standard*, Brussels.

CEN. (2003). *Eurocode 1: Actions on structures-Part 1-3: General actions - Snow loads*. *European Committee for Standard*, Brussels.

CEN. (2004). *Eurocode 8 : Design of structures for earthquake resistance - Part 1: General rules, seismic actions and rules for buildings (EN 1998-1:2004)*. *European Standard NF EN*, CEN, Brussels.

CEN. (2005). *Eurocode 1 — Actions on structures —Part 1-4: General actions - Wind actions*. *European Committee for Standard*, Brussels.

CEN. (2006). *Eurocode 8: Design of structures for earthquake resistance–Part 4: Silos, tanks and pipelines*. *European Committee for Standard*, Brussels.

CEN. (2007a). *Eurocode 3 : Design of steel structures —Part 4-2: Tanks*. *European Committee for Standard*, Brussels.

CEN. (2007b). *Eurocode 3 — Design of steel structures —Part 1-6: Strength and Stability of Shell Structures*. *European Committee for Standard*, Brussels.

Cordova, P., Deierlein, G., Mehanny, S. F., and Cornell, C. A. (2001). "Development of a two-parameter seismic intensity measure and probabilistic design procedure." *The Second U.S.- Japan Workshop on Performance-Based Earthquake Engineering Methodology for Reinforced Concrete Building Structures*, Sapporo, Hokkaido, 187–206.

Cornell, C. A. (1968). "Engineering Seismic Risk Analysis." *Bulletin of the Seismological Society of America*, 58(5), 1583–1606.

Cornell, C. A., and Krawinkler, H. (2000). "Progress and Challenges in Seismic Performance Assessment." *PEER Center News*, 3(2), 1–4.

Cortés, G., Nussbaumer, A., Berger, C., and Lattion, E. (2011). "Experimental determination of the rotational capacity of wall-to-base connections in storage tanks." *Journal of Constructional Steel Research*, Elsevier Ltd, 67(7), 1174–1184.

Cortes, G., and Prinz, G. S. (2017). "Seismic fragility analysis of large unanchored steel tanks considering local instability and fatigue damage." *Bulletin of Earthquake Engineering*, Springer Netherlands, 15(3), 1279–1295.

Cortes, G., Prinz, G. S., Nussbaumer, A., and Koller, M. G. (2012). "Cyclic Demand at the Shell-Bottom Connection of Unanchored Steel Tanks." *Proc., 15th World Conference on Earthquake Engineering*, Lisboa, Portugal.

Cruz, A. M., and Steinberg, L. J. (2005). "Industry Preparedness for Earthquakes and Earthquake-Triggered Hazmat Accidents in the 1999 Kocaeli Earthquake." *Earthquake Spectra*, 21(2), 285–303.

D'Ayala, D., Meslem, A., Vamvatsikos, D., Porter, K., and Rossetto, T. (2015). *Guidelines for Analytical Vulnerability Assessment - Low/Mid-Rise Buildings*. Vulnerability Global Component Project.

Dehghan Manshadi, S. H., and Maheri, M. R. (2010). "The effects of long-term corrosion on the dynamic characteristics of ground based cylindrical liquid storage tanks." *Thin-Walled Structures*, 48(12), 888–896.

DuBrowa, A. (2010). "Damaged Water Treatment plant in California." *Federal Emergency Management Agency*, <https://www.fema.gov/media-library/assets/images/57522#details> (Nov. 14, 2017).

Eads, L., Miranda, E., Krawinkler, H., and Lignos, D. G. (2013). "An efficient method for estimating the collapse risk of structures in seismic regions." *Earthquake Engineering & Structural Dynamics*, 42(1), 25–41.

Eads, L., Miranda, E., and Lignos, D. G. (2015). "Average spectral acceleration as an intensity measure for collapse risk assessment." *Earthquake Engineering & Structural Dynamics*, 44(12), 2057–2073.

Eidinger, J. M. (2012). "Performance of Water Systems during the Maule Mw 8.8 Earthquake of 27 February 2010." *Earthquake Spectra*, 28(S1), S605–S620.

European Pressphoto Agency. (2011). "The big pictures: The moment Japan's cataclysmic tsunami engulfed a nation." *Daily Mail*, <http://www.dailymail.co.uk/news/article-1365318/Japan-earthquake-tsunami-The-moment-mother-nature-engulfed-nation.html> (Nov. 14, 2017).

Fabbrocino, G., Iervolino, I., Orlando, F., and Salzano, E. (2005). "Quantitative risk analysis of oil storage facilities in seismic areas." *Journal of Hazardous Materials*, 123(1–3), 61–69.

FEMA. (2003). *HAZUS-MH MR4 Multi-hazard Loss Estimation Methodology, Technical Manual*. *National Institute of Building Sciences and Federal Emergency Management Agency (NIBS and FEMA)*, Washington D.C.

FEMA. (2009). *Quantification of Building Seismic Performance Factors*. FEMA P-695, prepared by Applied Technology Council for Federal Emergency Management Agency, Washington, D.C.

FEMA. (2012a). *Reducing the risks of nonstructural earthquake damage – A practical guide*. FEMA E-74, prepared by Applied Technology Council for Federal Emergency Management Agency and ATC Management and Oversight, Washington, D.C.

FEMA. (2012b). *Seismic Performance Assessment of Buildings*. FEMA P-58, prepared by the Applied Technology Council for the Federal Emergency Management Agency, Washington D.C.

Fragiadakis, M., and Vamvatsikos, D. (2010). "Fast performance uncertainty estimation via pushover and approximate IDA." *Earthquake Engineering & Structural Dynamics*, 39(6), 683–703.

Friends of the Earth Europe, and Transport & Environment. (2017). "TAR SANDS: COMING TO AN OIL REFINERY NEAR YOU?" <https://www.transportenvironment.org/sites/te/files/iframe_transportenvironment.html> (Nov. 14, 2017).

Gehl, P., Seyedi, D. M., and Douglas, J. (2013). "Vector-valued fragility functions for seismic risk evaluation." *Bulletin of Earthquake Engineering*, 11(2), 365–384.

Giardini, D., Woessner, J., Danciu, L., Crowley, H., Cotton, F., Grünthal, G., Pinho, R., Valensise, G., Akkar, S., Arvidsson, R., Basili, R., Cameelbeeck, T., Campos-Costa, A., Douglas, J., Demircioglu, M. B., Erdik, M., Fonseca, J., Glavatovic, B., Lindholm, C., Makropoulos, K., Meletti, C., Musson, R., Pitilakis, K., Sesetyan, K., Stromeyer, D., Stucchi, M., and Rovida, A. (2013). "Seismic Hazard Harmonization in Europe (SHARE): Online Data Resource."

Giovenale, P., Cornell, C. A., and Esteva, L. (2004). "Comparing the adequacy of alternative ground motion intensity measures for the estimation of structural responses." *Earthquake Engineering & Structural Dynamics*, 33(8), 951–979.

Girgin, S. (2011). "The natech events during the 17 August 1999 Kocaeli earthquake: aftermath and lessons learned." *Natural Hazards and Earth System Science*, 11(4), 1129–1140.

Godoy, L. A. (2016). "Buckling of vertical oil storage steel tanks: Review of static buckling studies." *Thin-Walled Structures*, 103, 1–21.

González, E., Almazán, J., Beltrán, J., Herrera, R., and Sandoval, V. (2013). "Performance of stainless steel winery tanks during the 02/27/2010 Maule Earthquake." *Engineering Structures*, 56(2013), 1402–1418.

Habenberger, J. (2015). "Fluid damping of cylindrical liquid storage tanks." *SpringerPlus*, Springer International Publishing, 4(1), 515.

Hansen, W. R. (1965). *Effects of the Earthquake of March 27,1964, At Anchorage, Alaska*. U.S.

Geological Survey Professional Paper 542–A, 68 p., 2 sheets, scales 1:2,400 and 1:480, https://pubs.usgs.gov/pp/0542a/.

Haroun, M. A. (1983). “Vibration studies and tests of liquid storage tanks.” *Earthquake Engineering & Structural Dynamics*, 11(2), 179–206.

Haroun, M. A., and Housner, G. W. (1981). “Earthquake Response of Deformable Liquid Storage Tanks.” *Journal of Applied Mechanics*, 48(2), 411.

Hatayama, K. (2008). “Lessons from the 2003 Tokachi-oki, Japan, earthquake for prediction of long-period strong ground motions and sloshing damage to oil storage tanks.” *Journal of Seismology*, 12(2), 255–263.

Hatayama, K. (2015). “Damage to Oil Storage Tanks from the 2011 Mw 9.0 Tohoku-Oki Tsunami.” *Earthquake Spectra*, 31(2), 1103–1124.

Housner, G. W. (1957). “Dynamic pressures on accelerated fluid containers.” *Bulletin of the Seismological Society of America*, 47(1), 15–35.

Housner, G. W. (1963). “The dynamic behavior of water tanks.” *Bulletin of the Seismological Society of America*, 53(2), 381–387.

Housner, G. W., Trinfunac, M. D., Frazier, G. A., Wood, J. H., Scott, R. F., Iwan, W. D., Jennings, P. C., and Brady, G. A. (1971). *Engineering features of the San Fernando earthquake of February 9, 1971*. Report No. EERL 71-02, Earthquake Engineering Research Laboratory, Pasadena, CA.

Iervolino, I., Fabbrocino, G., and Manfredi, G. (2004). “Fragility Of Standard Industrial Structures By a Response Surface Based Method.” *Journal of Earthquake Engineering*, 8(6), 927–945.

Innovative Engicon Solutions PVT. (2017). “Pipe Rack.” <http://innovativeengicon.in/gallery/> (Nov. 14, 2017).

Inoue, T. (1990). “Seismic Hazard Analysis of Multi-Degree-Of-Freedom Structures.” *Report No. RMS-8*, Reliability of Marine Structures, RMS-8, Stanford, California.

Jaiswal, O. R., Rai, D. C., and Jain, S. K. (2007). “Review of Seismic Codes on Liquid-Containing Tanks.” *Earthquake Spectra*, 23(1), 239–260.

Jalayer, F. (2003). “Direct Probabilistic Seismic Anaysis: Implementing Non-linear Dynamic Assessments.” Ph.D. dissertation, Dept. of Civil and Environmental Engineering, Stanford Univ., Stanford, CA.

Jayaram, N., Lin, T., and Baker, J. W. (2011). “A Computationally Efficient Ground-Motion Selection Algorithm for Matching a Target Response Spectrum Mean and Variance.” *Earthquake Spectra*, 27(3), 797–815.

Kalogerakou, M. E., Maniatakis, C. A., Spyrakos, C. C., and Psarropoulos, P. N. (2017). “Seismic response of liquid-containing tanks with emphasis on the hydrodynamic response and near-fault phenomena.” *Engineering Structures*, 153, 383–403.

Katsanos, E. I., and Vamvatsikos, D. (2017). “Yield frequency spectra and seismic design of code-compatible RC structures: an illustrative example.” *Earthquake Engineering & Structural Dynamics*, 46(11), 1727–1745.

Kazantzi, A. K., and Vamvatsikos, D. (2015). “Intensity measure selection for vulnerability studies of building classes.” *Earthquake Engineering & Structural Dynamics*, 44(15), 2677–2694.

Kazantzi, A. K., Vamvatsikos, D., and Lignos, D. G. (2014). “Seismic performance of a steel moment-resisting frame subject to strength and ductility uncertainty.” *Engineering Structures*, Elsevier Ltd, 78, 69–77.

Kildashti, K., Mirzadeh, N., and Samali, B. (2018). “Seismic vulnerability assessment of a case study anchored liquid storage tank by considering fixed and flexible base restraints.” *Thin-Walled Structures*, 123(October), 382–394.

Kilic, S., and Ozdemir, Z. (2007). “Simulation of Sloshing Effects in Cylindrical Containers under Seismic Loading.” *Proc., 6th LS-DYNA Anwenderforum*, Frankenthal.

Kishida, T. (2017). “Conditional Mean Spectra Given a Vector of Spectral Accelerations at Multiple Periods.” *Earthquake Spectra*, 33(2), 469–479.

Kohrangi, M., Bazzurro, P., and Vamvatsikos, D. (n.d.). “Implementing Conditional Spectrum based record selection for nonlinear dynamic analysis of 3D structural models: an introduction to vector IM based conditional spectra (under review).”

Kohrangi, M., Bazzurro, P., and Vamvatsikos, D. (2016a). “Vector and Scalar IMs in Structural

Response Estimation, Part I: Hazard Analysis." *Earthquake Spectra*, 32(3), 1507–1524.
Kohrangi, M., Bazzurro, P., and Vamvatsikos, D. (2016b). "Vector and Scalar IMs in Structural Response Estimation, Part II: Building Demand Assessment." *Earthquake Spectra*, 32(3), 1525–1543.
Kohrangi, M., Bazzurro, P., Vamvatsikos, D., and Spillatura, A. (2017a). "Conditional spectrum-based ground motion record selection using average spectral acceleration." *Earthquake Engineering & Structural Dynamics*, 44, 657–675.
Kohrangi, M., Vamvatsikos, D., and Bazzurro, P. (n.d.). "Conditional spectrum based record selection at multiple IM levels for IDA (under review)."
Kohrangi, M., Vamvatsikos, D., and Bazzurro, P. (2017b). "Site dependence and record selection schemes for building fragility and regional loss assessment." *Earthquake Engineering & Structural Dynamics*, 46(10), 1625–1643.
Krausmann, E., and Cruz, A. M. (2013). "Impact of the 11 March 2011, Great East Japan earthquake and tsunami on the chemical industry." *Natural Hazards*, 67(2), 811–828.
Lin, T., Haselton, C. B., and Baker, J. W. (2013a). "Conditional spectrum-based ground motion selection. Part I: Hazard consistency for risk-based assessments." *Earthquake Engineering & Structural Dynamics*, 42(12), 1847–1865.
Lin, T., Haselton, C. B., and Baker, J. W. (2013b). "Conditional spectrum-based ground motion selection. Part II: Intensity-based assessments and evaluation of alternative target spectra." *Earthquake Engineering & Structural Dynamics*, 42(12), 1867–1884.
Luco, N., and Bazzurro, P. (2007). "Does amplitude scaling of ground motion records result in biased nonlinear structural drift responses?" *Earthquake Engineering & Structural Dynamics*, 36(13), 1813–1835.
Luco, N., and Cornell, C. A. (2007). "Structure-Specific Scalar Intensity Measures for Near-Source and Ordinary Earthquake Ground Motions." *Earthquake Spectra*, 23(2), 357–392.
Malhotra, P. K. (1997). "Seismic Response of Soil-Supported Unanchored Liquid-Storage Tanks." *Journal of Structural Engineering*, 123(4), 440–450.
Malhotra, P. K. (2000). "Practical Nonlinear Seismic Analysis of Tanks." *Earthquake Spectra*, 16(2), 473–492.
Malhotra, P. K. (2005). "Sloshing Loads in Liquid-Storage Tanks with Insufficient Freeboard." *Earthquake Spectra*, 21(4), 1185–1192.
Malhotra, P. K., and Veletsos, A. S. (1994a). "Beam Model for Base-Uplifting Analysis of Cylindrical Tanks." *Journal of Structural Engineering*, 120(12), 3471–3488.
Malhotra, P. K., and Veletsos, A. S. (1994b). "Uplifting Analysis of Base Plates in Cylindrical Tanks." *Journal of Structural Engineering*, 120(12), 3489–3505.
Malhotra, P. K., and Veletsos, A. S. (1994c). "Uplifting Response of Unanchored Liquid-Storage Tanks." *Journal of Structural Engineering*, 120(12), 3525–3547.
Malhotra, P. K., Wenk, T., and Wieland, M. (2000). "Simple Procedure for Seismic Analysis of Liquid-Storage Tanks." *Structural Engineering International*, 10(3), 197–201.
Manos, G. C. (1991). "Evaluation of the earthquake performance of anchored wine tanks during the San Juan, Argentina, 1977 earthquakexs." *Earthquake Engineering & Structural Dynamics*, 20(12), 1099–1114.
Manos, G. C., and Clough, R. W. (1985). "Tank damage during the may 1983 coalinga earthquake." *Earthquake Engineering & Structural Dynamics*, 13(4), 449–466.
Manos, G. C., Shibata, H., and Shigeta, T. (1989). "Correlation of cylindrical tank wall buckling with an earthquake motion recorded at a small distance from the tank." *Earthquake Engineering & Structural Dynamics*, 18(2), 169–184.
McKenna, F., and Fenves, G. L. (2001). "The OpenSees Command Language Manual (1.2 edn)."
Mehanny, S. S. F. (2009). "A broad-range power-law form scalar-based seismic intensity measure." *Engineering Structures*, 31(7), 1354–1368.
Melissianos, V. E., Vamvatsikos, D., and Gantes, C. J. (2017). "Performance Assessment of Buried Pipelines at Fault Crossings." *Earthquake Spectra*, 33(1), 201–218.
MSMAware. (2014). "OSD for Below-Ground Storage." <http://msmaware.com/blog/documentation/on-site-detention/general-information-of-osd/osd-of-

below-ground-storage/> (Nov. 14, 2017).

Naito, C., Cox, D., Yu, Q. K., and Brooker, H. (2013). "Fuel Storage Container Performance during the 2011 Tohoku, Japan, Tsunami." *Journal of Performance of Constructed Facilities*, 27(4), 373–380.

Niwa, A., and Clough, R. W. (1982). "Buckling of cylindrical liquid-storage tanks under earthquake loading." *Earthquake Engineering & Structural Dynamics*, 10(1), 107–122.

Norio, O., Ye, T., Kajitani, Y., Shi, P., and Tatano, H. (2011). "The 2011 eastern Japan great earthquake disaster: Overview and comments." *International Journal of Disaster Risk Science*, 2(1), 34–42.

Nuzzo, R. (2014). "Scientific method: Statistical errors." *Nature*, 506(7487), 150–152.

O'Rourke, M. J., and So, P. (2000). "Seismic Fragility Curves for On-Grade Steel Tanks." *Earthquake Spectra*, 16(4), 801–815.

Oil and Gas club. (2015). "Question related to equipment and piping layout: - Part-2." <https://www.oilandgasclub.com/question-related-to-equipment-and-piping-layout-part-2/> (Nov. 14, 2017).

Önder, E., Tural, Ü., Aker, T., Kılıç, C., and Erdoğan, S. (2006). "Prevalence of psychiatric disorders three years after the 1999 earthquake in Turkey: Marmara Earthquake Survey (MES)." *Social Psychiatry and Psychiatric Epidemiology*, 41(11), 868–874.

Ormeño, M., Larkin, T., and Chouw, N. (2015a). "The effect of seismic uplift on the shell stresses of liquid-storage tanks." *Earthquake Engineering & Structural Dynamics*, 44(12), 1979–1996.

Ormeño, M., Larkin, T., and Chouw, N. (2015b). "Evaluation of seismic ground motion scaling procedures for linear time-history analysis of liquid storage tanks." *Engineering Structures*, 102(2015), 266–277.

Ozdemir, Z., Souli, M., and Fahjan, Y. M. (2010). "Application of nonlinear fluid–structure interaction methods to seismic analysis of anchored and unanchored tanks." *Engineering Structures*, Elsevier Ltd, 32(2), 409–423.

Ozdemir, Z., Souli, M., and M. Fahjan, Y. (2012). "Numerical Evaluation of Nonlinear Response of Broad Cylindrical Steel Tanks under Multidimensional Earthquake Motion." *Earthquake Spectra*, 28(1), 217–238.

Padgett, J. E., Nielson, B. G., and DesRoches, R. (2008). "Selection of optimal intensity measures in probabilistic seismic demand models of highway bridge portfolios." *Earthquake Engineering & Structural Dynamics*, 37(5), 711–725.

Pagani, M., Monelli, D., Weatherill, G., Danciu, L., Crowley, H., Silva, V., Henshaw, P., Butler, L., Nastasi, M., Panzeri, L., Simionato, M., and Vigano, D. (2014). "OpenQuake Engine: An Open Hazard (and Risk) Software for the Global Earthquake Model." *Seismological Research Letters*, 85(3), 692–702.

Phan, H. N., and Paolacci, F. (2016). "Efficient Intensity Measures for Probabilistic Seismic Response Analysis of Anchored Above-Ground Liquid Steel Storage Tanks." *Volume 5: High-Pressure Technology; Rudy Scavuzzo Student Paper Symposium and 24th Annual Student Paper Competition; ASME Nondestructive Evaluation, Diagnosis and Prognosis Division (NDPD); Electric Power Research Institute (EPRI) Creep Fatigue Workshop*, ASME, V005T09A010.

Phan, H. N., Paolacci, F., Bursi, O. S., and Tondini, N. (2017a). "Seismic fragility analysis of elevated steel storage tanks supported by reinforced concrete columns." *Journal of Loss Prevention in the Process Industries*, Elsevier Ltd, 47(2017), 57–65.

Phan, H. N., Paolacci, F., and Mongabure, P. (2017b). "Nonlinear Finite Element Analysis Of Unanchored Steel Liquid Storage Tanks Subjected To Seismic Loadings." *ASME 2017 Pressure Vessels and Piping Conference*, Waikoloa, Hawaii, United States.

Pitilakis, K., Franchin, P., Khazai, B., and Wenzel, H. (Eds.). (2014). *SYNER-G: Systemic Seismic Vulnerability and Risk Assessment of Complex Urban, Utility, Lifeline Systems and Critical Facilities*. Geotechnical, Geological and Earthquake Engineering, Springer Netherlands, Dordrecht.

Priestley, M. J. N., Wood, J. H., and Davidson, B. J. (1986). "Seismic Design of Storage Tanks." *Bulletin of the New Zealand Society for Earthquake Engineering*, 19(4), 272–284.

Prinz, G. S., and Nussbaumer, A. (2012a). "Fatigue analysis of liquid-storage tank shell-to-base connections under multi-axial loading." *Engineering Structures*, Elsevier Ltd, 40(2012), 75–82.

Prinz, G. S., and Nussbaumer, A. (2012b). "On the low-cycle fatigue capacity of unanchored steel liquid storage tank shell-to-base connections." *Bulletin of Earthquake Engineering*, 10(6), 1943–1958.

Raine, M. (2016). "Installation and commissioning of API 650 tanks." <https://issuu.com/christianbarthe/docs/installation_and_commissioning_of_a> (Nov. 14, 2017).

RASOR. (2015). "Risk Assessment for the Seismic protection Of industRial facilities, THALES." Final Technical Report, RASOR project, <http://excellence.minedu.gov.gr/thales/en/thalesprojects/379422>.

Razzaghi, M. S., and Eshghi, S. (2015). "Probabilistic Seismic Safety Evaluation of Precode Cylindrical Oil Tanks." *Journal of Performance of Constructed Facilities*, 29(6), 4014170.

Rondon, A., and Guzey, S. (2016). "Determination of localized stresses in the shell above anchor bolt chairs attachments of anchored storage tanks." *Thin-Walled Structures*, Elsevier, 98(2016), 617–626.

Rondon, A., and Guzey, S. (2017). "Fatigue evaluation of the API specification 12F shop welded flat bottom tanks." *International Journal of Pressure Vessels and Piping*, 149(2017), 14–23.

Rotter, J. M. (2006). "Elephant's foot buckling in pressurised cylindrical shells." *Stahlbau*, 75(9), 742–747.

Salzano, E., Garcia Agreda, A., Di Carluccio, A., and Fabbrocino, G. (2009). "Risk assessment and early warning systems for industrial facilities in seismic zones." *Reliability Engineering & System Safety*, Elsevier, 94(10), 1577–1584.

Salzano, E., Iervolino, I., and Fabbrocino, G. (2003). "Seismic risk of atmospheric storage tanks in the framework of quantitative risk analysis." *Journal of Loss Prevention in the Process Industries*, 16(5), 403–409.

Sezen, H., and Whittaker, A. S. (2006). "Seismic Performance of Industrial Facilities Affected by the 1999 Turkey Earthquake." *Journal of Performance of Constructed Facilities*, 20(1), 28–36.

Spritzer, J. M., and Guzey, S. (2017a). "Review of API 650 Annex E: Design of large steel welded aboveground storage tanks excited by seismic loads." *Thin-Walled Structures*, 112(September), 41–65.

Spritzer, J. M., and Guzey, S. (2017b). "Nonlinear numerical evaluation of large open-top aboveground steel welded liquid storage tanks excited by seismic loads." *Thin-Walled Structures*, Elsevier Ltd, 119(July), 662–676.

Steinberg, L. J., and Cruz, A. M. (2004). "When Natural and Technological Disasters Collide: Lessons from the Turkey Earthquake of August 17, 1999." *Natural Hazards Review*, 5(3), 121–130.

T.F. Warren Group. (2016). "Spheres (ASME) - Spherical shaped storage." <http://www.tfwarren.com/tarsco/products/asme-storage-spheres> (Nov. 14, 2017).

Talaslidis, D. G., Manolis, G. D., Paraskevopoulos, E., Panagiotopoulos, C., Pelekasis, N., and Tsamopoulos, J. A. (2004). "Risk analysis of industrial structures under extreme transient loads." *Soil Dynamics and Earthquake Engineering*, 24(6), 435–448.

Tank Connection. (2017). "Elevated water tanks." <http://www.tankconnection.midwestern.de/ask-the-expert/elevated-water-tanks> (Nov. 14, 2017).

Thoms, E. E., Haeussler, P. J., Anderson, R. D., and McGimsey, R. G. (2014). *1964 Great Alaska Earthquake—A Photographic Tour of Anchorage, Alaska*. U.S. Geological Survey Open-File Report 2014-1086, 48 p.

Tothong, P., and Cornell, C. A. (2008). "Structural performance assessment under near-source pulse-like ground motions using advanced ground motion intensity measures." *Earthquake Engineering & Structural Dynamics*, 37(7), 1013–1037.

Tothong, P., and Luco, N. (2007). "Probabilistic seismic demand analysis using advanced ground motion intensity measures." *Earthquake Engineering & Structural Dynamics*, 36(13), 1837–1860.

Trust Subsidiary Production Co. (2015). "Liquid Storage Tanks." <http://www.trustspco.com/index.php/fa/activiteis/petroshimi/202-2015-09-14-07-25-03> (Nov. 14, 2017).

Tsantaki, S., Adam, C., and Ibarra, L. F. (2017). "Intensity measures that reduce collapse capacity dispersion of P-delta vulnerable simple systems." *Bulletin of Earthquake Engineering*, Springer Netherlands, 15(3), 1085–1109.

Tural, Ü., Coşkun, B., Önder, E., Çorapçioglu, A., Yildiz, M., Kesepara, C., Karakaya, I., Aydin, M., Erol, A., Torun, F., and Aybar, G. (2004). "Psychological consequences of the 1999 earthquake in Turkey." *Journal of Traumatic Stress*, 17(6), 451–459.

Vakili, M., and Showkati, H. (2016). "Experimental and Numerical Investigation of Elephant Foot Buckling and Retrofitting of Cylindrical Shells by FRP." *Journal of Composites for Construction*, 20(4), 4015087.

Vamvatsikos, D. (2013). "Derivation of new SAC/FEMA performance evaluation solutions with second-order hazard approximation." *Earthquake Engineering & Structural Dynamics*, 42(8), 1171–1188.

Vamvatsikos, D. (2014). "Seismic Performance Uncertainty Estimation via IDA with Progressive Accelerogram-Wise Latin Hypercube Sampling." *Journal of Structural Engineering*, 140(8), A4014015.

Vamvatsikos, D., and Aschheim, M. A. (2016). "Performance-based seismic design via yield frequency spectra." *Earthquake Engineering & Structural Dynamics*, 45(11), 1759–1778.

Vamvatsikos, D., and Cornell, C. A. (2002). "Incremental dynamic analysis." *Earthquake Engineering & Structural Dynamics*, 31(3), 491–514.

Vamvatsikos, D., and Cornell, C. A. (2004). "Applied Incremental Dynamic Analysis." *Earthquake Spectra*, 20(2), 523–553.

Vamvatsikos, D., and Cornell, C. A. (2005a). "Developing efficient scalar and vector intensity measures for IDA capacity estimation by incorporating elastic spectral shape information." *Earthquake Engineering and Structural Dynamics*, 34(13), 1573–1600.

Vamvatsikos, D., and Cornell, C. A. (2005b). "Direct Estimation of Seismic Demand and Capacity of Multidegree-of-Freedom Systems through Incremental Dynamic Analysis of Single Degree of Freedom Approximation." *Journal of Structural Engineering*, 131(4), 589–599.

Vamvatsikos, D., and Cornell, C. A. (2006). "Direct estimation of the seismic demand and capacity of oscillators with multi-linear static pushovers through IDA." *Earthquake Engineering and Structural Dynamics*, 35(April 2004), 1097–1117.

Vamvatsikos, D., and Fragiadakis, M. (2010). "Incremental dynamic analysis for estimating seismic performance sensitivity and uncertainty." *Earthquake Engineering & Structural Dynamics*, 39(2), 141–163.

Vathi, M. (2016). "Structural Behaviour of Liquid Storage Steel Containers Under Strong Dynamic Excitation." Ph.D. dissertation, Dept. of Mechanical Engineering, University of Thessaly, Greece.

Vathi, M., and Karamanos, S. A. (2017). "A simple and efficient model for seismic response and low-cycle fatigue assessment of uplifting liquid storage tanks." *Journal of Loss Prevention in the Process Industries*, Elsevier Ltd, (Article in press).

Vathi, M., Karamanos, S. A., Kapogiannis, I. A., and Spiliopoulos, K. V. (2017). "Performance Criteria for Liquid Storage Tanks and Piping Systems Subjected to Seismic Loading." *Journal of Pressure Vessel Technology*, 139(5), 51801.

Vathi, M., Karamanos, S. A., Kapogiannis, I., and Spiliopoulos, K. (2015). "Performance Criteria for Liquid Storage Tanks and Piping Systems Subjected to Seismic Loading." *Proceedings of the ASME 2015 Pressure Vessels & Piping Division Conference*, Boston, Massachusetts, USA.

Vathi, M., Pappa, P., and Karamanos, S. A. (2013). "Seismic Response of Unanchored Liquid Storage Tanks." *Proc., ASME 2013 Pressure Vessels & Piping Division Conference*, Paris, France.

Veletsos, A. S., and Tang, Y. (1990). "Soil-structure interaction effects for laterally excited liquid storage tanks." *Earthquake Engineering & Structural Dynamics*, 19(4), 473–496.

Virella, J. C., Godoy, L. A., and Suárez, L. E. (2006). "Dynamic buckling of anchored steel tanks subjected to horizontal earthquake excitation." *Journal of Constructional Steel Research*, 62(6), 521–531.

Vrouwenvelder, T. (1997). "The JCSS probabilistic model code." *Structural Safety*, 19(3), 245–251.

Wasicek, M., Fischer, F. D., and Kolednik, O. (2008). "Auswirkung von monotoner und zyklischer Belastung auf die Undichtheit eines Tankbodenecks." *Stahlbau*, 77(7), 524–530.

Yang, T. Y., Moehle, J., Stojadinovic, B., and Der Kiureghian, A. (2009). "Seismic Performance Evaluation of Facilities: Methodology and Implementation." *Journal of Structural Engineering*, 135(10), 1146–1154.

Zama, S., Nishi, H., Hatayama, K., Yamada, M., Yoshihara, H., and Ogawa, Y. (2012). "On Damage of

Oil Storage Tanks due to the 2011 off the Pacific Coast of Tohoku Earthquake (Mw 9.0), Japan." *Proceedings of the 15th World Conference on Earthquake Engineering*, Lisboa, Portugal.
Zareian, F., Aguirre, C., Beltrán, J. F., Cruz, E., Herrera, R., Leon, R., Millan, A., and Verdugo, A. (2012). "Reconnaissance Report of Chilean Industrial Facilities Affected by the 2010 Chile Offshore Bío-Bío Earthquake." *Earthquake Spectra*, 28(S1), S513–S532.